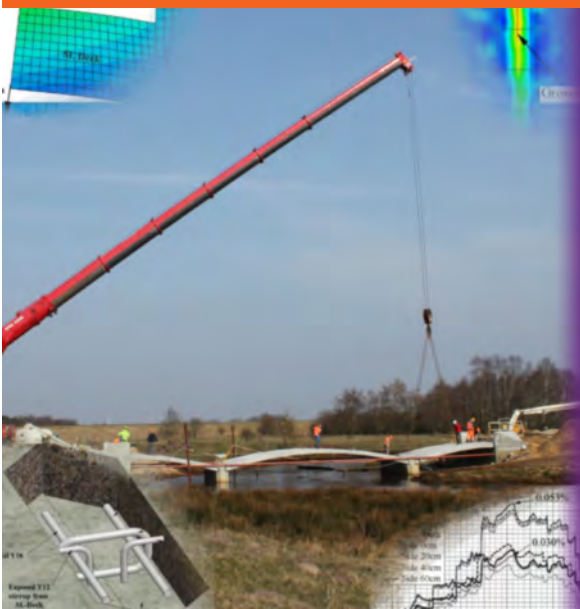


# Construction and Design of Post-Tensioned Pearl-Chain Bridges using SL-Technology



Philip Skov Halding

PhD Thesis

Department of Civil Engineering  
2016

DTU Civil Engineering Report R-350

# **Construction and Design of Post-tensioned Pearl-Chain Bridges using SL-Technology**

## **Supervisors**

Prof. Kristian Dahl Hertz, Technical University of Denmark.

Assoc. prof. Jacob Wittrup Schmidt, Technical University of Denmark, and COWI Denmark.

## **Assessment Committee**

Prof. Per Golterman (chair), Technical University of Denmark.

Prof. Matthew Gilbert, University of Sheffield.

Prof. Olga Popovic Larsen, Royal Danish Academy of Fine Arts.

## **Start date:**

February 1, 2013

## **Submission date:**

May 9, 2016

## **Copyright © 2016 by Philip Skov Halding**

Printed by GraphicCo

## **Department of Civil Engineering**

Technical University of Denmark

Building 118

DK-2800 Kgs. Lyngby

Denmark

*ISBN: 9788778774439*

*Report R-350*



## **PREFACE**

This thesis is submitted after a three year study at the Technical University of Denmark, and is the basis of the fulfillment of requirements for the Danish Ph.D. degree. The thesis is based on a number of papers, where most are appended. The Ph.D. studies were part of a larger project funded by Innovationsfonden. The public defense is scheduled to be on June 17<sup>th</sup> 2016.

Kgs. Lyngby May 9<sup>th</sup> 2016.

---

Philip Skov Halding



## ACKNOWLEDGEMENTS

First of all and most importantly, I wish to thank my two supervisor's professor Kristian D. Hertz and assoc. professor Jacob W. Schmidt for the great guidance and collaboration during my Ph.D.-period at DTU. Your support throughout the project has been tremendously valuable.

The project was a cooperation between industrial partners and the Technical University of Denmark, and it was funded by Innovationsfonden. Many thanks for the discussions and input during our working group meetings to my colleges in Abeo, Sweco, Skandinavisk Spændbeton, and Perstrup betonindustri.

Also, a special thanks to my friend and project manager Nicky E. Viebæk (Abeo) for the involvement and help in the practical preparations to the many full-scale tests performed.

Furthermore, I would like to recognize the efforts of the many Danish and foreign engineering students who have helped me when carrying out many of the tests presented in the thesis. Special thanks to post graduate Bryan J. Kennedy from University of Washington (now COWI).

Finally, thanks to the department of Civil Engineering at DTU, and to my Ph.D.-colleagues from the office for the always good atmosphere.



## ABSTRACT

Pre-fabricated closed-spandrel concrete arch bridges have existed for more than 50 years. Pearl-Chain (PC) Bridges are a new award-winning state-of-the-art segmental concrete arch bridge concept invented by professor Kristian Hertz. A PC-Arch can consist of a number of pre-tensioned low-weight SL-Decks. One SL-Deck is a combination of light aggregate concrete, and regular concrete. Curved post-tensioning ducts are cast into the elements, and several SL-Decks are post-tensioned together in an arch shape to become a PC-Arch. A PC-Bridge is built by erecting a number of adjacent PC-Arches and applying a filling layer of lower stiffness above the arches to level the road surface. The present Ph.D. thesis is part of a larger development project about Pearl-Chain Bridges funded by Innovationsfonden. The project also included another Ph.D. study about the developed materials used in Pearl-Chain Bridges. A row of companies have cooperated with the DTU-team in a consortium during the three year project period: Abeo, Perstrup Betonindustri, Skandinavisk Spændbeton og Sweco.

A method for calculation of the bending moment capacity was presented. The method was illustrated in a case study of a 30 m span PC-Bridge. The case showed that the pre-compression in the arch from pre-stressing, rise/to span ratio, and layer thickness of the filling as expected had influence on the capacity and could be altered to meet the capacity demands of a specific project. For an unevenly loaded bridge, in general, the lowest capacity was found to be in the joint between SL-Decks in the loaded side of the span, and in the SL-Deck in the non-loaded side. Arches under critical loading in the  $\frac{1}{4}$  point of the span have a higher positive than negative bending moment, and advantageously the PC-Arches are designed to have higher positive than negative bending moment capacities in the SL-Decks.

Concrete hinges were investigated for use in PC-Bridges. The true behavior of such hinges was far from ideal, and therefore had an influence of the overall static system. The responses of two types of hinges were investigated by full-scale testing, and numerical modelling. Despite of high levels of normal force in PC-Bridges, the result showed that a Mesnager inspired hinge type had a response similar to what was predicted in the literature. A specially designed saddle bearing also had elastic and plastic rotational resistance, but this hinge type was more practical to implement in a PC-Arch.

Two full-scale 13 m span PC-Arches were successfully assembled, post-tensioned and lifted into position next to each other on a test-foundation by use of a developed fast erection procedure. The same two arches were subsequently load-tested in the  $\frac{1}{4}$  point of the span in two tempi: 1) A test to  $\frac{2}{3}$  of the load carrying capacity,

where the behavior of the arches during loading was recorded and evaluated. It showed that the arches deflected as expected for a regular concrete arch, and that stresses are transferred between arches via so called Hammerhead joints. 2) A test to fracture to observe the ductility in the system, and fracture type. The collapse occurred after two plastic hinges were formed in the  $3/8$ , and  $5/8$  points of the span. Several warnings signs were observed when approaching the maximum loading.

## RESUMÉ

Der er blevet bygget forskellige præ-fabrikerede betonbuebroer i mere end et halvt århundrede. Perlekædebroer er et nyt prisvindende state-of-the-art betonbuebroskoncept, opfundet af professor Kristian Hertz fra DTU. En Perlekædebue består af et antal sammenspændte betonelementer, der stabiliseres af et svagere materiale. Elementerne er ofte forspændte såkaldte SL-Dæk med lav egenlast. Hvert SL-Dæk består af en kombination af letbetonblokke og normal beton. Derudover indeholder dækkene en buet kabelkanal til efterspænding, og når flere SL-Dæk sammenspændes, kan det gøres i en bueform, hvilket kaldes for en Perlekædebue. En Perlekædebro bygges af flere sammenstøbte Perlekædebuer ved siden af hinanden og har et fyldlag oven på buerne for at den overførte vej kan forløbe vandret. Dette Ph.D.-projekt udgør en del af et Innovationsfondsstøttet projekt om Perlekædebuebroer, hvor der bl.a. også er lavet et andet Ph.D.-projekt om de specielt udviklede materialerne i Perlekædebroer. En række virksomheder har i det tre år lange projekt samarbejdet med teamet på DTU i et projektkonsortium: Abeo, Perstrup Betonindustri, Skandinavisk Spændbeton og Sweco.

I afhandlingen til dette Ph.D.-projekt præsenteres en metode til beregning af momentbæreevnen af Perlekædebroer, og metoden illustreres i et eksempel på en bue med 30 m spænd. Eksemplet viste, at normaltrykket i buen påvirkes af for- og efterspændingen, højden af fyldlaget, samt højde til spænd forholdet af buen, og at dette har en vigtig betydning for bæreevnen. Ved at ændre normalkraften er det således muligt at optimere Perlekædebuernes bæreevne til et givent projekt. Ved belastning udelukkende i den ene side af buen var den laveste kapacitet i samlingen mellem SL-Dæk i den belastede side, mens det var i selve SL-dækket i den ubelastede side. Buer får større positivt moment i den belastede side end negativt moment i den ubelastede side, og dette stemmer fint overens med kapaciteten af SL-Dækket, hvor den positive momentkapacitet oftest er noget større.

To typer betonhængsler blev designet og testet med henblik på brug i Perlekædebroer. Betonhængsler er langt fra "ideelle" og vil yde betydelig rotationsmodstand, hvilket vil påvirke det statiske system. De to hængsler blev undersøgt i fuldskalaforøg og sammenlignet med numeriske modeller. Det viste sig, at det Mesnagerinspirerede hængsel opførte sig som forudset i litteraturen på trods af en høj normalkraftpåvirkning i Perlekædebuer. Et specialudviklet saddelehængsel viste også elastisk-plastisk opførsel og viste sig mest praktisk anvendeligt i Perlekædebuer.

To Perlekædebuer på 13 m spænd blev testet for at undersøge den praktiske opførsel ved proceduren for samling og efterspænding af buerne, samt når de løftes på plads på et forberedt fundament. Testen var en succes, og buerne kunne således

efterfølgende anvendes til et belastningsforsøg med last i  $\frac{1}{4}$  punktet af spændet. Forsøget var inddelt i to faser: 1) En test til  $\frac{2}{3}$  af brudbæreevnen, hvor buernes opførsel undersøgtes. Resultatet viste bl.a. at laster deles imellem buerne via såkaldte Hammerhovedsamlinger. 2) En test til brud, hvor bæreevne og brudtype blev undersøgt. Buerne brød som følge af to plastiske hængsler, der opstod i  $\frac{3}{8}$  og  $\frac{5}{8}$  punktet. Inden det endelige kollaps sås der adskillige varsler, når belastningen nærmede sig brudniveau.

## ABBREVIATIONS AND SYMBOLS

$\alpha$  = Rotation in hinge  
 $\alpha_{Rd}$  = Maximum rotation in hinge  
 $\alpha_t$  = Thermal expansion coefficient  
 $\delta_{down}$  = Downwards deflection of arch at distance  $d_{hinge}$  from hinge in loaded side  
 $\delta_{up}$  = Upwards deflection of arch at distance  $d_{hinge}$  from hinge in non-loaded side  
 $\Delta\phi$  = Extra angular deformation in area of arch from plastic hinges  
 $\mu$  = Moment distribution in beam with same loading as arch  
 $\rho_{pc}$  = Density of pervious concrete  
 $\rho_c$  = Density of regular concrete

$A_1$  = Area of arch  
 $A_2$  = Area of tension tie  
 $b_1$  = Hinge throat height  
 $b_2$  = Hinge body height  
 $c$  = Empirical hinge confinement factor  
 $d$  = Hinge width  
 $d_{hinge}$  = Distance from hinge to point of measured deflection in arch  
 $E$  = Young's modulus  
 $e^+$  = Eccentricity of thrust line to arch in loaded side  
 $e^-$  = Eccentricity of thrust line to arch in non-loaded side  
 $E_{cf}$  = Young's modulus of concrete foundation  
 $E_{cm}$  = Mean Young's modulus of concrete  
 $E_m$  = Young's modulus of mortar  
 $EI$  = Flexural stiffness  
 $f_{ck}$  = 5<sup>th</sup> percentile value of compressive cylinder strength of concrete  
 $F_{h_{TS}}$  = Horizontal reaction force from TS  
 $F_{v_{TS\_loaded}}$  = Vertical reaction force in loaded side of arch from TS  
 $F_{v_{TS\_non\_loaded}}$  = Vertical reaction force in non-loaded side of arch from TS  
 $F_{h_{UDL}}$  = Horizontal reaction force from UDL  
 $F_{v_{UDL\_loaded}}$  = Vertical reaction force in loaded side of arch from UDL  
 $F_{v_{UDL\_non\_loaded}}$  = Vertical reaction force in non-loaded side of arch from UDL  
 $g$  = Gravity constant  
 $g_{uni}$  = Sum of uniformly distributed self-weights  
 $g_{uni.fill}$  = Uniformly distributed part of self-weight from filling  
 $g_{uni.SL}$  = Uniformly distributed load from SL-Decks  
 $g_{uni.top}$  = Uniformly distributed load from top-plate  
 $H$  = Horizontal reaction force from a load  
 $h_{fill}$  = height of filling above crown  
 $H_t$  = Horizontal reaction force from temperature changes  
 $I$  = Second moment of area of arch  
 $K$  = hinge parameter  
 $k_1$  = Constant for one-way hinges  
 $L$  = Arch span  
 $L_{el}$  = Length of SL-element

$M$  = Bending moment  
 $m$  = Dimensionless hinge parameter  
 $M_{dead}$  = Bending moment from self-weight alone  
 $M_{neg}$  = Sum of moment contributions giving largest negative moment in arch  
 $M_{pos}$  = Sum of moment contributions giving largest positive moment in arch  
 $M_{pretension}$  = Bending moment from eccentric position of pre-stressing strand  
 $M_{rd+}$  = Calculated positive moment capacity  
 $M_{rd-}$  = Calculated negative moment capacity  
 $m_{SL}$  = Mass of SL-Deck  
 $M_{TS,neg}$  = Negative moment in non-loaded side of span from TS at loaded side of span  
 $M_{TS,pos}$  = Positive moment in loaded side of span from TS at loaded side of span  
 $M_{UDL,neg}$  = Negative moment in non-loaded side of span from UDL in loaded side of span  
 $M_{UDL,pos}$  = Positive moment in loaded side of span from UDL in loaded side of span  
 $N$  = Normal force  
 $N_{CSR}$  = Value of normal force reduction from creep, shrinkage and relaxation  
 $N_{dead}$  = Normal force from self-weight  
 $N_{post}$  = Normal force contribution from post-tensioning  
 $N_{pretension}$  = Normal force contribution from pre-tensioning  
 $N_{total}$  = Sum of all normal force contributions  
 $P$  = Concentrated vertical load on arch  
 $P_{axel,TS}$  = Design axel load from TS  
 $P_{SV,axel\#}$  = Concentrated force from axel of service vehicle  
 $R$  = Rise of arch  
 $r$  = Radius of circle  
 $rot_{ideal}$  = Calculated rotation in hinge if ideal based on measured deflection in arch  
 $s$  = Arch length  
 $s_p$  = Distance via centerline from springing to point p  
 $T$  = Temperature change  
 $t_{asphalt}$  = Thickness of asphalt layer  
 $v$  = Half the central angle of circle sector  
 $V_{UDL,lane}$  = Design UDL in notional lane 1  
 $V_{UDL,remain}$  = Design UDL in remaining areas next to driving lanes  
 $V_{UDL,sum}$  = Sum of all UDL loads from entire bridge width  
 $W$  = Total width of current bridge  
 $y_p$  = Vertical distance from springing to point p  
 $\emptyset$  = The angle between horizontal and a tangent to the arch at a point

DIC = Digital Image Correlation  
LAC = Light Aggregate Concrete  
LVDT = Linear Variable Differential Transformers  
PC = Pearl-Chain  
SL = Super-Light  
SLS = Serviceability Limit State  
SV = Service vehicle  
TS = Tandem system (load)  
UDL = Uniformly Distributed Load  
ULS = Ultimate Limit State

# CONTENTS

---

<b>1</b>	<b>Introduction .....</b>	<b>1</b>
1.1	Background.....	1
1.2	Scope.....	14
1.3	Thesis guide.....	14
<b>2</b>	<b>The Pearl-Chain Technology.....</b>	<b>17</b>
2.1	Principle of Pearl-Chain reinforcement.....	17
2.2	SL-Deck geometry and materials.....	19
2.3	Stresses and details.....	21
2.4	Case study of 30 m span PC-Bridge.....	22
<b>3</b>	<b>Influence of Concrete Hinges .....</b>	<b>31</b>
3.1	Background.....	32
3.2	Materials and geometry of test-specimens.....	32
3.3	Testing of the hinges.....	34
3.4	Implementation of the hinge response into the Pearl-Chain Arches.....	46
<b>4</b>	<b>Erection Procedure and Details .....</b>	<b>49</b>
4.1	Developed practical details .....	49
4.2	Post-tensioning of single arches.....	52
4.3	Lifting of single arches.....	55
4.4	Positioning on prepared foundations .....	57
<b>5</b>	<b>Test of arch Theory .....</b>	<b>59</b>
5.1	Preparing the test .....	59
5.2	Test results.....	68
<b>6</b>	<b>Pearl-Chain Bridge Projects.....</b>	<b>81</b>
6.1	Vorgod Creek Road Bridge.....	81
6.2	Hillerød Highway Pedestrian Bridge.....	95
<b>7</b>	<b>Conclusion.....</b>	<b>103</b>
7.1	Future research.....	105

<b>References .....</b>	<b>107</b>
<b>Appended papers.....</b>	<b>111</b>
<b><i>A</i> Precast Pearl-Chain Concrete Arch Bridges .....</b>	<b>113</b>
<b><i>B</i> Concrete Hinges for Pearl-Chain Bridges.....</b>	<b>129</b>
<b><i>C</i> Concrete Hinges .....</b>	<b>155</b>
<b><i>D</i> Assembly and Lifting of Pearl-Chain Arches .....</b>	<b>163</b>
<b><i>E</i> Full-Scale Load Tests of Pearl-Chain Arches.....</b>	<b>175</b>

# APPENDED PAPERS

## Journal papers:

### **Paper #1:**

Precast Pearl-Chain Concrete Arch Bridges

#### **Writers:**

Philip S. Halding (DTU), Kristian D. Hertz (DTU), Jacob W Schmidt (DTU/COWI)

#### **Publication:**

Published in Engineering Structures, 103, 214–227, 2015.

#### **Outline:**

The paper introduces the concept of Pearl-Chain Bridges. A calculation method is presented, and the capabilities of such bridges are exemplified with different spans, thicknesses etc. Basically, the concept is to post-tension straight precast concrete Super-Light Deck elements together in an arch shape.

### **Paper #2:**

Concrete Hinges for Pearl-Chain Bridges

#### **Writers:**

Philip S. Halding (DTU), Kristian D. Hertz (DTU), Jacob W Schmidt (DTU/COWI)

#### **Publication:**

Submitted to Magazine of Concrete Research, 2016

#### **Outline:**

This paper deals with the design and full-scale testing of two types of concrete hinges for use in Pearl-Chain Bridges. Models are developed to compare with test results and hinge behaviour is implemented in a global model of a Pearl-Chain Bridge.

### **Paper #5:**

Full-Scale Load Tests of Pearl-Chain Arches

#### **Writers:**

Philip S. Halding (DTU), Kristian D. Hertz (DTU), Jacob W. Schmidt (DTU/COWI),  
Bryan J. Kennedy (UW)

#### **Publication:**

Under review at Engineering Structures, 2015-2016.

#### **Outline:**

Two full-scale tests of Pearl-Chain Arches, where the first test is to approximately 2/3 of fracture load to observe the behaviour of the arches under loading, and the second test is to fracture.

### **Conference papers:**

#### **Paper #3:**

Concrete Hinges

#### **Writers:**

Philip S. Halding (DTU), Kristian D. Hertz (DTU), Jacob W Schmidt (DTU/COWI)

#### **Publication:**

Published in IASS-SLTE symposium proceeding, 2014.

#### **Outline:**

The development of a method for testing Mesnager inspired concrete hinges is outlined as well as the direct results from tests of 18 specially designed hinges.

#### **Paper #4:**

Assembly and Lifting of Pearl-Chain Arches

#### **Writers:**

Philip S. Halding (DTU), Kristian D. Hertz (DTU), Nicky E. Viebæk (Abeo), Bryan J. Kennedy (UW)

#### **Publication:**

Published in FIB symposium proceedings, 2015.

#### **Outline:**

Description of the special process of assembling, lifting, and positioning of two full-scale Pearl-Chain Arches.

### **Conference papers (not appended):**

#### **Paper #6:**

Pearl-Chain Arch Vaults

#### **Writers:**

Kristian D. Hertz (DTU), Philip S. Halding (DTU).

#### **Publication:**

Published in IASS-SLTE symposium proceeding, 2014.

#### **Outline:**

The paper describes the Pearl-Chain Technology, the basic principles behind it, and the possible applications.

# 1 INTRODUCTION

## 1.1 Background

Globally, the CO<sub>2</sub>-emission from cement production alone represents almost 4 % of the total emission [1]. Nevertheless, when comparing to other traditional building materials concrete is less polluting. The emission of CO<sub>2</sub> from manufacturing of concrete is approximately 5 % of that of steel for the same mass. Another material, light aggregate concrete has a CO<sub>2</sub>-emission similar to normal concrete per mass, but the emission per volume is less than half [2].

In order to reduce the greenhouse gas discharges when constructing concrete structures it is often a (costly) option to optimize the shape and geometry to the load, and hereby require less material. An example of such optimization is to replace a uniformly loaded beam with an arch. In Denmark smaller span concrete arch bridges less than 50 m have not been economically competitive for more than half a century, because of the requirement of complicated formwork which is expensive and slow to build. Highway bridges are instead often made as concrete beam bridges or concrete frame bridges.

If the arch bridge could be reintroduced in an economically competitive version with state-of-the art concrete technologies we would save large amounts of CO<sub>2</sub> because of the reduced amount of concrete. This is the basic idea behind the development of Pearl-Chain Arch Bridges. To become competitive, the cost is reduced by using CO<sub>2</sub>-friendly mass-produced pre-fabricated elements, and furthermore by aiming to reduce the arch erection time to less than a day.

### 1.1.1 Closed-spandrel arch bridges

Traditional closed-spandrel arch bridges date all the way back to the Romans ([3], [4]). The erection method has since that time included scaffolding to support the unfinished arch of stone, or later of masonry or concrete. Concrete arches were always in-situ cast and formwork was needed on top of the scaffolding ([5], [6]). It was not until the 1960s when pre-fabricated concrete elements were introduced that the first developments in pre-cast arches took place. Different precast arch solutions have since been introduced for closed-spandrel arches of spans up to

approximately 30 m. Examples are: BEBO, NUCON, TechSpan, Matiere and Macrete FlexiArch, though other systems exist as well ([3], [7]–[14]). See *Figure 1* for a simplified system with the typical closed-spandrel precast arch bridge terminology.

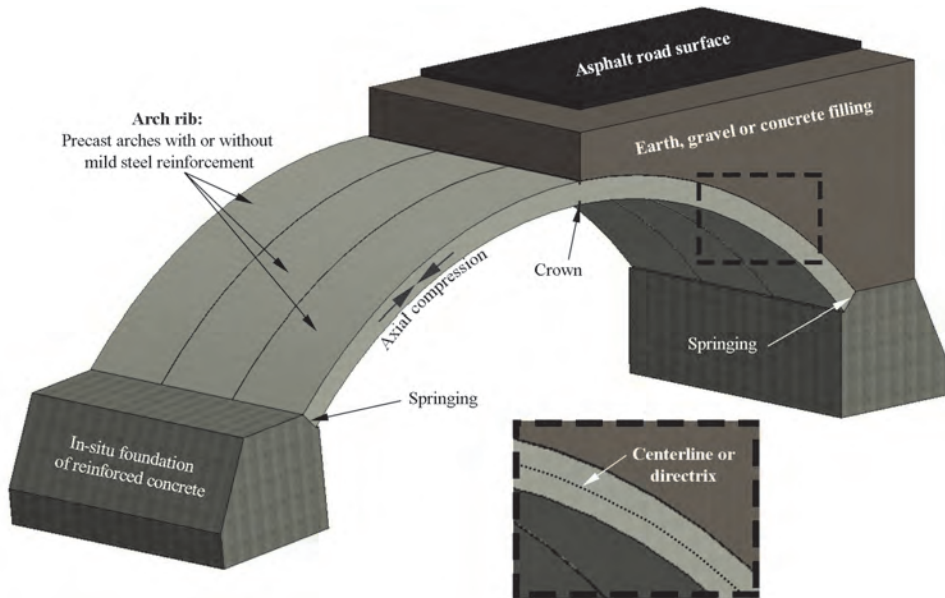


*Figure 1: Simplified assembly of a typical closed-spandrel precast arch bridge.*

NUCON and Macrete FlexiArch use smaller straight precast concrete elements put together in an arch shape, while BEBO, Matiere and TechSpan cast larger pieces so that one arch consists of one, two or three pieces. The benefit of smaller straight pieces is the possibility of stacking the elements during transportation, where larger curved precast segments need large trucks and take more space on the truck. On the other hand, larger curved precast arch parts have the benefit of fitting perfectly to the desired arch shape, where smaller straight segments will not follow the optimal continuous centre line [15]. The optimal line is here defined as a shape where the total dead load does not create significant bending moments in the arch. All the concepts offer quick assembly (without scaffolding), and lifting by either one or two cranes. Some arches require pouring of joints after positioning, some do not. Concepts that rely on soil-structure interac-

*Closed-spandrel arch bridges have a filling material at the spandrel (between the arch and the above road slab). Open-spandrel arches with the road above the arch usually have columns or walls to support the road.*

tion have strict guidelines for how to compact the filling. There may also be requirements to the level of filling above the crown, and with any increase in the filling height there will be an increase in the sizes of the bridge ramps to the above road. It is possible to reduce the ramps and the waste of space in the traffic clearance profile by changing the curvature of the arch, so that the arch is less curved above the traffic clearance profile.

Even though all the mentioned concepts exist they are not typically the first choice when building new highway bridges in Denmark because of the presented challenges.

None of the existing types of pre-fabricated closed-spandrel arch systems take advantage of pre-stressing in either the concrete elements or in the combined structure. Some consist of plain concrete but most have mild steel reinforcement. Many of the concepts include hinges, but none of them have defined the response of the arch when implementing concrete hinges, which are not behaving ideally. An overview of the concepts is given in Table 1.

### 1.1.2 Loads on closed-spandrel arch bridges

The critical loads on arch bridges are non-symmetrically positioned, e.g. caused by a heavy vehicle ([16]–[18]) in one side of the span. Uniformly distributed traffic load (UDL) over the entire span is not a worst-case-scenario in regard to bending moments because the arch-shape is designed to resist this type of loading producing axial forces in the arch rib, while the increase in bending moment is small. This depends on the chosen shape.

A UDL can actually help to stabilise the arch structure. If the UDL is applied as a permanent load from an increased height of the filling material above the crown, it will act as a pre-compression of the arch rib (cf. *Figure 1*). An increase in the compression in the arch can make it more resistant to bending moments from heavy concentrated loads. On the contrary, if the pre-compression is too large the arch cross-section will fail by exceeding the compressive strength of the concrete when subjected to a relatively small bending moment.

The optimal arch shape when subjected to a UDL is a parabola. In theory, this shape will resist the load and give rise only to an axial force in the arch rib, so no bending moments or shear will occur [19]. Dead load from the arch alone will, theoretically, not create any bending and shear in the arch rib when the catenary shape is used [8]. The circular shape deviates from the other shapes in case of a large rise to span ratio, but is similar to the catenary and parabola for small rise to span ratios. *Figure 2* shows two examples of arch shapes. The first example is a parabola, catenary, and

circle shape with a low rise to span ratio of 1/13, and the other is for a medium rise to span of 4/15.

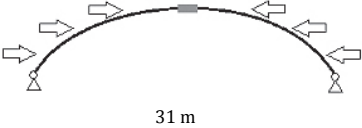
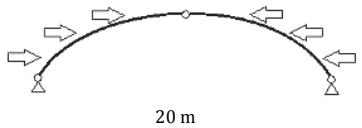
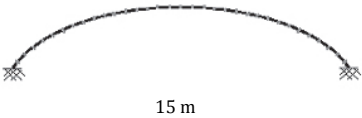
Concept	Advantages	Disadvantages	Schematic Figure and Largest Span
BEBO (1965)	Small footings, perfect fit to desired shape, pre-stressed via large amount of soil, can change curvature over the span.	Wasting space, difficult stacking of curved elements during transportation, needs two cranes, large ramps, in-situ casting of joint at crown, strict guidelines for filling, difficult production of curved elements.	 31 m
Matiere (1980s)	Good utilization of traffic clearance profile, only one crane for lifting, no in-situ casting after lifting.	Difficult stacking of curved elements during transportation, difficult production of elements.	 20 m
NUCON (1995)	No corrosion of reinforcement, lifting by one crane, automatic interlocking of concrete elements, easy stacking and transportation of small elements.	No reinforcement, risk of high stress concentrations in joints, temporary ties during lifting, complicated casting of the elements due to interlocking system	 20 m
Tech-Span (2004)	Small footings, perfect fit to desired shape, statically determined (in theory), can change curvature over the span	Wasting space, difficult stacking of curved elements during transportation, needs two cranes, large ramps, in-situ casting of joint at crown, strict guidelines for filling.	 20 m
Macrete Flexi-Arch (2008)	Only one crane for lifting, no in-situ casting after lifting, easy transportation, no corrosion of reinforcement, small ramps.	No reinforcement, risk of high stress-concentrations in joints, filling is pure concrete. Only small spans.	 15 m

Table 1: Comparison of the described pre-fabricated concrete arch systems.

Wilson [20] claims that a rise to span of 1/5 is typical, and that the final ratio depends on the site conditions. In general, there appears to be no consistency in the size of the rise to span ratios in the literature, but detailed shape optimization, as explained by Ruzicka [21], is not worth the effort for low rise to span ratios. This assertion is verified by the work of Findlay [17] and Han [19]. The results of Han's FE model shows insignificant difference in the distribution of axial force, bending moment and shear of different arch shapes having a rise to span of 1/10. Now it

seems that a flat arch is always preferable, since it can be used whatever the shape. However, bridges with low rise to span ratios are limited mainly by the soil stiffness at the abutments. If bridges are built on bed rock or if the horizontal forces can be resisted by a tension tie with high stiffness, arch bridges can have low rise to span ratios.

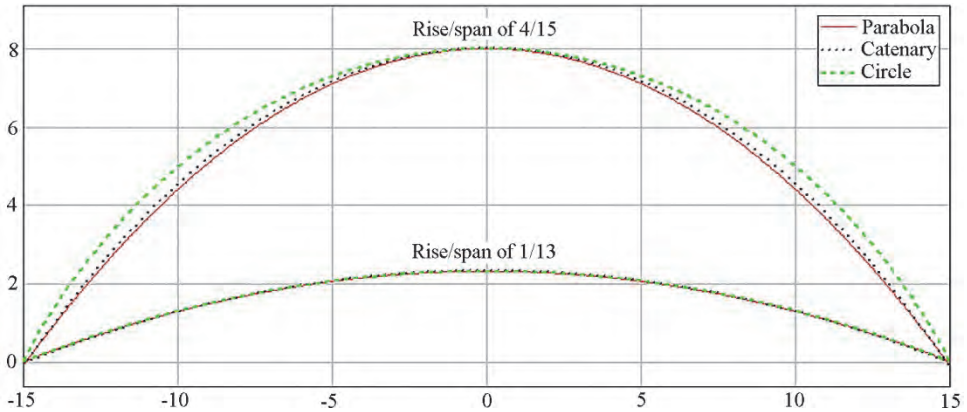


Figure 2: Arch shapes from parabola, catenary, and circle.

### 1.1.2.1 Temperature and time dependent deformations

For statically indeterminate arch systems (two-hinged or hinge-less arch), temperature changes and creep create additional stresses in the arch.

A temperature growth will increase the rise (if a constant span is assumed), and a negative bending moment develops in the arch rib. The opposite happens for a temperature decrease. Lai [22] explains how temperature changes should always be taken into consideration when designing concrete arch bridges. He gives a term, derived by use of Castigliano’s first theorem, for the increase in horizontal reaction force,  $H_t$ , in a two-hinged arch when a temperature change,  $T$ , occurs. A similar but reduced term is given by Finlay [17]:

$$H_t = \frac{\alpha_t \cdot T \cdot L}{\int_0^l y_p^2 \frac{ds_p}{EI}} \tag{1.1}$$

Where  $y_p$  is the vertical distance from the level of the springings to a point on the directrix in the arch rib,  $s_p$  is distance along the directrix from the left springing to that same point (see Figure 1), and  $\alpha$  is the thermal expansion coefficient of the mate-

rial.  $E$ ,  $I$ , and  $L$  are Young's modulus, the moment of inertia and the span of the arch, respectively. The expression in the numerator,  $\alpha \cdot T \cdot L$ , is the total horizontal displacement of the abutments due to temperature changes if the arch was free to move.

From the above equation bending moment and axial force distributions in the arch rib are found by:

$$M = H_t \cdot y \quad (1.2)$$

$$N = H_t \cdot \cos\emptyset \quad (1.3)$$

Where  $\emptyset$  is the angle between horizontal and a tangent to the arch at the point. The sizes of the contributions to  $M$  and  $N$  from temperature changes are often insignificantly small when compared to the critical live loads.

Other papers have discussed the issues of increased bending moments from temperature changes in arch bridges as well ([18], [23]), and Wilson [20] presented a range of tests showing the effects of temperature and creep. Steinberg [24] reported the use of flat jacks at the crown to jack up arches when they settle, to avoid problems with creep. The creep and shrinkage causes a reduction in the rise. By jacking up the arch directly after the positioning on the abutments the calculated level of reduction of the rise can be counteracted.

#### 1.1.2.2 *Dead Load*

The moment capacity depends on the normal force, and the normal force depends on live load, self-weight, and possible pre-stressing.

There is ambivalence when evaluating the effects of the self-weight in pre-fabricated arch bridges. Unlike straight beam bridges the self-weight contributes to the pre-compression of the arch which is often an advantage. But pre-fabricated arches are lifted in place by crane, and to lift further the self-weight of the arch alone has to be kept as low as possible. But it is not preferred to have a large amount of dense filling above the arch rib, since the ramps of the above road will become longer and more expensive when a thick layer of filling is applied. Also, an increase in the self-weight increases both the vertical and horizontal reaction force, which again leads to a requirement for larger footings.

#### 1.1.2.3 *Live Loads*

The biggest challenge for arches is concentrated loads on one half of the span only. Vertical forces acting close to the  $\frac{1}{4}$  point of the span of an arch causes a positive

bending moment in the arch rib below the force, but at the same time a negative bending moment in the opposite unloaded half. The pre-compression, due to the arch shape and self-weight, helps resisting these bending moments to a certain extent. This happens by withstanding tension in the arch rib as a reduction in the pre-compression. A large concentrated load around the arches  $\frac{1}{4}$  point is the worst case, but the back filling material in closed-spandrel arch bridges distributes a concentrated load from a wheel to a larger area on the surface of the arch. For shallow arches this relieving effect is not as beneficial as for high rise arches.

In reality the heaviest trucks and trains have many axels distributing the load over a large area on small span bridges. They may contribute with the greatest total weight, but not give rise to the biggest bending moments in small arch bridges. Other less heavy vehicles may be more critical in regard to bending moments because of a more concentrated weight distribution. For instance, a so called Tandem System has only 1.2 m between its two axels of each 300 kN [25], which can cause a too high loading level when positioned in proximity of the  $\frac{1}{4}$  point of the arch span.

### 1.1.3 Hinges in arch structures

Historically, concrete arch bridges have had between zero and three hinges. A one-hinged arch has a hinge at the crown (rarely seen), a two-hinged arch has one hinge at each springing (the connection between arch and abutment), and a three-hinged arch has hinges at all the three locations, see *Figure 3*.

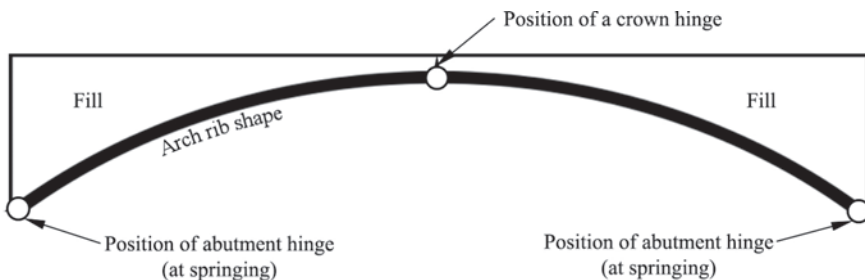


*Figure 3: Schematic figure of the positions of hinges in arch bridges.*

A three-hinged arch solution has both advantages and disadvantages. It is statically determinate and has the advantage of avoiding an increased bending moment from shrinkage and creep, temperature changes, and settlement of the foundations. On the other hand, such a system has no additional reserve strength when the abutments settle, the rise decreases, and the horizontal reaction force thereby increases.

In arches with a low rise to span ratio, even a small decrease in the rise generates a large increase in the horizontal reaction force at the abutment. Therefore, shallow arches are often designed with two or no hinges. This ensures that the arch resists the settlement by an increased bending moment. An arch without hinges is an option as well, but the two-hinged system solution allows some uneven vertical abutment settlements, which can create an undesirable stress level near the springings in the static system without hinges.

It is very difficult to apply ideal concrete hinges (with zero bending moment) in real arch structures, and complicated to investigate the actual response. The response of such hinges will be in between an ideal hinge, and a fixed joint. Consequently, the structure is often constructed based on an idealized or simplified static system which is applied with the assumption of zero bending moments in the hinges.

### 1.1.3.1 *The concrete hinge*

The first type of concrete hinge was a so called saddle bearing (originally developed by German Claus Köpcke in 1880) where basically two concrete surfaces with similar radii were connected in compression – one with concave and one with convex shape [26]. The rotation would then happen with a resistance from the friction between the surfaces. Sometimes a thin sheet of lead was put in between the concrete surfaces to reduce friction.

The saddle bearing evolved into two surfaces with different radii, which means that the rotation in the hinge had more of a rolling character compared to the sliding in the first saddle bearing type ([27], [28]).

In the start of the 20<sup>th</sup> century Mesnager and Freyssinet each developed a new type of concrete hinge by reducing the cross section height,  $b_2$ , of the concrete at the hinge position to  $b_1$ , see *Figure 4*. The reduced cross section is called the hinge throat. In the figure is shown a longitudinal section cut in a crown hinge.

First, Augustin Mesnager created such hinge with crossing reinforcement through the hinge throat. His design was focused on the mild steel reinforcement and disregarded the concrete in the throat area. The steel bars were designed to transfer both shear and normal forces and the job of the concrete was to protect against corrosion.

Freyssinet had a similar design but without the crossing mild steel bars in the throat so that section forces had to entirely be transferred through the concrete. In the throat the concrete is subjected to multi-axial stress as described by Base [28]. The normal stress from the arch structure changes direction in a bottleneck shape near the throat and creates a lateral confinement of the concrete in the throat. The confined concrete has a capacity up to several times higher than the unconfined cylinder strength. For “one-way hinges” Griezic et al. [29] introduced an empirical con-

finement factor based on test results. The factor is limited to the value 1.7 regardless of the  $b_1$  to  $b_2$  ratio:

$$c = \frac{1}{1 - 0.5k_1 \left[ 1 - \frac{b_1}{b_2} \right]} \quad (1.4.)$$

The parameter  $k_1$  is 1.1 for “one-way hinges”. Moreell [30] describes how Mesnager tested full-scale hinges and found that the concrete in the hinge throat, that he would ignore in regard to load carrying capacity, would actually increase the fracture load in the order of 33 % compared to a throat with exposed mild steel bars only.

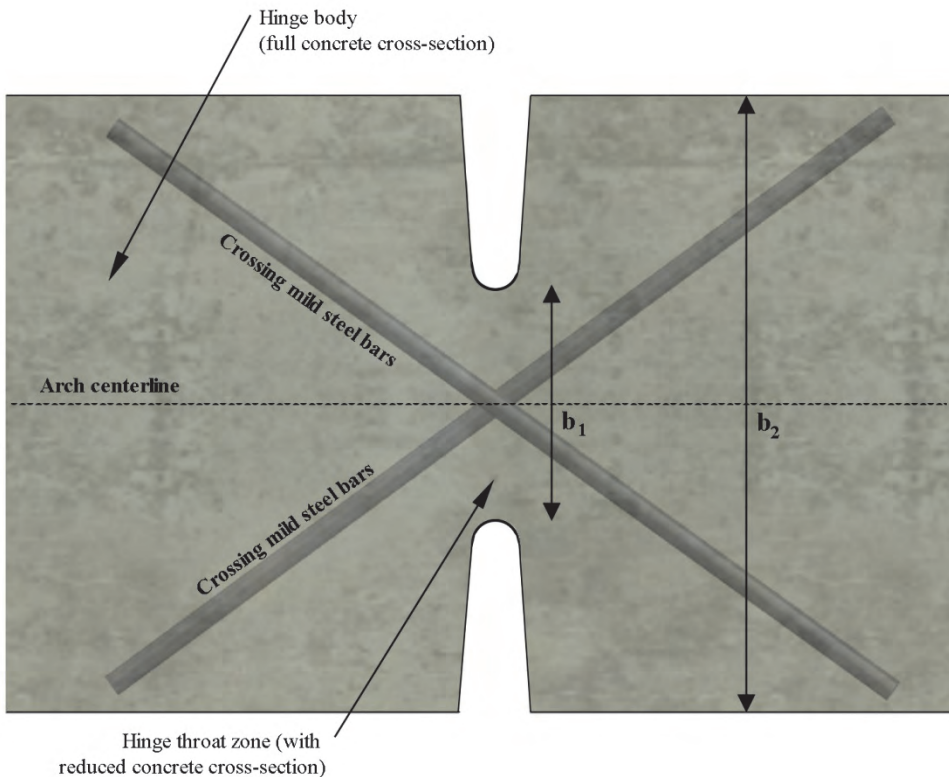


Figure 4: Mesnager and Freyssinet type concrete crown hinge with reduced height at the hinge throat. Can be positioned at crown or springings, cf. Figure 3.

For use of the Mesnager type of concrete hinges in constructions the rotation limits are important and were investigated several times ([27], [28], [30]–[34]). The limits vary in the literature and there seem to be no consensus in the definition of the lim-

its for use in SLS state. Values between 0.004 rad and 0.01 rad were proposed based on hinge testing for different geometries and normal forces. Leonhardt ([34], [32]) developed design guidelines including a suggested size of the maximum rotation,  $\alpha_{Rd}$ , in ‰:

$$\alpha_{Rd} = \frac{12800N_d}{b_1 \cdot d \cdot E_{com}} \quad (1.5.)$$

The area of the hinge throat in m<sup>2</sup> is  $b_1 \cdot d$ , and  $N_d$  and  $E_{com}$  are the normal force in MN, and the Young's modulus in MN/m<sup>2</sup>, respectively.

Leonhardt's guidelines included also suggested sizes of the hinge throat, the geometry of the recesses at the throat, transverse tensile forces in the hinge body, and rotation-moment characteristics. In the literature tested hinge characteristics are most often presented as rotation-moment plots. Leonhardt though proposed a universal rotation-moment relationship applicable for different geometries, normal forces, and concrete stiffness:

$$m = \frac{M}{N \cdot b_1} \quad (1.6.)$$

$$K = \frac{8N}{9 \cdot b_1 \cdot d \cdot E} \quad (1.7.)$$

$$\frac{\alpha}{K} = \frac{1}{(1 - 2m)^2} \quad (1.8.)$$

$m$  is a dimensionless parameter taking into account the normal force,  $N$ , and is the ordinate of the universal hinge response curve. It is valid for  $m > 1/6$ . In the interval of  $0 < m < 1/6$  the hinge response is assumed linear with a straight line from origo to the response curve. The angle of rotation in the hinge,  $\alpha$ , is divided by a constant,  $K$ . This ensures that the calculated abscissa take into account the concrete stiffness,  $E$ , the geometry of the hinge, and the normal force. The universal hinge response curve is verified by several tests with different sizes of normal force. The curve is seen in *Figure 5*. The hinge rotation limit in Eq. 1.5. is based on the point in the figure, where the crack reaches the middle of the throat ( $m = 1/3$ ).

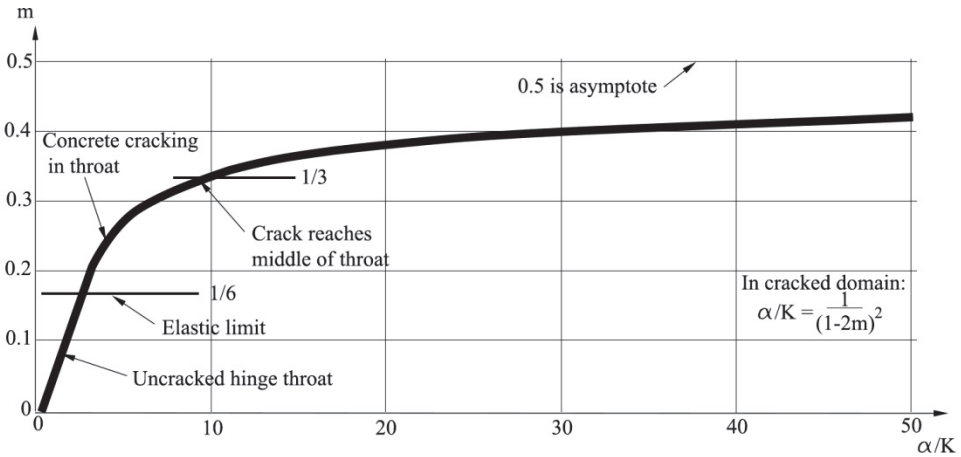


Figure 5: Universal hinge response proposed by Leonhardt and Reimann [32].

### 1.1.4 Load-testing of full-scale arches

Concrete arches can be load-tested and evaluated in a number of ways depending on the objective of the test. In the following is presented some of the methods used previously.

The difference between elastic and plastic ultimate strength calculations for statically indeterminate, concrete arches was addressed by Jain [35]. He studied circular, two-hinged arches subjected to a concentrated load at the  $\frac{1}{4}$  point of the span. Beyond the elastic limit, when the concrete starts cracking, and the moment of inertia and material stiffness decrease, his proposed plastic calculation method gave a load carrying capacity 50% to 100% higher than obtained elastically. The plastic response of a two-hinged arch begins when approaching the ultimate load. First, a plastic hinge forms below the loading point due to the maximum, positive bending moment. After further loading, another plastic hinge forms on the non-loaded side at the location of the largest negative bending moment. The second plastic hinge leads to collapse of the structure.

Jain dealt with a static system with a steel tension tie of a given stiffness,  $E_s$ , and area,  $A_2$ , to resist the horizontal force from the concrete arch of span,  $L$ . The arch had stiffness,  $E_c$ , cross sectional area,  $A_1$ , and moment of inertia,  $I$ . Without taking areas of plastic deformations into account, the horizontal reaction force,  $H$ , was:

$$H_{elastic} = \frac{\int \mu \cdot y \cdot ds}{\int y^2 ds + L \left( \frac{I}{A_1} + \frac{E_c}{E_s} \cdot \frac{I}{A_2} \right)} \quad (1.9)$$

The parameter,  $y$ , is the equation of the arch shape, and  $\mu$  is the bending moment distribution of a similar beam (with no horizontal force). The small length,  $ds$ , is along the arch centerline axis. From having the arch reactions he calculated the thrust line, and found the normal force in the arch at any point on the span. The positive bending moment was much larger below the load compared to the negative moment in the non-loaded  $\frac{1}{4}$  point. To achieve the optimal load carrying capacity, moment redistribution had to occur. That happened when the first plastic hinge was formed below the load where the moment was largest. At a certain length of the span below the point load, the concrete was in the plastic domain of the working curve. This additional angular deformation generated an increase in the horizontal reaction force and the line of thrust therefore became less inclined, compared to the purely elastic case. This change is illustrated in *Figure 6*.

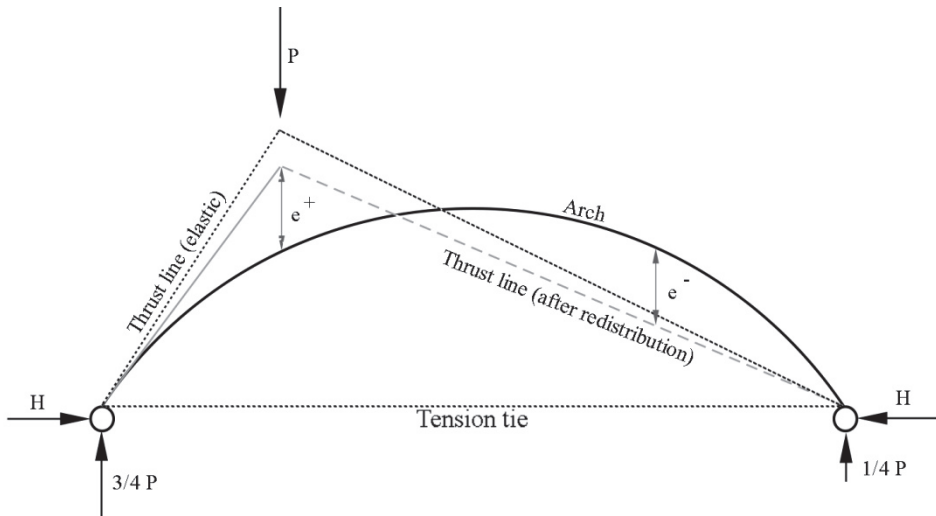


*Figure 6: Thrust lines of arch loaded in  $\frac{1}{4}$  point of span.*

In the figure the thrust line is shown for the elastic case and for the case with moment redistribution from plastic hinges. The optimal condition was a situation where the concrete could undergo enough angular deformation in the plastic hinge for the bending moment to reach the same level in the non-loaded  $\frac{1}{4}$  point of the span as in the loaded  $\frac{1}{4}$  point of the span. The eccentricity of the thrust line to the arch shape is shown in *Figure 6* in the loaded-,  $e^+$ , and the non-loaded side,  $e^-$ . The horizontal reaction including plastic hinges was:

$$H_{pl\_hinge} = \frac{\int \mu \cdot y \cdot ds + E_c I \sum \Delta \phi \cdot y \cdot ds}{\int y^2 ds + L \left( \frac{I}{A_1} + \frac{E_c}{E_s} \cdot \frac{I}{A_2} \right)} \quad (1.10.)$$

$E_c I \sum \Delta\phi \cdot y \cdot ds$  is the extra outward movement of the arch ends due to the part of the arch span that had developed plastic strains. The potential extra outward movement was withstood as an increased  $H$ .  $\Delta\phi$ , is the extra angular deformation compared to the elastic case.

Jains proposed theory only included arches with the same cross section properties along the span. With that limitation the method was verified after several tests.

Marshall et al. [36] provided practical engineering guidelines based on experimental tests of three closed-spandrel, reinforced concrete arches. Those arches had span lengths 12.8 m, 6.1 m, and 11 m. Their arches were cast into abutment walls, and soil-structure interaction was considered. Their 12.8 m span arch was tested during erection, during the compaction of the filling material, and later for a live load of 253 kN. The 6.1 m and the 11 m span arches were tested in a lab to fracture with symmetric point loads at the crown and close to the crown. Strain gauges were implemented in both tests, and were applied on the top and bottom of the arches at various positions along their spans. With this instrumentation, bending curvature (and therefore moment) could be calculated and correlated to the applied load for various points in the span. The 6.1 m span arch failed in shear close to the fixed connection at the abutment support. Oppositely, the tested 11 m span arch displayed a more ductile failure, with larger bending deformations before the ultimate load was applied.

Zhang et al. [37] used a similar method to determine the ultimate capacity of two existing, 20 m long, arch ribs. They measured strains at different span locations by instrumenting the top, bottom, and ribs of the arches. The vertical displacements were monitored at several span locations, and the abutments' horizontal settlement was also measured. The arches were loaded with point loads of the same magnitude in both  $\frac{1}{4}$  points and at the crown. A plastic hinge was observed in the  $\frac{1}{8}$  point of the span as the load increased and large cracks became visible before the ultimate load was applied. Their tested arches failed with a sudden shear fracture at the springings.

Another full-scale test was described by McGrath and Mastroianni [38]. An 8.5 m long, closed-spandrel arch bridge was loaded with a real, tandem-load truck. The bridge was further tested with a loading beam. That beam was connected to adjacent ground anchors, which were used to pull the beam downward onto the bridge. This loading simulated one axle of a heavy vehicle. Cracking was observed, but the bridge was not loaded to fracture.

## **1.2 Scope**

Before the beginning of the Ph.D.-project the theoretical idea of Super-Light Decks, and Pearl-Chain reinforcement had never in practice been combined into a Pearl-Chain Bridge structure. Therefore, the main success criterion of the work in the Ph.D. was to develop these technologies from concepts to buildable arch structures.

### **1.2.1 Research hypothesis and related objectives**

The hypotheses of the overall project related to the present Ph.D.-studies were:

- 1) It is possible to build a bridge using a number of centrally post-tensioned Pearl-Chain Arches made from Super-Light composite SL-Deck elements provided with lateral connections between the arches, and hinges at the supports?
- 2) Can construction and mounting time for a bridge be significantly reduced by developing a post-tensioning assembly technique, where Pearl-Chain Arches are post-tensioned together and lifted to their final location?

Based on the hypotheses, the following objectives were identified. It is the objective to:

- Determine a method for calculation of the load bearing capacity of the bridge from Pearl-Chain Arches.
- Design and test (in full-scale) hinges for use in Pearl-Chain structures, and investigate the behavior of the hinges, and the effect of the subcomponent to the response of the global static arch system.
- Design practical details for Pearl-Chain Bridges: Transverse connections, connections to foundations, and altered Super-Light Deck geometry for use in Bridges.
- Develop and test (in full-scale) an assembly and lifting method for Pearl-Chain Arches.
- Verify the functionality of Pearl-Chain Arches and the developed details by monitoring a full-scale test bridge during loading.
- Investigate the load carrying capacity and fracture type of a Pearl-Chain Bridge loaded to collapse.
- Build a full-scale functional Pearl-Chain Bridge in Denmark.

## **1.3 Thesis guide**

The thesis deals with a range of subjects within the Pearl-Chain Bridge technology. The first chapters focus on the Pearl-Chain concept and hinges. Then, the challenges

and solutions when erecting Pearl-Chain Arches is described via an assembly and lifting test of two full-scale 13 m span arches. After the erection-test the same two arches are load-tested to investigate the behavior of the individual elements and the global structure when loaded stepwise to the point of fracture. Finally, two applied Pearl-Chain Bridge projects cases are presented, where one was built in Denmark in 2015.

- Chapter 2 presents the technology: Pre-tensioning of individual Super-Light Decks, Post-tensioning of arches and so on. A method for analytic calculation of the capacity of Pearl-Chain Bridges is proposed and demonstrated as well.
- Chapter 3 is about concrete hinges and the development of concrete hinges for use in Pearl-Chain Bridges. It includes data from full-scale tests of two hinge types, and numerical models for comparison.
- Chapter 4 describes the erection procedure from individual Super-Light Decks to a finished arch. The erection procedure was tested with two 13 m span arches.
- Chapter 5 is regarding two subsequent tests of the erected arches from chapter 4. The arches were tested in the  $\frac{1}{4}$  point of the span in two tempi: i) to  $\frac{2}{3}$  of fracture load to monitor the arch behavior, and ii) to fracture.
- Chapter 6 presents two Pearl-Chain Bridge cases: Vorgod Creek Road Bridge, and Hillerød Highway Pedestrian Bridge, where the first one was designed and built during the Ph.D.-period.

The red thread and progress of the thesis is illustrated in *Figure 7* together with the primary connections between the different chapters and the appended papers.

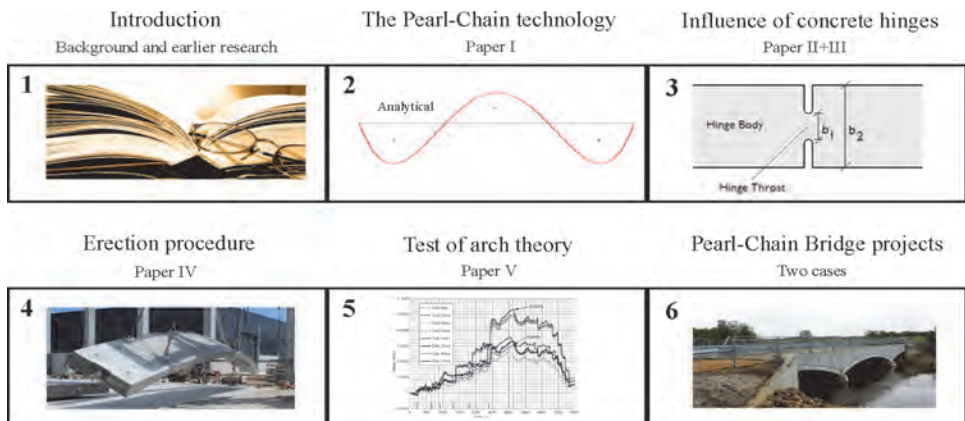


*Figure 7: Connection between chapters in thesis and appended papers.*



## 2 THE PEARL-CHAIN TECHNOLOGY

Chapter 2 is an introduction to the Super-Light Deck elements, and Pearl-Chain Arches. The technologies are elaborated, and in a theoretical design case of a 30 m span bridge, the Pearl-Chain Bridge load bearing calculation method is illustrated. The chapter is based on the journal paper #1: “Precast Pearl-Chain concrete arch bridges”.

The aim of the studies in the chapter is to find a method for how to calculate the capacity of Pearl-Chain Bridges, and to explore the design limits of Pearl-Chain Arches (in a case) limited to calculations of single arches in a Pearl-Chain Bridge.

### ***2.1 Principle of Pearl-Chain reinforcement***

The Pearl-Chain (PC) reinforcement technology is basically to tension elements together in a given shape. Each segment consists of pre-fabricated concrete with a cast-in curved duct. Post-tensioning cables are lead through the ducts in all segments, and the cables are then tensioned so that the segments stand in compression, and become one large curved structure. The technology is patented [39]. *Figure 8* shows an example of the PC principle with a circular arch consisting of eight pre-cast elements held together by post-tensioning cables through the ducts. The ducts are curved in a circular arch shape with a radius corresponding to the desired circle shape. The parameter,  $\alpha$ , is the angle between two elements.

#### **2.1.1 Pre-tensioning and post-tensioning concept**

The post-tensioning cables follow the shape of the arch, while the visible appearance shows the non-continuous shape of the joined concrete segments (SL-Decks). When the post-tensioning cables follow the desired arch shape when suited inside the curved ducts, the force from post-tensioning only introduces normal stresses in the arch and no bending moments.

The SL-Deck consists of a combination of light aggregate concrete (LAC) blocks (3MPa characteristic cylinder compressive strength) below and regular concrete

(55MPa characteristic cylinder compressive strength) above. The end surfaces of each SL-Deck are given a slight inclination enabling several elements to be joined together in an arch shape. In the joints the direction of the post-tensioning cables is perpendicular to the end surface. The SL-Deck is a composite of light- and normal concrete, but closest to the joint to the next SL-Deck it consists of at least 200 mm massive regular concrete. This insures an even transfer of forces between the elements, and a neutral axis in the middle of the cross-section, at the level of the cables. When the corrugated cable ducts form a 90 degree angle with the end surfaces of the SL-Deck elements, the cables go from one SL-Deck to the next without sudden bending.

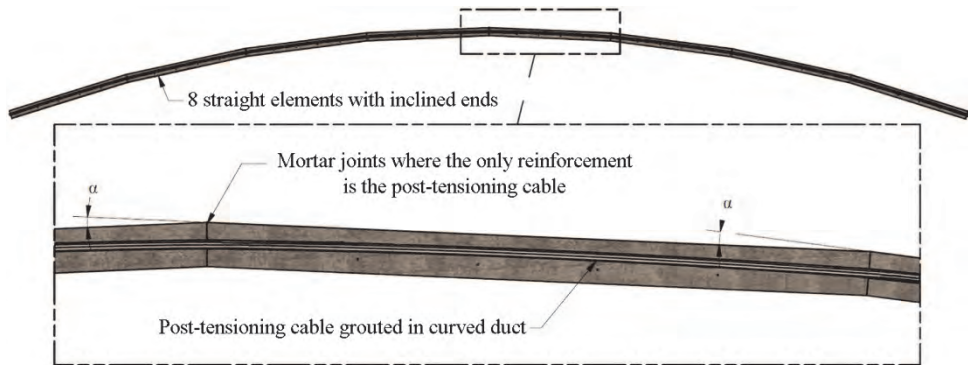


Figure 8: Side elevation of a PC-Arch consisting of eight elements, and close-up of cut where the post-tensioning cable ducts are visible.

In Figure 9 some of the regular concrete in an SL-Deck is cleared away in order to obtain a view of the geometry of the LAC blocks and reinforcement solution. In this case the PC-Arch has four LAC blocks across with a width of 1.65 m. Pre-tensioning strands are positioned as shown in the figure, and the duct with the post-tensioning cables is placed in the middle of the deck at a height that ensures that it will not create a bending moment in the arch bridge – only an axial thrust. This is possible since the neutral axis changes depending on the cross-section in the element: At the massive concrete (at each end) the neutral axis is in the middle, and in other cross-sections the neutral axis is above the middle because of the LAC blocks having a low stiffness.

Reinforcement bars are positioned between the blocks in the transverse direction. The transverse reinforcement is applied to distribute the load on the deck to the longitudinal ribs between the blocks, and because of the handling of each element during SL-Deck production and bridge erection, see Chapter 4. Furthermore, it resists downward forces coming from the tightened post-tensioning cable, and helps to transfer forces transversely from one arch to another.

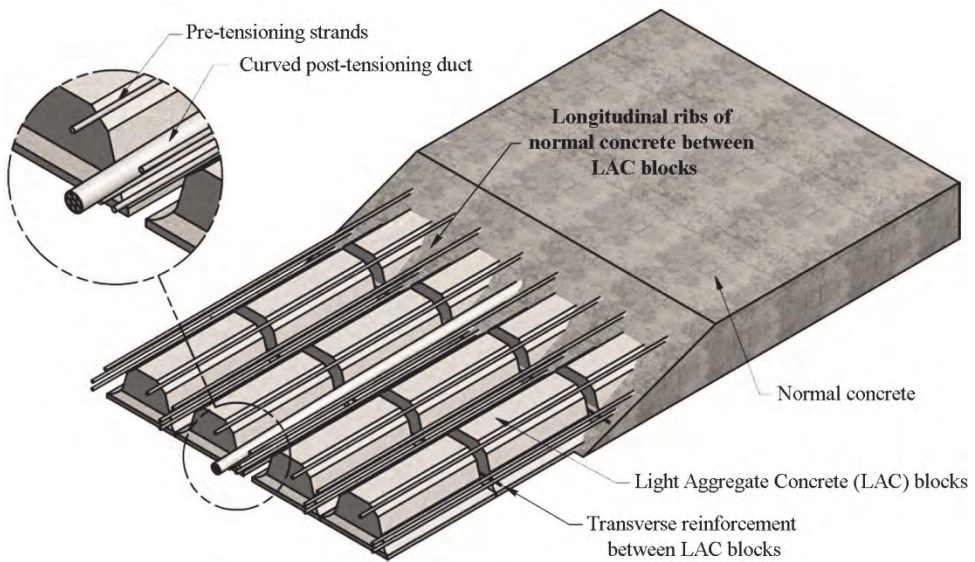


Figure 9: View of the interior of an SL-Deck element for PC-Bridges.

This example of an SL-Deck and a PC-Bridge can be combined in many ways. The configuration of pre-stressing strands can be altered, the height and number of the LAC blocks can be adjusted, the total deck height and width can be altered, and more post-tensioning cables can be added. The flexibility of the design enables civil engineers to use the technology in almost any arch shape. Elements of equal length create a circular shape, and different length elements can form a shape with a curvature changing over the span. Also, the PC concept can be used as vaults in buildings, and other structures [40].

## 2.2 SL-Deck geometry and materials

SL is an abbreviation for Super-Light, and the brand name is due to the low self-weight of the SL-Decks compared to decks with plain concrete.

A PC-Bridge has the lowest bending moment capacity either in the SL-Decks or in the joints between the SL-Deck elements. The joints consist of a special mortar having characteristic compressive strength of at least 80 MPa [41], which is higher than that of the regular concrete in the SL-Deck elements (55 MPa). The post-tensioning cables are the only reinforcement in the cross section in the joints.

The 55 MPa regular concrete has a density of 2300 kg/m<sup>3</sup>, while the 3 MPa LAC blocks are approximately 800 kg/m<sup>3</sup>.

In the SL-Deck cross section a number of pre-tensioning strands are chosen. In the below example, see *Figure 10*, each element of 1.65 m width has 8 pre-tensioning strands in the top of the cross section with 50 mm concrete cover to the top surface. In the bottom of the cross-section between LAC blocks are 4 strands with 75 mm concrete cover to the bottom, and 2 strands with a 112.5 mm concrete cover to the bottom. All strands have at least a space of 25 mm, and 50 mm concrete cover to the LAC blocks. Additionally, there are two strands at each side with 50 mm concrete cover to the sides. All strands have a cross-sectional area of 93 mm<sup>2</sup> and a characteristic ultimate strength of 1860 MPa. Both top and bottom strands are pre-stressed to e.g. 50% of the 0.1% proof stress of the steel. The density of all steel is 7850 kg/m<sup>3</sup>.

The LAC blocks are the same as those used in 220 mm SL-Decks for buildings, but a 270 mm deck height is required for use in bridges due to increased concrete covers. This means that 50 mm additional regular (55 MPa) concrete is applied in the top of the cross section compared to the 220 mm SL-Deck for buildings. When increasing the height of the cross-section even further, more regular concrete can be added in the top of the cross section depending on the desired cross-section height.

Instead of the 2.4 m SL-Deck width that is normally used in buildings, 1.65 m SL-Decks can be used in Pearl-Chain Bridges to reduce the mass of each arch. Reducing the mass is beneficial for larger arch spans, since the PC-Arches are lifted into place by a crane. The minimum required width is 1.65 m when having four LAC blocks across. 50 mm of normal concrete is required as a minimum on both sides of the SL-Deck and between the two middle blocks regardless of the total deck width. When transverse shear connections are used between adjacent PC-Arches, the required width of each arch is increased. In the example of a four LAC block SL-Deck, the minimum width is then 1.75 m.

The LAC blocks consist of the 3 MPa concrete, and between the blocks in the longitudinal direction is placed transverse stainless steel reinforcing bars of at least Y6 with strength of 550 MPa. Stainless steel is required since the concrete cover is smaller than required for the transverse bars.

The post-tensioning duct is centrally positioned in the middle between LAC blocks, and can contain a number of cables each with a cross-sectional area of 150 mm<sup>2</sup>. The strength of the wires is equal to the pre-tensioning strands, and post-tensioning is performed to typically 90% of the 0.1% proof stress of the steel.

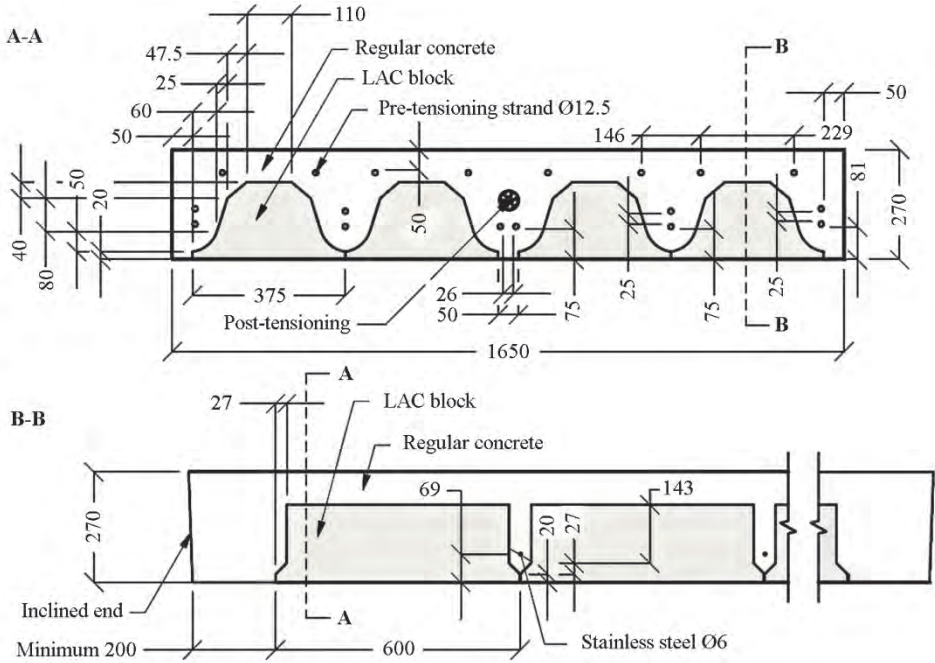


Figure 10: Cross-section (A-A) and longitudinal section (B-B) of a SL-Deck. Unit is mm.

### 2.3 Stresses and details

The regular concrete in the SL-Decks forms ribs stabilized by the LAC blocks. In a cross section having the ribbed profile axial stresses will be more concentrated. When going from a ribbed cross section to the massive concrete cross sections at the ends, the concentrated stresses will distribute into the rectangular shape.

When pre-tensioning the SL-Decks the interaction between concrete and strands take place evenly along the strands. After release from the pre-tensioning bed the strands shorten and compress the concrete. Subsequently, the SL-Decks are post-tensioned together. The post-tensioning is placed in a way which applies an evenly distributed normal stress at the ends of each SL-Deck. The post-tensioning will further compress the concrete, and at the same time reduce the tension in the strands. It is expected that the concrete will be additionally compressed in the ribs as explained above. See Figure 11.

The ribs are designed for resisting positive bending moments, and the expectation is that the negative bending moment capacity is lower than the positive. For use in arch bridges this is not a problem, since the load often causes a large positive bending moment and a smaller negative bending moment.

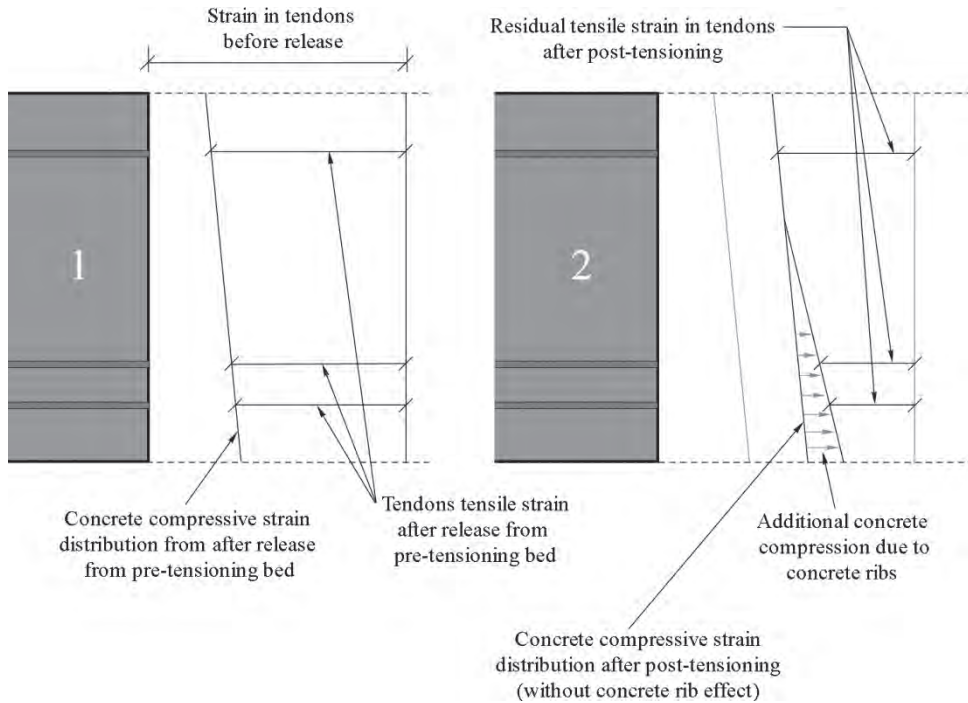


Figure 11: 1) Strain after release strands from pre-tensioning bed. 2) Strain after post-tensioning.

## 2.4 Case study of 30 m span PC-Bridge

To exemplify the PC-concept a case study of a PC-Bridge is evaluated based on a specified calculation method. Some input parameters in the calculation are varied to illustrate the structural behavior. Furthermore, calculated bending moments, axial thrusts, etc. are compared with results from an FE-model in Robot Structural Analysis.

### 2.4.1 Calculation method

Finding the theoretical moment capacity is at this point done assuming ideal hinges. The general input parameters required for such calculation are:

- Number of hinges and choice of arch shape.
- Number of SL-Decks in one arch.
- Rise and span.
- Level of interaction with adjacent arches.

- SL-Deck thicknesses and widths.
- Stress level and number of pre-tensioning strands and post-tensioning wires.
- Position of pre-tensioning strands.
- Height of filling material.
- The material properties.

In order to investigate the capacity and to draw influence lines for the bending moment, reactions, and axial force of a point load moving across the bridge, analytical calculations are performed.

Superposition is then used when adding influence lines for the loads corresponding to each axle of a chosen type of vehicle.

Initially the number of hinges, the arch shape, the level of interaction with adjacent arches, and the rise to span ratio are selected. The number of SL-Decks is chosen, and the length of each element is calculated. The amount of post-tensioning is picked, and the overall weight is calculated based on the geometry and material data. Temperature loads are found as well.

Having calculated the axial stiffness, the static stiffness, and the flexural stiffness of the SL-Decks, the bending moment capacities are found for different normal forces. The normal force changes depending on the position of the live load on the arch. For shallow arches the distribution of force from the live load is conservatively assumed to act on the arch rib exactly below the point where the concentrated load is positioned on the road surface. For every position of a vehicle the axial force and load carrying capacity must be calculated. The capacity is then compared to the bending moment from the load of the vehicle. Calculations are performed in steps of 0.3 m for the position of the vehicles, and also in steps of 0.3 m around the  $\frac{1}{4}$  points of the span of the arch.

A chart of the calculation process is shown in *Figure 12*. “Checked by FEM” means that calculations at this step are to be verified by a numerical model.

Stability issues are not investigated in this study, since the filling material and adjacent arches have a stabilizing effect. Also, the approach does not take phenomena such as possible plastic hinges into account.

#### 2.4.1.1 FE-Model

FE calculations performed in Robot Structural Analysis [42] are based on massive concrete sections. Using the found stiffness of the chosen SL-Deck a solid concrete deck element with similar stiffness is modelled instead. In the analytical approach it is assumed that the arch shape is similar to the circular post-tensioning cables, but

in the FE-model we calculate the elements always having the neutral axis in the middle of the cross section. This difference in approach results in an insignificant error. An example of the difference between numerical and analytical calculation can be seen in *Figure 13*. It shows the moment distribution of a 30 m span circular arch of width 1.65 m subjected to dead load including self-weight from the arch, filling to the top point of the arch, and a road slab.

Similarly, normal forces can be found, and combinations of moment and normal force can be determined for different positions of an applied load.

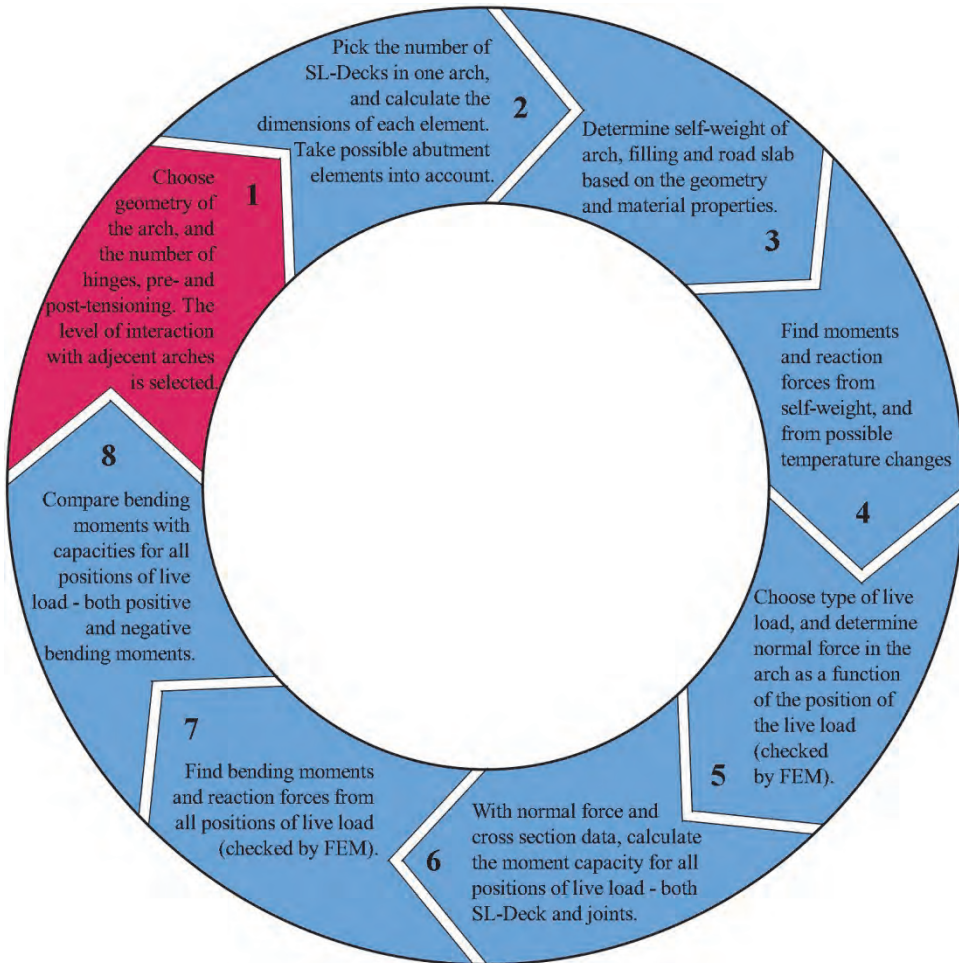


*Figure 12: 8 step flow chart of the iterative load-bearing calculation method for PC-Bridges.*

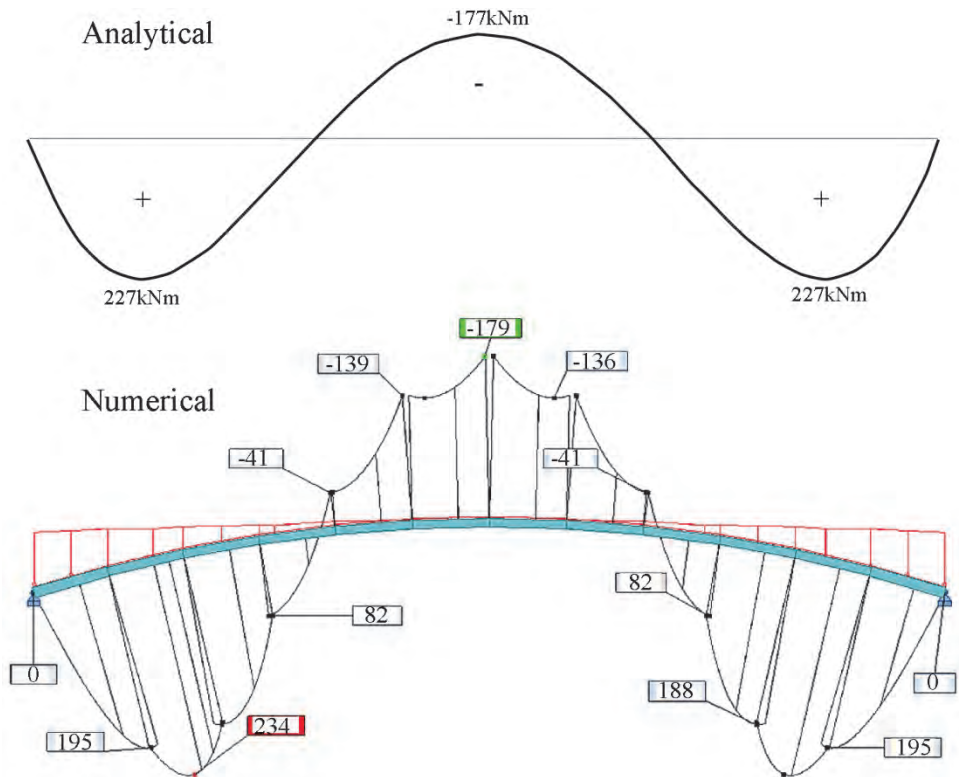


Figure 13: Analytical and numerical bending moment distribution. Unit is kNm.

## 2.4.2 Essential information

Information required when performing the load carrying calculation:

- The arches in PC-Bridges are not vulnerable to shrinkage and creep due to pre-tensioning of the individual pre-fabricated SL-Deck elements, and the post-tensioning before erection. Simply, the initial time-dependent deformations have already occurred before the arches are positioned.
- Relaxation in the strands and cables will still fully occur.
- The developed backfilling material for PC-Bridges consists of a granular material called pervious concrete with a density,  $\rho_{pc}$ , of about 1800 kg/m<sup>3</sup>. It is perfectly drained so that no pore water is present. Should any rain perforce the road slab and drain through the pervious concrete, holes at the

lowest elements will lead the water away from the spandrel area. Therefore, the drained density of the filling is used in the calculation.

- The filling is often spread out on the arch and levelled to the height of the crown (for small ramps), but depending on the bridge geometry, the height of the filling can be increased to any level above the crown (for larger pre-compression of the arch).
- On top of the pervious concrete is a road slab of  $4 \text{ kN/m}^2$  which corresponds to the build-up of a regular paved road.
- It is assumed that the change in temperature is uniform in the arch rib. The thermal expansion coefficient,  $\alpha$ , of the regular concrete is  $5 \cdot 10^{-5} \frac{\text{m}}{\text{mK}}$ .

### 2.4.3 Design Examples

Examples of design of a 30 m span Pearl-Chain Bridge are now presented. The objective is to investigate the effects on the bending moment capacities when altering the following design parameters:

- The thickness of the SL-Decks (270 mm, 320 mm, 370 mm, and 420 mm) with a fixed size of the LAC blocks similar to the example in *Figure 10*.
- The rise to span ratio (1/13, 1/10, and 1/7.5) with the supports being infinitely stiff.
- The number of post-tensioning cables (7, 9, and 13).
- The level of filling above the crown (0m, 1m, and 2m) with a road slab above the filling. The properties of the materials are presented in section 2.2.

The investigated arches are subjected to a test load consisting of two point loads. The point loads are 112 kN and 64 kN, respectively. The distance between the loads is 3 m. The loading is the same in all cases. An overview of the bending moment capacities for combinations of the different parameters is seen in *Figure 14*. In the figure "SL42 1/13" means a SL-Deck with deck thickness of 420 mm in an arch with

*Fixed case design parameters:*

- *Span: 30 m*
- *Shape: Circular*
- *Width of SL-Deck: 1.65 m*
- *Number of elements: 12*
- *Static system: 2-hinged*
- *Pre-tensioning: Cross-section from Figure 10*

rise to span of 1/13. Note that the iterative approach described in *Figure 12* is not performed in the example. This is because the calculations are based on input parameters (such as e.g. the rise to span ratio) that have been pre-defined and do not require iteration. Safety-coefficients are not implemented in the case study calculations.

All capacities in *Figure 14* are found as the smallest numerical value of the capacities in

the SL-Decks or the joints between SL-Decks. In almost all cases, the positive bending moment capacities are limited by the joints between SL-Decks, and the negative bending moment capacities are limited by a cross section with LAC blocks in the SL-Decks. The transfer of forces to adjacent arches has not been taken into account in the example.

*Figure 15* shows the relationship between the normal force in the cross section and the SL-Deck moment capacities for the case with a rise to span ratio of 1/13. For the positive bending moment the capacity increases when the normal force increases. The normal force increases when the number of post-tensioning cables increases, and when the amount of filling gets larger. All the points in the figure refer to combinations of the parameters similar to what is shown in *Figure 14*. In the figure we only study the behaviour based on the capacity of a cross section inside the SL-Deck. Because of the shape of the cross section in the SL-Decks it is expected that the negative bending moment capacity is lower than the positive. At a certain level of the normal force the negative bending moment capacity begins to decrease with an increasing normal force. For positive bending the same occurs but at a larger normal force, and the difference is because of the cross section geometry with the LAC blocks in the bottom. As explained in Chapter 1, the worst load we can apply to any arch is large and concentrated close to the  $\frac{1}{4}$  point of the span, such as the load in the case study. Such load will generate a large positive moment below the load in the loaded side, and a smaller, but not insignificant, negative moment in the non-loaded side of the arch. A larger positive bending moment capacity is therefore required, and this is obtained when using SL-Decks. Depending on the given load it is easy to adjust the bending moment capacities of a PC-Bridge by adding or removing post-tensioning cables or pervious concrete (filling) in the design process.

When comparing the bending moment capacities of the 1.65 m wide SL-Decks from *Figure 15* with the joints between the SL-Deck elements it is seen that the positive bending moment of the joints is lower than that of the SL-Deck in many cases. This means that a possible fracture due to an applied positive bending moment will occur in the joint and not in the SL-Deck. This means that warnings of the bridge being loaded close to its capacity may be observed as cracks or spalling of concrete in the joints at or close to the  $\frac{1}{4}$  point of the span. *Figure 16* shows the positive moment capacity of the joints compared to the capacity of the SL-Decks.

Now, the influence of the pervious concrete filling and the rise to span ratio is investigated. The filling adds to the level of pre-compression in the arch. *Figure 17* shows the order of magnitude of the effect of this pre-compression in case of a 270 mm SL-Deck, and a 420 mm SL-Deck with 7 post-tensioning cables. The positive bending moment capacity is nearly similar for the 270 mm SL-Deck having 2 m of pervious concrete filling above the crown of the arch compared to the 420 mm SL-Deck with 0 m of filling.

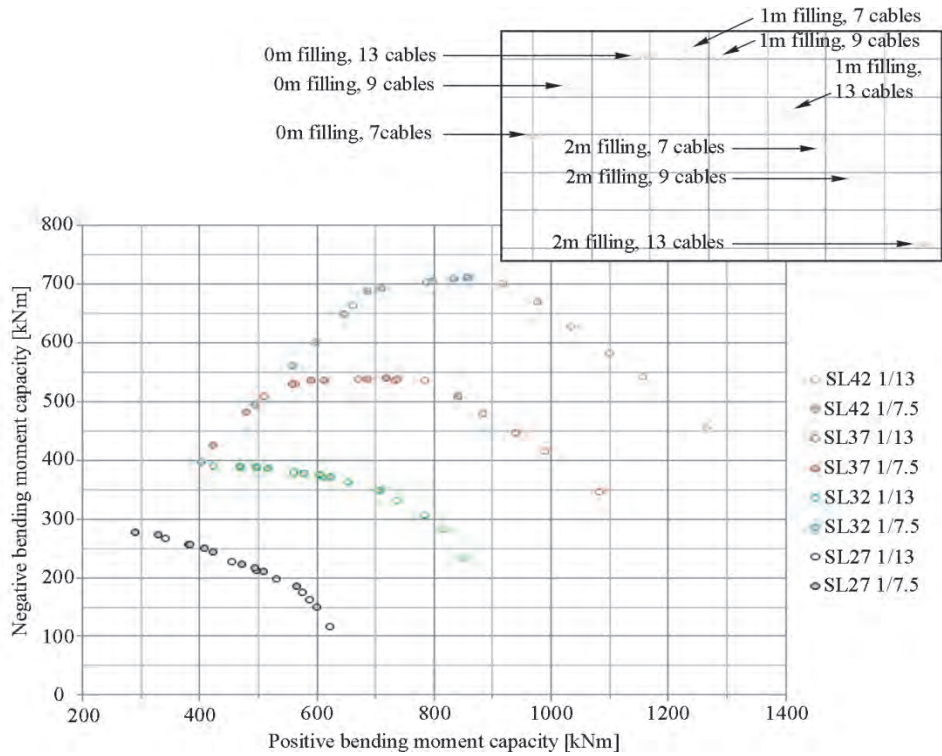


Figure 14: Positive- and negative bending moment capacities for PC-Arches.

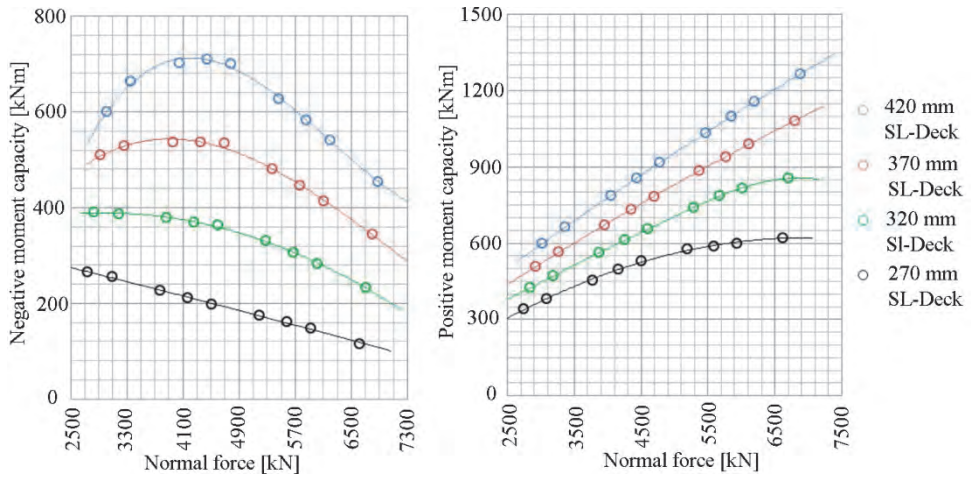


Figure 15: Capacities as function of normal force for rise/span of 1/13.

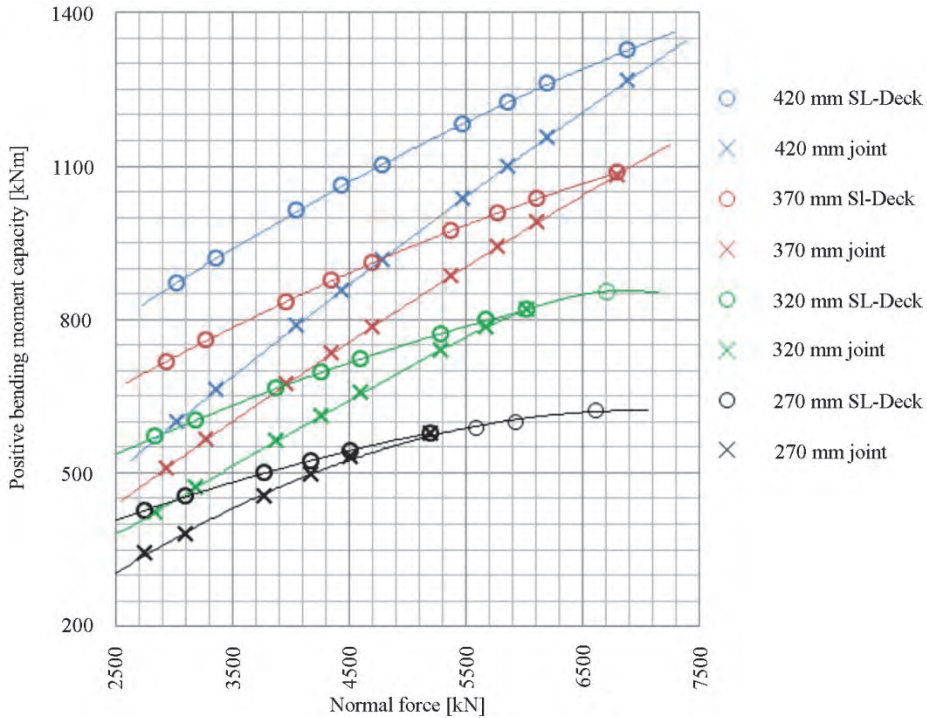


Figure 16: Capacities of joint vs. SL-Deck as function of normal force. Rise/span is 1/13.

As expected the moment capacity decreases when the rise of the arch gets larger. The shape of the arch is still circular in all cases no matter which rise to span ratio we consider. This is why the small difference between the capacities of the 270 mm (2 m filling) and 420 mm (0 m filling) SL-Decks do not change significantly at different rise to span ratios. When we see some change in the difference it can be explained by the previous concrete filling above the crown being a uniformly distributed load. The arch has a circular form which does not resist the uniformly distributed load perfectly like a parabola would. Therefore, an increased initial positive bending moment is applied to the arch when adding an extra layer of filling. Note also that an increase in the normal force may still reduce the negative moment capacity (for the given geometries in this theoretical case study).

The number of post-tensioning cables may be determined by the requirements when lifting the arch, and if it is necessary to reduce the normal force a change in the rise to span ratio is a solution when the filling is already 0 m above the crown of the arch.

A comparison between the presented PC-Bridge concept and the existing prefabricated closed spandrel arch bridge concepts from Chapter 1 is found in the appended Paper I.

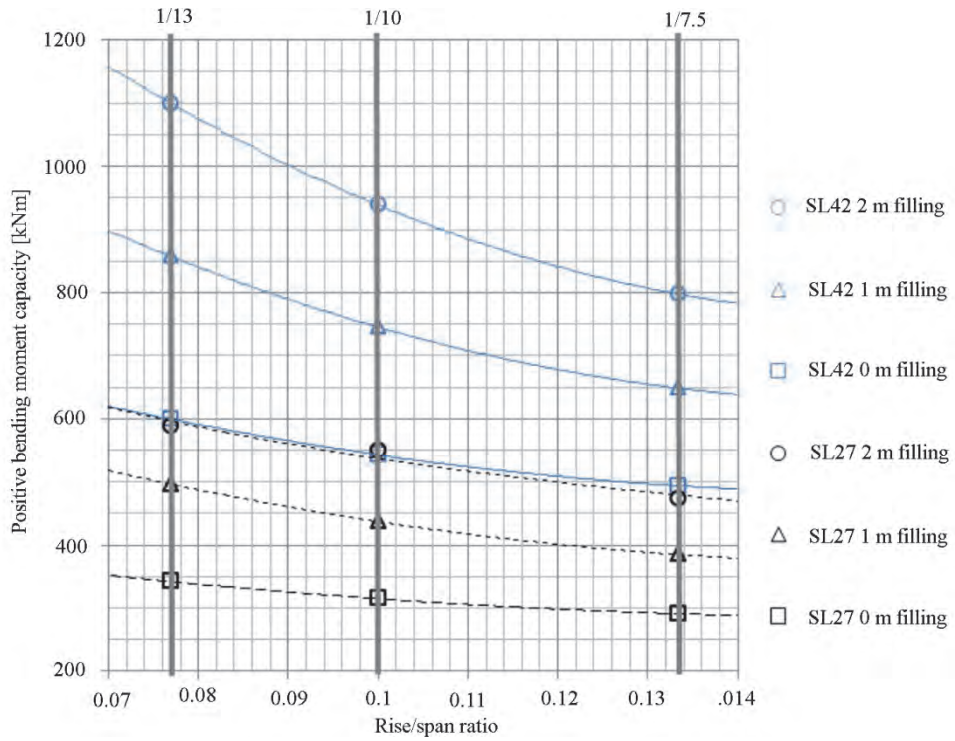
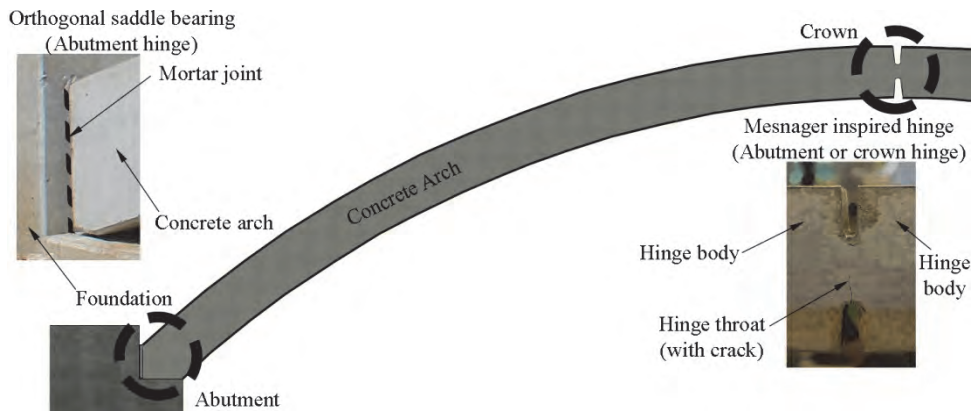


Figure 17: Capacities as function of rise/span. 7 post-tensioning cables are used.

# 3 INFLUENCE OF CONCRETE HINGES

This chapter describes the tests of two types of designed concrete hinges intended for use in Pearl-Chain Arches. The results from the tests are compared with numerical models for a thorough evaluation of each hinge type.

The two types of concrete hinges: i) a Mesnager and Freyssinet inspired hinge, and ii) an orthogonal saddle bearing type hinge, both shown in *Figure 18*. The Mesnager type hinge has been used many times in arch bridges in the first part of the last century, while the orthogonal saddle bearing hinge is specially invented for use in PC-Bridges.



*Figure 18: The two types of investigated hinges for PC-Arches. The Mesnager hinge can be used as abutment hinge as well as crown hinge.*

The chapter is based on the journal paper #2: “Concrete Hinges for Pearl-Chain Bridges”, and the conference paper #3: “Concrete Hinges”.

The scope of the hinge tests:

- Investigate the response of the two hinge systems using component-scale testing and numerical modelling.
- Implement the hinge responses into a global structural model of the Pearl-Chain Bridge to investigate the changes in structural response compared to the ideal hinge, and a fixed connection.

### 3.1 Background

The true behavior of hinges used in concrete arch structures has a significant influence on the overall static system. A resistance towards rotation in hinges means that the static system is not as intended if designed with ideal zero bending moment hinges similar to what was done in the case in Chapter 2. Instead, the distribution of forces and bending moments is somewhere in between the two extremes: The ideal hinge, and a fixed connection, *Figure 19*.

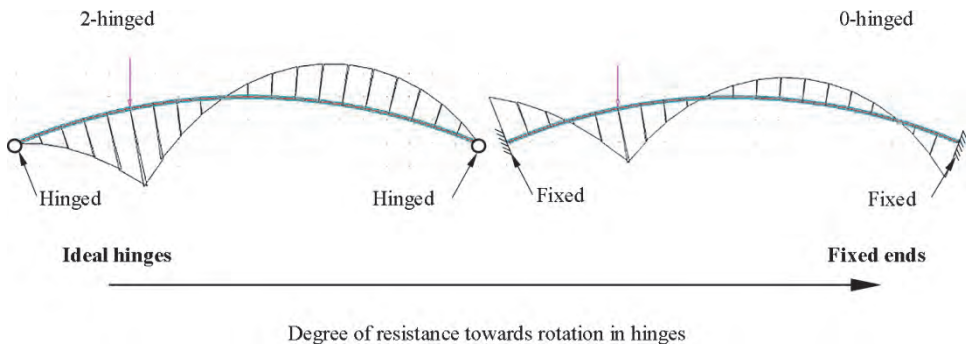


*Figure 19: Influence of hinge rotational resistance on bending moment distribution in 2-hinged arch.*

The Pearl-Chain Bridges differ from many other closed-spandrel arch bridge types by having a higher level of pre-compression in the arch rib. Self-weight contributes to the normal force in all arches, but having post-tensioning at the same time increases the normal force significantly compared to “plain” concrete arches with only mild steel reinforcement. Furthermore, the concept so far is intended for low rise to span constructions, rise/span = 1/13, where the normal force from the self-weight and payload is high. The relatively high level of normal force may affect the functionality of the hinges in these arches. It is therefore a requirement for the Pearl-Chain Arch hinges to be functional at this high level of normal force. Another requirement is to stay below the level in ULS,  $m = 1/3$ , proposed by Leonhardt and Reimann, where cracking in the hinge reaches half way through the throat, cf. *Figure 5*. They also propose a limit of  $m = 1/6$  (initiation of crack in throat) in SLS.

### 3.2 Materials and geometry of test-specimens

The regular concrete in Pearl-Chain Arches has characteristic compressive cylinder strength of 55 MPa, and Characteristic Young’s modulus of 41 GPa. The same type of

concrete was used in both types of hinges. In the Mesnager inspired hinge type the concrete properties were tested to be  $f_{ck\_mes} = 55$  MPa, and  $E_{c0k\_mes} = 33$  GPa. For the orthogonal saddle bearing hinge the same test values were  $f_{ck\_ort} = 59$  MPa, and  $E_{c0k\_ort} = 39$  GPa. The mild steel was the same in both types of specimens as well. The strength of the steel was 550 MPa.

Figure 20 shows the test specimens for the Mesnager inspired hinge test. Three geometries of the throat were tested, which is the reason for the three different length values given in the close-up on the right in the figure. To more easily handle the elements in the lab, the test specimens had reduced width compared to a Pearl-Chain Arch. The tested specimens had crossing reinforcement through the throat with a total of four crosses of two Y10 mild steel bars at each cross. The hinge body was sufficiently reinforced to avoid splitting from transverse forces next to the throat.

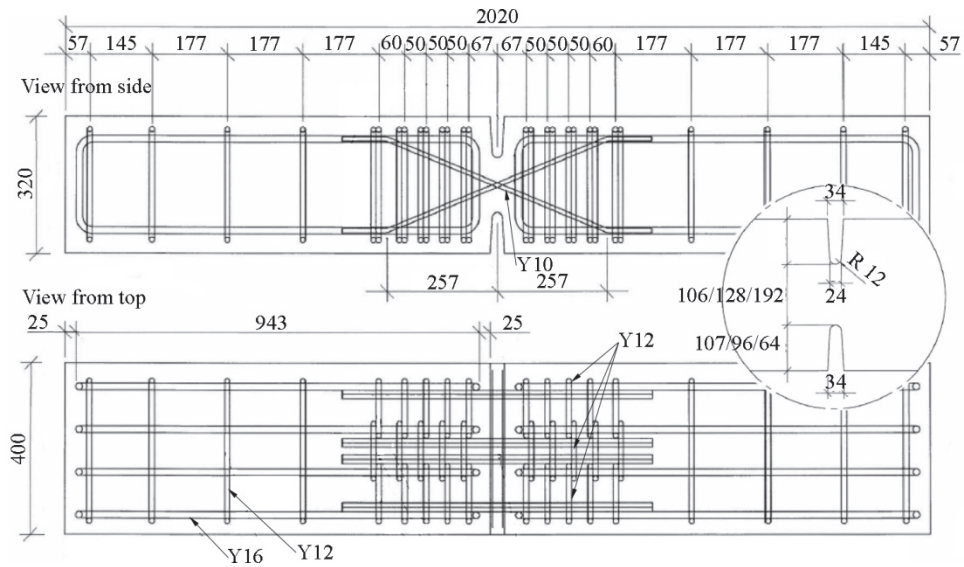


Figure 20: Geometry of test-specimen for the Mesnager inspired hinge test. Unit is mm.

In Figure 21 the specimen for testing the orthogonal saddle bearing hinge is shown. The orthogonal concrete surfaces at the end of the specimen are connected to a rigid foundation with similar surfaces. Mortar is poured between the opposite surfaces, and this connection has the studied hinge-behavior. The test-specimens have full width of 1.75 m.

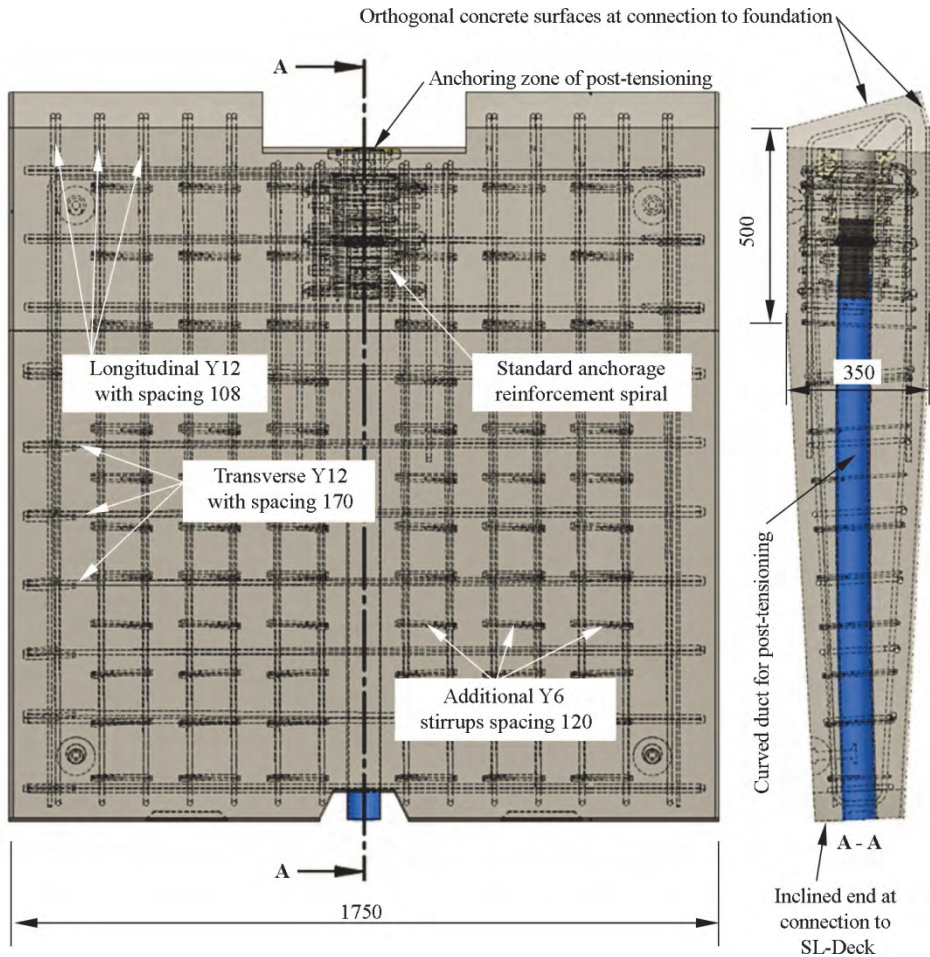


Figure 21: Concrete element specimen used for orthogonal saddle bearing hinges. Unit is mm. By courtesy of Perstrup Betonindustri.

### 3.3 Testing of the hinges

The two developed hinge candidates for possible application in Pearl-Chain Bridges were tested and analyzed. Full-scale tests were performed on both types: The Mesnager inspired hinge type was tested at the Technical University of Denmark, and the orthogonal saddle bearing was implemented in two loaded Pearl-Chain Arches tested in Jutland in Denmark.

#### 3.3.1 Testing of the Mesnager inspired hinges

In Paper #3 [43] it was found that the best hinge ratio,  $b_1/b_2$ , was  $1/3$  based on tests of three different ratios. Larger hinge ratios of  $4/10$  and  $6/10$  were unfit for use in

Pearl-Chain structures due to cracking from the throat into the hinge body. Hence, the more detailed investigations in this paper includes the ratio  $b_1/b_2 = 1/3$  alone. Eight specimens were tested with the  $1/3$  ratio, five with the  $4/10$  ratio, and three with the  $6/10$  ratio.

### 3.3.1.1 Test method

Extensive efforts were made to create a test-setup that would simulate the conditions of the hinge in a Pearl-Chain Arch. Instead of having a post-tensioning duct inside the test specimens and two complex anchorage zones, it was chosen to compress the specimens on the end surfaces to create the large normal force similar to the one from pre-stressing, and arch loads. This was the best possible practical solution when having specimens of only 2 m in length.

First, specially designed steel profiles were pre-stressed to the ends of the test-specimen to achieve the required normal force. The steel profiles were two HEB 300 welded together, and the pre-stressing was applied via two threaded rods of M42 – one next to the specimen in each side. Six Belleville springs were used in each connection between steel profile, and threaded rod to ensure free rotation. The normal force was initially 1000 kN (changed with up to 8 % during testing). The deviation in normal force was measured by four strain gauges on the M42 threaded rods.

The test-setup was a four-point-bending creating a constant bending moment between the presses. A rigid steel test-frame was built with two hydraulic presses pushing down onto the top surface of the test specimen positioned on two supports on the floor. The setup is seen in *Figure 22*.

Measurements of rotation were performed on the top surface of the hinge body, and across the recesses in the throat. The top surface measurements were of the vertical deflections in six locations – three in each side of the throat with spacing 300 mm. These measurements were intended to show if any significant bending occurred in the hinge body during testing. Any interfering vertical settlements of the arch supports were recorded at both supports. *Figure 23* shows the measuring equipment and the position of it.

The measurements across the recesses in the top and bottom of the throat were more directly recording the deformations, though it was expected that the bottom recess measurement would be affected by cracking in the throat when exceeding the elastic limit ( $m = 1/6$ ).

The tests were video recorded and the rotations were verified by visual interpretation from the recordings.

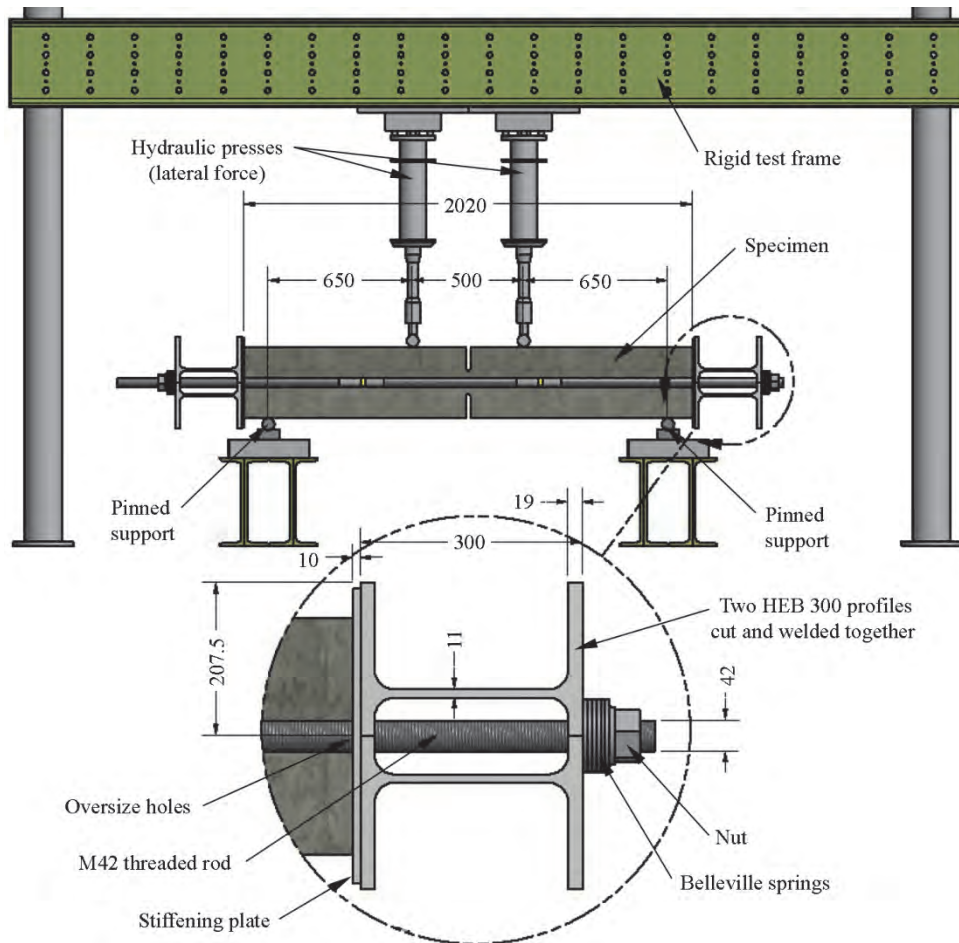
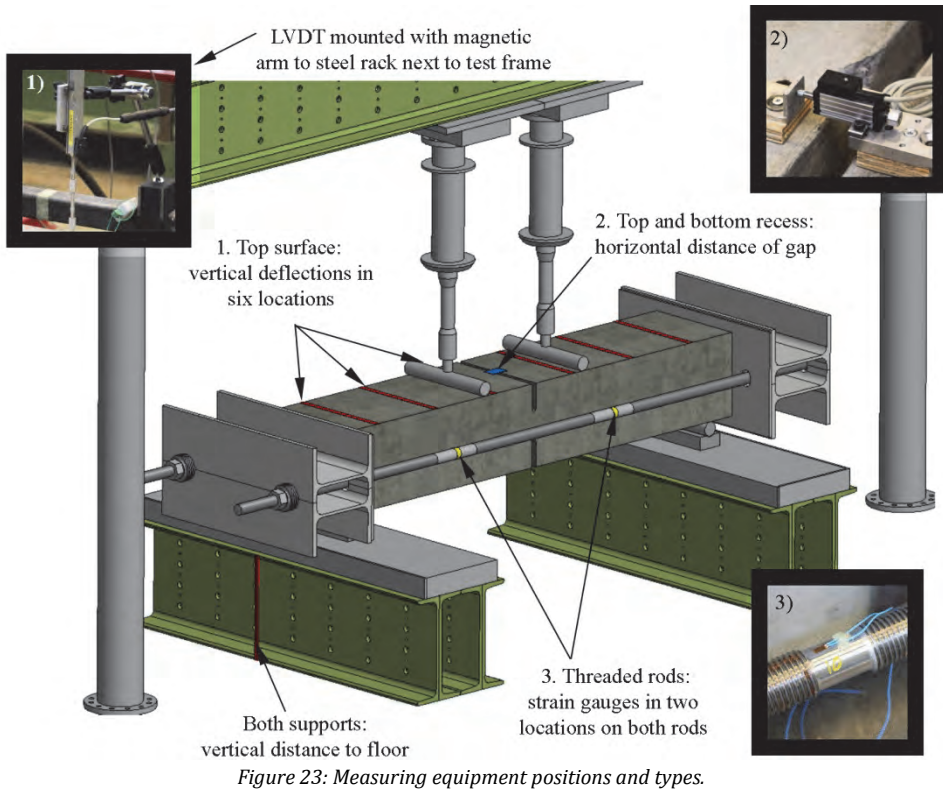


Figure 22: Test-setup for Mesnager inspired hinge type tested at DTU [2]. Unit is mm.

### 3.3.1.2 Test results

Results for the hinge ratio 1/3 showed that the elastic limit for the hinge type at the given normal force was at a rotation of 0.0018 rad, and moment of 20 kNm. The rotational stiffness was hence 10,600 kNm/rad, and there was a 3 % deviation in this value depending on the measuring method: top surface of body or in recess of throat. Failure (max bending moment) occurred at 0.019 rad and 40 kNm. The specimens showed no cracks except for in the hinge throat, which was anticipated. The hinge responses are seen in Figure 24, Figure 25, and Figure 26 (measured on top of test specimen), where the average curves, and fracture points for the different specimens are shown as well.

The hinge ratios  $b_1/b_2 = 4/10$  had a rotational stiffness of 14,200 kNm/rad, and  $b_1/b_2 = 6/10$  had 37,600 kNm/rad. In the figure, points of largest moment for ratio  $b_1/b_2 = 6/10$  are not given due to large deviations depending on the measuring method used.



### 3.3.1.3 Comparison between test, model and theory

To compare the universal hinge response curve by Leonhardt and Reimann to the hinge response from the tests we use Eq. 1.6., 1.7., and 1.8. The altered plot of the average hinge response from the tested hinge specimens are matched with the one proposed in *Figure 5*. When testing the hinges measurements showed that the normal force deviated with up to 8 % during testing. Therefore, two alternate curves are given as well with a plot of the hinge response assuming 8 % higher or 8 % lower normal force, see *Figure 27*.

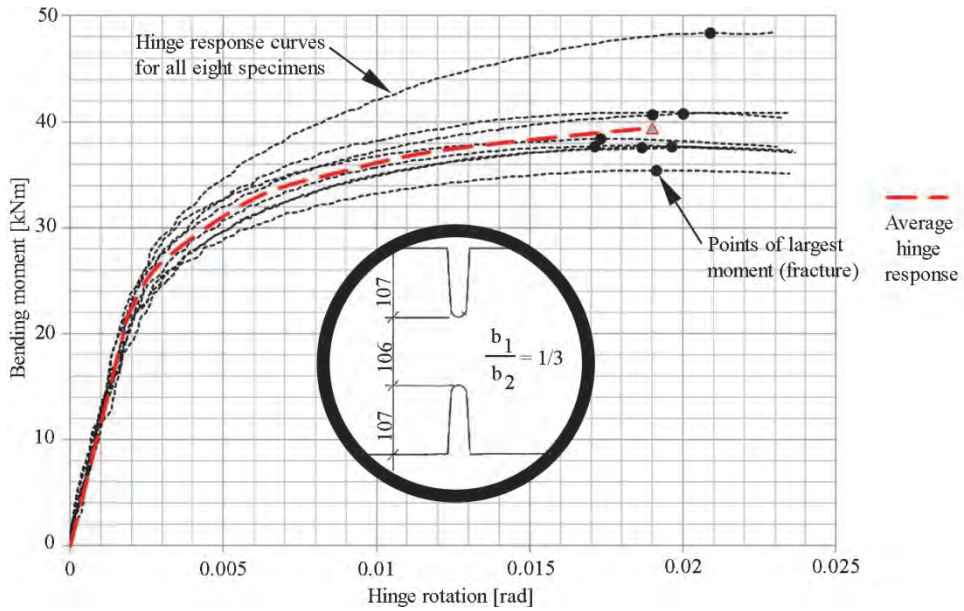


Figure 24: Hinge responses from the tested specimens,  $b_1/b_2 = 1/3$ . Unit is mm.

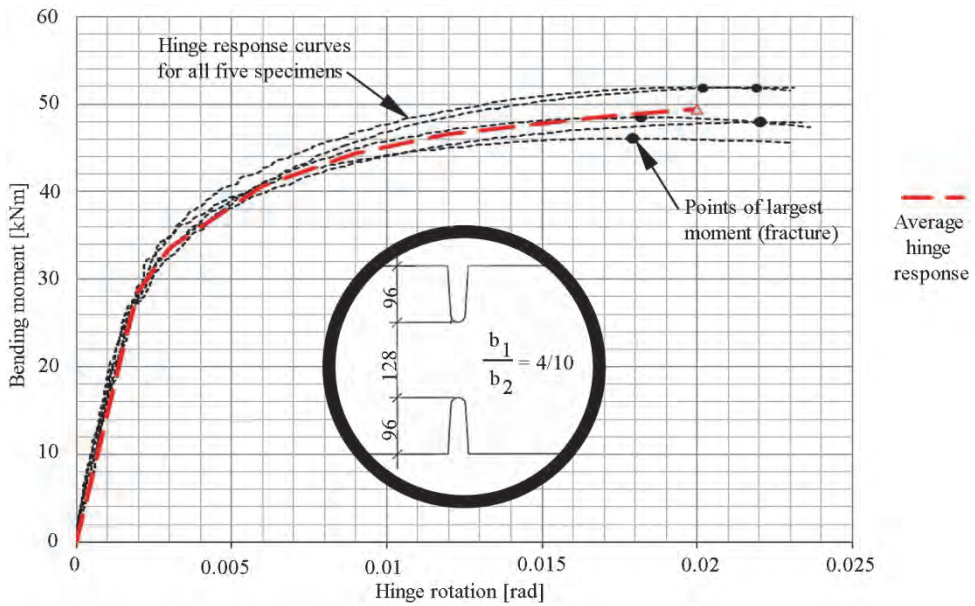


Figure 25: Hinge responses from the tested specimens,  $b_1/b_2 = 4/10$ . Unit is mm.

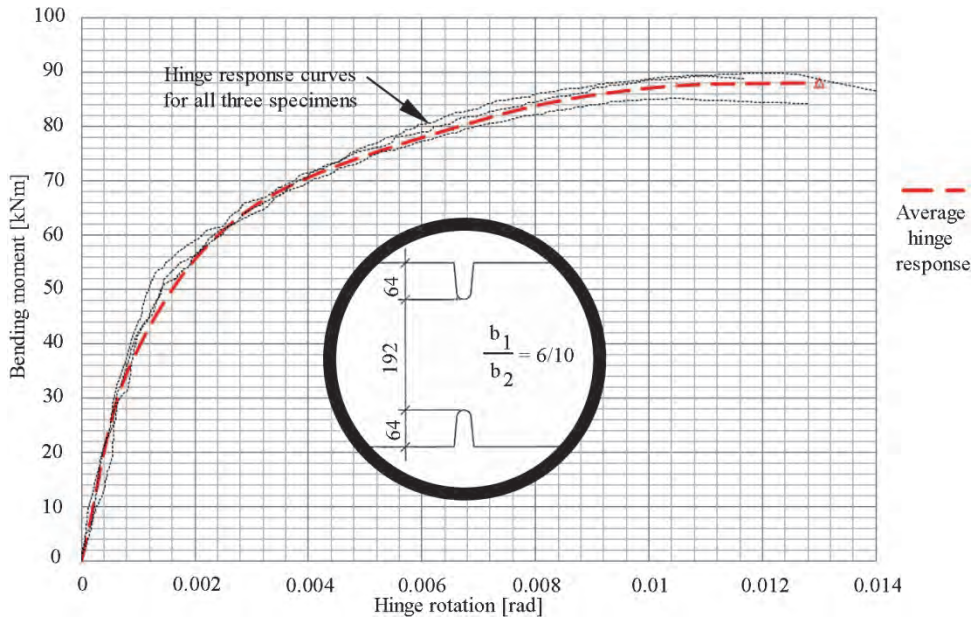


Figure 26: Hinge responses from the tested specimens,  $b_1/b_2 = 6/10$ . Unit is mm.

The comparison shows that the tested hinge response is comparable to the universal hinge response curve. It is therefore found that the relatively high level of normal force is not a hindrance for applying the model by Leonhardt and Reimann. Still, the reason why the rotational limit should be  $m = 1/3$  (crack half way through throat) is unclear. Base [28] tested Mesnager hinges in working condition with cracks up to  $2/3$  through the throat. This can be explained by two observations: i) the crossing reinforcement go into tension to help resist the moment, when the crack becomes larger than  $b_1/2$ , and ii) the concrete confinement increases as the crack length develops cf. Eq. 1.4.

There is a high margin of safety using the  $m = 1/3$  limit but even then there might be a challenge with ingress of water to the crossing reinforcement. An even more conservative approach is to stay below the  $m = 1/6$  limit to avoid corrosion in the mild steel in the throat. Use of this type of hinge in the domain between  $m = 1/6$ , and  $m = 1/3$  would require stainless steel in the hinge throat region.

A numerical model is created in Abaqus [44] (without the reinforcement) to compare with the tested response in the elastic un-cracked domain. The results are seen in Figure 28. The geometry, material properties, and applied loads are similar to the tested hinges. The numerical model gives a 9 % higher rotation compared to the tested hinge. Creating a denser mesh than the shown does not change the output significantly. As shown in the figure the effect of the normal force does not account for the difference either.

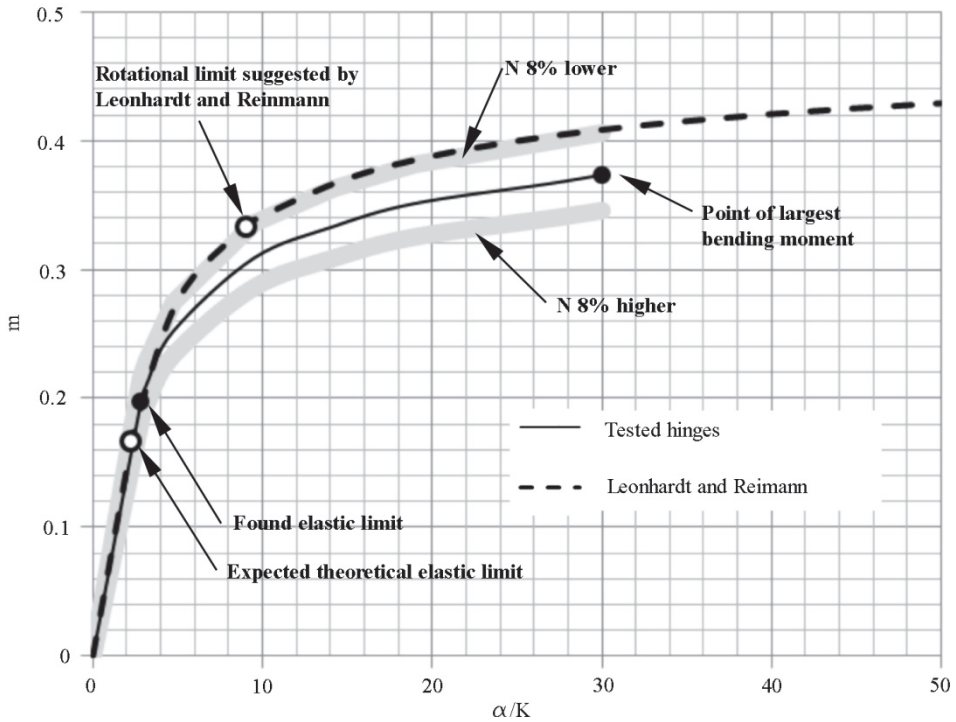


Figure 27: Tested hinge response ( $b_1/b_2 = 1/3$ ) compared to universal response model by Leonhardt and Reimann.

The reason for the 9 % dissimilarity is a degree of fixation of the test-setup that does not exist in the numerical model or in a real concrete hinge in an arch structure. If we fix the supports of the hinge specimen in the model the rotation decreases to approximately half. When there is a degree of fixation at the supports the static system changes, and the bending moment becomes less than expected for a given load.

### 3.3.2 Testing of the orthogonal bearing hinges

This type of hinge was developed to be implemented in a load test of two full-scale Pearl-Chain Arches of 13 m span. The test was performed in two tempi: 1) A test to 2/3 of the load carrying capacity and 2) a test to fracture. The relevant results of the behavior of the orthogonal saddle bearing hinges were primarily gathered from the non-destructive first test.

#### 3.3.2.1 Test method

Two Pearl-Chain Arches of 1.75 m width were positioned next to each other on a stiff concrete foundation (and tension tie),  $E_{cf} = 36$  GPa, with no possibility of horizontal settlement [45], see Figure 29. The span was 13 m, and rise 1 m. A plateau was

cast in concrete on top of the arches at the  $\frac{1}{4}$  point of the span, and heavy steel weights were positioned on the plateau during the test. The abutment elements (elements in each end of each arch) were designed with orthogonal concrete surfaces to fit to two similar surfaces in the foundation. When positioning the arches, wedges were placed between arch and foundation, and the gap was poured with a mortar of stiffness,  $E_m = 23$  GPa. The mortar gap,  $t$ , was approximately 6 cm in the loaded side and 8 cm in the non-loaded side.

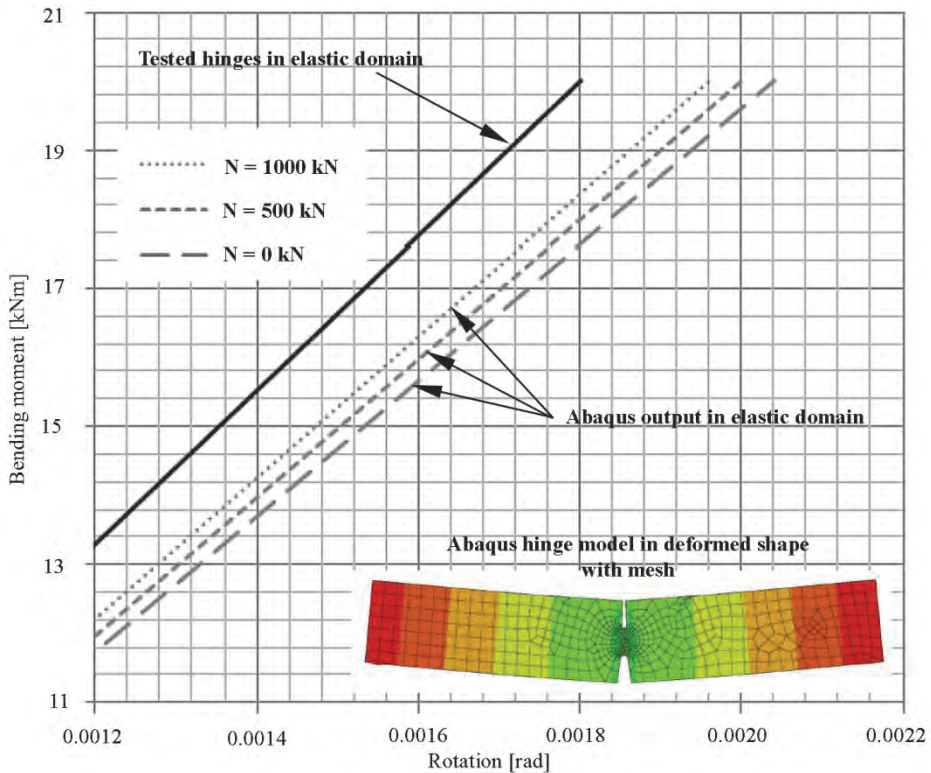


Figure 28: Abaqus model output vs. tested hinge in elastic domain.

Measurements of the hinge behavior were performed using ARAMIS DIC software (Digital Image Correlation) [46]. After taking photographs of the relevant surface, the software compares the photo taken during loading to a reference photo. The output from ARAMIS was utilized in finding the rotation of the hinges, and to spot the first appearing cracks, see Figure 30. The figure shows a fully formed crack in top of the hinge in the loaded side of the arch.

The normal force was calculated based on the arch geometry and the applied load and self-weight. Post-tensioning was anchored in the abutment elements and do in this case not contribute to the normal force in the hinges.

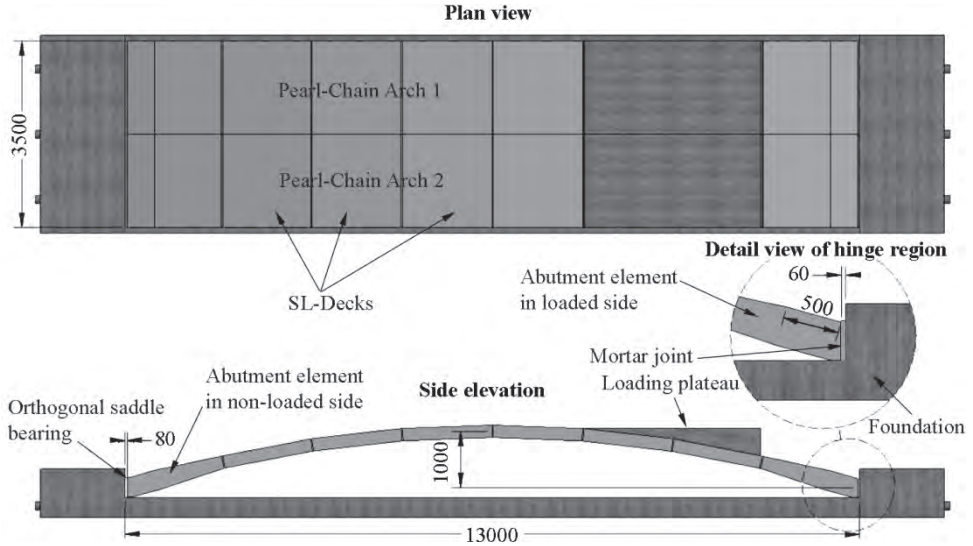


Figure 29: Test setup for full-scale Pearl-Chain Arch test with orthogonal saddle bearing hinges. Unit is mm.

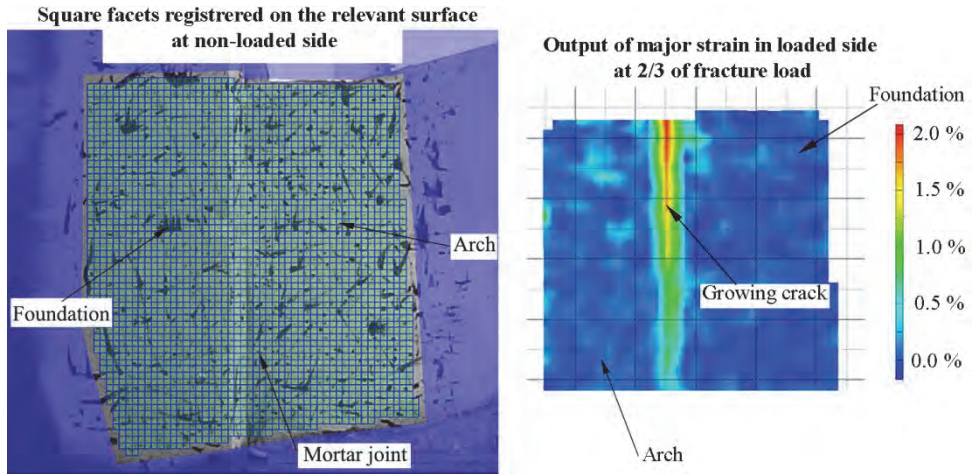


Figure 30: ARAMIS. Top: The used facets (non-loaded side). Bottom: Cracking in surface between foundation and mortar (loaded side).

At the point of first cracking in the hinge regions at the elastic limit, the load was approximately,  $P_{\text{elastic}} = 300 \text{ kN}$  (including load from plateau), giving a normal force in the hinges of approximately,  $N_{\text{elastic}} = 891 \text{ kN}$ . This value is applied in a numerical model of the orthogonal saddle bearing created in Abaqus.

The deflections of the tested arches were monitored by Linear Variable Differential Transformers (LVDT's) during loading. At  $d_{\text{hinge}} = 500$  mm from the hinge point in the loaded side the deflection was  $\delta_{\text{down}} = 0.30$  mm downwards, and at the same distance from the hinge point in the non-loaded side the deflection upwards was  $\delta_{\text{up}} = 0.29$  mm. Both measurements of the deflections were at the load  $P_{\text{elastic}}$ .

### 3.3.2.2 Test results

Figure 31 and Figure 32 show comparisons between ARAMIS results from the test, and the numerical model in Abaqus. In the figures the influence of the thickness of the mortar joint,  $t$ , and the Young's modulus,  $E_m$ , have been investigated. The response of the joints is evaluated by two different methods: 1) The rotation is shown coming from the deformation of the mortar joint alone, and 2) the total rotation is shown at the surface between the arch, and the mortar joint (not including the deformations in the 500 mm of arch). An ideal hinge would in the tested setup give a total rotation of:

$$rot_{\text{ideal}} = \tan^{-1} \left( \frac{\delta_{\text{down}}}{d_{\text{hinge}}} \right) = 0.0006 \text{ rad}$$

### 3.3.2.3 Comparison between test and model

The measured values from ARAMIS are within 22 % of the total values from the Abaqus model, when applying the same properties of stiffness and mortar thickness. When comparing to the rotation of an ideal hinge though, the rotation measured in ARAMIS is only around 1/3 of  $rot_{\text{ideal}} = 0.0006$  rad. This indicates that the joints perform as practically fixed in the un-cracked region.

The results show that it is possible to some extent to affect the level of rotation in the elastic region from altering the mortar thickness, and Young's modulus. The effect of such alteration on the other hand is not abundant. For instance it is seen in Figure 32 that the trend line curves of the total rotations from the model are close to each other and even overlapping for stiffness above 15 GPa.

Beyond the elastic limit of the material cracking occurs. The elastic to plastic behavior was recorded with ARAMIS as well, see Figure 33. It is seen from the figure that the hinges behave fixed primarily in the elastic region of the response curves (prior to cracking). After cracking initiates, the gap between the measured rotations with ARAMIS and the calculated ideal rotations (from LVDTs) decreases. Actually, the transition from un-cracked to cracked state happens prior to the recorded first visible signs of cracks. This may be due to unrecorded micro-cracking in front of the crack tip.

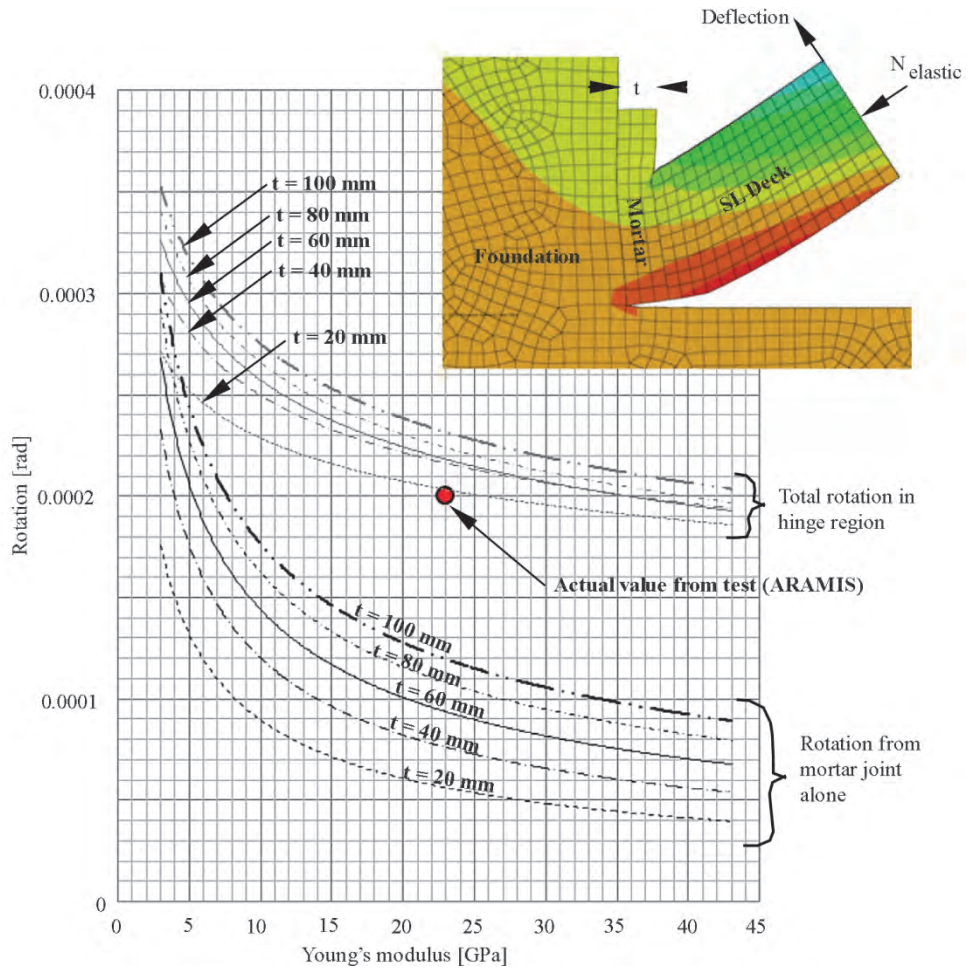


Figure 31: Rotation in non-loaded side for different thicknesses,  $t$ , and values of Young's modulus of the mortar.

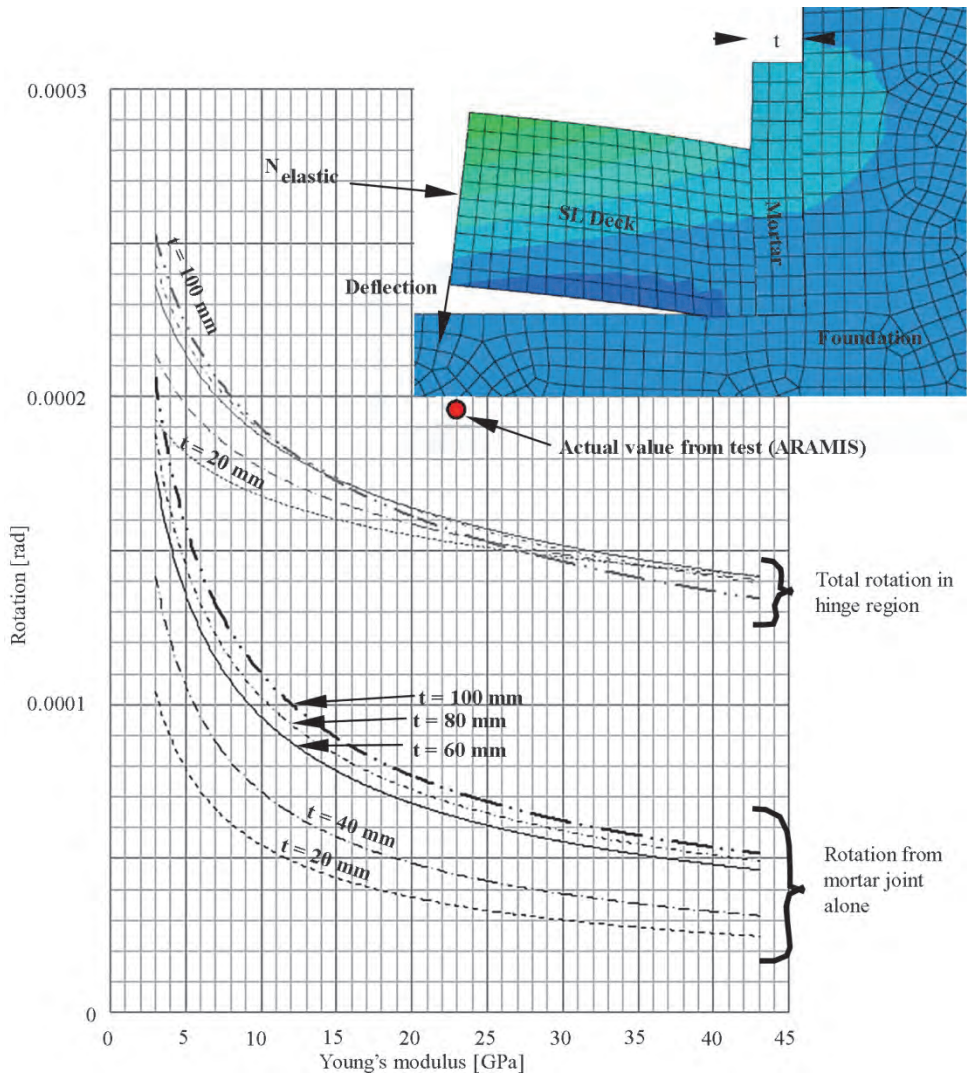
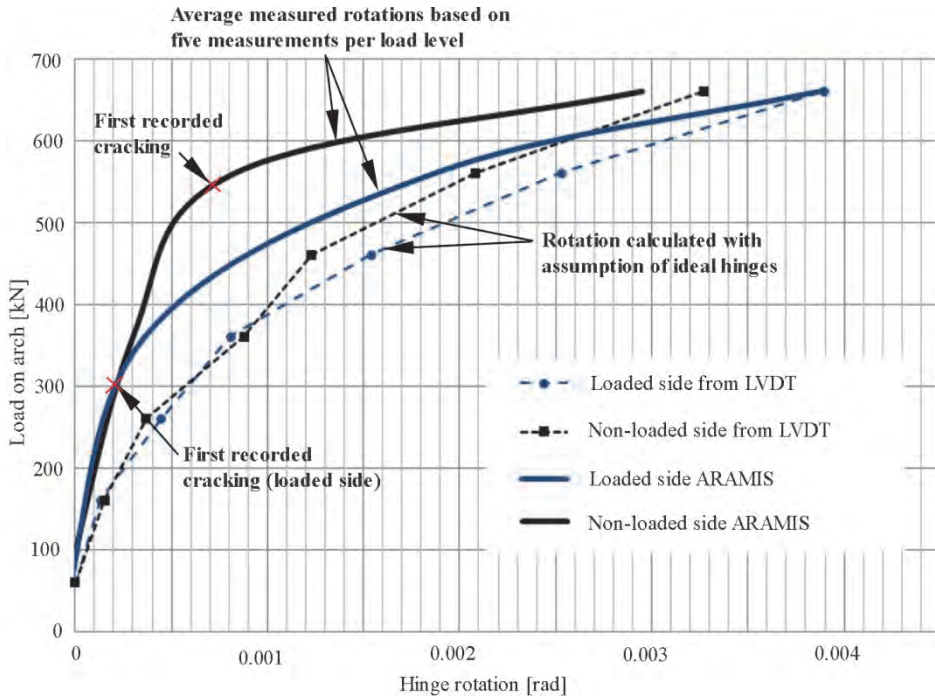


Figure 32: Rotation in loaded side for different thicknesses,  $t$ , and values of Young's modulus of the mortar.



### 3.4 Implementation of the hinge response into the Pearl-Chain Arches

The normal force in the tested Mesnager inspired hinges were 1000 kN which corresponds to 7.8 MPa of normal stress in the hinge body. The level of normal stress is based on what is found in a fully traffic loaded Pearl-Chain Bridge with rise to span of 1/13 and span of 30 m. In the orthogonal saddle bearing hinges from the 13 m span test the normal stress was 1.3 MPa. This 83 % difference could have an influence when comparing the hinges. In *Figure 28* we found that the effect of the normal force on the hinge response in the elastic region was relatively small.

The proportionality limit for the Mesnager inspired hinge was 0.0018 rad, which is close to four times the value of the orthogonal saddle bearing hinge (*Figure 33*). Despite of the smaller rotation capacity in the elastic domain, the orthogonal saddle bearing hinge has several practical advantages compared to the Mesnager type:

- For application in pre-fabricated arches, the developed abutment element is easy to implement as a pre-fabricated “pearl” in the Pearl-Chain, and the mortar connection to the foundation is simple to create.

- The hinge (mortar joint) has fewer problems with corrosion of reinforcement. Nevertheless, observations from loading at 2/3 of collapse load of the two tested 13 m span arches showed cracks propagating into the abutment element.
- The abutment element works as an anchorage block for the post-tensioning, which means no pre-stressing in the hinge. In the Mesnager hinge the post-tensioning would conceivably have to propagate through the hinge throat, and be anchored outside that region.
- Even beyond the 2/3 of collapse load the hinges still acted as intended (despite of large cracks), and the final collapse of the two arches occurred in the span of the arch – not in the springing hinges.

Advantages of the Mesnager inspired hinge type:

- The larger rotation in the elastic region is important in certain types of arches.
- A well-defined rotation-moment curve from lab-testing exists for simple implementation in programs for global structural analysis such as Robot Structural Analysis [42]. A true rotation-moment curve for the orthogonal saddle bearing hinge can only be found in the future by complicated lab testing.
- The hinge type is well tested and documented for use in other arch structures over a range of years.
- Can be used as crown hinge.

To exemplify the influence of the local hinge response, the curve from *Figure 24* is implemented in a global model in Robot Structural Analysis. The model is similar to the tested 13 m span Pearl-Chain Arches. *Figure 34* shows the difference in bending moment going from ideal hinges to the true hinge response to fixed ends. The load in the figure is equal to 2/3 of the fracture load in the full-scale test.

In the example in the figure the hinge is in the plastic domain of the hinge response curve, which is beyond the limit for serviceability state (at first cracking  $m = 1/6$ ). Actually, the hinge in the loaded side is exactly at the  $m = 1/3$  limit suggested in the ULS by Leonhardt and Reimann, where the crack has reached the middle of the throat.

In the real test of the two Pearl-Chain Arches, the orthogonal saddle bearing hinge in the loaded side had a crack of  $3/4$  of the height of the mortar joint. At that stage the crack followed the surface between mortar and foundation in one side of the bridge, while the crack at the opposite side grew into the abutment element.

Due to the simplicity, the practical advantages, and the behavior seen at the test, the orthogonal saddle bearing hinge has been chosen for use in the first ever build

Pearl-Chain Bridge in the summer of 2015 in Denmark: the “Vorgod Creek Bridge”. More about this bridge in Chapter 6.

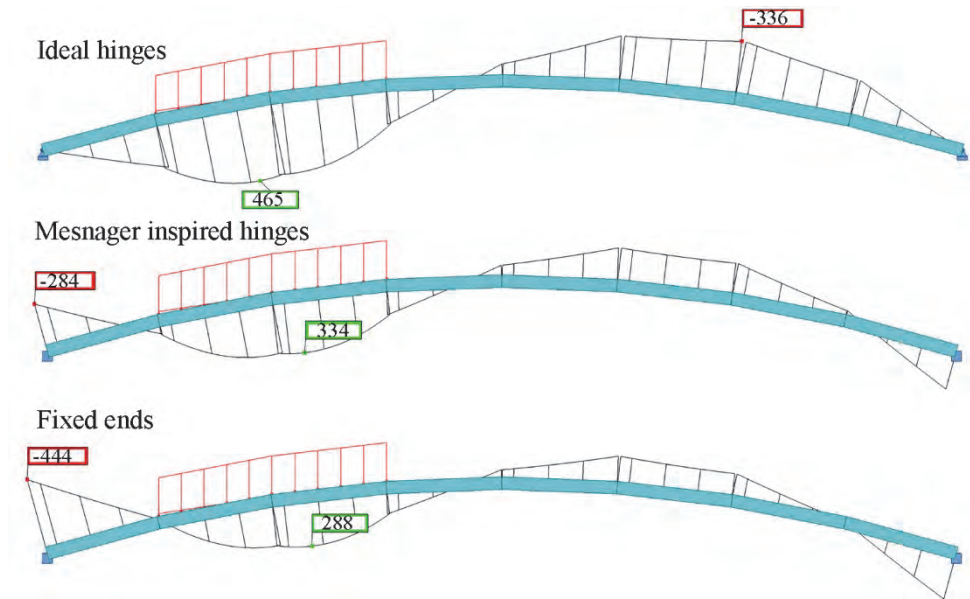


Figure 34: Behavior of global structure depending on support properties. Unit is kNm.

# 4 ERECTION PROCEDURE AND DETAILS

Chapter 4 deals with some of the practical challenges when building a Pearl-Chain Bridge. Details developed during the Ph.D.-study are presented. A full-scale assembly-, lifting-, and positioning test of two 13 m span PC-Arches is used as an example of the erection method. A 6 m span, PC-Arch was previously tested [47], and the earlier 6 m span test-arch was mainly produced to verify the assembly method of the three SL-Decks it consisted of.

The two new 13 m span arches consisted of six SL-Deck elements, and two specially designed abutment elements. The SL-Decks for the test had thickness of 220 mm which is less than the minimum limit of 270 mm for SL-Decks in bridges. Subsequently to the erection test, the two arches were to be load-tested, and to be able to reach fracture, the thickness of the SL-Decks had to be reduced. Results from the succeeding load tests are given in Chapter 5.

The chapter is primarily based on the conference paper #4: “Assembly and lifting of Pearl-Chain arches”, but also on the journal paper #1: “Precast Pearl-Chain concrete arch bridges”.

The scope of the full-scale tests of the assembly and lifting process was to verify 1) that the post-tensioning method and developed details worked in practice, 2) that the fast lifting and transportation of PC-Arches was possible by crane or truck, and 3) that adjacent arches could be positioned next to one another to build a PC-Bridge.

## ***4.1 Developed practical details***

Some practical details were developed in order to assemble and erect the PC-Arches: The connections between SL-Deck elements, the connections between PC-Arches, and abutment elements.

### **4.1.1 Connections between SL-Deck Elements**

The inclined ends of the SL-Decks are given rough surfaces and shear locks for adequate transfer of shear forces. The roughness is achieved by applying a retarder on the surface of the mold, casting the concrete, and then washing away the layer of unhardened cement paste at the surface of the elements leaving the aggregates visible.

When the joint between SL-Decks are cast, the elements are positioned vertically (on edge) in the desired position. Post-tensioning ducts are connected, a formwork is applied, and a special mortar is poured in the cavity between the elements.

The joints are reinforced by the post-tensioning cables only, but additional mild steel bars can be applied longitudinally (this was not done in the lifting test). This can be achieved by adding recesses in the SL-Decks in which the bars can be positioned (overlapping the joints). Subsequently, mortar is cast in the recesses.

### **4.1.2 Connections Between PC-Arches**

Forces can be transferred between adjacent PC-Arches. A so called Hammerhead joint recess was designed and positioned in the sides of each SL-Deck.

The Hammerhead joints consist of a transverse, 550 MPa Y12 reinforcement steel bar embedded in a recess formed in the strong concrete. The steel bar goes from the concrete into the Hammerhead recess where it bends 180 degrees (with a bending radius of 96 mm) and continues back into the concrete again, see *Figure 35*. In the lifting test, the recess length was 500 mm, the depth was 113 mm, and the width was 110 mm.

After placing adjacent arches, the Hammerhead joint recesses of each arch become aligned with each other and pieces of rebar are put on the inside of the bended Y12 in the longitudinal direction. Then, the longitudinal rebar pieces is connected by a rebar hoop that goes around both bars. In the test, the longitudinal bars and the hoops were both 550 MPa Y16. Finally, the whole thing is cast out with a >55 MPa mortar. The arches are positioned 10 mm apart, and therefore it is necessary to use a construction foam as a formwork between the two arches to contain the mortar during the Hammerhead joint pour.

Each of the described Hammerhead joints can transfer a shear force of more than 2.5 tonnes. Due to the hoop around the longitudinal bars, the joint remains functional even if the arches are not perfectly aligned.

The bars in Hammerhead joints may have to be stainless steel if applied close to the surface of the SL-Decks.

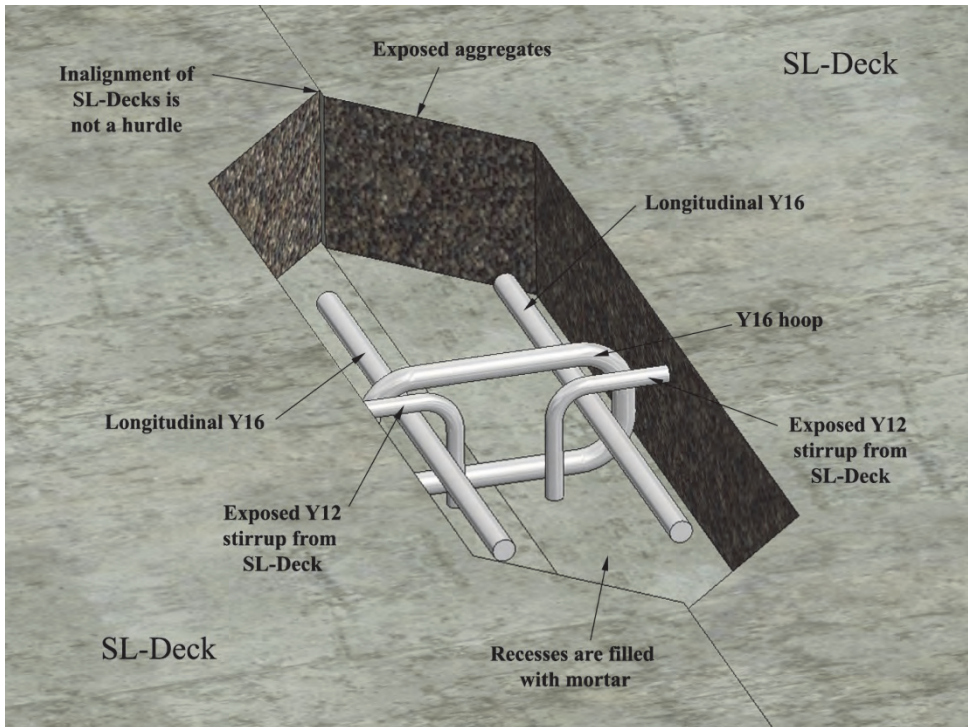


Figure 35: Hammerhead joint recesses on sides of two adjacent SL-Decks.

### 4.1.3 Abutment Elements

The specially designed prefabricated concrete elements at each end of a PC-Arch are called abutment elements. The hinge behavior in the connection between the abutment element and the foundation was investigated in Chapter 3 (the orthogonal saddle bearing hinge).

Often these elements have to be made of massive concrete with additional mild steel reinforcement compared to the SL-Deck elements. This is not because of the connection to the abutments but to the large stress concentration from anchoring the post-tensioning cables. When the concentrated stresses at the area of the anchoring are distributed to the entire cross section large transverse forces develop. Therefore, transverse bars and stirrups are built into the abutments elements. An example of abutment element geometry is seen in *Figure 36*, and a reinforcement solution was presented earlier, cf. *Figure 21*.

The direction of the curved duct is orthogonal to the end surface where the abutment element meets the first SL-Deck. The inclined end of the abutment element is similar to the inclined ends of the SL-Decks with a rough surface and shear locks.

An abutment element consists of the same concrete (55 MPa compressive cylinder strength) as the SL-Decks, but is not pre-tensioned.

When required draining holes can lead water through the abutment elements away from the arch bridge.

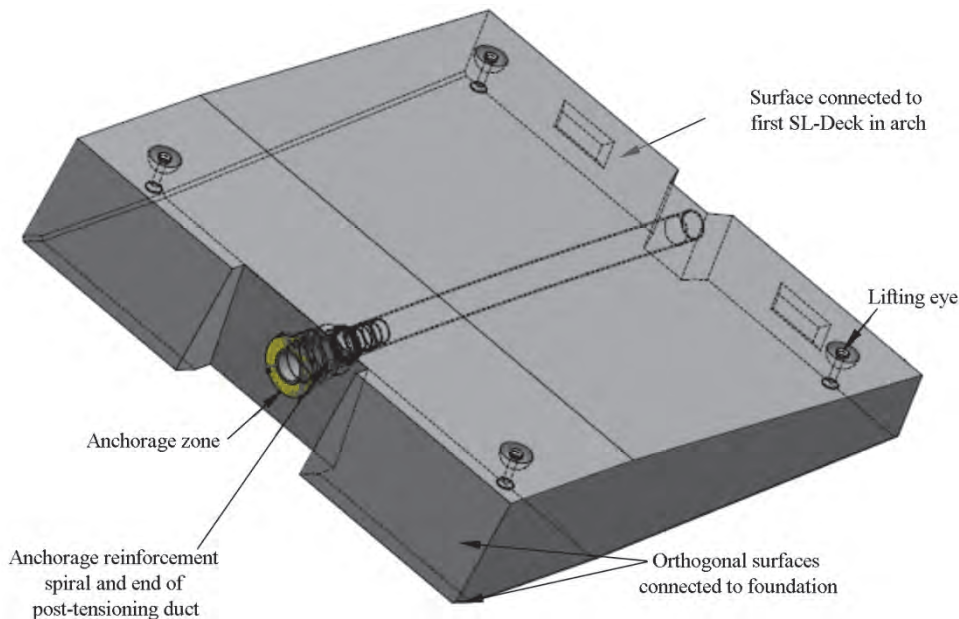


Figure 36: Possible geometry for an abutment element. By courtesy of Perstrup Betonindustri.

The thickness of the abutment elements was tapered from 350 mm at the anchorage end for the post-tensioning (500 mm from the anchorblock location) to 220 mm at the connection to the SL-decks.

## 4.2 Post-tensioning of single arches

SL-Decks are fabricated indoors in 100 m long pre-tensioning lanes. The LAC blocks are initially positioned in the mold in desired numbers by a specially developed block machine. Spacers are put in to separate the individual SL-Decks in the lane, and transportation threads are positioned. Pre-tensioning strands are stressed, transverse mild steel reinforcement is placed, and recesses for joints are filled out before the pre-tensioning bed is poured with concrete. After initial hardening the produced SL-Decks are transported by crane to a storage location where further hardening takes place. When the desired level of hardening, creep and shrinkage is reached the SL-Decks are ready to be implemented in a PC-Arch.

All elements in the two test-arches had a curved cable duct for a 7C15 post-tensioning cable. An overview of the components in one arch is seen in *Figure 37*. Detail A in the figure shows a mortar joint between two SL-Decks at the crown of the arch, and Detail B illustrates the anchorage zone of the post-tensioning cable in the abutment element. The rise is 1 m, and the elements were in this case cast at least seven days before the assembly.

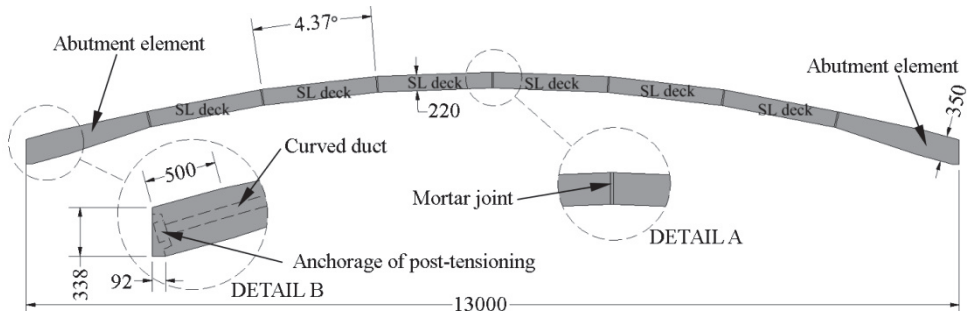


*Figure 37: One PC-Arch consisting of six SL-Decks and two abutment elements. Unit is mm.*

The width of each test arch was 1.75 m, and the SL-Deck elements were 220 mm thick.

All elements were placed on their edge on shims on the ground for post-tensioning. A leveled ground surface is a requirement for this approach. Ends of cable ducts from each element were connected and formwork was put up for in-situ casting of the mortar joints between the elements. The compressive cylinder strength of the mortar was >80 MPa after 28 days. The special mortar was designed and tested to remain homogeneous when being poured over a height of up to 2.4 m [41].

Two days later, the mortar was hardened enough for the post-tensioning to take place. The cable was post-tensioned to 90 % of the 0.1 percent proof stress of the steel, giving a force of 221 kN per wire. This force will decrease over time with up to 20 % due to anchorage seating loss, shrinkage, creep, and relaxation.

When the arches were post-tensioned with a cable through the curved ducts in the elements, the curvature of the cable resulted in a downwards force along the duct. Shortly after the post-tensioning of both arches, visible cracks were formed in the longitudinal direction through the mortar joints between the elements. The cracks were only found between SL-Decks and not at the joints to the abutment elements. They also only occurred in the bottom surface of the elements. Increasing the SL-Deck thickness and the cross reinforcement will in future arches increase the crack resistance. Furthermore, the curing time of the concrete and mortar before post-tensioning has an influence. In a previous test where the concrete had been cured

for a longer time these cracks did not appear although the thickness of the deck and the pre-stressing force were identical. In later PC-Arches (the applied case in Chapter 6) additional reinforcement was applied transversely below the ducts in the SL-Decks and sufficient curing time was applied to avoid any cracking which potentially could lead to corrosion of the tendon.

The last part of the pre-lifting assembly was grouting the cable duct.

See *Figure 38* for pictures of the assembly steps. A) was the vertical positioning in the desired shape (darker surfaces are the LAC blocks, B) was at time when formwork was put up for casting of joints, C) was two days later when formwork was removed, and post-tensioning was performed, and D) was after the cable duct had been grouted, and the arch was ready for lifting

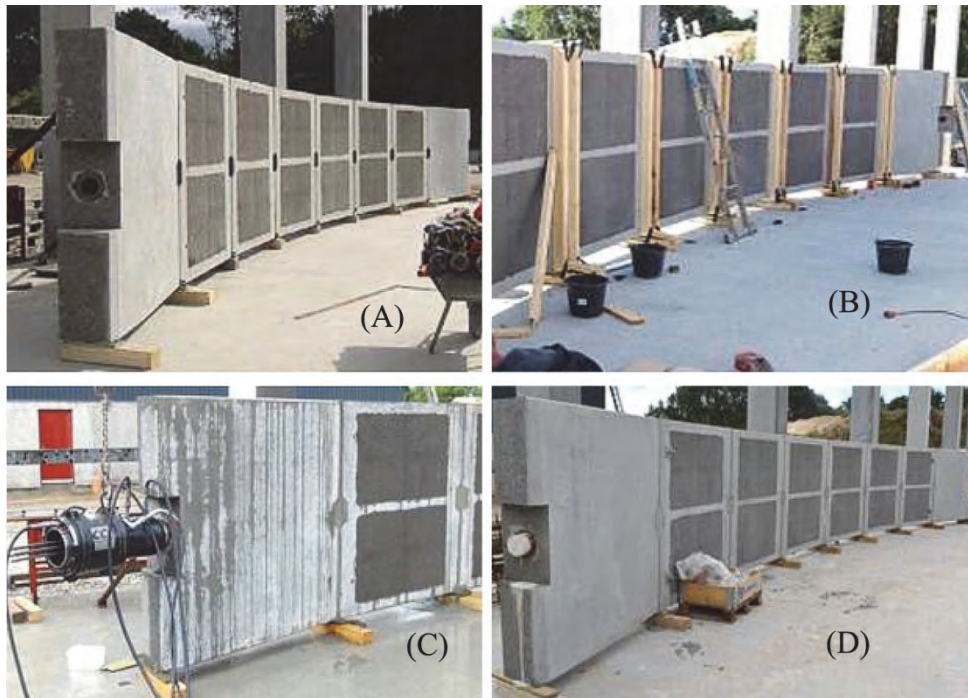


*Figure 38: Assembly steps for PC-Arch.*

This method was selected in order to minimize crane time, which is often a costly component of bridge construction. If the PC-Arches were assembled on temporary scaffolding, a large, mobile crane would be required to lift and erect the arch before the next arch assembly could begin. By assembling each arch on its side, a smaller, less expensive crane mounted on a truck can be used to handle the individual SL-

Decks. After assembling several PC-Arches, a larger crane can then be brought to the site to quickly erect all the arches at the same time.

### **4.3 Lifting of single arches**

In general the lifting points, for the process of lifting a whole arch, are positioned in the regular concrete in the SL-Decks. This is because the resistance to punching shear is better than in areas, where the LAC blocks are present.

The optimal lifting method in the lifting test was determined on beforehand with analyses in the FE-program: Autodesk Robot Structural Analysis, and by simple hand calculations (not included in the thesis). Mid-air rotation of the arch was necessary, and the number and position of lifting points were studied to minimize bending moments during the lift. The lifting sequence can be summarized as:

- 1) Using two lifting points to vertically lift the arch from its “on-side” orientation.
- 2) Connecting two additional lifting points, and then rotating the assembly in mid-air.
- 3) Transporting the arch in its horizontal orientation.

#### **4.3.1 Lifting points and rotation in mid-air**

At first the arch was lifted in two points. This first vertical lift should be performed without the arch slanting to the side when leaving its supports. The balance points were found to be slightly into the first SL-Decks next to the abutment elements.

When hanging in the air, the arch was then rotated and transported to the site of erection. Rotating and lifting the arch in its horizontal orientation with the same lifting points used for the initial vertical lift resulted in bending moments less than the arch’s capacity. Therefore, the same lifting points were chosen for both vertical and horizontal lifting (although two additional points were added for the horizontal lift). The optimal position for the four-point, horizontal lifting of the arch is two points approximately in the middle of the first SL-Decks adjacent to the abutment elements on each end. However, positioning the lifting points here was not chosen due to the LAC blocks in the SL-Decks in this area. *Figure 39* shows the position of the final lifting points (circled in red).

A factor of 1.65 was applied to the static analysis results in order to account for dynamic loading.

During this assembly and lifting test, the mid-air rotation was performed by a small crane as well as a large truck working together. They lowered the arch onto a temporary support, supporting the arch at the  $\frac{1}{4}$  points. Thereafter, the truck could

lift and transport the arch to the erection site. In future Pearl-Chain Bridge erections, such maneuvering can be performed with one mobile crane alone, by means of a crane hoist. In future Pearl-Chain bridges, the arch elements should be assembled next to the erection site so that the total number of arches for the PC-Bridge can be lifted and put on prepared foundations one by one with a mobile crane.

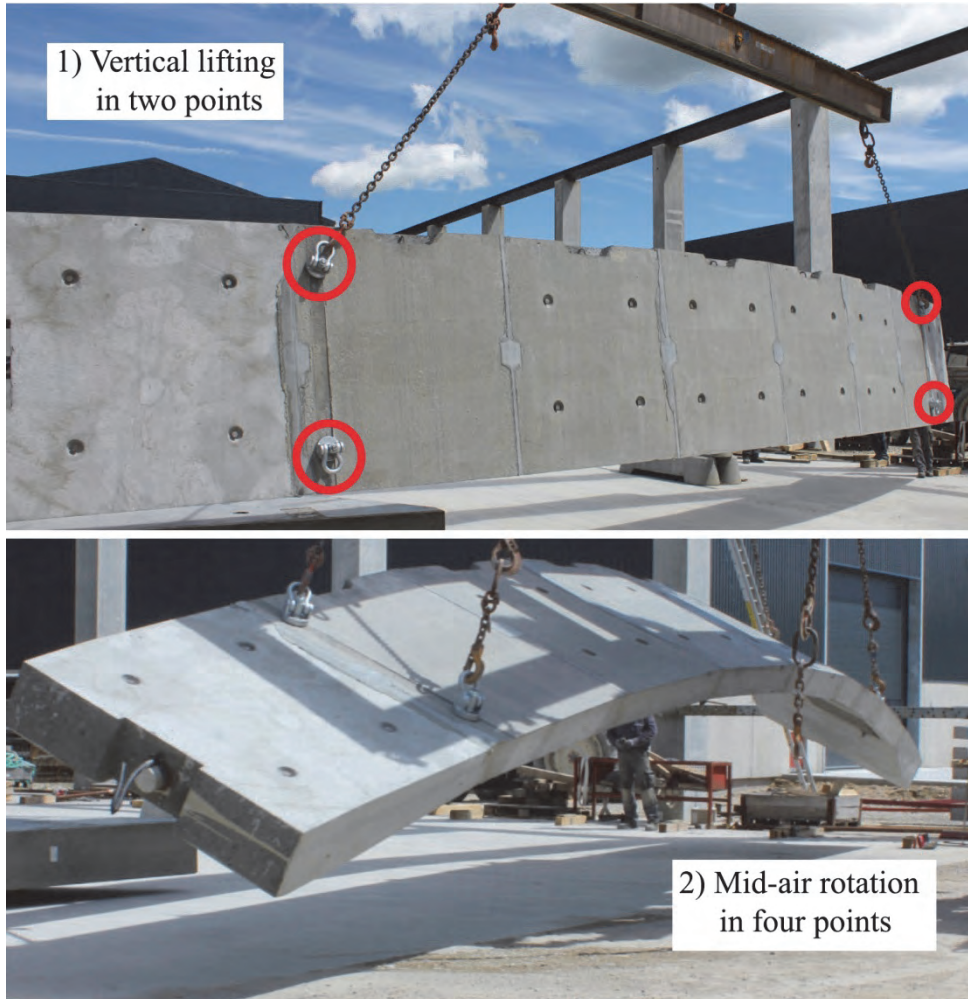
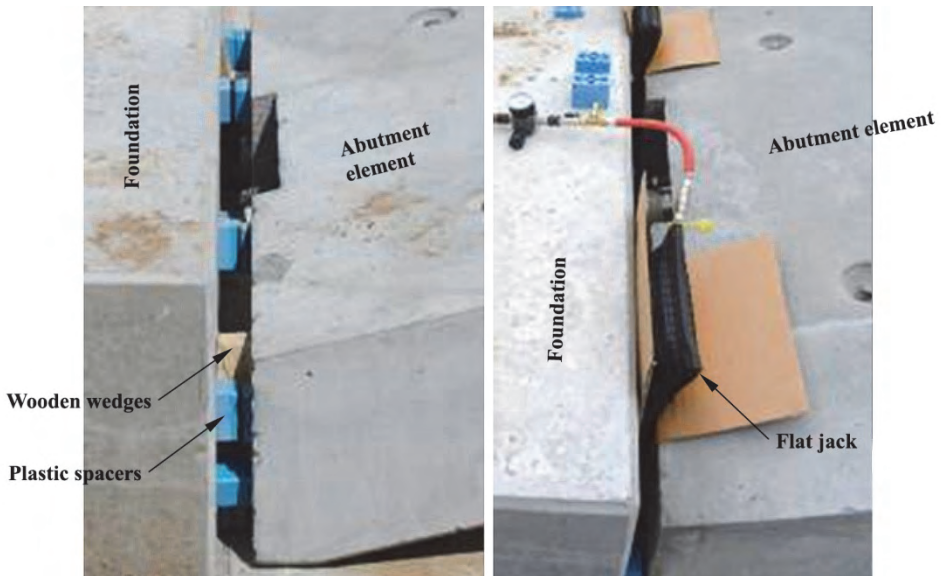


Figure 39: Lifting and mid-air rotation of PC-Arch.

## 4.4 Positioning on prepared foundations

Positioning of the arches on a prepared foundation was a significant part of the assembly process. The design was made with space between the foundation and the arches when positioning them on the foundation. Since the arches transfer horizontal forces as well as vertical forces to the abutments, the positioning has to be precise. Even small horizontal settlements of the arch springings will incorporate undesired bending moments in the arch.

Two methods were tried when positioning the arches: The first PC-Arch was positioned on the foundation, and plastic and wood wedges were put in the space to regulate the span length. The span of the second PC-Arch was adjusted by two hydraulic flat jacks at each springing. The latter method was less time consuming. The remaining space between the arches and the foundation was later cast out with a mortar. The hinge behavior of the „Orthogonal saddle bearing“ springings were previously analysed in Chapter 3. *Figure 40* shows the two methods for positioning the arches at the foundation. On the left is seen the method using wooden wedges and plastic spacers, and on the right the position of the arches were held by 6 bar of hydraulic pressure in flat jacks.



*Figure 40: Connection detail between foundation and arch.*



*Figure 41: Two adjacent PC-Arches after assembly and lifting.*

After pouring the mortar between the arch and foundation the two PC-Arches were ready to be prepared for subsequent load-testing (*Figure 41*), which is the content of Chapter 5.

# 5 TEST OF ARCH THEORY

The two PC-Arches in Chapter 4 were assembled and lifted into position on a foundation. Now, the same two 13 m span arches are used when performing two load-tests in Chapter 5: Test 1) Experimental results on the behavior of the PC-Arches, and the SL-Decks when used in an arch. Test 2) Ultimate load carrying capacity of the PC-Arches. Conservatively, no pervious concrete filling was used on top of the arches in the tests.

The chapter is based on the journal paper #5: “Full-scale load tests of Pearl-Chain Arches”.

The scope of the load tests was to:

- Monitor deflections and strains during loading, and determine if forces were transferred between arches.
- Investigate the behavior of the straight SL-Decks during loading, when used in an arch structure.
- Compare the ultimate load from testing with an analytical model.
- Identify any clear warnings before the ultimate capacity was reached.

## ***5.1 Preparing the test***

In Test 1, the arches were loaded with a total of 66.0 tonnes (648 kN) at the  $\frac{1}{4}$  point of the span. Ten months later, they were re-tested in Test 2 to determine the load carrying capacity, which was 98.8 tonnes (970 kN). Both tests were scheduled for the same day, but due to problems with the loading crane, Test 2 was delayed.

### **5.1.1 Geometry and materials**

The geometry and level of pre-stressing was given previously in Chapter 4: Each of the two arches consisted of eight elements (six SL-Decks and two abutment elements). The SL-Decks were approximately 1.60 m long, 1.75 m wide, and 220 mm in

section height. This gave space for four LAC blocks across and two lengthwise in each deck element. The resulting area of the normal concrete in an arch cross section with LAC blocks was 0.196 m<sup>2</sup>. The SL-Decks had 10 pre-tensioned mono strands in the bottom of the cross section with a concrete cover of 60 mm, and 10Y20 bars (550 MPa mild steel) in the top of the cross section with concrete cover of 30 mm. The material properties of the strands were the same as the post-tensioning cables. See *Figure 42* for section cuts of the SL-Decks

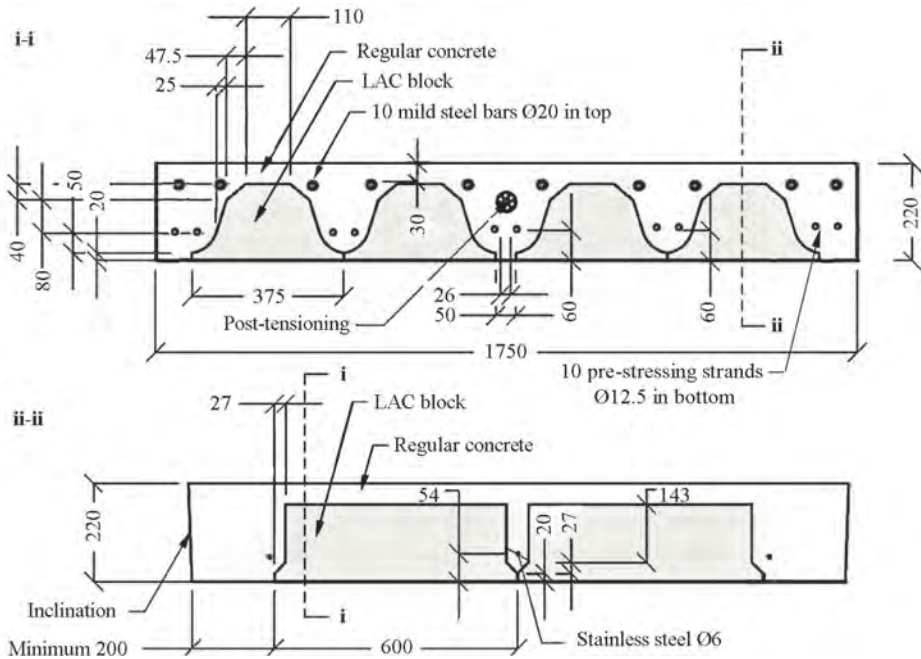


*Figure 42: Detailed section cuts of SL-Deck type in the test arches.*

The normal concrete had a characteristic compressive cylinder strength of  $f_{ck} = 59$  MPa and a Young's modulus of  $E_{cm} = 39$  GPa. The concrete's theoretical strain at maximum stress was  $\epsilon_{c1} = 0.26$  ‰. *Figure 43* is based on 28 day tests of the uniaxial compressive strength ( $f_{cm}$ ) combined with values of the Young's modulus ( $E_{cm}$ ) and strains ( $\epsilon_{c1}$  and  $\epsilon_{cu1}$ ) calculated with the Eurocode 2 [48]. Cored specimens were tested after the collapse in Test 2 and still gave approximately the same Young's modulus and strength.

The true curve would have been dependent on a variety of factors (e.g., mix design, aggregate size and type, and admixtures).

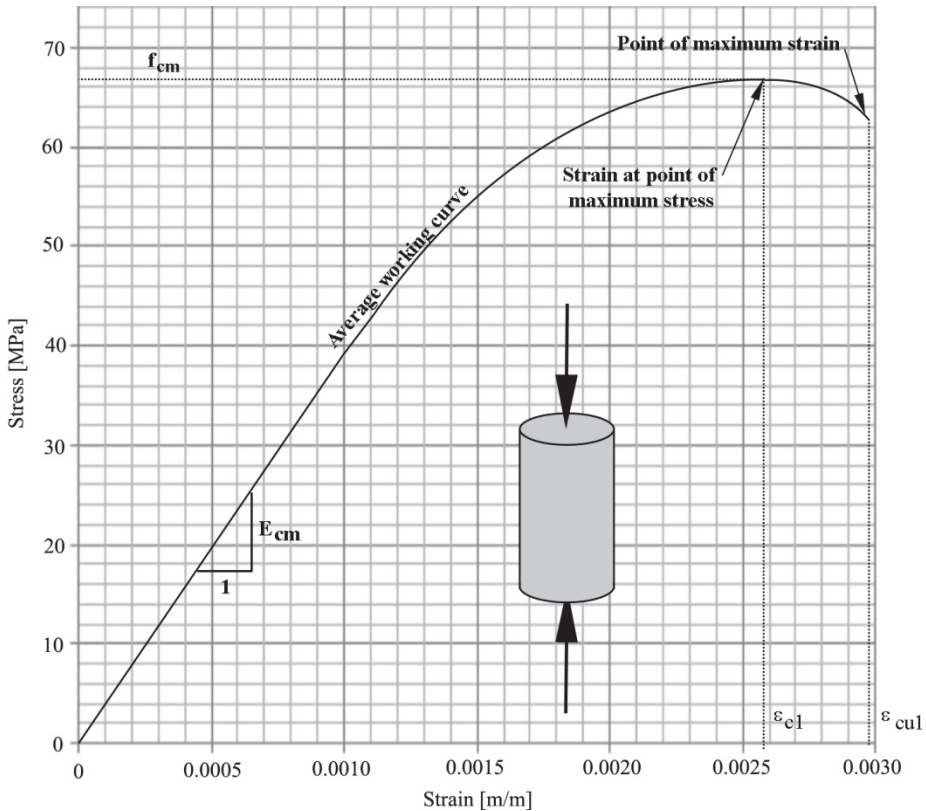


Figure 43: Theoretical working curve for the normal concrete in the SL-Decks.

Reinforced concrete plateaus were cast on top of the arches between the 1/8 and 3/8 points of the span. These plateaus provided a level, horizontal surface for load application at the span's 1/4 point. Both arches had their own, isolated plateau, each weighing an estimated 30 kN. Individual plateaus were chosen because one goal was to determine if an asymmetrical load would be shared between the arches. Therefore, a gap between the plateaus prevented the premature transfer of force at the load point.

The two arches were tied together with Hammerhead joints in every SL-Deck. The Hammerhead joint mortar had compressive cylinder strength of 12 MPa, and a Young's modulus of 23 GPa.

To avoid test result interference from horizontal settlement of the abutments, a post-tensioned abutment plate was cast as a foundation for the test arches. It consisted of concrete with characteristic compressive cylinder strength of 43 MPa, and a corresponding Young's modulus of 36 GPa. Three 7C15 post-tensioning cables were used to post-tension the abutment plate (similar to those in the arches). The

distance between the ducts was 1.2 m. The ends of the abutment plate were also heavily reinforced with mild steel. *Figure 44* shows the test setup.

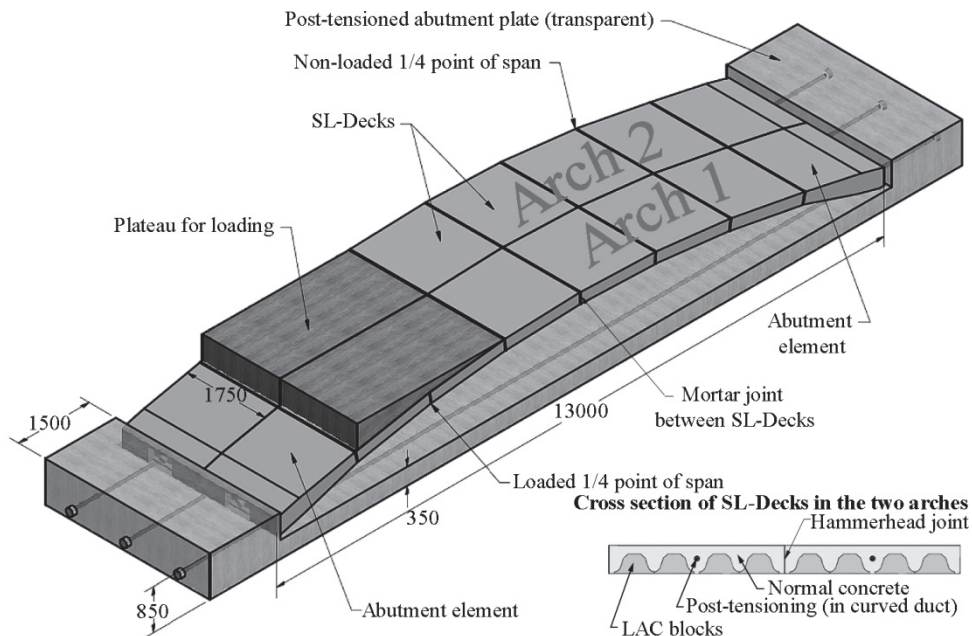


*Figure 44: Test setup of two 13 m span PC-Arches placed on a post-tensioned abutment plate. Unit is mm.*

Mortar was poured between the PC-Arches and the abutment plate. This was done to provide a smooth, continuous bearing surface for the lateral and vertical support reactions. Statically, it was expected that these joints – which lacked any sort of crossing reinforcement – would show a hinge response. In Chapter 3 this connection, a “orthogonal saddle bearing hinge”, was investigated in detail.

## 5.1.2 Measurement Methods

### 5.1.2.1 Arch Deflections

Deflections were measured with three different methods: LVDT’s, a leveling instrument, and the ARAMIS (DIC) system.

Twelve LVDT’s were attached to different locations of the arches. Two of the LVDT’s measured the horizontal settlement of the abutments, while the other 10 measured vertical deflections along the span.

Vertical deflections were also measured by using a leveling instrument. The instrument was placed approximately 7 m from the side of “arch 1”. Rulers were attached to the sides of both arches, and the deflection was measured through the leveling instrument when the load was applied. A total of 12 rulers were attached: 7

on “arch 1” and 5 on “arch 2”. The leveling instrument was used both to verify the readings from the LVDT’s, which were more accurate and precise, and to measure the deflections at locations where the LVDT’s could not be applied. This was at the loading plateau, and at the  $\frac{3}{4}$  joint, where detailed photographs were taken.

Figure 45 shows the position and notation of all LVDT’s and rulers. The measuring devices were positioned as close to the joints between SL-Decks as possible, and the joints were each given a location name: A, B, C, etc. The LVDT’s named 1 and 2 measured the horizontal movement of the abutments at the end of “arch 1”.

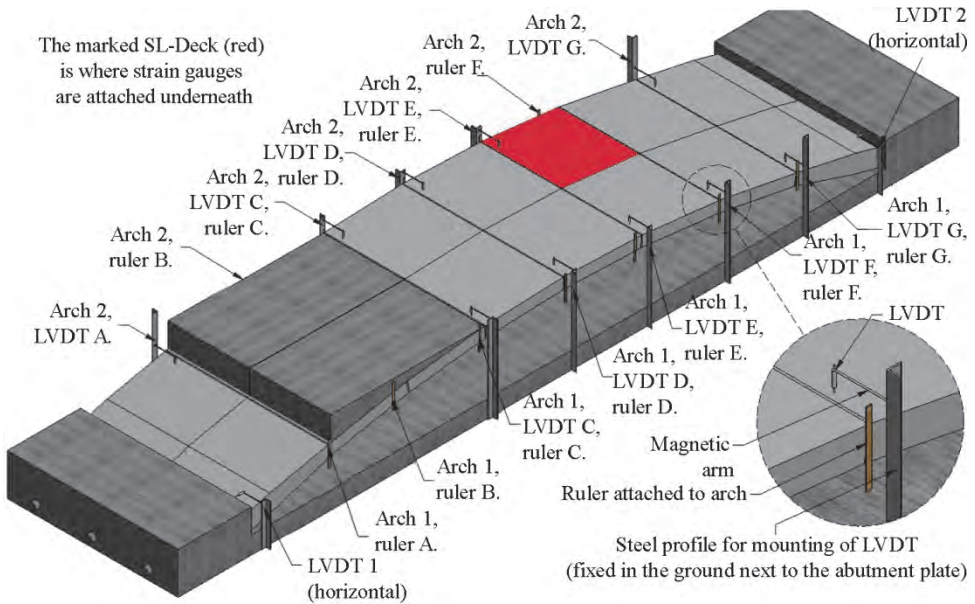


Figure 45: Position of all LVDT’s and rulers for measurement of deflections on “arch 1” and “arch 2”.

The third method relied on the ARAMIS software.

### 5.1.2.2 Strain Measurements

Two methods were used to acquire strain measurements on the arches: ARAMIS and concrete strain gauges.

ARAMIS was introduced in Chapter 3, and is a software package with Digital Image Correlation technology [46], and is based on photographs taken before and during testing.

Photographs were taken on the side of the arches for processing in ARAMIS. The first two cameras were in location B (the loaded  $\frac{1}{4}$  point of the span), two other cameras were in location F (the non-loaded  $\frac{1}{4}$  point of the span), and the last two cameras were placed at the joints to the abutment plate in both ends of “arch 2”, see

Chapter 3. All cameras were perpendicularly aligned to the arch surface, and several spot lights gave indirect light for best possible photos. The 2d ARAMIS version was used.

Strains were also obtained with concrete strain gauges, which were applied underneath “arch 2” (the SL-Deck is marked red in *Figure 45*). Eight, 50 mm long, concrete strain gauges were attached, which measured the strain in the longitudinal direction of the arch. They were positioned at location F, in two rows of four strain gauges, as shown in *Figure 46*. A longitudinal spacing of 200 mm between gauges was used for each row, and all gauges were placed on the deck’s normal concrete. In *Figure 46*, the dark rectangles are the bottoms of the LAC blocks. Line A is the position of a cross section in the SL-Deck through only normal concrete, and line B is the position of a cross section with both normal concrete and LAC blocks. The bottom of the non-loaded side was expected to be in compression during testing. Furthermore, it was expected to be one of the critical locations when approaching the ultimate load carrying capacity. The other important locations were in the  $1/8$ ,  $1/4$ , or  $3/8$  points of the span in the loaded side.

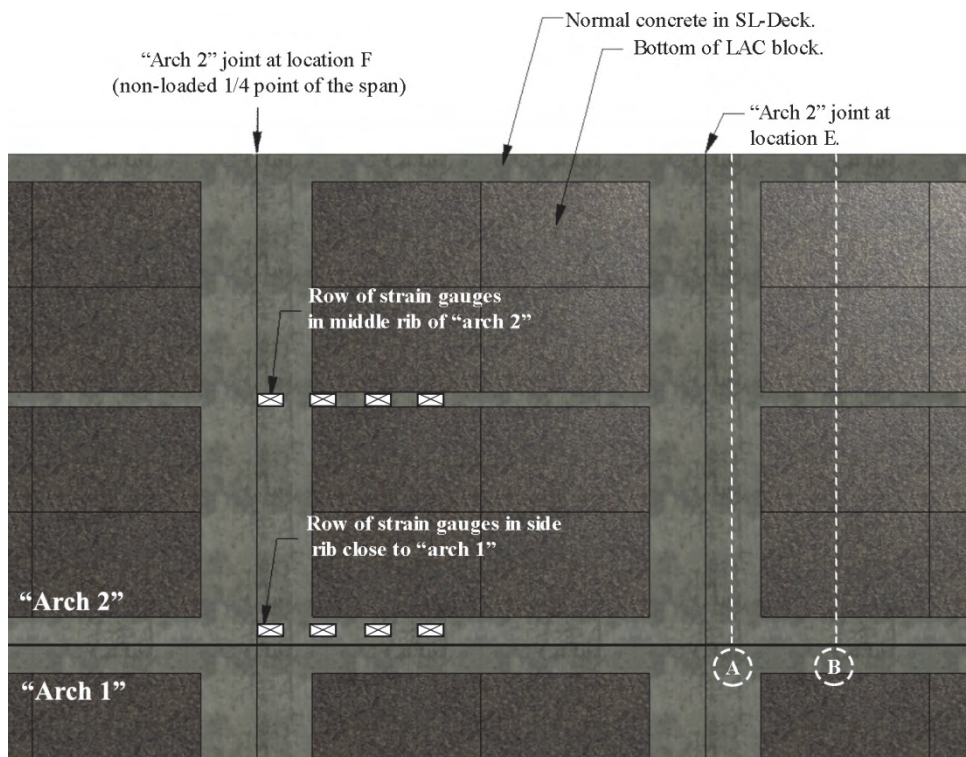


*Figure 46: View from underneath “arch 2” at the joint at location F (for locations see Figure 45).*

### 5.1.3 Analytical calculations

Before testing the arches, analytical calculations were performed in order to determine the initial strains at the most critical positions, and the expected load at fracture.

#### 5.1.3.1 Initial strains

The self-weight (including the plateaus), pre-tensioning force within the individual SL-Decks, and the post-tensioning force were included in this calculation. *Figure 47* shows the sequence of initial loadings. State I is the strain distribution after pre-tensioning the SL-Deck. State II represents the post-tensioning of the arch and the application of its self-weight. States IIIA and IIIB represent the strain distributions at the loaded and non-loaded  $\frac{1}{4}$  points, respectively, after applying the weight of the loading plateau. Those  $\frac{1}{4}$  points were the theoretically most critical locations in the span assuming the load as being concentrated at the  $\frac{1}{4}$  point. In reality the load on the plateaus was expected to be uniformly distributed from the  $\frac{1}{8}$  to  $\frac{3}{8}$  of the span in the first load steps. Later as the arch deflects, the load would be expected to concentrate in the regions of the  $\frac{1}{8}$  of the span, and the  $\frac{3}{8}$  of the span. This is due to the plateaus having a bending stiffness as well.

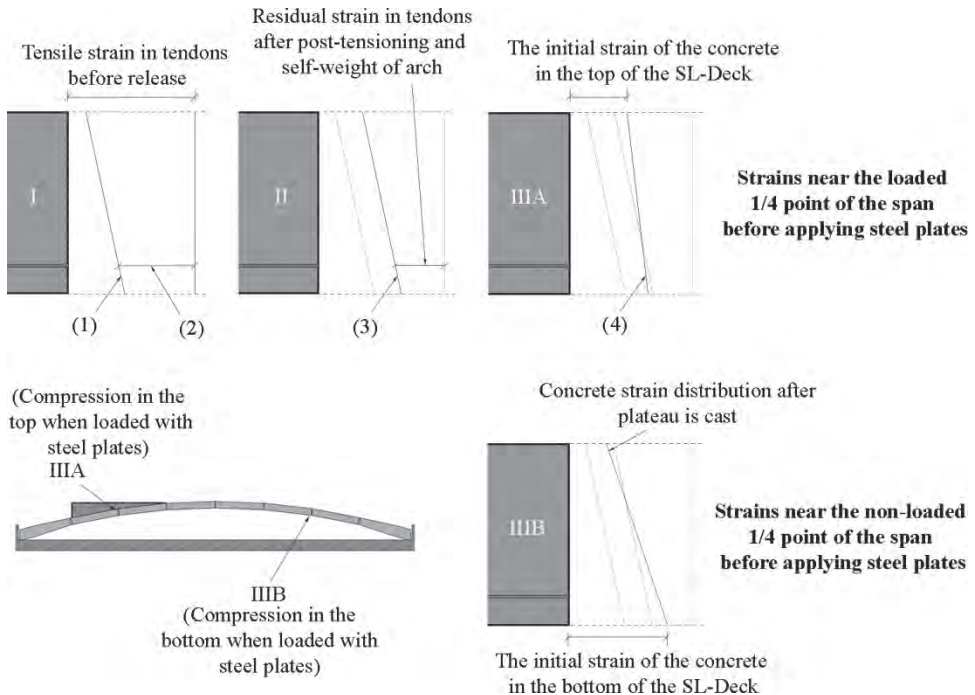


*Figure 47: Initial elastic strain distributions in a SL-Deck in two positions before loading with steel blocks. The size of the strain distributions are not to scale.*

In *Figure 47* (1) is the concrete compressive strain distribution from after release from pre-stressing bed, (2) is the tendons tensile strain after release from pre-stressing bed, (3) is the increased concrete compressive strain after post-tensioning and arch self-weight, and (4) is the final initial concrete strain distribution after the plateau is cast near the loaded  $\frac{1}{4}$  point of the span.

The normal force in each arch from the initial contributions, less the expected initial losses, was 3251 kN. The calculated contributions to the normal force were: 166 kN for the arch dead load, 1520 kN for the eccentric pre-stressing strands, 1544 kN for the central post-tensioning cable, and 107 kN for the plateau dead load. The bending moment from the eccentric pre-tensioning was negative. In a cross section with LAC blocks it was -111 kNm, and in a cross section of only normal concrete it was -76 kNm. In the joints between SL-Decks there were no contributions from pre-tensioning.

The moment contribution from the dead load of the plateau was 43 kNm close to the loaded  $\frac{1}{4}$  point of the span, and -28 kNm close to the non-loaded  $\frac{1}{4}$  point of the span. By Navier's formula we achieve the following elastic, compressive strains:

- In the bottom of the non-loaded side around location F:
  - With a full cross section of normal concrete the strain was 0.038%.
  - With a cross section including LAC blocks the strain was 0.10%.
  - In the joints between SL-Decks the strain was 0.0136%.
- In the top of the loaded side around location B:
  - With a full cross section of normal concrete the strain was 0.0142%.
  - With a cross section including LAC blocks the strain was 0.0073%.
  - In the joints between SL-Decks the strain was 0.0049%.

The SL-Decks were chosen to have pre-tensioning in the bottom of the cross section only (cf. *Figure 42*), and this, along with the position and mass of the plateau, is the reason for the largest initial strain in the bottom of the non-loaded side.

### 5.1.3.2 *Expected load at fracture*

The load at fracture was at first calculated to be 56 tonnes (550 kN) with the assumption of the full load being concentrated in the  $\frac{1}{4}$  point of the span. As mentioned, the true static system is closer to two point loads in the  $\frac{1}{8}$  point, and  $\frac{3}{8}$  points of the span. This is the basis of the following simplified calculation:

By using Eq. 1.9 the horizontal reaction is determined. The steel tension tie properties are changed to fit the properties of the abutment plate in the test:

$$H_{elastic} = \frac{\int \mu(x) \cdot y(x) \cdot ds}{\int y(x)^2 ds + L \left( \frac{I_{arch}}{A_{arch}} + \frac{E_{arch}}{E_{plate}} \cdot \frac{I_{arch}}{A_{plate}} \right)}$$

Then the bending moment,  $M(x)$ , and normal force,  $N(x)$ , is found. An example of the shape of the moment distributions is seen in *Figure 48*.

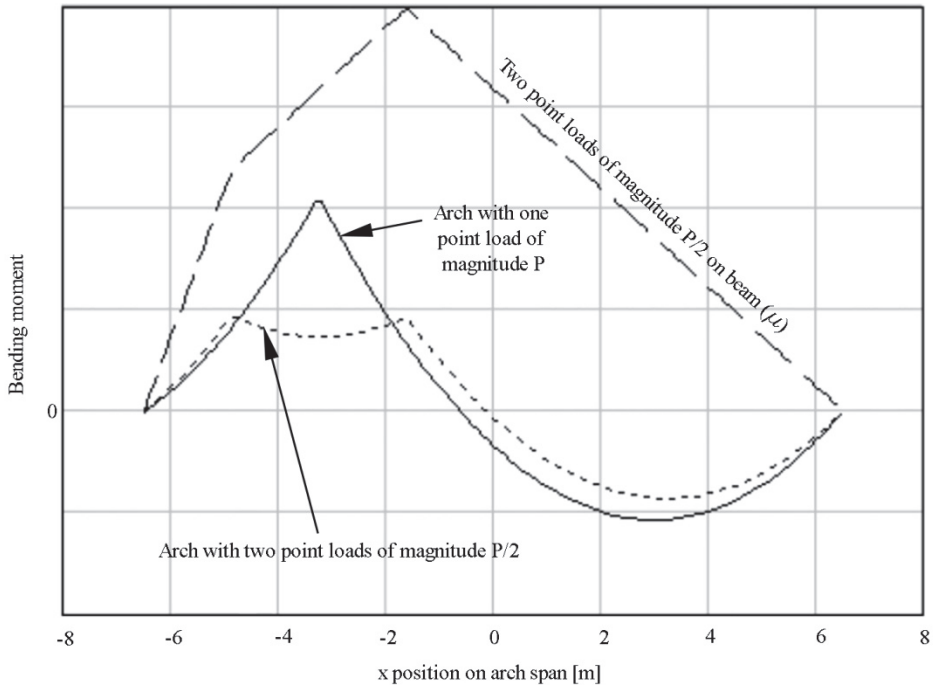


Figure 48: Bending moment in the arch from applied load.

The  $M(x)$ , and  $N(x)$  depend on the total load,  $P$ . The bending moment capacity of the arch depends on the normal force. Using an iterative approach the direct load carrying capacity is found in terms of  $P$ :

1. Choose a  $P$ , calculate  $H$ , and find  $M(x)$ , and  $N(x)$ .
2. In the assumed most critical positions ( $1/8$ ,  $1/4$ , and  $3/8$  of the span in the loaded side, and the  $1/4$  point of the span in the non-loaded side) calculate  $N$  and  $M$ .
3. For the different magnitudes of  $N$  find the moment carrying capacity,  $M_d$ , of the three possible cross sections in the arch: A section with LAC blocks in the SL-Deck (*Figure 42*), a section with no LAC blocks in the SL-Deck, and a section through a joint between SL-Decks. In this step the value of  $N$  from

the load,  $P$ , is increased by the normal force from pre-stressing and dead load.

4. Compare the numerical value of  $M$  and  $M_d$  for all the positions on the arch span, and all types of cross sections in these positions. In this step the relevant initial bending moments are added to  $M$  found from the load,  $P$ . If  $|M| < |M_d|$  in all possible combinations, then increase  $P$  and repeat the iteration.

By means of this purely elastic approach the load carrying capacity was found to be  $P = 86.5$  tonnes. The capacity is found to be reached in the non-loaded side in the  $\frac{1}{4}$  point of the span in a cross section with LAC blocks. At that point only little capacity is left in the loaded side in the  $\frac{3}{8}$  point of the span in the joint between SL-Decks. Therefore, the effect of possible plastic hinges is presumably insignificant.

## **5.2 Test results**

The bridge assembly was tested with two separate phases, with different investigative objectives for each test. In Test 1, deflections and strains were measured during loading to 66 tonnes (648 kN), when the test was stopped for safety reasons. This first test gave evidence for the transfer of forces through the Hammerhead joints, and permitted the study of the distribution of strains within an SL-Deck. Test 2, on the other hand, was conducted in order to determine the specimen's ultimate load capacity, and to observe its collapse mechanism. *Figure 49* shows a photograph taken during Test 1.

Test 1 was performed with the following procedure. The two arches were loaded with steel blocks, each weighing 10 tonnes (98 kN). First "arch 1" was loaded with one block, and then "arch 2" was loaded with one block. This sequence repeated until three blocks were positioned on each arch, and then the arches were unloaded in reverse order. In Test 1, the maximum applied load at the  $\frac{1}{4}$  point of the span was 66 tonnes (648 kN), which included the mass of the plateaus. Test 2 was executed similarly, but with blocks weighing 6.4 and 10 tonnes. The specimen was loaded to failure of the arches, which occurred at a total load of 98.8 tonnes (970 kN). *Figure 50* shows the loading as function of time for Test 2.

### **5.2.1 Test 1 – testing in the linear elastic range**

#### *5.2.1.1 Deflections and deformations*

The deflections measurements from the LVDT's were similar to those measured by the leveling instrument.



Figure 49: Test 1. Six steel blocks, each weighing 10 tonnes, were set on the plateaus on "arch 1" (near side in photograph) and "arch 2".

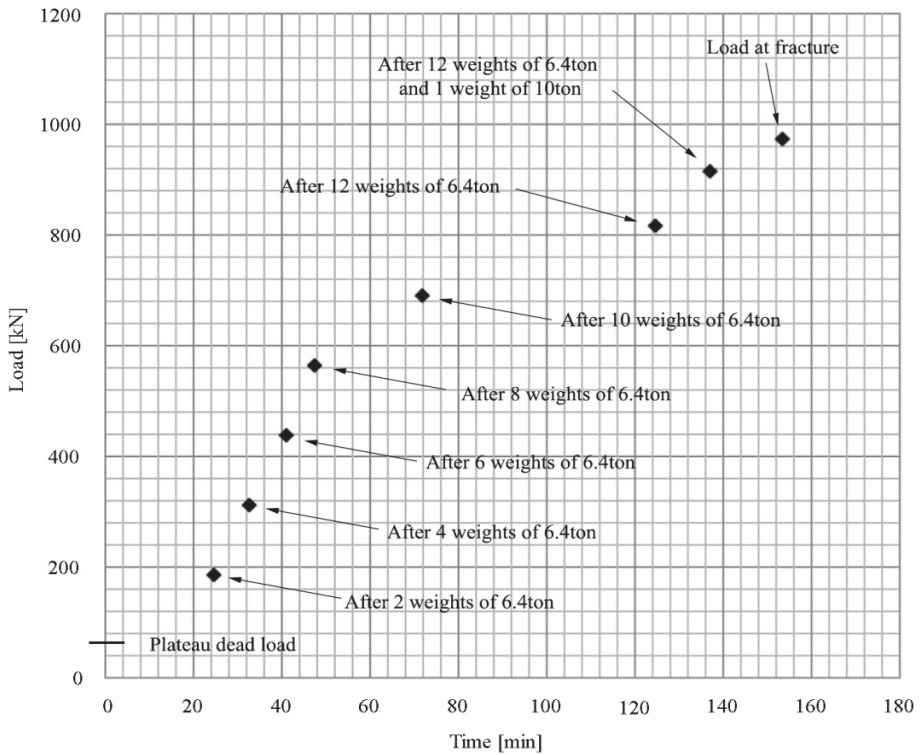
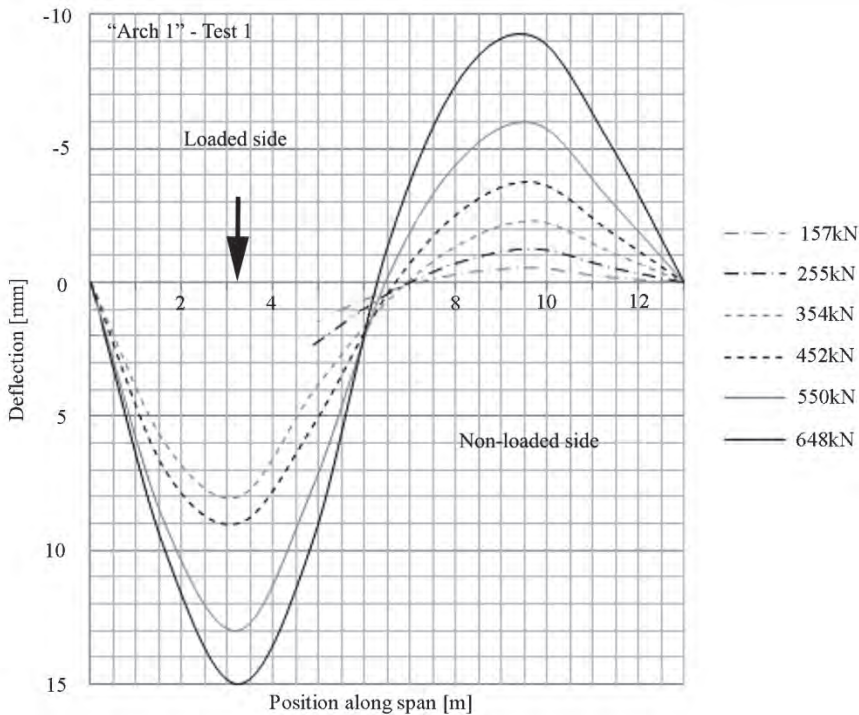


Figure 50: Loading sequence for Test 2.

Because of the LVDT's gave readings every five seconds, whereas the rulers were only read after every change in loading, only the LVDT data is presented here. In *Figure 51*, the deflection of "arch 1" is given, and in locations of no LVDT instruments, the deflections given by adjacent LVDT's have been supplemented with readings from the leveling instrument. For very small deflections, however, the leveling instrument lacked the resolution needed for useful results. During Test 1, the largest deflection on the loaded side was 15 mm. In Test 2, this value was 32 mm at the load level before fracture.



*Figure 51: Deflection of "arch 1" for various total loads (accumulated from both arches) at the ¼ point of the span, not including self-weight.*

*Figure 52* shows the measured deflections of each arch as the loading progressed. The plot indicates that the Hammerhead joints transferred forces between the arches. However, there was some deviation between the deflections because of the unsymmetrical loading. The deflection in "arch 1" increased both when load was applied to "arch 1", but also when applied to "arch 2". The results from LVDT 1 and LVDT 2, measuring horizontal settlement of the abutments, showed insignificant deflections of less than 1/3 of a mm. Therefore, all deflections in "arch 1" when applying load on "arch 2" must come from forces being transferred through the Hammerhead joints.

By comparing the arches' deflections at locations C, D, E, and G, it appears that the position closest to the loading plateau, had the largest difference in the deflection between the two arches. In *Figure 52*, it is seen that at position C, "arch 1" deflected more than "arch 2" when the load was applied to "arch 1", and vice versa. This did not happen in the same way for positions D, E, and G. This trend was expected because the forces being transferred through the Hammerhead joints were likely largest at the location of applied load, but were smaller when moving away from that position. The Hammerhead joints were designed to transfer more than 100 kN vertical force each.

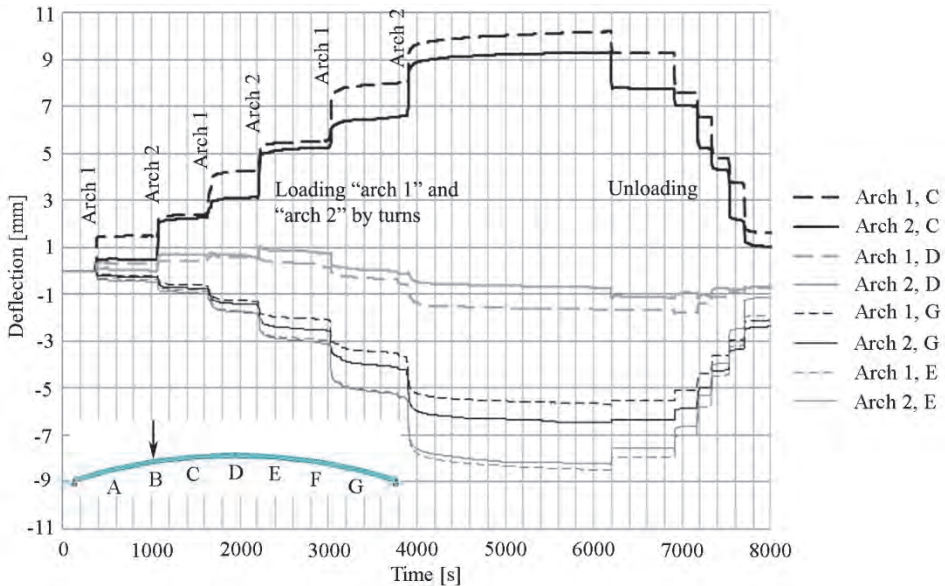


*Figure 52: Test 1. Comparison of deflections of "arch 1" and "arch 2" at location C, D, E, and G (downwards is considered positive).*

An ARAMIS system was used to monitor the arch deformation near the loaded and non-loaded  $\frac{1}{4}$  points of the span (locations B and F, respectively). Vertical deformations found by ARAMIS corresponded well with the measurements from the LVDT's and the leveling instrument. Digital Image Correlation (DIC) enables crack growth analysis by limiting the display output to strains above a certain value. Such analyses were complete for both the loaded and non-loaded  $\frac{1}{4}$  points of the span. The non-loaded  $\frac{1}{4}$  point (location F) did not show any cracking after applying the total of 66 tonnes, while some cracks appeared in the loaded  $\frac{1}{4}$  point of the span (location B). *Figure 53* shows the location of the DIC measurements (a), the vertical deflection contour plot at 648 kN load (b), and the identified cracks at 648 kN load (c). One crack developed between the plateau and arch, and another one from the

arch into the plateau. Neither of those cracks affected the behavior of the arch itself. The plateau was not designed to transfer any significant shear to the arch – only direct vertical load. Therefore, some sliding between the two surfaces was expected. The separation was expected and verified the assumption of the static system being with two concentrated forces: one force at the 1/8 of the span, and one at the 3/8 of the span. The plateaus likely had a large bending stiffness, and as the arch settled below the plateau, the load went from being uniformly distributed on the arch to being two point loads on the arch – one close to the 1/8 point of the span, and one close to the 3/8 point of the span. This was due to the arch deflecting more than the plateau, so that the contact surface was limited to the two areas close to the 1/8 and 3/8 points.

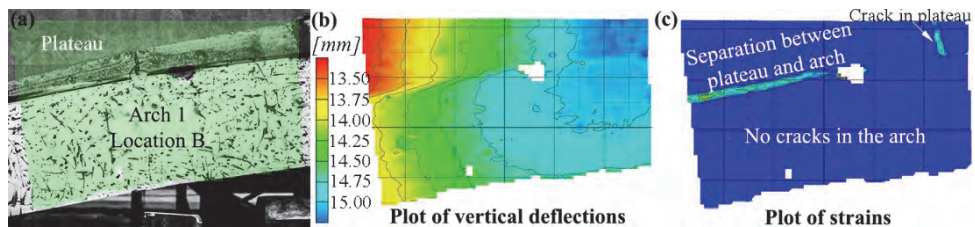


Figure 53: At 648 kN load: ARAMIS output for the loaded quarter point at location B on the side of arch 1.

### 5.2.1.2 Strains in SL-Decks

At location F on “arch 2”, concrete strain gauges were attached to the underside of the arch, see *Figure 46*. The measured strains (in the longitudinal direction of the span) are shown in *Figure 54*. The vertical tick marks on the time axis indicate the time when each new 98 kN load was applied.

The results show that the largest measured strains developed in the concrete ribs in a cross section of the SL-Deck where the LAC blocks were located. This was expected, since the cross sectional area of the normal concrete was smaller in this zone compared to the zone with no LAC blocks at the ends of an SL-Deck. The thinnest rib was in the middle of the element, and the strains there were approximately 100% larger (at location “Mid 60 cm”) compared to the cross section without LAC blocks (at location “Mid 0 cm”). The strain gauge at “Mid 20 cm” was positioned at the transition between the cross sections with and without LAC blocks. Here, the magnitude of the strain was between the two extremes, since the normal force in the SL-Deck was being transferred from the large rectangular concrete section to the rib, which had a smaller cross sectional area.

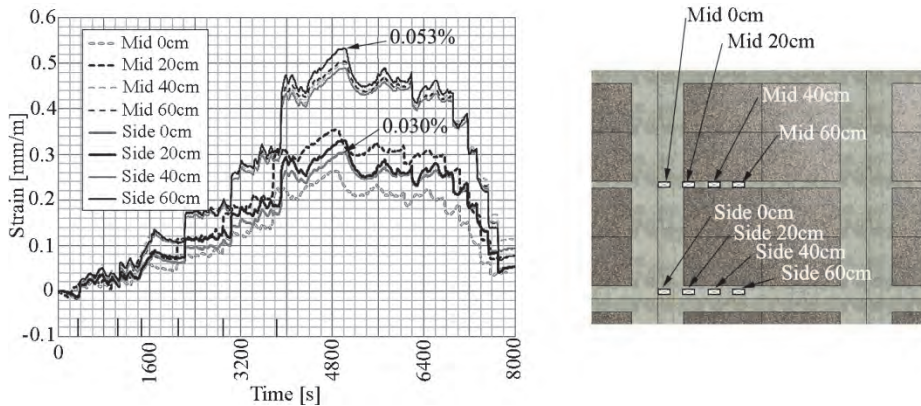


Figure 54: Strains from the eight strain gauges during Test 1 (not including initial strains).

The same trend occurred for the strain gauges at the side of the SL-Deck, although the concentration of the strains occurs a little further into the side rib. Where the “Mid 40 cm” and the “Mid 60 cm” measurements are almost similar, the difference between the “Side 40 cm”, and “Side 60 cm” measurements are up to 9%. Also, the increase in strain from “Mid 0 cm” to “Mid 20 cm” was close to 40%, while the increase from “Side 0 cm” to “Side 20 cm” was less than 9%. The reason for the difference in how fast the strains concentrated was due to the ribs’ relative sizes - the side rib was wider than the middle rib. Furthermore, a Hammerhead joint was located in proximity of the strain gauges “Side 40 cm” and “Side 60 cm”. This could have had an effect on the results.

## 5.2.2 Test 2 – Testing to failure

The fracture load was 98.8 tonnes (970 kN) which was 14% higher than the analytically calculated result of 86.5 tonnes (849 kN). Plastic hinges formed in both the loaded and non-loaded side of the arches during the last loading interval: from 94% to 100% of the fracture load. So they did not contribute to a 50% to 100% larger load capacity as explained by Jain [35], who stated that this occurs for arches with rectangular concrete cross sections and mild steel reinforcement.

Several different damage warnings were observed in the structure before the ultimate capacity was applied. Figure 55 shows three photographs at the moment of collapse: 1. Plastic hinges forming on the loaded side, and then on the non-loaded side. 2. Loss of structural stability (a four hinged arch which is free to move) at the moment of fracture. 3. Final collapse.



*Figure 55: Sequence of observed failures preceding collapse.*

### 5.2.2.1 Test of theory

The collapse occurred after two plastic hinges developed in the arch. The plastic hinges formed at the  $3/8$  and  $5/8$  points of the span. Theoretically, the most critical positions were expected to be in the  $3/8$  of the span in the loaded side, and at the  $1/4$  point of the span in the non-loaded side, but only if the specimen behaved as a two-hinged arch. The cross sections where the hinges formed though were the same as predicted: In the joint in the loaded side and in the SL-Deck with LAC blocks in the non-loaded side.

Hinge behavior was assumed at the interfaces between the foundation plate and the arch ends because reinforcement was not used to tie those elements together. At a low level of load ( $< 300$  kN), however, the ARAMIS analysis showed limited rotation at the abutments, which suggested that the support connections were close to being fixed instead of hinged. At larger loads ( $> 300$  kN), clear hinge effect was observed, although it remained far from an ideal hinge with zero bending moment. A plot based on numerical calculations in the program Robot Structural Analysis [42] shows the difference in bending moment distributions, see *Figure 56*.

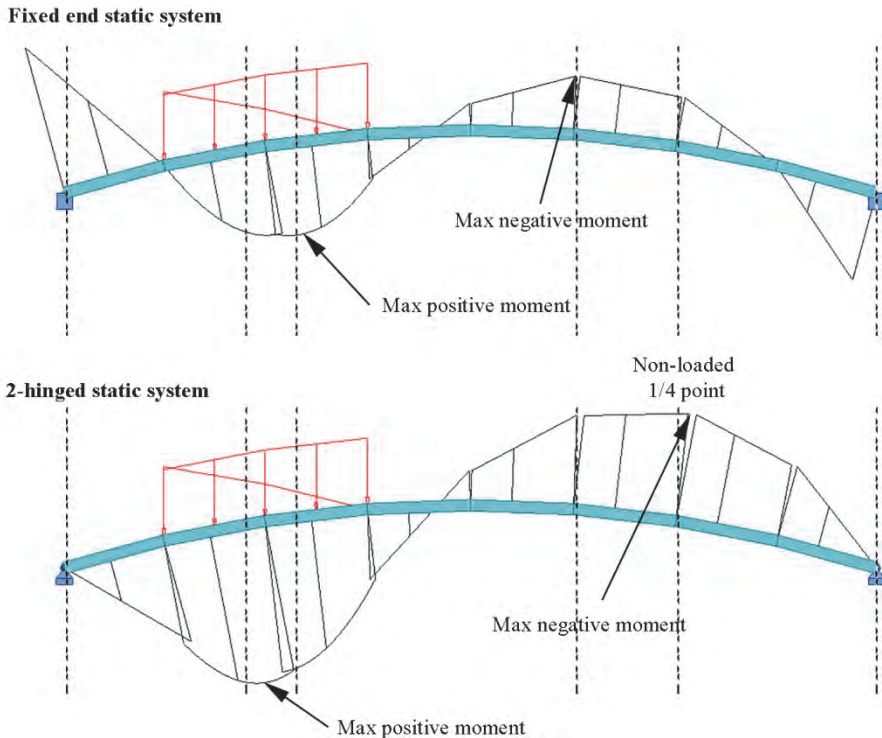


*Figure 56: Bending moment distribution in fixed vs. 2-hinged arch of same geometry as the tested arches.*

The true static system would have been somewhere between the two extremes. This may be the reason why the fracture occurred closer to the crown of the arch in the non-loaded side. Also, a small degree of fixation in the hinges may have reduced the bending moments and hereby give an increase in the load carrying capacity compared to the calculated value. In fact, when checking the load carrying capacity based on an arch with fixed ends, and a load corresponding to the fracture load from the test, there would still be a remaining moment capacity of +102 kNm and -105 kNm in the loaded and non-loaded side, respectively.

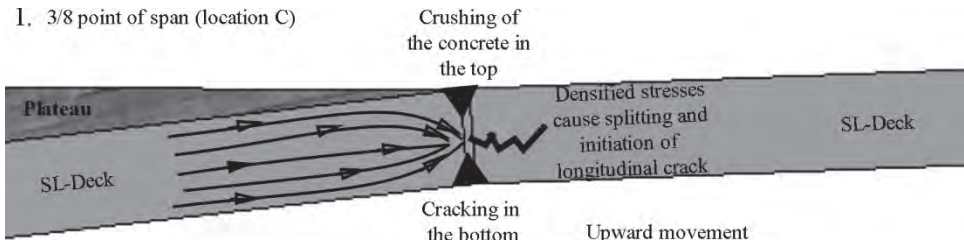
The expected failure mechanism was compressive crushing of the concrete in the bottom of the non-loaded side, or in the top of the cross section in the loaded side of the span. The actual failure was more complex due to the rotation in the points of the plastic hinges and the SL-Deck geometry in combination with the local stresses from the plateau used for loading. The following observations were made just before the ultimate capacity was reached:

1. A plastic hinge formed at the 3/8 point of the span on the loaded side of the arch. The plastic hinge concentrated the stresses in that location, since the concrete crushed at the top and a transverse crack opened at the bottom. A longitudinal crack developed in the middle of the adjacent deck element, which was likely caused by a splitting mechanism that resulted from the concentrated normal load being transferred between the deck elements.
2. A plastic hinge formed in the 5/8 point of the span, at which point the arch became an unstable structure (having four hinges). The 3/8 point was pushed downwards, and the 5/8 point was lifted upwards. This movement would have created a shear force, which would exacerbate the cracking at the 3/8 point of the span.
3. The deflections and crack propagation occurred very quickly. As the plastic hinges moved upwards and downwards, the longitudinal crack lengthened in the mid-depth of the SL-Deck. The crack stayed in the middle of the cross section, probably because of the mild steel reinforcement and the pre-stressing strands in the top and bottom of the cross section.

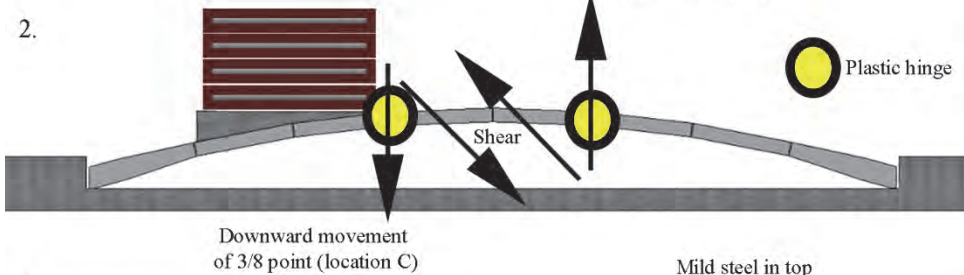
*Figure 57* depicts the observations leading to collapse.

*Figure 58* shows photographs of the large longitudinal crack in the loaded side (3/8 point of span – location C), and crushing of concrete on the underside of the arch in the non-loaded side (5/8 point of span – location E).

1. 3/8 point of span (location C)



2.



3.

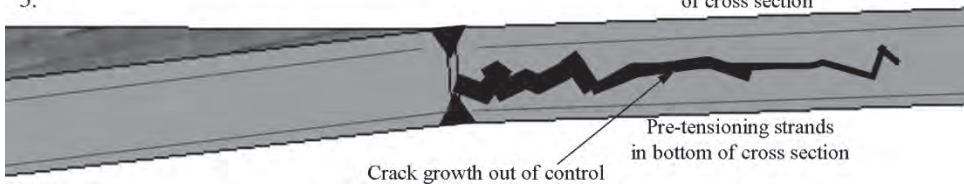


Figure 57: Sequence of events leading to final collapse.



Figure 58: Photographs taken after collapse: longitudinal crack at 3/8 point (left) and crushed LAC at 5/8 point (right).

The PC-Arches seemed to form both plastic hinges nearly simultaneously. If this was true, then the same load resulted in concrete crushing strains at the 3/8 and 5/8 locations. With this damage observation, the results from the elastic analyses can be used to predict the load at failure.

Other reasons for the 14 % difference between the calculated load capacity and the actual capacity are:

- Multiaxial stresses in the SL-Decks. We have shown how the stresses concentrate inside the SL-Deck and the confinement of the concrete may give a different working curve with a higher compressive strength compared to the one presented earlier.
- The strength of the LAC blocks has not been accounted for in the analytical calculations. The load bearing capacity is based on the normal concrete only.

### 5.2.2.2 Warnings before fracture

Highly pre-stressed construction members (arches in particular) are often assumed to have a brittle, unwarned fracture. However, the tested PC-Arches showed several warning signs before the collapse occurred. *Figure 59* shows the change in system stiffness. On the main vertical axis the load is plotted as function of the deflections for all load levels in the loaded  $\frac{1}{4}$  point – locations B – and the non-loaded  $\frac{1}{4}$  point – location F. On the secondary vertical axis the corresponding stiffnesses are seen. There is clear system ductility since the stiffness decreases as the load and deflections increase. The figure is based on data from Test 2.

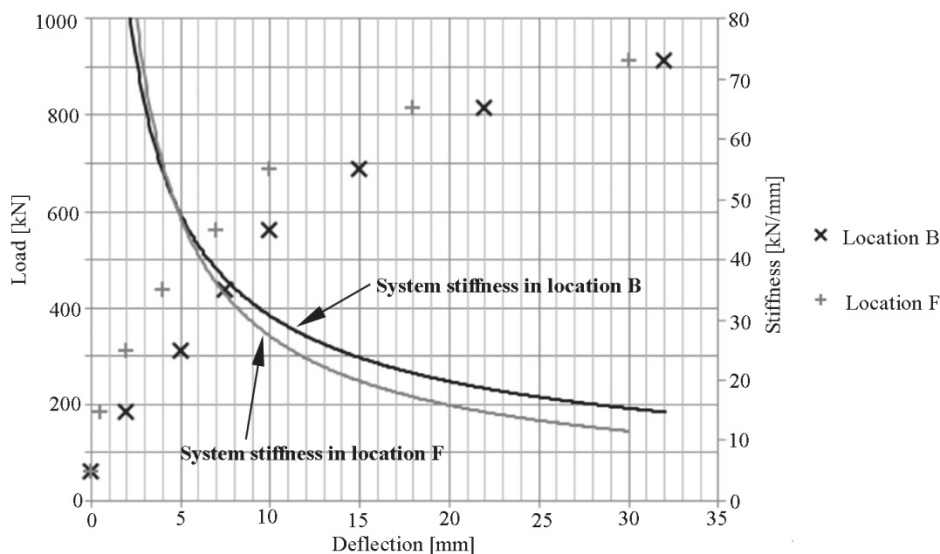


Figure 59: Deflections in location B and F at different loads, and corresponding system stiffness.

The first visible cracks were seen at the connection to the abutments where the hinge rotation took place. *Figure 56* compared analyses of the two-hinged and fixed

end static systems, and showed that the largest bending moment resulted at the abutments if fixed.

The cracks at the support “hinges” were initially observed at a load of approximately 300 kN, and grew as a result of additional loading. This means that visible cracks at the abutments were seen at a load level of 31% of the fracture load. At several locations, cracks were observed in the bottom of the loaded side of the arch at 84% to 94% of the fracture load. The non-loaded  $\frac{1}{4}$  point of the span was closely monitored, but cracks were not observed there. However, cracking was observed in the top of the cross section at the  $\frac{5}{8}$  point of the span, where the plastic hinge developed before the collapse. Extensive concrete spalling was observed in the bottom of the arch close to that same location, also at 84% to 94% of the fracture load.

An interesting observation was that all cracking initiated at the connections between the SL-Decks and mortar joints, which seemed to be the weakest link.



# 6 PEARL-CHAIN BRIDGE PROJECTS

Two PC-Bridges have been projected during the Ph.D.-study: The first one was a road bridge crossing the Vorgod Creek in Jutland in Denmark, and the second one was a pedestrian bridge over a highway in Hillerød north of Copenhagen in Denmark. The road bridge project was built in 2015, and the pedestrian bridge, unfortunately, did not win the tender process.

Both projects are described and evaluated in regard to the performance of the developed technologies contained within both of the two bridge types.

The scope of the chapter is to illustrate 1) the practical application of PC-Bridges in two projects (one using a tension tie system, and one without a tension tie), and 2) the real-world challenges when going from “lab to market” (or “test-arch to finished bridge”) with a new state-of-the-art technology.

## 6.1 Vorgod Creek Road Bridge

Vorgod Creek is situated in the countryside in Jutland in Denmark. An old passing of the creek required renewing, and after giving an offer for the built, the municipality chose to build the first ever Pearl-Chain Bridge. The finished PC-Bridge is seen in *Figure 60*.

### 6.1.1 Introduction to the site and project requirements

The old bridge is shown in *Figure 61*. It had two intermediate supports and three spans of 9 m.

The new bridge also has two intermediate supports, and it has a max span of 13 m and a total length of 26 m with one notional lane. Because of the rural location the road bridge is in the Danish Bridge Class 2 [49], which means that the bridge must resist special vehicles up to 80 tonnes from eight axels. Eurocode 1 (part 2) [25] defines the required loads on road bridges. In this case, the most important loads are the special vehicle and a so called Tandem System (TS). A TS load consists of two heavy axels with a small spacing of only 1.2 m and an axel load of up to 300 kN (unamplified value in notional lane 1). At the same time as the TS a uniformly dis-

tributed load (UDL) of up to  $9 \text{ kN/m}^2$  is applied (also in lane 1) in the unfavorable parts of the span. Another UDL of  $2.5 \text{ kN/m}^2$  is applied in remaining areas in the unfavorable parts of the span. The site has poor soil conditions. We do not look closer into braking forces, wind loads, etc. in the following simplified load bearing calculations.



Figure 60: The finished Vorgod Creek PC-Bridge. Courtesy of Abeo A/S.

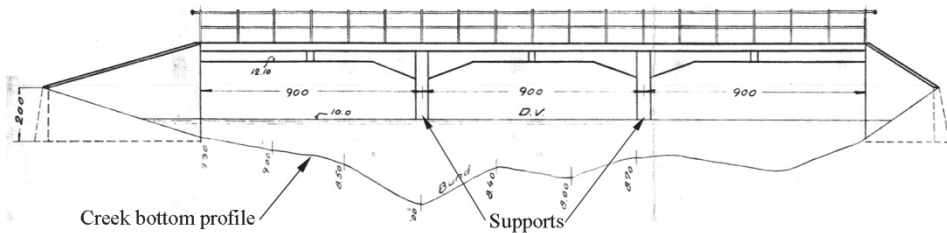


Figure 61: The old bridge at the crossing of Vorgod Creek.

## 6.1.2 The static system and assumptions

Just like the old bridge, the new PC-Bridge has piled foundations with piles down to 10 m below the terrain. The poor soil conditions were a problem if the arches should have delivered a large horizontal reaction force. Therefore, the chosen solution was to create a tied arch consisting of one main span of 13 m, and two side spans of 6.5 m.

The main span consists of a full arch with a rise to span  $1/13$ . This arch is formed by four adjacent PC-Arches with a total width of 6 m (two PC-arches with width 1.75 m and two with 1.25 m). Each PC-arch consists of 6 SL-Decks and 2 abutment elements, similar to the tested arches in Chapter 5. The side spans are half-arches and each half-arch consists of two SL-Decks and two abutment elements each. Figure 62 is a plan view of the arches in the superstructure and a longitudinal section.

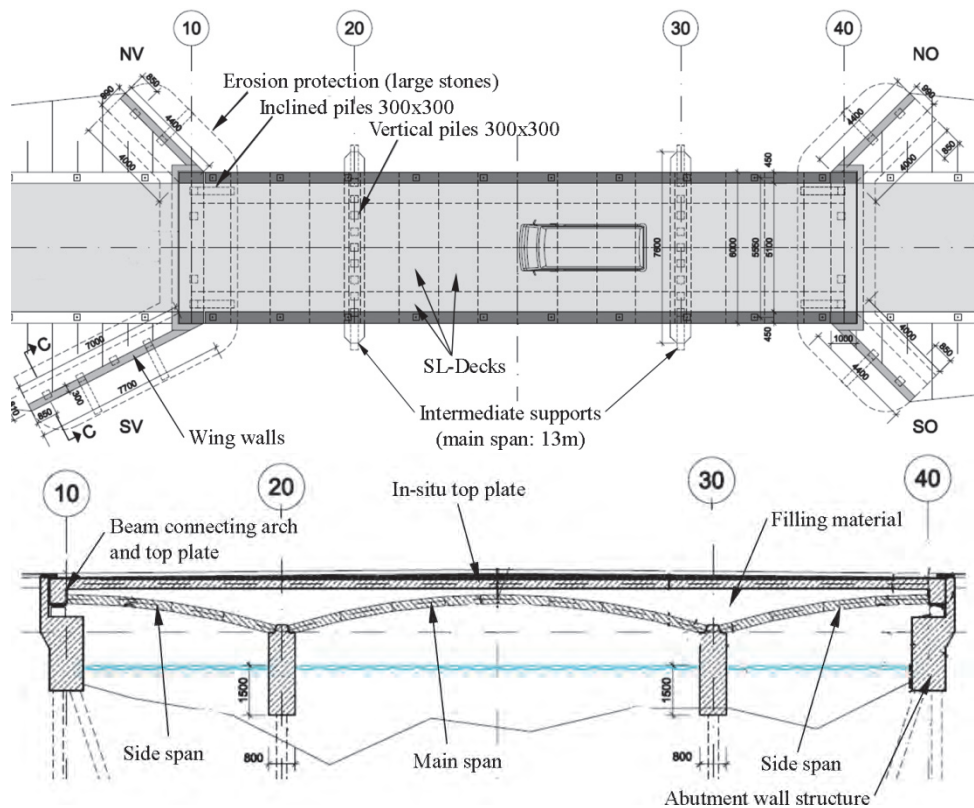


Figure 62: The new PC-Bridge at Vorgod Creek. Top: Plan view. Bottom: Longitudinal section. Courtesy of Sweco Denmark.

The horizontal reaction forces from one span are transferred to the span next to it. The horizontal forces from the side spans towards the abutments are resisted in a “top plate” tie as tension. The top plate is an in-situ cast and post-tensioned concrete plate covering the whole width of the bridge.

Edge beams in both sides of the bridge are integrated in pre-fabricated side-walls. On top of the vertical side-walls the crash barrier is positioned, and force on the crash barrier from a vehicle is transferred to the arches via stiffened orthogonal steel profiles attached to both arch and side wall. A cross section of the bridge at the position of the crown of the main span is seen in Figure 63.

It is conservatively assumed that a load on the road surface is acting directly on the arch below the point of the loading. The bending moment capacity from the 300 mm top plate and the pervious (draining) concrete between top plate and arches are not taken into consideration.



ness. Because of the compulsory water membrane and for aesthetic reasons though, this was not pursued.

A compulsory water membrane can be omitted in case of a top plate tensioned in both longitudinal and transverse direction. For the Vorgod Creek Bridge the top plate was post-tensioned in the longitudinal direction, and a membrane had to be installed.

A discussion is now whether or not the top plate was actually being tensioned in two directions: The longitudinal post-tensioning will (because of Poisson's ratio) expand the concrete transversely. This leads to transverse compression for two reasons:

- 1) The top plate is confined by the side walls, which are rigidly attached to the arches below.
- 2) The top plate is in-situ cast on top of the very porous pervious concrete layer, and hence, there is a good connection between the two. When the top plate expands sideways, the pervious concrete resists this enlargement.

#### 6.1.3.2 Side walls

Several suggestions for the design of side walls were discussed in the PC-working group. It was clear from the above mentioned reasons that side walls were dictated to be installed together with a water membrane.

The final design is seen in *Figure 60*. Several walls are installed, and each wall has the same width as the below SL-Deck in the PC-arch. There are pros and cons with this solution. Having many individual walls with joints in the same positions as the PC-arches below is an aesthetical solution, and it allows for each joint to distort a little when the bridge deforms when loaded. On the other hand having many elements gives a larger number of crane lifts and more joints to seal. An alternative solution could be larger side walls, e.g. only four pre-fabricated walls on each side of the bridge instead of the 16 elements in the chosen design. The Danish Road Directory is also keen on slim edge beam designs, and such could potentially be achieved for this type of PC-Bridge with inclined side walls held in by transverse ties.

One challenge with having transverse permanent ties through filling of pervious concrete, and also with the chosen design, is that the pervious concrete must be compacted to work as intended. To compact it special machines are required to maneuver on top of the filling whenever a certain thickness is poured. For the chosen design the side elements are connected to the arches via steel profiles, and the side elements are cast with long mild steel bars – for connection to the top plate – sticking out of the inside surface. This ended up as a practical difficulty in the Vorgod Creek Bridge project since the steel was in the way when compacting the filling layer.

### 6.1.3.3 Abutment connection detail

An interesting detail is the connection between the abutment, the PC-half-arches, and the top-plate tie, see *Figure 64*. Because of the static system, where all horizontal forces are kept within the system, the abutment structure in reinforced concrete is only approximately 1.3 m at the thickest point. In addition to a downward reaction force the abutments should resist a lifting force. This is achieved by means of vertical post-tensioning of the abutment structure, where the abutment and the bridge are joined in compression through a bearing. Minor rotations of the bridge at the bearing are possible since a 30 mm horizontal space is located between top plate and abutment wall. This leaves room for temperature bridge elongations as well.

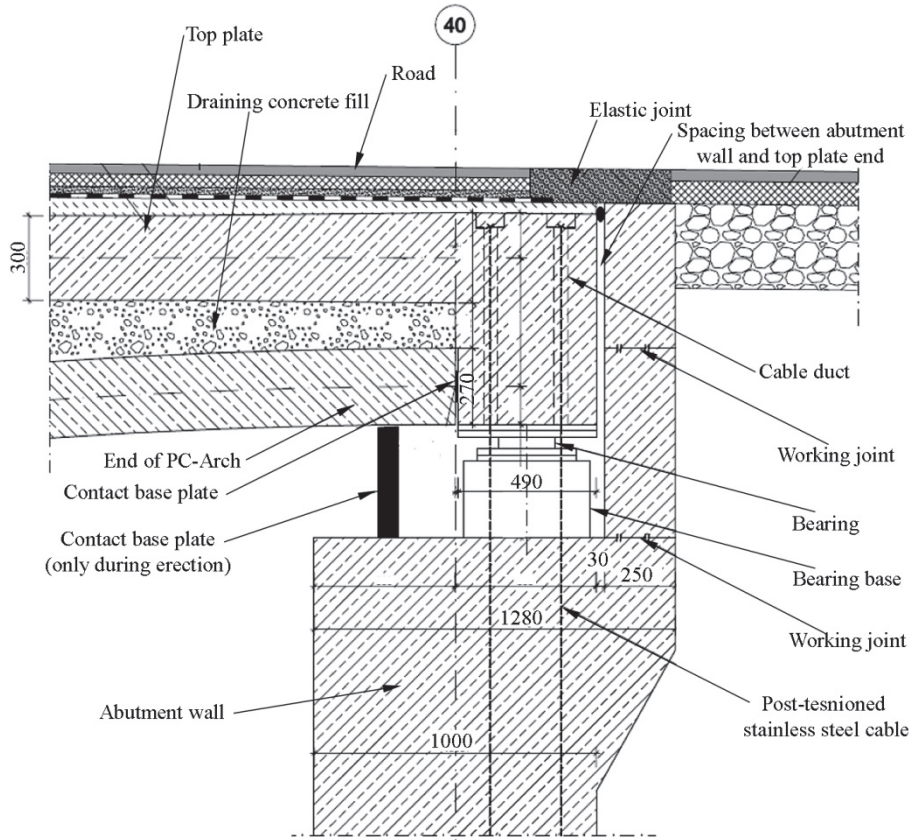


*Figure 64: Abutment connection detail. By courtesy of Sweco Denmark. Owned by Perstrup Betonindustri.*

### 6.1.4 Erection procedure

Before the erection took place the old bridge was dismantled, and the abutments and intermediate supports were removed. The new supports and abutments were cast in advance of the erection day, and the PC-arch elements were ordered from the factory. The arches were assembled and post-tensioned at the factory shortly before being transported to the bridge site. At the day of erection, all 12 arches were installed within half a working day by one crane. Because of the three-span system there was a challenge in regard to horizontal reactions from the arches self-weight during erection. For this reason, two temporary ties (threaded rods) were put in the main span between the intermediate supports, and further two were put in between the intermediate support and the abutment structure in both sides of the bridge. Also, a temporary post-tensioning system was used between the abutment walls all across the entire creek to be able to regulate the distance between the abutments during erection, and after erection. The sequence of the erection of the arches is given here (see also *Figure 65*):

1. Positioning of the temporary ties between supports in all three spans.
2. The inner two PC-arches of the main span were lifted into position on the intermediate supports.
3. Two half-arches were positioned – one in each side – and in continuation of the positioned main arches. The arches now continuously reach from one abutment to the other.
4. The temporary post-tensioning systems between the abutment walls (one in each side of the bridge) were tensioned simultaneously. They would stay tensioned until the top plate could take over the horizontal reaction forces. To achieve horizontal connection between the abutment walls and the arches, temporary wedges were inserted in the gap between the bridge and the abutment.
5. The rest of the arches were lifted into position, and all joints are poured with mortar.

During the installation it was clear that the half PC-arches had sufficient stiffness and load carrying capacity to stand by themselves without horizontal support. After the installation of the arches the side elements were lifted into position as well, and were attached to the arches. The pervious concrete was then poured and compacted in layers according to the specifications [50]. Finally, the top plate was cast, and after hardening and post-tensioning, the temporary post-tensioning between the abutments was removed. The final details (road, crash-barrier, etc.) were implemented and the bridge was opened in early summer of 2015.



Figure 65: Vorgod Creek Bridge after erection of the 12 PC-arches.

### 6.1.5 Simplified load bearing calculation

Only the full arch in the main span is treated in the following simplified calculation. The method used in this example is not identical to the method used for the actual project design.

The top plate and the pervious concrete filling were conservatively assumed to not contribute to the load bearing capacity – they only contribute as dead load. The previously described TS is used as live load, and is positioned in the  $\frac{1}{4}$  point of the span. Figure 66 illustrates the arch parameters.

Initially the arch length and hereby the length of each pre-fabricated element is determined:

The equation of the circular shape is:

$$y(x) = R - \left| r - \sqrt{r^2 - x^2} \right| \quad (6.1)$$

The angle,  $v$ , at the circle center, and the arch length are:

$$v = \sin^{-1} \left( \frac{\left(\frac{l}{2}\right)}{r} \right) = 17.5 \text{ deg} \quad (6.2)$$

$$s = 2 \cdot v \cdot r = 13.2 \text{ m} \quad (6.3)$$

We choose to have eight elements of equal length in the arch, which gives an element length of:

$$L_{el} = \frac{s}{8} \cong 1.65 \text{ m} \quad (6.4.)$$

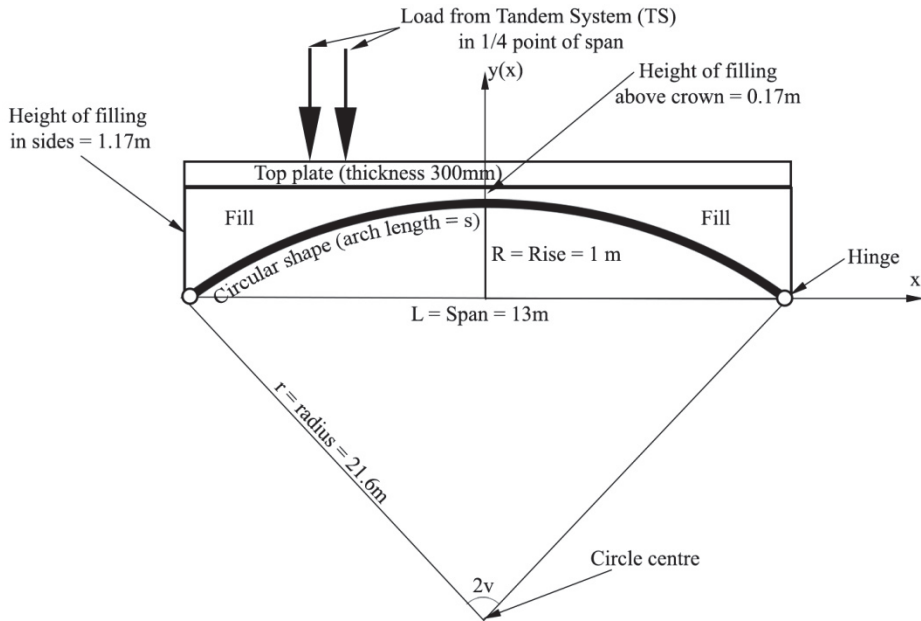


Figure 66: Vorgod Creek main span geometry and coordinate system. Bridge width,  $W$ , is 6m.

Six of the elements are SL-Decks, and two are abutment elements. When the outer dimensions of each SL-Deck are known we find the number of LAC blocks in each type of SL-Deck. The first type had a width of 1.25 m and space for two blocks transversely, and the other type had a width of 1.75 m and space for four LAC blocks transversely. The lengths were the same, and they both had space for two rows of blocks lengthwise. In total each type would have four and eight blocks, respectively. The 1.25 m wide SL-Deck ended up with a self-weight of 5.78 kN/m<sup>2</sup>, and design flexural stiffness of  $EI = 58 \text{ MNm}^2$ , and the 1.75 m wide SL-Deck had self-weight of 5.62 kN/m<sup>2</sup> and design flexural stiffness of 64.6 MNm<sup>2</sup> (based on a deck thickness of 270 mm similar to the one presented in Paper I). A similar deck in plain concrete would have a self-weight of 6.63 kN/m<sup>2</sup>. The safety coefficient is 1.54 for pre-fabricated concrete including high consequence class addition.

### 6.1.5.1 Normal force contributions

Now, the normal force from the total self-weight is found as contributions from the arch, the filling, and the top plate. The arch, the top plate, and the layer of fill above the crown of the arch are assumed to be uniformly distributed. The pervious concrete was measured to have density of  $\rho_{pc} = 2092 \text{ kg/m}^3$ , and the top plate consisted of concrete of density  $\rho_c = 2500 \text{ kg/m}^3$ . The width of the bridge,  $W$ , was 6 m. Figure 67 shows the different loads and reactions of the bridge.

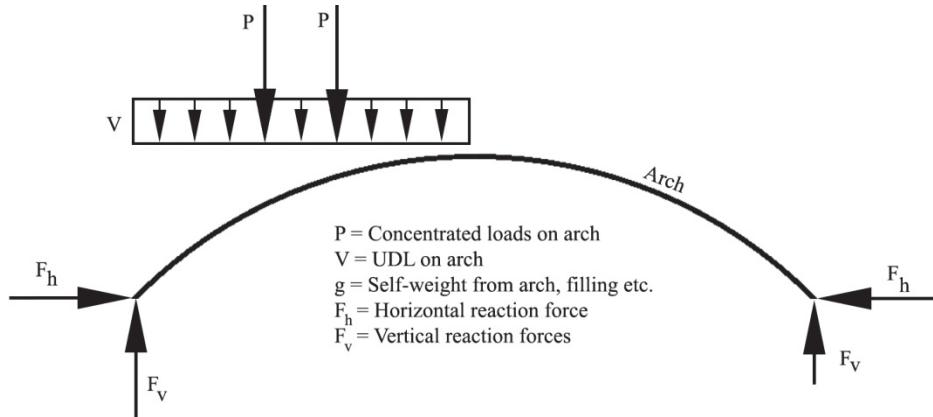


Figure 67: Loads and reactions of arch. Abbreviations are found in the beginning of the thesis.

Horizontal and vertical reaction force from uniformly distributed self-weights:

$$\begin{aligned}
 g_{uni} &= g_{uni.fill} + g_{uni.SL} + g_{uni.top} = 0.17m \cdot 6m \cdot 2092 \frac{kg}{m^3} \cdot g + & (6.5) \\
 &2 \left( 5.62 \frac{kN}{m} \cdot 1.75m + 5.78 \frac{kN}{m} \cdot 1.25m \right) + 0.3m \cdot 2500 \frac{kg}{m^3} \cdot 6m \cdot g = \\
 &21.0 \frac{kN}{m} + 34.1 \frac{kN}{m} + 44.2 \frac{kN}{m} = 99.3 \text{ kN/m}
 \end{aligned}$$

$$\begin{aligned}
 F_{h\_uni} &= \frac{g_{uni} \cdot L^2}{8 \cdot R} \cong 2100 \text{ kN} & (6.6) \\
 F_{v\_uni} &= g_{uni} \cdot \frac{L}{2} \cong 645 \text{ kN}
 \end{aligned}$$

In equations 6.5. and 6.6. it is assumed (to simplify the calculation) that the arch is hinged at the crown. This can be done since the results are very similar for 2-hinged and 3-hinged arches with no horizontal settlement.

Vertical reaction force from filling below crown of arch:

$$g_{fill}(x) = (R - y(x)) \cdot W \cdot 2092 \frac{kg}{m^3} \cdot g \quad (6.7)$$

$$F_{v\_fill} = \frac{1}{2} \int_{-\frac{L}{2}}^{\frac{L}{2}} g_{fill}(x) dx \cong 227.3 \text{ kN} \quad (6.8.)$$

The horizontal reaction from filling below crown level is found by finding the center of gravity of the filling and then take moment around the springing of the arch. Figure 68 shows the situation.

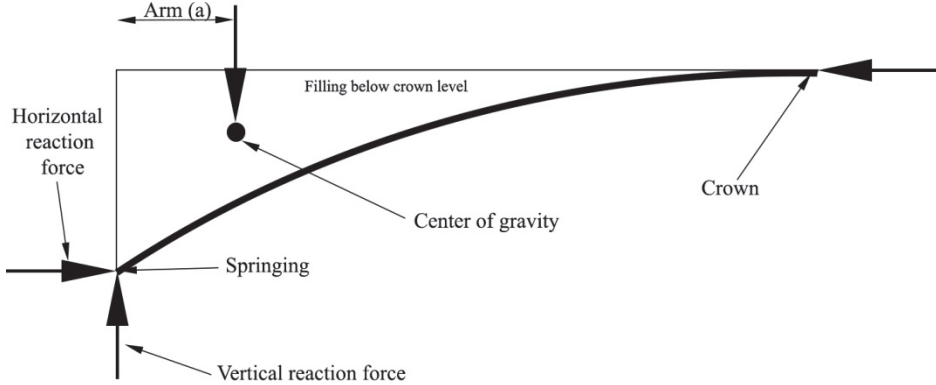


Figure 68: Center of gravity of filling below the level of the crown (one half of the bridge).

The arm,  $a$ , is calculated to be 1.62 m, and this gives:

$$F_{h\_fill} = \frac{a \cdot F_{v\_fill}}{R} = 367 \text{ kN} \quad (6.9.)$$

Now, the reaction forces from the TS live load are calculated. Conservatively, we assume the axels to act directly on the arch at the position below the location of the TS-vehicle. The  $y$ -coordinate of each axel is:

$$y\left(-\frac{L}{4} - 0.6 \text{ m}\right) = 0.66 \text{ m} \quad (6.10.)$$

$$y\left(-\frac{L}{4} + 0.6 \text{ m}\right) = 0.84 \text{ m} \quad (6.11.)$$

The Danish design axel load is found according to EC 1991-2, and the national annex [52]. The safety coefficient is 1.4, and the high consequence class coefficient is 1.1. For Bridge Class 2 the adjustment factor for the TS load is 0.8, and 0.33 for the UDL in the driving lane (3 m width). For remaining areas (2.1 m width) the UDL factor is 1.00. The used loads can be seen in 6.1.1., and the design loads are then:

$$P_{axel\_TS} = 300 \text{ kN} \cdot 1.1 \cdot 1.4 \cdot 0.8 \cong 370 \text{ kN} \quad (6.12.)$$

$$V_{UDL\_lane} = 9 \text{ kN/m}^2 \cdot 1.1 \cdot 1.4 \cdot 0.33 \cdot 3 \text{ m} \cong 13.7 \text{ kN/m} \quad (6.13.)$$

$$V_{UDL\_remain} = 2.5kN/m^2 \cdot 1.1 \cdot 1.4 \cdot 1.00 \cdot 2.1m \cong 8.1kN/m \quad (6.14.)$$

$$V_{UDL\_sum} = 13.7 \frac{kN}{m} + 8.1 \frac{kN}{m} \cong 21.8 \frac{kN}{m} \quad (6.15.)$$

The contributions to the reaction forces are found similarly to the self-weight contributions. The results are:

$$F_{v\_UDL\_loaded} = \frac{3}{4} V_{UDL\_sum} \cdot \frac{L}{2} = 106.3kN \quad (6.16.)$$

$$F_{v\_UDL\_non\_loaded} = \frac{1}{4} V_{UDL\_sum} \cdot \frac{L}{2} = 35.4kN \quad (6.17.)$$

$$F_{h\_UDL} = \frac{F_{v\_UDL\_loaded} \frac{L}{2} - V_{UDL\_sum} \frac{L}{4}}{R} = 230.3kN \quad (6.18.)$$

$$F_{v\_TS\_loaded} = 2 \frac{3}{4} P_{axel\_TS} = 555kN \quad (6.19.)$$

$$F_{v\_TS\_non\_loaded} = 2 \frac{1}{4} P_{axel\_TS} = 185kN \quad (6.20.)$$

$$F_{h\_TS} = \frac{1.5P_{axel\_TS} \frac{L}{2} - 2P_{axel\_TS} \frac{L}{4}}{R} = 1202kN \quad (6.21.)$$

Because of the low rise to span ratio the horizontal reaction force is almost the same as the normal force in the arch. The sum of all normal force contributions are then the normal force from the self-weight, the live loads, pre-tensioning and post-tensioning. Pre-tensioning is performed to 50 % of the 0.1% proof stress (1634 MPa), and there are 18 strands in the 1.75 m wide SL-Decks and the idealized area is 0.287 m<sup>2</sup>. The total normal force in the SL-Deck from this is 1146 kN. There are 10 strands in the 1.25 m wide SL-Decks and the idealized area is 0.245 m<sup>2</sup>. The total normal force in the SL-Deck from this is 595 kN. The position of the strands is similar to presented in Chapter 2, *Figure 10*. The safety coefficient for pre-tensioning and post-tensioning including additional high consequence coefficient is 1.32.

$$N_{pretension} = 2 \cdot (1146kN + 595kN) = 3481kN \quad (6.22.)$$

The contribution from pre-tensioning acts only inside the SL-Decks, and not in the joints.

Post-tensioning cables in each of the four arches was Freyssinet 7C15 strands stressed to 70% of the 0.1% proof stress of the steel giving a normal force contribution of 910 kN each. The steel strength and safety factors are equal for all pre-stressing.

$$N_{post} = 4 \cdot 910 kN = 3640 kN \quad (6.23.)$$

Reductions from creep, shrinkage and relaxation (CSR) due to pre-tensioning, post-tensioning and self-weight are subtracted from the total sum of normal forces:

$$N_{CSR} = -2979 \text{ kN} \quad (6.24.)$$

$$N_{total} = N_{pretension} + N_{post} + F_{h\_UDL} + F_{h\_TS} + F_{h\_uni} + F_{h\_fill} + N_{CSR} = \quad (6.25.)$$

$$3481 \text{ kN} + 3640 \text{ kN} + 230.3 \text{ kN} + 1202 \text{ kN} + 2100 \text{ kN} + 621 \text{ kN} +$$

$$(-2979 \text{ kN}) \cong 8295 \text{ kN}$$

Temperature changes of 30 °K cause a change in this normal force in magnitude ±1 to 2 % cf. Eq. 1.1.

### 6.1.5.2 Bending moment contributions

A small bending moment is built into the structure from self-weight and pre-tensioning, since the PC-Arch shape is not perfectly adapted to the distribution of the dead load. The moment from pre-tensioning is divided into a positive contribution from the top strands in each SL-Deck, and a negative contribution from the bottom strands. The sum of these contributions is -4.9 kNm for the 1.25 m wide SL-Deck, and -18.4 kNm for the 1.75 m wide SL-Deck. The total moment from pre-tensioning over the whole width is then:

$$M_{pretension} = 2 \cdot (-4.9 \text{ kNm}) + 2 \cdot (-18.4 \text{ kNm}) = -46.6 \text{ kNm} \quad (6.26.)$$

We assume that no bending moments come from the post-tensioning, which is located at the or close to the neutral axis in the SL-Decks. The moment distribution from self-weight (without the eccentric pre-tensioning) is given in *Figure 69*.



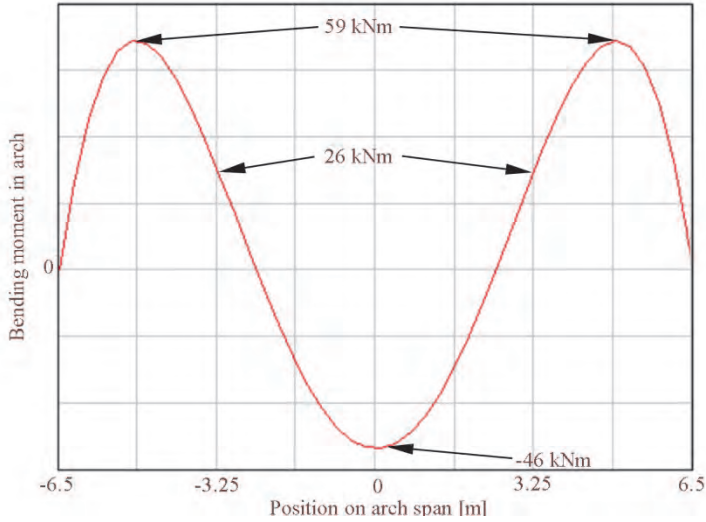


Figure 69: Bending moment in main span of Vorgod Creek Bridge from dead load (not included eccentric pre-tensioning).  $M_{dead} = 26 \text{ kNm}$ .

The two axels in the TS-system load (eq. 6.12) are giving a positive bending moment below the TS at the  $\frac{1}{4}$  point of the span of approximately:

$$M_{TS\_pos} = -F_{h\_TS} \cdot y \left( \frac{L}{4} \right) + F_{v\_TS\_loaded} \cdot \frac{L}{4} = 897 \text{ kNm} \quad (6.27.)$$

In the non-loaded  $\frac{1}{4}$  point of the span the negative bending moment from the TS system becomes:

$$M_{TS\_neg} = -F_{h\_TS} \cdot y \left( \frac{L}{4} \right) + F_{v\_TS\_nonloaded} \cdot \frac{L}{4} = -305 \text{ kNm} \quad (6.28.)$$

The UDL load (eq. 6.15) is applied in the unfavorable part of the span which is assumed to be in the half of the arch where the TS system is located. The positive and negative bending moments from the UDL load in the loaded and non-loaded  $\frac{1}{4}$  points of the span are:

$$M_{UDL\_pos} = -F_{h\_UDL} \cdot y \left( \frac{L}{4} \right) + F_{v\_UDL\_loaded} \cdot \frac{L}{4} - V_{UDL\_sum} \cdot \frac{L}{4} \cdot \frac{L}{8} = 57 \text{ kNm} \quad (6.29.)$$

$$M_{UDL\_neg} = -F_{h\_UDL} \cdot y \left( \frac{L}{4} \right) + F_{v\_UDL\_nonloaded} \cdot \frac{L}{4} = -59 \text{ kNm} \quad (6.30.)$$

The largest positive and negative bending moment from the above contributions in the loaded and non-loaded  $\frac{1}{4}$ -points of the span is then (pre-tensioning included):

$$M_{pos} = M_{pretension} + M_{dead} + M_{TS_{pos}} + M_{UDL_{pos}} = 933 \text{ kNm} < 1179 \text{ kNm} = M_{rd+} \quad (6.31.)$$

$$M_{neg} = M_{pretension} + M_{dead} + M_{TS_{neg}} + M_{UDL_{neg}} = -385 \text{ kNm} > -866 \text{ kNm} = M_{rd-} \quad (6.32.)$$

The bending moment in combination with the normal force found earlier can be resisted by the four PC-arches ( $M_{rd}$ ) with the chosen thickness of 270 mm.

## 6.2 Hillerød Highway Pedestrian Bridge

The bridge site is north of Copenhagen in Denmark. An old pedestrian beam bridge was removed after accidentally being run into by a truck. The submitted PC-Bridge solution for a new bridge across the highway is seen in *Figure 70*.



*Figure 70: Visualization of Hillerød Highway PC-Bridge proposal. By courtesy of Abeo. Drawn by Henning Larsen Architects Denmark.*

### 6.2.1 Introduction to the site and the project requirements

The below road has two lanes of highway traffic – one lane in each direction. The span of the old dismantled bridge was 30 m, and the total width was 3.24 m. The existing foundations are reusable to some extent, and therefore the span of the new bridge is 30 m as well. The soil conditions are in this case sufficiently good to obtain the horizontal force from the PC-Bridge.

It is a pedestrian bridge in Bridge group 3 [49], and it has to resist an UDL on the unfavorable parts of the span (characteristic value of 5 kN/m<sup>2</sup>), and the accidental presence of a service vehicle (SV). The Eurocode [25] defines the SV to use: It con-

sists of two axels with a spacing of 3.0 m. The front axel contains an 80 kN mass, and the back axel has 40 kN. The Danish Road Directory demand to multiply these values with a factor 1.5, and further by a safety coefficient of 1.4. We do not look closer into horizontal forces, crowd loads, etc. in the following simplified load bearing calculations.

### 6.2.2 The chosen static system and assumptions

The width of the new bridge is  $W = 3.0$  m, and it consists of two PC-Arches of 1.5 m each. Also, each arch consists of 12 pre-fabricated elements – 2 abutment elements, and 10 SL-Decks. The arches are connected transversely to one another in all SL-Decks by Hammerhead joints and are assumed to act as one when loaded. The connection to the abutments are hinged (assumed resistance free rotation), and the arches transfer a horizontal force to the foundations. The arch rise to span ratio is 1/13, and above the arches are filler with a top surface,  $h_{\text{fill}}$ , 250 mm above the crown. The filling material (pervious concrete) does not contribute to the load bearing capacity, and a load on the asphalt surface is assumed to act directly in the arch below the point without spreading of the force through the filling. On top of the pervious concrete is a layer of  $t_{\text{asphalt}} = 70$  mm asphalt cover. Furthermore, side walls are assumed to not contribute to the load carrying capacity. The thickness of the side walls is 250 mm.

### 6.2.3 Example of load bearing calculation

The calculation method from the case in Paper I is used in this example to find the dimensions of the PC-Arches in the Hillerød Highway Pedestrian Bridge. The program Robot Structural Analysis [42] is made use of to visually explain the different steps of the method.

#### 6.2.3.1 Step 1 + 2

- *Choose the geometry of the arch, and the number of hinges, pre-stressing strands and post-tensioning cables. The level of interaction with adjacent arches is selected.*
- *Pick the number of SL-Decks in one arch and calculate the dimensions of each element. Take possible abutment elements into account.*

The geometry of the arch is defined above (span of  $L = 30$  m, and width of  $W = 3.0$  m). With a rise to span of 1/13 the rise is,  $R = 2.31$  m. The arch is initially chosen to be 2-hinged with a 320 mm thick SL-Deck, and the selected pre-tensioning (12 strands) in each of the two PC-arches has a sum of positive 1.5 kNm from the eccen-

tric position of the strands. Again the pre-tensioning is performed to 50% of the 0.1% proof stress (1634MPa) in all strands. This gives a normal force contribution in each SL-Deck of  $N_{\text{pretension}} = 791 \text{ kN}$ .

For post-tensioning is chosen the same solution as in the Vorgod Creek Bridge with 7C15 in each of the two arches. This was 910 kN in each arch.

The Hammerhead joints give full interaction between the arches, and they resist any loads together.

It is decided to have all 12 elements with the same length (including the two abutment elements). The circle radius is  $r = 49.9 \text{ m}$ , and the start inclination and arch length are:

$$v = \sin^{-1}\left(\frac{L/2}{r}\right) = 17.5 \text{ deg} \quad (6.33.)$$

$$s = 2 \cdot v \cdot r = 30.47 \text{ m} \quad (6.34.)$$

Each element is then  $30.47 \text{ m} / 12 = 2.54 \text{ m}$  in length. This leaves room for three LAC blocks in the longitudinal direction. Transversely, there is room for three blocks, but since the post-tensioning cable must be positioned in the center only two blocks are put in.

### 6.2.3.2 Step 3 + 4

- Determine self-weight of arch, filling and road slab based on the geometry and material properties.
- Find moments and reaction forces from self-weight, and from possible temperature changes.

The density of the pervious concrete is similar to in the Vorgod Creek Bridge. The concrete in the side walls has density of  $\rho_c = 2500 \text{ kg/m}^2$  – which is the same as the asphalt layer – and represent 1/6 of the bridge width. The SL-Decks have mass  $m_{SL} = 5.85 \frac{\text{kN}}{\text{m}^2}$ . The total dead load at the springings and at the crown is:

$$g_{\text{springing}} = \left(m_{SL} + \frac{5}{6} \cdot \rho_{pc} \cdot g \cdot (R + h_{fill}) + \frac{1}{6} \cdot \rho_c \cdot g \cdot (R + h_{fill})\right) W + t_{\text{asphalt}} \cdot \rho_c \cdot g \cdot W = 182 \text{ kN/m} \quad (6.35.)$$

$$g_{\text{crown}} = \left(m_{SL} + \frac{5}{6} \cdot \rho_{pc} \cdot g \cdot h_{fill} + \frac{1}{6} \cdot \rho_c \cdot g \cdot h_{fill}\right) W + t_{\text{asphalt}} \cdot \rho_c \cdot g \cdot W = 35 \text{ kN/m} \quad (6.36.)$$

The response of the structure to the dead load is illustrated in *Figure 71*. Furthermore, a temperature change of 30 K would give a moment of magnitude  $\pm 19 \text{ kNm}$ .

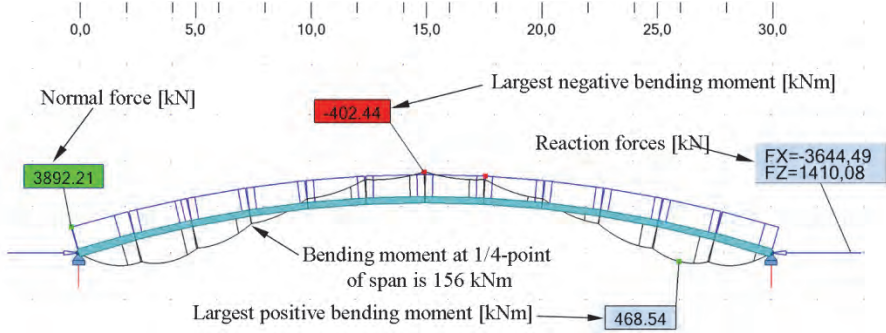


Figure 71: Self-weight loads applied in Robot Structural Analysis.

### 6.2.3.3 Step 5

- Choose type of live load, and determine normal force in the arch as a function of the position of the live load.

The SV and UDL live loads are (including amplification (1.5), safety coefficient (1.4), and consequence class multiplication (1.1):

$$P_{SV\_axel1} = 80 \text{ kN} \cdot 1.5 \cdot 1.4 \cdot 1.1 = 184.8 \text{ kN} \quad (6.37.)$$

$$P_{SV\_axel2} = 40 \text{ kN} \cdot 1.5 \cdot 1.4 \cdot 1.1 = 92.4 \text{ kN} \quad (6.38.)$$

$$V_{UDL} = 5 \frac{\text{kN}}{\text{m}^2} \cdot W \cdot 1.4 \cdot 1.1 = 23.1 \frac{\text{kN}}{\text{m}} \quad (6.39.)$$

The normal force contribution from the SV-load alone is given in Figure 72.

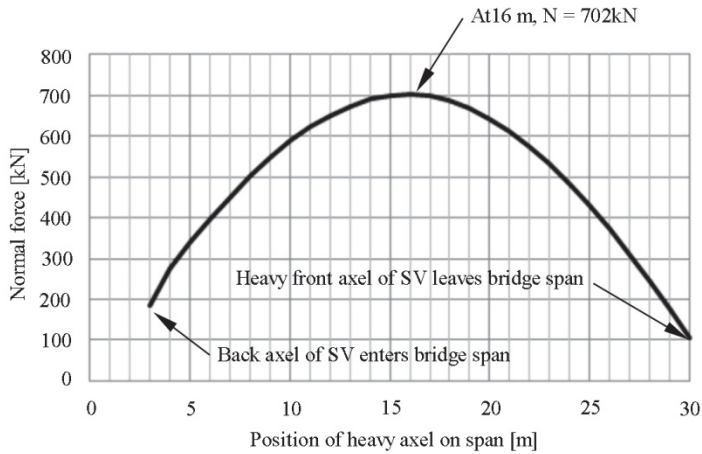


Figure 72: Influence line for normal force from SV-load at the springing of the bridge.

The UDL-load gives a normal force in the arch of  $N_{UDL} = 619$  kN. The total normal force before applying the SV-load, and including losses from CSR ( $N_{CSR} = -1946$  kN) is then:

$$N_1 = N_{prestress} + N_{post} + N_{dead} + N_{UDL} + N_{CSR} = 5967kN \quad (6.40.)$$

To this could be added both normal force increases from temperature and possible abutment settlement. That is not done in this example.

#### 6.2.3.4 Step 6+7+8

- With normal force and cross section data, calculate the moment capacity for all positions of live load – both SL-Decks and joints.
- Find bending moments and reaction forces from all positions of live load.
- Compare bending moments with capacities for all positions of live load – both positive and negative bending moments.

Three types of cross sections must be checked depending on the vehicle position: 1) In the SL-Deck with LAC blocks, 2) in the SL-Deck without LAC blocks, and 3) in the joint between the elements. In the joints of course the normal force from pre-tensioning is not acting, and will be subtracted (and the CSR losses are reduced). In Robot Structural Analysis the bending moment from the SV-load is evaluated as a moving load, and the maximum and minimum values are shown as the output in Figure 73. The figure includes all loads (also self-weights and UDL), and the UDL is positioned on the left half of the arch. The moments are given in all points for all

possible positions of the SV-vehicle driving from left to right with the heavy axel in front.

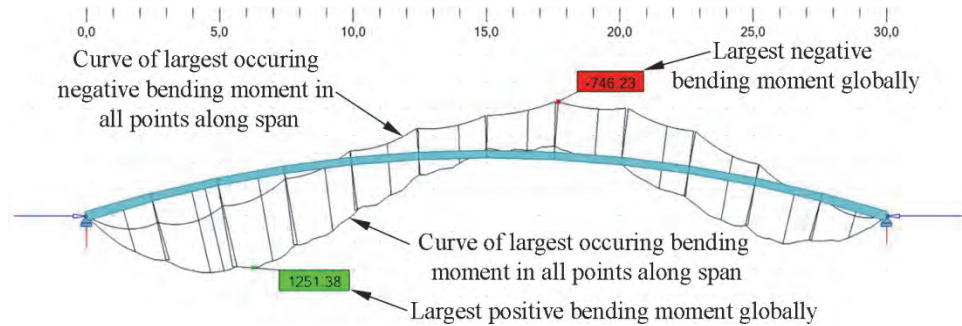


Figure 73: Largest positive and negative bending moment in all points on PC-arch span for all possible positions of SV-load. Unit is kNm.

To find the actual most critical combination of N and M for the arch, the influence line of the normal force from applying the SV-load should be evaluated in all points of the span, and then used to determine the capacity of the cross-section in all points for all positions of load. Then the capacities in each point of the span should be compared to the moment from the applied load in the same location of the load. In order to illustrate the method the following expected critical positions are taken out for further evaluation in the Hillerød Highway Bridge example:  $x = 6$  m (approximate point of largest positive moment in SL-Deck), and  $x = 17.5$  m (approximate point of largest negative moment in joint).

Normal force influence lines are drawn with the moment capacity and moment loads for the two chosen positions on the bridge span, see Figure 74. The capacities are larger than the bending moments from the loads for all positions of the SV-load. The same is the case for all other points on the bridge span, and hence, the bridge can resist the applied loads used in this simplified example.

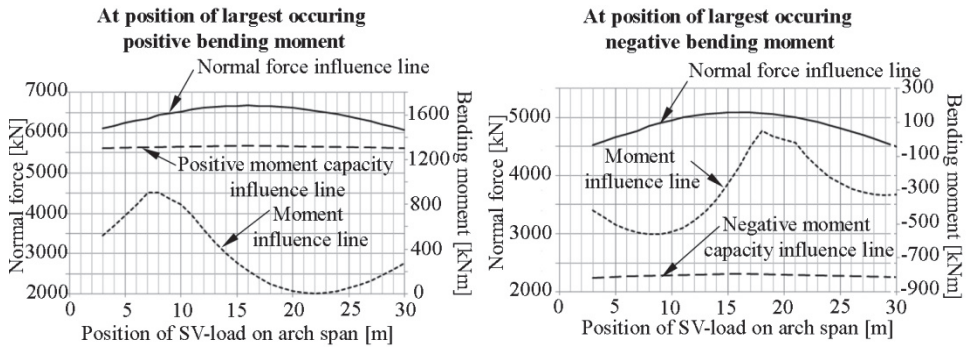


Figure 74: Influence lines of normal force, bending moment from loads, and bending moment capacity.

If the capacity was not sufficiently large (or much too large) the steps 1 to 8 could be repeated for design optimization.



# 7 CONCLUSION

The hypothesis and related objectives of the thesis were proved. During the Ph.D.-studies the concept of Pearl-Chain Bridges were intensively investigated and developed to be able to design, erect, and full-scale test Pearl-Chain Arches. The results of the tests lead to the successful erection of the first ever fully functional Pearl-Chain Bridge in 2015.

First, a load carrying calculation method had to be developed for the complicated geometry of the arches, and with both pre-tensioning, and centrally positioned post-tensioning. But before the calculation method was developed, a new design of the Super-Light Deck, with at least 270 mm thickness, had to be created for specific use in bridges. For use in buildings the Super-Light Decks are 220 mm.

Based on ideal hinges, a case study of a circular 30 m span two-hinged Pearl-Chain Bridge was presented in Chapter 2 to show the influence of the parameters: Number of post-tensioning cables, rise to span ratio, height of the filling, and height of the Super-Light Decks. It was found that Pearl-Chain Bridges can be designed to resist bending moments from specific loads by adjusting the normal force through changing the above parameters. The proposed calculation method was also used in an applied case in Chapter 6.

The theoretical case study also showed that the joints between Super-Light Deck elements often are weaker than the Super-Light Decks when they are subjected to a positive bending moments. In general the negative bending moment capacity is smallest in the Super-Light Decks. It has to be taken into consideration that the negative moment capacity starts decreasing before the positive moment capacity does, when the normal force in the cross section is increased. This is due to the cross section being ribbed, and a combination of normal concrete and light aggregate concrete.

Having the basic analytical understanding of the behaviour of loaded Pearl-Chain Arches the next step was to develop and investigate the response of Pearl-Chain

Bridges with concrete hinges at the abutments. Implementing concrete hinges would have an influence on the static system due to rotational resistance in such hinges. Two concrete hinge types were designed and full-scale tested in Chapter 3. For a Mesnager type hinge, the results of specimens with hinge ratio 1/3 showed that the relationship between rotation and bending moment was comparable to a universal hinge response curve by Leonhardt and Reimann despite of a relatively large normal force in the tested specimens. An Abaqus model of the tested Mesnager hinges gave results within 9% of the tested.

Orthogonal saddle bearing type hinges were tested as part of a full-scale Pearl-Chain Arch load-test. The arch span was 13 m and loaded in the  $\frac{1}{4}$  point of the span. The hinges were monitored with Digital Image Correlation software, ARAMIS, in both the loaded and non-loaded side. At the elastic limit, the rotation difference was up to 22 % between test and an Abaqus model.

The orthogonal saddle bearing was evaluated as being practical, and easy to implement, but with only the hinge response data available found in this thesis. The Mesnager inspired hinge type was tested and documented over many years, but the combination of a hinge throat and central post-tensioning was an obstacle for practical use.

To show the significance of the local hinge response, the rotation-moment-data from the test of the Mesnager inspired hinge was built into a global model of the 13 m span Pearl-Chain Arches in a finite element simulation. The results from this exercise revealed that the Mesnager inspired hinge would be beyond the suggested rotational limit when the arches were loaded to  $\frac{2}{3}$  of the fracture load.

The technique of the assembly and lifting of Pearl-Chain Arches was tested at the construction of two 13 m span test arches. The practical procedure was evaluated in Chapter 4 and includes the individual assembly and post-tensioning of each arch, the lifting technique, and the positioning on a prepared foundation. It was chosen to assemble and post-tension the Super-Light Decks "on edge" (rotated 90° from the erected position of the arch so that all Super-Light Decks touch the ground at the same time), and then rotate the Pearl-Chain Arch in the air before positioning. Both methods worked as smooth and fast as intended, though cracks appeared longitudinally across the joints between Super-Light Decks after post-tensioning. The best method for positioning the arch on the foundation was by use of hydraulic flat jacks between arch and foundation followed by pouring of a mortar.

The two test arches were subsequently loaded in Chapter 5, to investigate if Super-Light Decks in a Pearl-Chain Arch would deflect similar to an ordinary concrete arch,

to monitor the connection details, and to analyze the type of fracture and the load carrying capacity. The following important results were found:

- The straight Super-Light Decks in Pearl-Chain Arches worked as intended. The light aggregate concrete blocks formed ribs in the Super-Light Decks which lead to a concentration of the stresses and possibly multiaxial compression.
- The lateral connections called Hammerhead joints transferred forces between arches, and the two arches deflected similarly when loaded on one arch only.
- The load at collapse was 970 kN which was 14% higher than the calculated ultimate load of 849 kN based on ideal abutment hinges. Possible reasons for the difference were: i) the abutment hinges had a rotational resistance, and must have decreased the bending moment and increased the capacity, ii) the strength in the Super-Light Decks close to the ribs may have been higher due to the multiaxial stresses, iii) the stabilizing effect of the light aggregate concrete blocks was not considered.
- Several damage warnings were observed before final collapse. First, the connections to the abutments started cracking at around 31% (300 kN) of the fracture load. Later, the arches cracked on the bottom of the loaded side, and concrete began spalling off from the bottom of the non-loaded side. This damage occurred at 84% to 94% of the fracture load.
- Finally, large deformations occurred (plastic hinges) in the arches when the last 6% of the fracture load was applied.

To reach the final objective, the first ever Pearl-Chain Bridge was built in Denmark in 2015 (Chapter 6). The lifting and positioning of the 12 Pearl-Chain Arches in the applied case was performed in half a working day by one crane.

## **7.1 Future research**

Two interesting aspects of the Pearl-Chain Bridge technology have not yet been explored.

First, the possibility of utilizing the strength and stiffness of the pervious concrete filling and the concrete road slab, and consider it when calculating the load carrying capacity of the arch. Small scale models of such a “sandwich Pearl-Chain Bridge” structure has already been tested at DTU. The initial results showed a large increase in load carrying capacity (more than a factor 8), compared to a plain arch loaded in the  $\frac{1}{4}$  point of the span.

Secondly, considering soil-structure interaction for Pearl-Chain Bridges with a higher rise to span ratio could, in some cases, be a better solution than the shallow arches investigated in this thesis.

## REFERENCES

- [1] NRMCA, "Concrete CO2 Fact Sheet," 2012.
- [2] K. D. Hertz and A. Bagger, "CO2 emissions from Super-light Structures," in *Proceedings of the International Association for Shell and Spatial Structures (iabse-ias) Symposium 2011 "taller, Longer, Lighter"*, 2011.
- [3] J. Bernini, N. Fitzsimons, and W. Heierli, "Overfilled Precast Concrete Arch Bridge Structures," in *IABSE Congress Report*, 2000, pp. 380–387.
- [4] C. O'Connor, "Development in Roman stone arch bridges," *Endeavour*, vol. 18, no. 4, pp. 157–162, Jan. 1994.
- [5] R. Heim, "Eisenbetonbogenbrücken im Landschaftsbild," *Internationales Organ für Betonbau*, 1914.
- [6] "Difficult falsework erection for 242-ft. concrete arch," *Engineering News*, 1916.
- [7] A. Wakeman, "The nucon arch - Plain precast concrete arch systems," *ARCH BRIDGES*, pp. 645 – 652, 1995.
- [8] D. Hutchinson, "Application and design of segmental precast arches," *Geotechnical Special Publication*, no. 126 I, pp. 452 – 459, 2004.
- [9] B. Boughton, "Precast reinforced concrete arch and portal units," *Concrete (London)*, vol. 39, no. 3, 2005.
- [10] Macrete, "www.macrete.com/flexiarch," 2014. .
- [11] P. Proctor and K. Seow, "Bridge replacement using low profile three hinged pre-cast arch in Newfoundland," in *2000 Annual Conference Abstracts - Canadian Society for Civil Engineering*, 2000.
- [12] G. E. Tan, T. B. Ong, K. K. Choong, and C. Y. Ong, "A New Form of Precast Closed Spandrel Arch Bridge System," *7th International Conference on Arch Bridges*, pp. 195–202, 2013.

- [13] FlexiArch, "Bendy Bridge," *New Civil Engineering International*, Nov-2008.
- [14] D. Mckittrick, "Contractor design and design build finance and operate, the increasing use of manufactured arches.," *ARCH BRIDGES*, pp. 683 – 691, 1995.
- [15] P. E. Mondorf, *Concrete bridges*. Polyteknisk forlag, 2006.
- [16] V. J. Elmont, "Test-loading until breaking point of a 100-foot arch bridge," *Canadian Engineer*, 1913.
- [17] A. H. Finley, "Deck participation in concrete arch bridges," *Civil Engineering (New York)*, vol. 2, no. 11, pp. 685 – 689, 1932.
- [18] W. S. Wilson, "Reinforced concrete arch bridges," *Surveyor*, vol. 88, no. 2272, pp. 143 – 146, 1935.
- [19] M. Han, S. Lee, J. Sim, and S. Jeon, "The Effects of Design Parameters on Structural Behavior of Arch Rib," in *7th International Conference on Arch Bridges*, 2013, pp. 125–132.
- [20] W. M. Wilson, "Tests of reinforced concrete arch bridges," *Association Internationale Des Ponts Et Charpentes -- Memoires*, vol. 5, pp. 375 – 422, 1938.
- [21] J. Ruzicka and L. Vrablik, "Shape Optimization of Arch and Shells Centerline," in *7th International Conference on Arch Bridges*, 2013, pp. 211–216.
- [22] L. L. Y. Lai, "Thermal effects on load rating of reinforced concrete arch bridges," *Structures Congress 2013: Bridging Your Passion With Your Profession - Proceedings of the 2013 Structures Congress*, pp. 479 – 490, 2013.
- [23] O. H. F. Hackedorn, "Three-hinged concrete arch bridge, Brookside Park, Cleveland," *Engineering News*, 1906.
- [24] H. E. Steinberg, "Eliminating initial stresses in concrete arch bridges," *Concrete and Constructional Engineering*, vol. 27, no. 6, pp. 326 – 327, 1932.
- [25] "EN 1991-2, Traffic Loads on Bridges." pp. 35–38, 2003.
- [26] S. Marx and G. Schacht, "Gelenke im massivbau," *Beton- und Stahlbetonbau*, vol. 105, pp. 27–35, 2010.

- [27] J. Dix, "Betongelenke unter oftmals wiederholter Druck- und Biegebeanspruchung," *Deutscher Ausschuss Für Stahlbeton*, vol. 150, p. 41, 1962.
- [28] G. D. Base, "Tests on four prototype reinforced concrete hinges," *Cement and Concrete Association -- Research Report*, 1965.
- [29] A. Griezic, "Stress-strain characteristics of confined concrete in column 'hinges,'" *Aci Materials Journal*, vol. 95, no. 4, pp. 419 – 428, 1998.
- [30] B. Moreell, "Articulations for concrete structures -- Mesnager hinge," *American Concrete Institute -- Journal*, vol. 7, no. 1, pp. 123 – 124, 1935.
- [31] R. W. Kluge, "Tests of reinforced concrete hinges," *Concrete and Constructional Engineering*, vol. 35, no. 12, pp. 605 – 615, 1940.
- [32] F. Leonhardt and H. Reimann, "Betongelenke -- Versuchsbericht, Vorschlaege zur Bemessung und konstruktiven Ausbildung," *Deutscher Ausschuss Fuer Stahlbeton*, pp. 1 – 34, 1965.
- [33] I. H. E. Nilsson, "Belastningsförsök på ofullständiga betongleder," *Nord Betong*, no. 6, pp. 17 – 22, 1977.
- [34] S. Marx and G. Schacht, "Concrete Hinges – Historical Development and Contemporary Use," in *Proceedings of the 3rd fib International Congress – 2010*, 2010, pp. 1–22.
- [35] O. P. Jain, "Ultimate strength of reinforced concrete arches," *American Concrete Institute -- Journal*, vol. 32, no. 6, pp. 697 – 713, 1960.
- [36] J. D. Marshall, J. B. Anderson, R. L. Meadows, and T. J. Jensen, "Full-Scale Testing of Three-Sided Precast Concrete Arch Sections," *Journal of Bridge Engineering*, vol. 19, no. 12, p. 04014051, Dec. 2014.
- [37] J. Zhang, C. Li, F. Xu, and X. Yu, "Test and Analysis for Ultimate Load-Carrying Capacity of Existing Reinforced Concrete Arch Ribs," *Journal of Bridge Engineering*, vol. 12, no. 1, pp. 4–12, Jan. 2007.
- [38] T. J. McGrath and M. E.P., "Finite-element modeling of reinforced concrete arch under live load," *Transportation Research Record*, no. 1814, pp. 203 – 210, 2002.

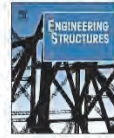
- [39] K. D. Hertz, "Light-weight load-bearing structures reinforced by core elements made of segments and a method of casting such structures," 08160304.5, 2010.
- [40] K. D. Hertz and P. S. Halding, "Super-light pearl-chain arch vaults," in *Proceedings of the Iass-slte 2014 Symposium*, 2014.
- [41] M. S. M. Lund, M. Arvidson, and K. K. Hansen, "Mechanical and Moisture Properties of Mortar Joints in Pearl-Chain Bridges," 2014.
- [42] "Robot Structural Analysis Professional." Autodesk, 2013.
- [43] P. S. Halding and K. D. Hertz, "Concrete Hinges," in *Proceedings of the Iass-slte 2014 Symposium*, 2014.
- [44] "Abaqus/CAE." Dassault Systèmes, 2012.
- [45] P. S. Halding, K. D. Hertz, N. E. Viebæk, and B. Kennedy, "Assembly and lifting of Pearl-Chain arches," *Proceedings of Fib Symposium 2015*, 2015.
- [46] "Aramis." GOM mbH, 2013.
- [47] P. S. Halding, K. D. Hertz, J. W. Schmidt, and B. Kennedy, "Full-Scale Load Tests of Pearl-Chain Arches," *Engineering Structures*, 2016.
- [48] "EN 1992-1-1 Design of concrete structures." 2008.
- [49] D. R. Directory, "Broer. Vejledning til belastnings- og beregningsgrundlag." p. 70, 2010.
- [50] M. S. M. Lund, K. K. Hansen, R. Truelsen, and L. Johansen, "Pervious concrete fill in Pearl-Chain Bridges: Using small-scale results in full-scale implementation," *Construction and Building Materials*, vol. 106, pp. 404–414, Mar. 2016.
- [51] M. S. M. Lund, "Experimental Study of Properties of Pervious Concrete used for Bridge Superstructure," *Proceedings of the 12th International Symposium on Concrete Roads*, 2014.
- [52] Danish Road Directory, "EN 1991-2 DK National Annex." p. 10, 2009.

## APPENDED PAPERS

- A. Paper I: Precast Pearl-Chain Concrete Arch Bridges**
- B. Paper II: Concrete Hinges for Pearl-Chain Bridges**
- C. Paper III: Concrete Hinges**
- D. Paper IV: Assembly and Lifting of Pearl-Chain Arches**
- E. Paper V: Full-Scale Load Tests of Pearl-Chain Arches**



# A PRECAST PEARL-CHAIN CONCRETE ARCH BRIDGES



## Precast Pearl-Chain concrete arch bridges



Philip Skov Halding<sup>\*,1</sup>, Kristian Dahl Hertz<sup>1</sup>, Jacob Wittrup Schmidt<sup>2</sup>

Technical University of Denmark, Department of Civil Engineering, Building 118, DK-2800 Kgs. Lyngby, Denmark

### ARTICLE INFO

#### Article history:

Received 5 March 2015

Revised 1 September 2015

Accepted 8 September 2015

#### Keywords:

Concrete

Arch

Pre-stressing

Post-tensioning

Pearl-Chain Bridge

Super-Light Deck element

Light aggregate

Theoretical case study

Bending moment capacity

Structural behavior

### ABSTRACT

A Pearl-Chain Bridge is a closed-spandrel arch bridge consisting of a number of straight pre-fabricated so called Super-Light Deck elements put together in an arch shape by post-tensioning cables. Several Pearl-Chain arches can be positioned adjacent to each other by a crane to achieve a bridge of a desired width. On top of the arch is a filling material to level out the surface of the above road. The filling only transfers vertical loads to the arch.

The geometry and material properties of Super-Light Decks are presented, and we refer to several full-scale tests of Pearl-Chain arches where the technology was used. We also study other important components and details in the Pearl-Chain Bridge concept and review the effects of different types of loads.

A theoretical case study of a circular 30 m span Pearl-Chain Bridge is presented showing the influence of a number of parameters: The number of post-tensioning cables, the rise to span ratio, the height of the filling, and the height of the Super-Light Decks. We find that Pearl-Chain Bridges can be adjusted to resist specific moment loads by changing the normal force in the arch cross section by altering the above parameters. It is also found that the negative bending moment capacity starts decreasing before the positive bending moment capacity does, when the normal force in the cross section is increased. This is because of the cross section of the Super-Light Decks include a combination of normal concrete and light aggregate concrete with light aggregate concrete blocks in the bottom of the cross section.

The positive bending moment capacity is therefore often larger than the negative, and that corresponds well with the required capacities when a concentrated load close to the quarter point of the span is applied. Such load is critical for arches, and gives a large positive bending moment below the load and a smaller negative bending moment in the unloaded side.

When the Pearl-Chain Bridge concept is compared to other pre-fabricated arch bridge solutions we find a number of advantages when using Pearl-Chain Bridges: Straight elements, combination of normal concrete and light aggregate concrete, flexible design control, and joint details.

© 2015 Elsevier Ltd. All rights reserved.

### 1. Introduction

Closed-spandrel arches have been a rare choice for bridge structures in the past 50 years. Now a new invention from the Technical University of Denmark – The Pearl-Chain Technology – reintroduces the closed-spandrel arch bridge in a modern version. This paper introduces the concept of Pearl-Chain Bridges (PC Bridges) and assesses the capabilities of such bridges with different spans, thicknesses and reinforcement solutions. Basically, the concept is to post-tension straight precast concrete elements together in an arch shape. The pre-fabricated elements used are called

Super-Light Decks (SL Decks) since they consist of a combination of light-aggregate concrete and regular concrete which gives a low self-weight of the arch. Post-tensioning is done with cables through curved ducts in the SL Decks.

Such Pearl-Chain arches are lifted by crane, and positioned on prepared foundations. The bridge width depends on the amount of arches being placed next to each other. Transfer of forces between adjacent arches is possible through specially designed in-situ cast shear locks. A special filling material is poured on top of the arch rib. See Fig. 1 for a general closed-spandrel arch bridge terminology.

The first use of arches dates at least back to the Egyptians in 3000 B.C., and later Roman engineers built vaults and arch bridges [1]. Stone was often the building material for arches and continued to be so for millennia until the introduction of iron bridges, steel bridges, and finally reinforced concrete bridges in the late 19th century [2,3].

\* Corresponding author. Tel.: +45 4525 1811.

E-mail addresses: [psh@byg.dtu.dk](mailto:psh@byg.dtu.dk) (P.S. Halding), [khz@byg.dtu.dk](mailto:khz@byg.dtu.dk) (K.D. Hertz), [jws@byg.dtu.dk](mailto:jws@byg.dtu.dk) (J.W. Schmidt).

<sup>1</sup> Tel.: +45 4525 1950.

<sup>2</sup> Tel.: +45 4525 1773.

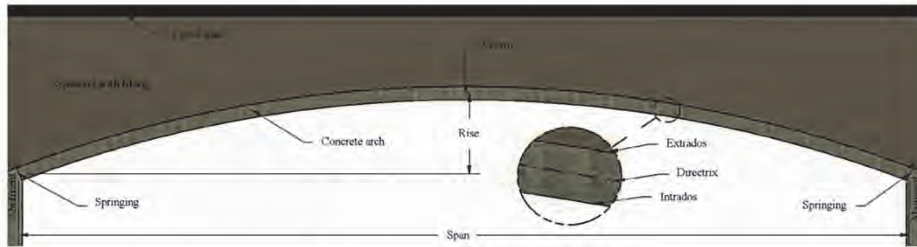


Fig. 1. Side elevation of classical closed-spandrel arch bridge. The crown is the top-point of the arch through the directrix (centerline), and the springings are the areas where the arch meets the abutments. The span is the horizontal distance between the springings at the level of the directrix, and the rise is the vertical distance from the chord between springings to the crown.

Robert Maillart (1872–1940) is probably the best-known engineer to have worked with concrete arch bridges. He made a major contribution to the development of this field in the beginning of the 20th century [4]. Zastavni [5] reviews Maillart's development from the early three-hinged arch bridges to non-hinged arches, and later deck-stiffened bridges. Maillart's work showed the limits of slender arch bridges, until Freyssinet's pre-stressing technique made it less expensive to build even longer spans.

Most closed-spandrel arch solution required in-situ casting and complex scaffoldings making the erection cost and time less competitive compared to other bridge solutions. Heim [6] shows an example of the extent of a typical early 20th century scaffolding solution for concrete arch bridges. Another problem was in-situ casting in cold weather [7], but with the introduction of pre-fabricated concrete elements in the 1960s such concerns became largely irrelevant for buildings and to some extent for bridges.

Different precast arch solutions have since been introduced for closed-spandrel arches. Examples are: BEBO, NUCON, TechSpan, Matiere and Macrete FlexiArch, though other systems exist as well [1,2,8–14].

### 1.1. Existing pre-fabricated arch concepts

NUCON and Macrete FlexiArch use smaller straight precast concrete elements put together in an arch shape, while BEBO, Matiere and TechSpan cast larger pieces so that one arch consists of one, two or three pieces. The benefit of smaller straight pieces is the possibility of stacking the elements during transportation, where larger curved precast segments need large trucks and take more space on the truck. On the other hand, larger curved precast arch parts have the benefit of fitting perfectly to the desired arch shape, where smaller straight segments will not follow the optimal continuous center line [15]. We define the optimal line as a shape where the total dead load does not create significant bending moments in the arch. All the concepts offer quick assembly (without scaffolding), and lifting by either one or two cranes. Some arches require pouring of joints after lifting, some do not. Concepts that rely on soil–structure interaction have strict guidelines for how to compact the filling. There may also be requirements to the level of filling above the crown, and with any increase in the filling height there will be an increase in the sizes of the bridge ramps to the above road. It is possible to reduce the ramps and the waste of space in the traffic clearance profile by changing the curvature of the arch, so that the arch is less curved above the traffic clearance profile.

BEBO started creating pre-fabricated arches for closed spandrel bridges back in 1965, where the first full-scale test took place [1]. Their arches have a high rise to span ratio, and rely on soil–structure

interaction, between the arch and the filling material, to have sufficient load-carrying capacity. The first BEBO arches consisted of several small, pre-fabricated, straight concrete segments that had to be assembled and cast together on site. The assembly procedure was solved by placing the elements on temporary scaffolding during the pour of the concrete in the joints. Later, the concept was changed so that one arch consisted of only one or two curved concrete pieces if the span is less or more than 14.6 m. Now, the erection could be performed having only one in-situ cast joint at the crown, and the assembly did not require formwork or scaffolding. The foundation is a spread footing and the springings of the arch are cast together with the footing without reinforcement, which allows a rotation. BEBO, though, claim that their closed-spandrel arches with high rise to span ratio exhibit practically no rotations at the hinges. The system allows spans of approximately 30 m, and any width is possible by adding several arches next to each other. Two cranes are required for lifting.

Marcel Matiere's pre-fabricated arch bridge concept, from the early 1980s, consists of three segments: two abutment elements, and one "roof" element [9,14]. The abutment elements include both a pre-fabricated foundation and an abutment wall with a slight curvature. The "roof" element is placed on the abutment elements, and the connections between the elements are functioning as hinges. The largest Matiere arch span is 20 m, and because the abutment elements can stand without support only one crane is required for the erection. Like BEBO the Matiere arches have a large rise to span ratio, but the largest Matiere arches have shallow "roof" element, which reduces the waste of space around the traffic clearance profile.

In 1995, the NUCON arch was an experiment in creating pre-fabricated high-strength concrete arches without reinforcement. Wakeman [2] explains the idea of building an arch of several small segments, inspired by old brick arches. All segments would be put next to each other and attached by wires to a lifting beam, so that the whole arch could be lifted in place in one piece. Each concrete piece was formed to interlock with the adjacent one, but at least two different types of elements were required for the correct assembly. Temporary ties had to be put in during the lift, but then the erection could be performed without scaffolding and with only one crane. After the assembly and lifting, the NUCON arch would not require any in-situ casting in the joints between elements. The span of the arch concept is not mentioned, but several arches next to each other would give the desired bridge width, and the static system is hingeless.

TechSpans arches (from 2004) are very similar to BEBO with two curved parts assembled at the crown [8,11]. One difference is the static system, where TechSpan puts in a metal plate creating a hinge when casting in-situ at the crown. This gives a

three-hinged arch, which is a statically determinate structure. The span is up to 20 m, with a rise to span of 0.3–0.4 for road bridges. Again, the soil–structure interaction is an essential part of the load-carrying capacity, and special requirements to the filling material are given. Each arch is 1.5 m wide, and 200 mm in height. Two cranes are required for lifting.

Macrete FlexiArch is the most recent invention (from 2008) with spans of up to 15 m [10,13,16,17]. The FlexiArch is very similar to the NUCON arch with many small straight pre-fabricated concrete segments put together similar to a brick arch. Each arch is assembled already before being transported to the erection site: a flexible membrane is attached to all the elements so that the arch can be transported as one flat piece. Then, as a crane lifts the arch the membrane holds together the small elements which naturally fall into an arch shape. The static system is hingeless, with concrete being poured as filling material.

Table 1 shows a summary of the different concepts.

The Pearl-Chain technology, presented in this paper, introduces both pre-stressing of the individual SL Decks, and post-tensioning to assemble the SL Deck elements in the desired shape. This is new from previously developed pre-fabricated arch systems. The density of the SL Deck is smaller than a massive concrete deck, and therefore lifting of larger spans is possible. Also, the post-tensioning method can provide a larger moment capacity to the arch, which allows even larger spans to be lifted, and for larger live loads to be resisted. The pre-compression of the arch comes from the pre-stressing, and post-tensioning, but also from the dead-load including backfilling material on the arch. The role of the filling in this study is purely to distribute loads vertically from the above road surface to the arch.

Tension and cracks do not occur until relatively large unsymmetrical loads are applied to the PC Bridge. The tension is initially resisted as a reduction in the pre-compression. The assembly and lifting procedure has already been successfully full-scale tested [18], see test-lifting in Fig. 2.

The concept is currently aimed at low rise-to span ratios and limited layers of filling above the arch crown. This reduces the sizes of the ramps, and the waste of space above the traffic clearance profile. Furthermore, lower rise to span ratios increases the pre-compression of the SL Deck elements.

Like NUCON and Macrete FlexiArch the Pearl-Chain Bridges consist of straight elements for easy transportation and stacking, and the unique design of the SL Decks and the curved ducts allows the post-tensioning cable to follow the arch shape even when elements are straight. This is state-of the art among pre-fabricated arch concepts.

Also, Pearl-Chain Bridges have excellent fire- and acoustical properties due to the light-aggregate concrete in the SL Decks used [19]. These topics, though, will not be addressed further in this paper, but makes the technology applicable for vaults in buildings too. Finally, the SL Deck is mass produced for application in buildings, which means that the price of the elements is low, and the bridge concept will therefore also have a commercial benefit.

The aim of the paper is to explore the design limits of PC arches through theoretical case examples. Furthermore, the presented PC Bridge concept will be compared to existing pre-fabricated arch concepts to show the advantages of PC technology.

## 2. The Pearl-Chain technology

The patented Pearl-Chain Reinforcement is invented at the Technical University of Denmark and commercialized by a spin-out company. It enables engineers to apply several straight SL Decks put together, and still be able to attain a desired centreline position. This is achieved through the Pearl-Chain principle, where

the concrete elements are post-tensioned together in the desired arch shape with curved ducts cast into the straight concrete elements.

The objective of this chapter is to introduce the geometry and materials of the SL Deck, to present the post-tensioning technique, and to explain conceptual details such as connections between SL Decks.

### 2.1. Pre-stressing and post-tensioning concept

The post-tensioning cables follow the shape of the arch, while the visible appearance shows the non-continuous shape of the joined concrete segments (SL Decks). When the post-tensioning cables follow the desired arch shape when suited inside the curved ducts, the force from post tensioning can introduce normal stresses only in the arch and no bending moments.

Both a full-scale PC arch consisting of three elements, and two arches of 13 m span have already been successfully assembled and tested [18,20]. All the tested arches had curved post-tensioning through straight SL Decks. Fig. 3 shows an example of the PC principle with a circular arch consisting of eight precast elements held together by post-tensioning cables through the ducts. The ducts are curved in a circular arch shape with a radius corresponding to the desired circle shape.

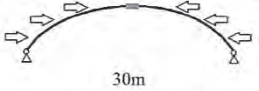
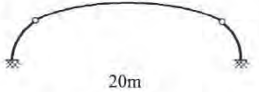
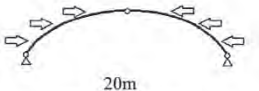
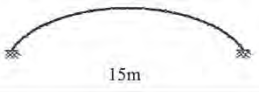
The SL Deck consists of a combination of light aggregate concrete blocks (3 MPa characteristic cylinder compressive strength) below and regular concrete (55 MPa characteristic cylinder compressive strength) above. The ends of each SL Deck are given a slight inclination enabling several elements to be joined together in an arch shape. In the joints the direction of the post-tensioning cables is perpendicular to the end surface. The SL Deck is a composite of light- and normal concrete, but closest to the joint to the next SL Deck it consists of at least 200 mm massive regular concrete. This insures an even transfer of forces between the elements, and a neutral axis in the middle of the cross-section, at the level of the cables. When the corrugated cable ducts form a 90° angle with the end surfaces of the SL Deck elements, the cables go from one SL Deck to the next without sudden bending.

In Fig. 4 some of the normal concrete in an SL Deck is cleared away in order to obtain a view of the geometry of the light-aggregate concrete blocks and reinforcement solution. In this case the PC arch has four light aggregate concrete blocks across with a width of 1.65 m. Pre-stressing strands are positioned as shown in the figure, and the duct with the post-tensioning cables is placed in the middle of the deck at a height that ensures that it will not create a bending moment in the arch bridge – only an axial thrust. This is possible since the neutral axis changes depending on the cross-section in the element: At the massive concrete (at each end) the neutral axis is in the middle, and in other cross-sections the neutral axis is above the middle because of the light aggregate blocks having a low stiffness.

Reinforcement bars are positioned between the blocks in the transverse direction. The transverse reinforcement is applied to distribute the load on the deck to the longitudinal grooves between the blocks, and because of the handling of each element during SL Deck production and bridge erection. Furthermore, it resists downward forces coming from the tightened post-tensioning cable, and helps to transfer forces transversely from one arch to another.

This example of an SL Deck and a PC Bridge can be combined in many ways. The configuration of pre-stressing strands can be altered, the height of the light aggregate concrete blocks can be adjusted, the total deck height and width can be altered, and more post-tensioning cables can be added. The flexibility of the design enables civil engineers to use the technology in almost any arch shape. Elements of equal length create a circular shape, and different length elements can form a shape with a curvature changing

**Table 1**  
Comparison of the described pre-fabricated concrete arch systems.

Concept	Advantages	Disadvantages	Schematic figure and largest span
BEBO (1965)	Small footings, perfect fit to desired shape, pre-stressed via large amount of soil, can change curvature over the span	Wasting space, difficult stacking of curved elements during transportation, needs two cranes, large ramps, in-situ casting of joint at crown, strict guidelines for filling, difficult production of curved elements	 30m
Matiere (1980s)	Good utilization of traffic clearance profile, only one crane for lifting, no in-situ casting after lifting	Difficult stacking of curved elements during transportation, difficult production of elements	 20m
NUCON (1995)	No corrosion of reinforcement, lifting by one crane, automatic interlocking of concrete elements, easy stacking and transportation of small elements	No reinforcement, risk of high stress concentrations in joints, temporary ties during lifting, complicated casting of the elements due to interlocking system	 20m
TechSpan (2004)	Small footings, perfect fit to desired shape, statically determined (in theory), can change curvature over the span	Wasting space, difficult stacking of curved elements during transportation, needs two cranes, large ramps, in-situ casting of joint at crown, strict guidelines for filling	 20m
Macrete FlexiArch (2008)	Only one crane for lifting, no in-situ casting after lifting, easy transportation, no corrosion of reinforcement, small ramps	No reinforcement, risk of high stress-concentrations in joints, filling is pure concrete. Only small spans	 15m



**Fig. 2.** Positioning of post-tensioned Pearl-Chain arch consisting of six SL Decks and two abutment elements (summer 2014). The span is 13 m.

over the span. Also, the PC concept can be used as vaults in buildings, and other structures [21].

## 2.2. Super-light deck geometry and materials

A PC Bridge has the lowest bending moment capacity either in the SL Decks or in the joints between the SL Deck elements. The joints consist of a special mortar having characteristic compressive strength of at least 80 MPa [22], which is higher than that of the regular concrete in the SL Deck elements (55 MPa). The post-tensioning cables are the only reinforcement in the cross section in the joints.

In the SL Deck cross section a number of pre-stressing strands are chosen. In the below example, see Fig. 5, each element of 1.65 m width has 8 pre-stressing strands in the top of the cross section with 50 mm concrete cover to the top surface. In the bottom of the cross-section between light aggregate concrete blocks are 4 strands with 75 mm concrete cover to the bottom, and 2 strands with a 112.5 mm concrete cover to the bottom. All strands have at least a space of 25 mm, and 50 mm concrete cover to the light aggregate concrete blocks. Additionally, there are two strands at each side with 50 mm concrete cover to the sides. All strands have

a cross-sectional area of 93 mm<sup>2</sup> and a characteristic ultimate strength of 1860 MPa. Both top and bottom strands are pre-stressed to e.g. 50% of the 0.1% proof strength of the steel. The light aggregate concrete blocks are the same as those used in 220 mm SL Decks, but a 270 mm deck height is required for use in bridges due to increased concrete covers. This means that 50 mm additional regular (55 MPa) concrete is applied in the top of the cross section compared to the 220 mm SL Deck for buildings. When increasing the height of the cross-section even further, more regular concrete can be added in the top of the cross section depending on the desired cross-section height.

Instead of the 2.4 m SL Deck width that is normally used in buildings, 1.65 m SL Decks can be used in Pearl-Chain Bridges to reduce the mass of each arch. Reducing the mass is beneficial for larger arch spans, since the PC arches are lifted into place by a crane. The minimum required width is 1.65 m when having four light aggregate blocks across – two in each side of the post-tensioning cables. 50 mm of normal concrete is required as a minimum on both sides of the SL Deck and between the two middle blocks regardless of the total deck width.

The light aggregate concrete blocks consist of the 3 MPa concrete, and between the blocks in the longitudinal direction is

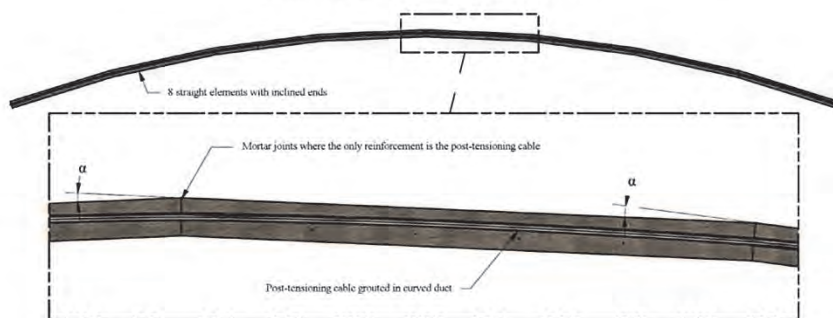


Fig. 3. Side elevation of a Pearl-Chain arch consisting of eight elements. In the bottom is a close-up of a cut of the bridge, where the curved ducts inside elements are visible, and join together in the desired arch shape.  $\alpha$  is the angle between two elements.

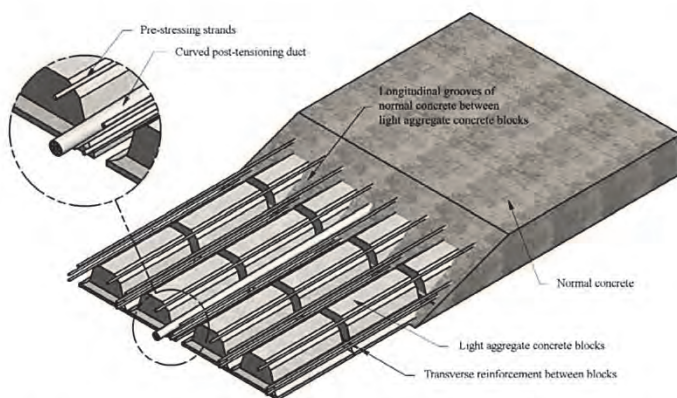


Fig. 4. View of the interior of an SL Deck element for PC Bridges. Light aggregate concrete blocks are positioned in a pattern with four blocks per 1.65 m width of the SL Deck. The duct is positioned in the middle of the deck. Pre-stressing strands are in the longitudinal direction, and slack reinforcement runs in the transverse direction between the blocks.

placed transverse stainless steel reinforcing bars of at least Y6 with strength of 550 MPa. Stainless steel is required since the concrete cover is smaller than required for the transverse bars.

The post-tensioning duct is positioned in the middle between blocks, and contains a number of cables each with a cross-sectional area of 150 mm<sup>2</sup>. The strength of the wires is equal to the pre-stressing strands, and post-tensioning is performed to typically 90% of the 0.1% proof strength of the steel.

### 2.3. Stresses and details

The regular concrete in the SL Decks forms ribs stabilized by the light-aggregate concrete blocks. In a cross section having the ribbed profile axial stresses will be more concentrated. When going from a ribbed cross section to the massive concrete cross sections at the ends, the concentrated stresses will distribute into the rectangular shape.

When pre-stressing the SL Decks the interaction between concrete and strands take place evenly along the strands. After release from the pre-stressing bed the strands shorten and compress the

concrete. Subsequently, the SL Decks are post-tensioned together. The post-tensioning is placed in a way which applies an evenly distributed normal stress at the ends of each SL Deck. The post-tensioning will further compress the concrete, and at the same time reduce the tension in the strands. It is expected that the concrete will be additionally compressed in the ribs as explained above. See Fig. 6.

The ribs are designed for resisting positive bending moments, and the expectation is that the negative bending moment capacity is lower than the positive. For use in arch bridges this is not a problem, since the load often causes a large positive bending moment and a smaller negative bending moment. The case study later in the paper demonstrates this difference in the moment capacities.

A number of important details are relevant when reviewing the PC concept: The connections between SL Deck elements, the connections between PC arches, abutment elements, lifting points, and hinges. The hinges have a significant influence on the static system. This is covered in the "Simplified Static System" section.





Fig. 7. SL Deck elements on edge positioned on shims on the ground during pour of joints. The bottom of the SL Decks is visible, and the darker areas are the bottom of the light aggregate concrete blocks.

when the Hammerhead joint is cast. The bars in Hammerhead joints may have to be stainless steel if applied close to the surface of the SL Decks. More information can be found in another article by the authors [18].

### 2.3.3. Abutment elements

The prefabricated concrete elements at each end of a PC arch are called abutment elements. Often these elements have to be made of massive concrete with additional reinforcement compared to the SL Deck elements. This is not because of the connection to the abutments but to the large stress concentration from anchoring the post tensioning cable. When the stresses at the area of the anchoring are distributed to the entire cross section large transverse forces develop. Therefore, transverse bars and stirrups are built into the abutments elements. An example of a possible geometry of an abutment element is seen in Fig. 8.

The direction of the curved duct is orthogonal to the end surface where the abutment element meets the first SL Deck. The inclined end of the abutment element is similar to the inclined ends of the SL Decks with a rough surface and shear locks.

An abutment element will consist of the same concrete (55 MPa) as the SL Deck elements, but may not be pre-stressed. When required draining holes can lead water through the abutment elements away from the bridge.

### 2.3.4. Lifting points

In general the lifting points, for the process of lifting a whole arch, are positioned in the regular concrete in the SL Decks. This is because the resistance to punching shear is better than in areas, where the light aggregate concrete blocks are present.

Four-point lifting of two 13 m span PC arches has already been described by the authors [18] including mid-air rotation of the arches. Additional lifting points can be created if necessary for lifting of larger spans.

## 3. Simplified static system and loads

As introduced previously, typical concrete arch bridges have between zero and three hinges. It seems impossible to have ideal hinges (zero bending moment) in arch structures, buried under an often compacted filling material. And we therefore apply an idealized or simplified static system.

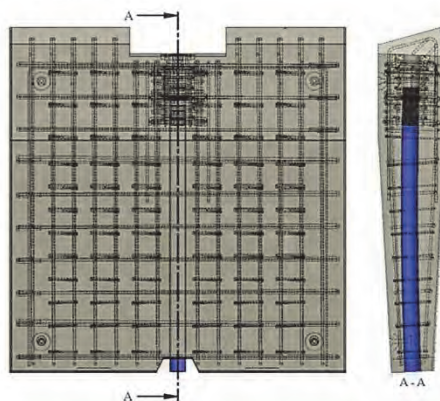


Fig. 8. Example of an abutment element for a PC Bridge showing one possible reinforcement solution. Section A shows a view through the curved duct (in blue) that ends in a standardized reinforced anchoring area. By courtesy of Perstrup Betonindustri. (For interpretation of the references to colour in this figure legend, the reader is referred to the web version of this article.)

A three-hinged arch solution has both advantages and disadvantages. It is statically determinate and has the advantage of avoiding an increased bending moment from shrinkage and creep, temperature changes, and settlement of the abutments. On the other hand, such a system has no additional reserve strength when the abutments settle, the rise decreases, and the horizontal reaction force thereby increases. In arches with a low rise to span ratio, even a small decrease in the rise can generate a large increase in the horizontal reaction force. Therefore, shallow arches are often designed with two or no hinges. This ensures that the arch resists the settlement by an increased bending moment. The PC test-arches built so far have been shallow, and therefore two-hinged solutions were chosen. An arch without hinges is an option as well, but the two-hinged system solution allows some uneven vertical abutment settlements, which can create an undesirable stress level in the hingeless system.

In the present work it is assumed that the horizontal reaction forces and horizontal settlements are withstood by either a rigid tension tie system, or by the ground being prepared. Concrete hinges were considered for use in PC Bridges, and specially designed hinges have already been full-scale tested at the Technical University of Denmark [23], see Fig. 9. The results showed that the designed concrete hinges had relatively small linear elastic rotation domains. As a consequence this type of hinge was not chosen for PC Bridges. Instead a type of saddle bearing hinge was implemented connecting the abutment and the abutment element in the built PC arches with a two-hinged static system (see more in [18]).

Determining the optimal static system for arch bridges was investigated by Zastavni [5], who built a very simple “topology decision-making tree” based on historical arch bridges. His parameters when deciding the static system included: The loading, the span, the support conditions, and the rise to span ratio.

### 3.1. Loading scheme

The critical loads on PC Bridges are non-symmetric, e.g. caused by a heavy vehicle [24–26]. Uniform traffic load over the entire

span is not a worst-case-scenario because the arch-shape is designed to resist this type of loading producing axial forces in the arch rib, while the increase in bending moment is small. This depends on the chosen shape. A uniformly distributed load can actually help to stabilize the arch structure. If the uniformly distributed load is applied as a permanent load from an increased height of the filling material above the crown, it will act as a pre-compression of the arch rib. An increase in the compression in the arch can make it more resistant to bending moments from heavy concentrated loads. On the contrary, if the pre-compression is too large the PC cross section will fail by exceeding the compressive strength of the concrete when subjected to a relatively small bending moment.

The optimal arch shape when subjected to a uniformly distributed load is a parabola. In theory, this shape will resist the load and give rise only to an axial force in the arch rib, so no moments or shear will occur [16]. Dead load from the arch alone will, theoretically, not create any bending and shear in the arch rib when the catenary shape is used [8]. The circular shape deviates from the other shapes in case of a large rise to span ratio, but is similar to the catenary and parabola for small rise to span ratios. Fig. 10 shows two examples of arch shapes. The first example is a parabola, catenary, and circle shape with a low rise to span ratio of 1/13, and the other is for a medium rise to span of 4/15. The tested full-scale PC arches had circular shape and a rise to span of 1/13.

Wilson [27] claims that a rise to span of 1/5 is typical, and that the final ratio depends on the site conditions. In general, there appears to be no consistency in the size of the rise to span ratios in the literature, but detailed shape optimization, as explained by Ruzicka [28], is not worth the effort for low rise to span ratios. This assertion is verified by the work of Findlay [25] and Han [16]. The results of Han's FE model shows insignificant difference in the distribution of axial force, bending moment and shear of different arch shapes having a rise to span of 1/10. Now it seems that a flat arch is always preferable, since it can be used whatever the shape. However, as explained earlier, bridges with low rise to span ratios are limited mainly by the soil stiffness at the abutments. If bridges are built on bed rock or if the horizontal forces can be resisted by a tension tie, arch bridges can have very low rise to span ratios. A tension tie solution was used in the first tests of PC arches. The initial choice for PC arches was the rise to span of 1/13. This was due to the acceptable fit of the circular shape (similar length SL Decks), to the level of pre-compression in the arch (optimizing the load bearing capacity), and to the low rise (for simple practical application). Several solutions for challenges with horizontal reaction forces are possible but this is not within the scope of this paper.

### 3.1.1. Temperature and time dependent deformations

When choosing a two-hinged or hinge-less arch system, temperature changes and creep create additional stresses in the PC arch.

A temperature growth will increase the rise (if a constant span is assumed), and a negative bending moment develops in the arch rib. The opposite happens for a temperature decrease. Lai [29] explains how temperature changes should always be taken into consideration when designing concrete arch bridges. He gives a term, derived by use of Castigliano's first theorem, for the increase in horizontal reaction force,  $H_t$ , in a two-hinged arch when a temperature change,  $T$ , occurs. A similar reduced term is given by Findlay [25]:

$$H_t = \frac{\alpha \cdot T \cdot I}{\int_0^s y^2 \frac{ds}{EI}} \quad (1)$$

where  $y$  is the vertical distance from the level of the springings to a point on the directrix in the arch rib,  $s$  is distance along the directrix

from the left springing to that same point, and  $\alpha$  is the thermal expansion coefficient of the material.  $E$ ,  $I$ , and  $I$  are Young's modulus, the moment of inertia and the span of the arch, respectively. The expression in the numerator,  $\alpha \cdot T \cdot I$ , is the total horizontal displacement of the abutments due to temperature changes if the arch was free to move.

From the above equation bending moment and axial force distributions in the arch rib are found by:

$$\begin{aligned} M &= H_t \cdot y \\ N &= H_t \cdot \cos\theta \end{aligned}$$

where  $\theta$  is the angle between horizontal and a tangent to the arch at the point. For PC Bridges the bending moment and normal force contribution from temperature changes are included in the load bearing capacity calculations. The size though, is often insignificant when compared to the critical live loads. For instance a 30 m span two-hinged PC Bridge with a rise to span of 1/13 (and cross section similar to Fig. 5) will develop a maximum of 14 kN m additional positive or negative bending moment for a 30 K temperature change.

It is assumed that the change in temperature is uniform in the arch rib. The thermal expansion coefficient of the regular concrete is  $5 \cdot 10^{-5}$  m/mK.

Other papers have discussed the issues of increased bending moments from temperature changes in arch bridges as well [26,30], and Wilson [27] presented a range of tests showing the effects of temperature and creep. The arches in PC Bridges are not vulnerable to shrinkage and creep due to pre-stressing of the individual pre-fabricated SL Decks, and the post-tensioning before lifting. Simply, the initial time-dependent deformations have already occurred before the arches are positioned. Steinberg [31] reported the use of flat jacks at the crown to jack up arches when they settle, to avoid problems with creep. The residual creep and shrinkage causes a reduction in the rise. By jacking up the arch directly after the positioning on the abutments the calculated level of reduction of the rise can be counteracted. Experimentation with this flat jack method has been tested during the erection of the tested PC arches [18].

Relaxation in the strands and cables will still occur.

### 3.1.2. Dead load

The moment capacity depends on the normal force, and the normal force depends on all of the following parameters: pre-stressing, post-tensioning, live load, and self-weight.

There is ambivalence when evaluating the effects of the self-weight in pre-fabricated arch bridges. Unlike straight beam bridges the self-weight contributes to the pre-compression of the arch. But pre-fabricated arches are lifted in place by crane, and to lift further the self-weight of the arch alone has to be kept as low as possible. But we do not prefer a large amount of dense filling above the arch rib, since the ramps of the above road will become longer and more expensive when a thick layer of filling is applied. Also, an increase in the self-weight increases both the vertical and horizontal reaction force, which again leads to a requirement for larger footings.

The self-weight depends on the exact configuration of the SL Decks and the material properties of the filling and road slab. The 55 MPa concrete has a density of 2300 kg/m<sup>3</sup>, while the light-aggregate blocks are approximately 800 kg/m<sup>3</sup>. The low self-weight of the blocks lowers the total weight of a PC arch, and therefore enables lifting with an increased lever arm.

The density of all steel is 7850 kg/m<sup>3</sup>. The number of SL Decks in one arch also has an influence on the self-weight of the arch alone.

The backfilling material in the PC Bridges which were used in the tests and the first actual projects consists of a granular material with a density of about 1800 kg/m<sup>3</sup>. It is perfectly drained so that

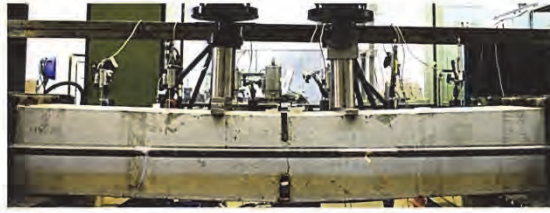


Fig. 9. Example of possible post-tensioned full-scale concrete hinge for PC arches being tested at the Technical University of Denmark.

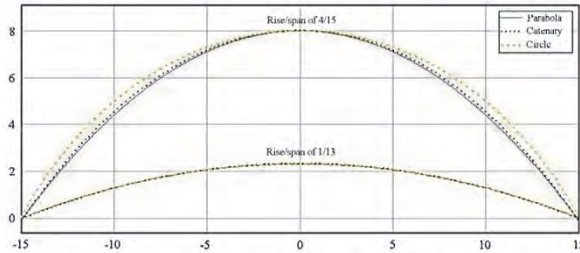


Fig. 10. Comparison between parabola, catenary and circle for rise to span of 1/13 and 4/15, respectively.

no pore water is present. Should any rain perforce the road slab and drain through the filling material, holes at the abutment elements will lead the water away from the spandrel area. The filling material is often spread out on the arch and leveled to the height of the crown (for small ramps), but depending on the bridge geometry, the height of the filling can be increased to any level above the crown (for larger pre-compression of the arch).

On top of the backfilling is usually a road slab of about  $4 \text{ kN/m}^2$ . This corresponds to a regular paved road.

### 3.1.3. Live loads and lifting

The challenge for arches is concentrated loads on one half of the span only. Vertical forces acting close to the  $\frac{1}{4}$  point of the span of an arch causes a positive bending moment in the arch rib below the force, but at the same time a negative bending moment in the opposite unloaded half. The pre-compression, due to the arch shape and level of self-weight, helps resisting these bending moments to a certain extent. This happens by withstanding tension in the arch rib as a reduction in the pre-compression. A large concentrated load around the  $\frac{1}{4}$  point is the worst case, but the back filling material in closed-spandrel arch bridges distributes a concentrated load from a wheel to a larger area on the surface of the arch. For shallow arches this relieving effect is not as beneficial as for high rise arches.

In general the heaviest trucks and trains have many axles distributing the load over a large area on small span bridges. They may contribute with the greatest total weight, but not give rise to the biggest bending moments in small arch bridges. Other less heavy vehicles may be more critical in regard to bending moments because of a more concentrated weight distribution. For instance, a so called Tandem System has only 1.2 m between its two axles of each 300 kN [32], which can be challenging when positioned in proximity of the  $\frac{1}{4}$  point of the arch span. Fig. 11 shows 66 tons test-loading on two PC arches in the  $\frac{1}{4}$  point of the span.

As explained earlier, lifting is performed in four or more points on the arch, and the number of lifting points can be increased for larger spans. We do not go further into detail with the lifting procedure in this work.

## 4. Case study of PC Bridge

To exemplify the PC concept a case study of a PC Bridge is evaluated based on a specified calculation method. Some input parameters in the calculation are varied to illustrate the structural behavior. Furthermore, calculated bending moments, axial thrusts, etc. are compared with results from an FE model in Robot Structural Analysis.

### 4.1. Calculation method

Finding the theoretical moment capacity was done assuming ideal hinges. The general input parameters required for such calculation were:

- Number of hinges and choice of arch shape.
- Number of SL Decks in one arch.
- Rise and span.
- Level of interaction with adjacent arches.
- SL Deck thicknesses and widths.
- Stress level and number of pre-stressing strands and post-tensioning wires.
- Position of pre-stressing strands.
- Height of filling material.
- The material properties.

In order to investigate the capacity, and to draw influence lines for the bending moment, reactions, and axial force of a point load moving across the bridge, analytical calculations were performed.



Fig. 11. Test of two PC arches with 66 tons of load in the critical 1/4 point of the span.

Superposition was then used when adding influence lines for the loads corresponding to each axle of a chosen type of vehicle.

Initially the number of hinges, the arch shape, the level of interaction with adjacent arches, and the rise to span ratio were selected. The number of SL Decks was chosen, and the length of each element was calculated. The amount of post-tensioning was picked, and the overall weight could be calculated based on the geometry and material data. Temperature loads were found as well.

Having calculated the axial stiffness, the static stiffness, and the flexural stiffness of the SL Decks, the moment capacities were found for different normal forces. The normal force changes depending on the position of the live load on the arch. For shallow arches the distribution of force from the live load was conservatively assumed to act on the arch rib exactly below the point where the concentrated load is positioned on the road surface. For every position of a vehicle the axial force and load carrying capacity must be calculated. The capacity is then compared to the bending moment from the load of the vehicle. Calculations were performed in steps of 0.3 m for the position of the vehicles, and also in steps of 0.3 m around the  $\frac{1}{4}$  points of the arch.

A chart of the calculation process is shown in Fig. 12.

Stability issues were not investigated in this study, since the filling material and adjacent arches have a stabilizing effect.

#### 4.1.1. FE-model

FE calculations performed in Robot Structural Analysis [33] are based on massive concrete sections. Using the found stiffness of the chosen SL-Deck a solid concrete deck element with similar stiffness is modeled instead. In the analytical approach it is assumed that the arch shape is similar to the circular post-tensioning cables, but in the FE model we calculate the elements always having the neutral axis in the middle of the cross section. This difference in approach results in an insignificant error. An example of the difference between numerical and analytical calculation can be seen in Fig. 13. It shows the moment distribution of a 30 m span circular arch of width 1.65 m subjected to dead load including self-weight from the arch, filling to the top point of the arch, and a road slab.

Similarly, normal forces can be found, and combinations of moment and normal force can be determined for different positions of an applied load.

#### 4.2. Design examples

Examples of design of a 30 m span Pearl-Chain Bridge are now presented. The objective is to investigate the effects on the bending moment capacities when altering the design parameters.

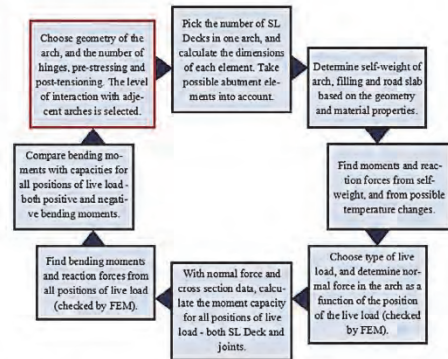


Fig. 12. Flow chart of calculations of moment capacity of PC Bridges. The initial step in the design iteration is marked in red. (For interpretation of the references to colour in this figure legend, the reader is referred to the web version of this article.)

In the following case some of the geometric parameters are fixed: The span is 30 m, the shape is circular, the width is 1.65 m, the arch consists of 12 elements, two abutment hinges are included, and the number, size and force of pre-stressing strands is identical to the strands presented in Fig. 5. To illustrate the structural behavior the following parameters were investigated for different values:

- The thickness of the SL Decks (270 mm, 320 mm, 370 mm, and 420 mm) with a fixed size of the light aggregate concrete block similar to the example in Fig. 5.
- The rise to span ratio (1/13, 1/10, and 1/7.5) with the supports being infinitely stiff.
- The number of post-tensioning cables (7, 9, and 13).
- The level of filling above the crown (0 m, 1 m, and 2 m) with a road slab above the filling. The properties of the materials are presented in Section 2.2.

The investigated arches are subjected to a test load consisting of two point loads. The point loads are 112 kN and 64 kN, respectively. The distance between the loads is 3 m. The loading is the same in all cases. An overview of the bending moment capacities for combinations of the different parameters is seen in Fig. 14. In the figure "SL42 1/13" means a SL Deck with deck thickness of 420 mm in an arch with rise to span of 1/13. Note that the iterative approach described in Fig. 12 is not performed in the example. This

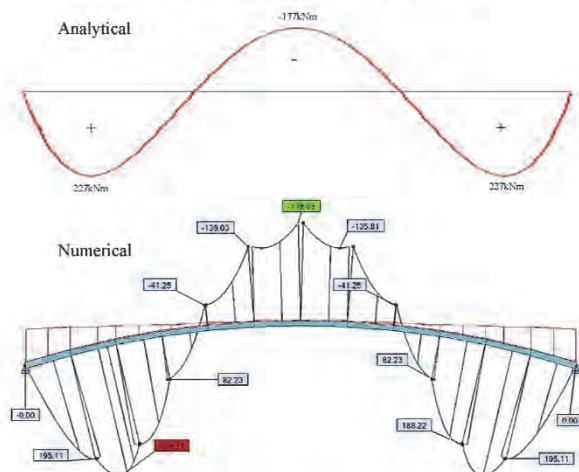


Fig. 13. Output example from Robot Structural Analysis compared to analytical solution. It shows a moment distribution when a 30 m arch is applied self-weight alone. Units are kN m.

is because the calculations are based on input parameters (such as e.g. the rise to span ratio) that have been pre-defined and do not require iteration. Safety-coefficients are not implemented in the case study calculations.

All capacities in Fig. 14 are found as the smallest numerical value of the capacities in the SL Deck or the joints between SL Decks. In almost all cases, the positive bending moment capacities are limited by the joints between SL Decks, and the negative bending moment capacities are limited by a cross section in the SL Decks. The transfer of forces to adjacent arches has not been taken into account in the example.

Fig. 15 shows the relationship between the normal force in the cross section and the SL Deck moment capacities for the case with a rise to span ratio of 1/13. For the positive bending moment the capacity increases when the normal force increases. The normal force increases when the number of post-tensioning cables increases, and when the amount of filling gets larger. All the points in the figure refer to combinations of the parameters similar to what is shown in Fig. 14. In the figure we only study the behavior based on the capacity of a cross section inside the SL Deck. Because of the shape of the cross section in the SL Decks it is expected that the negative bending moment capacity is lower than the positive. At a certain level of the normal force the negative bending moment capacity begins to decrease with an increasing normal force. For positive bending the same occurs but at a larger normal force, and the difference is because of the cross section geometry with the light aggregate blocks in the bottom. The worst load we can apply to any arch is a large point load close to the  $\frac{1}{4}$  point of the span, such as the load in the case study. Such load will generate a large positive moment below the load in the loaded side, and a smaller, but not insignificant, negative moment in the unloaded side of the arch. We therefore require a larger positive moment capacity which is obtained when using SL Decks. Depending on the given load it is easy to adjust the capacities of a PC Bridge by adding or removing post-tensioning cables or filling material in the design process.

When comparing the bending moment capacities of the 1.65 m wide SL Decks from Fig. 15 with the joints between the SL Deck elements we discover an essential detail. In most of the studied cases the positive bending moment of the joints is lower than that of the SL Deck. This means that a possible fracture due to an applied positive moment will occur in the joint and not in the SL Deck. This means that warnings of the bridge being loaded close to its capacity may be observed as cracks or spalling of concrete in the joints at or close to the quarter point of the span. Fig. 16 shows the positive moment capacity of the joints compared to the capacity of the SL Decks for similar combinations from the case study.

Now, we investigate the influence of the filling material and the rise to span ratio. As mentioned, the filling will add to the level of pre-compression. Fig. 17 shows the order of magnitude of the effect of this pre-compression in case of a 270 mm SL Deck, and a 420 mm SL Deck with 7 post-tensioning cables. The positive moment capacity is nearly similar for the 270 mm SL Deck having 2 m of filling material above the crown of the arch compared to the 420 mm SL Deck with 0 m of filling. As expected the moment capacity decreases when the rise of the arch gets larger. The shape of the arch is still circular in all cases no matter which rise to span ratio we consider. This is why the small difference between the capacities of the 270 mm (2 m filling) and 420 mm (0 m filling) SL Decks do not change significantly at different rise to span ratios. When we see some change in the difference it can be explained by the filling above the crown being a uniformly distributed load. The arch has a circular form which does not resist the uniformly distributed load perfectly like a parabola would. Therefore, a larger initial positive bending moment is applied to the arch when adding an extra layer of filling. Note also that an increase in the normal force may still reduce the negative moment capacity (for the given geometries in this theoretical case study).

The number of post-tensioning cables may be determined by the requirements when lifting the arch, and if it is necessary to reduce the normal force a change in the rise to span ratio is a solution when the filling is already 0 m above the crown of the arch.

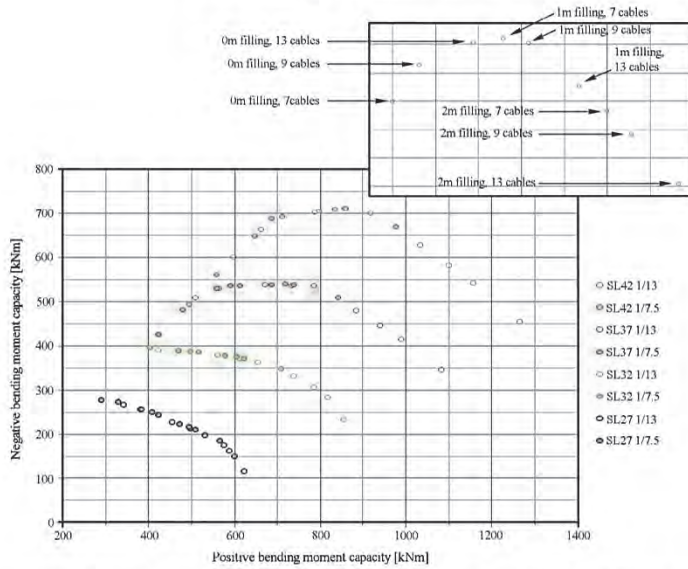


Fig. 14. Relation between positive and negative bending moment capacity of PC arches. Combinations are plotted with different SL Deck cross sections, rise to span ratios, level of backfilling, and number of post tensioning cables. The sequence of plotted combinations is shown in the top right corner.

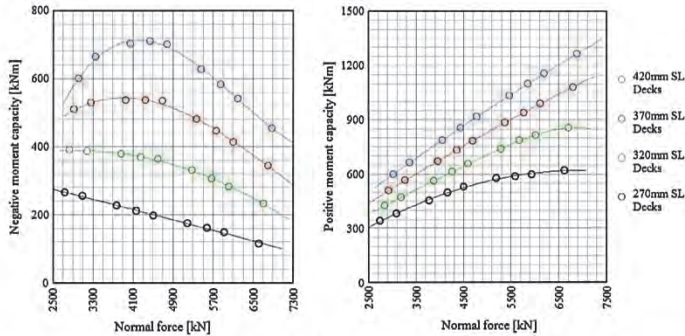


Fig. 15. Negative and positive bending moment capacity for SL Decks in one arch as a function of the normal force in the cross section. The rise to span ratio is 1/13. The four different SL Deck thicknesses are plotted, and each circle represents one combination from the case.

5. Comparison of Pearl-Chain Bridges and existing concepts

We now compare the Pearl-Chain Bridge technology to other prefabricated arch bridge concepts. In general it should be noted that the results in the case are conservative since the calculations are based on one arch only, assuming no interaction with adjacent arches and no bending capacity of the road slab. The force from a concentrated load on the road surface was also assumed to act exactly at an area on the arch directly below, though the road slab and filling material would distribute the force to a larger area.

When we compare the special properties of PC Bridges with the other closed-spandrel pre-fabricated arch bridge concepts

mentioned earlier in the introduction, substantial differences become evident:

1. The first obvious advantage is the straight SL Deck elements. The easy stacking of straight elements enables a more efficient transportation than for concepts where curved elements are used. The Macrete Flexiarch has the same advantage of transporting straight elements, though they are limited by the length of the truck during transportation, where the shorter SL Decks can be stacked on top of each other instead. Also, the bed where the SL Decks are cast can easily be adjusted to create SL Decks of any length. By decreasing the length of an

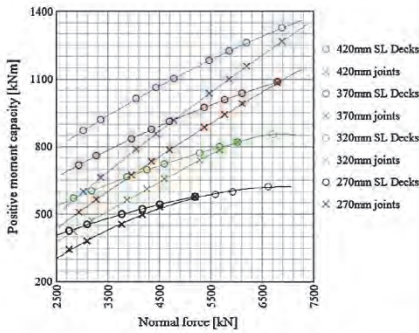


Fig. 16. Positive moment capacity of SL Decks and joints as function of the normal force in the cross section. The rise to span ratio is 1/13. Each mark represents one combination from the case.

element, and giving the post-tensioning duct a larger curvature the bridge shape can be changed to whatever may be required in a specific project.

2. A significant feature is the combination of the normal concrete, and the light-aggregate concrete. The SL Deck cross section ensures a sufficient bending moment capacity, but with a lower weight than the other concepts. The cross-section is designed so that the positive bending moment capacity is large, and that the negative bending moment capacity somewhat smaller. This corresponds with the worst loading situations on arches, where a large concentrated load (close to the 1/4 point of the span) gives a large positive moment below the load and a smaller but not insignificant negative moment in the unloaded half of the arch. The lower arch self-weight makes it possible to lift further with only one crane. BEBO for instance change from a one-crane lifting sequence into a two-crane lift when the span exceeds 14.6 m. Lifting further, and with only one crane, minimizes the traffic disturbance during the erection, and is less expensive. As a bonus the light aggregate blocks underneath a PC arch have

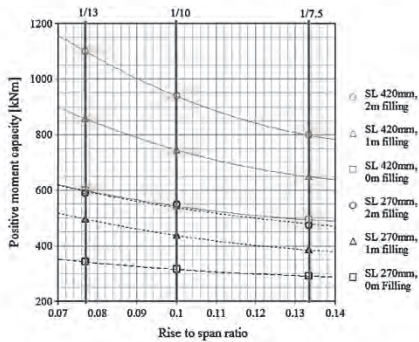


Fig. 17. Positive moment capacity as a function of the rise to span ratio for PC arches with 7 post-tensioning cables. SL Decks of height 270 mm and 420 mm are used with different amounts of filling. The rise to span ratios 1/13, 1/10, and 1/7.5 are combinations from the case.

excellent acoustical properties compared to a regular concrete surface.

3. Another advantage is the ability to control the pre-compression in PC arches. With pre-stressing of the SL Deck elements and post-tensioning of the arch it is possible to completely control, and optimize the normal stress in the arch. All other concepts do this only by adjusting the rise to span ratio, and the amount and density of the filling material. Furthermore, the level of shrinkage and creep is reduced for PC arches due to the pre-stressing before assembly, and post-tensioning before lifting.
4. The assembly is performed with only casting concrete in the Hammerhead joints between the arches. The joints between each SL Deck in an arch are cast before the arch is lifted into position. This is somewhat similar to the concepts by BEBO, and TechSpan, where the crowns of all adjacent arches are cast together in-situ. The use of “concrete against concrete” in compression as seen in the concepts by NUCON, Matiere and Macrete is not chosen for PC arches. This is because of the challenges with a high level of pre-stressing of arch structures, where small irregularities in the compressed concrete surfaces could cause stress concentrations and cracking. The joints between each SL Deck in an arch are in many situations weaker than the SL Decks under the action of positive bending moment. When a joint is positioned at or close to the 1/4 point of the span, the expectation is to achieve fracture in the joint with a possible warning from cracking or spalling of concrete before failure.
5. As mentioned earlier large horizontal reaction forces occur for low rise to span ratios, and if a PC Bridge is designed without a rigid tension tie, this may limit the possibilities of the concept because of requirements for expensive foundation solutions. Another solution is to utilize the soil-structure interaction like e.g. TechSpan does. But this does not have sufficient effect on low rise to span arches. The already built PC arches have successfully used a tension tie system, and future research by the authors will investigate a new method to reduce the large horizontal reaction forces.

The above considerations show that the PC Bridge concept is versatile as well as flexible. PC Bridges are expected to be used in a wide range of spans, also exceeding 30 m, which was the basis of the case study.

6. Conclusion

Pearl-Chain Bridges are closed-spandrel arch bridges consisting of straight pre-fabricated Super-Light Deck elements joined together in an arch shape by post-tensioning cables. Several Pearl-Chain arches are positioned beside each other by crane to achieve the desired bridge width, and a filling material is placed in top of the arches to achieve a road surface at a desired level. Properties and geometry of all components in Pearl-Chain Bridges are presented.

A case study of a circular 30 m span Pearl-Chain Bridge is presented to show the influence of the parameters: Number of post-tensioning cables, rise to span ratio, height of the filling, and height of the Super-Light Decks. A method for capacity calculations is presented, and it is found that Pearl-Chain Bridges can practically be designed to resist specific bending moments by adjusting the normal force through changing the above parameters. This is illustrated in an example in the case where a 270 mm Super-Light Deck with 2 m of filling above the crown has the same positive moment capacity as a 420 mm Super-Light Deck with 0 m of filling above the crown. The positive moment capacity is often larger than the negative, and this corresponds well with the required capacity

when the most critical loads are applied: A concentrated load close to the  $\frac{1}{4}$  point of the span, which gives a large positive moment below the load and a smaller negative moment in the unloaded side.

The theoretical case study also shows that the joints between Super-Light Deck elements often are weaker than the Super-Light Decks for positive bending moments. Therefore, fracture may occur in the joints with possible warnings from cracking or spalling. In general the negative bending moment capacity is smallest in the Super-Light Decks. It has to be taken into consideration when designing Pearl-Chain Bridges that the negative moment capacity starts decreasing before the positive moment capacity does, when the normal force in the cross section is increased. This is due to the fact that the cross section of the Super-Light Deck elements is a combination of normal concrete and light aggregate concrete.

When Pearl-Chain Bridges are compared to other pre-fabricated arch bridge solutions we find a number of advantages including the use of straight elements, the state-of-the-art combination of normal concrete and light-aggregate concrete, the flexible control of the pre-compression from pre-stressing and post-tensioning, and finally, the connection details and assembly method. The largest disadvantage for the Pearl-Chain concept is the large horizontal reaction forces that must be resisted by either large abutment constructions or a tension tie system.

### 6.1. Future research

All calculations were performed in two dimensions, and any out of plane behavior was not included. Another interesting detail that could be investigated is the effect of settlement of the abutments, and choosing the requirements of the soil at erection sites. Furthermore, developing new solutions to reduce the horizontal reaction forces is relevant.

Finally, testing the type of fracture at ultimate load, and exploring the strain and stresses of the SL Deck when used in PC Bridges are interesting when determining the span limits for the technology.

### Acknowledgements

The authors wish to thank Innovationsfonden for funding the research in Pearl-Chain Bridges. Also, we are grateful for the cooperation with the project manager Nicky Eide Viebæk from the company Abeo A/S, and the rest of the Pearl-Chain Bridge working group consisting of the representatives from the companies: Grøntmij, Skandinavisk Spændbeton, and Perstrup Betonindustri.

### References

- [1] Bertini J. Overfilled precast concrete arch bridge structures. BEBO of America; 2000.
- [2] Wakeman A. The NUCON arch – plain precast concrete arch systems. Arch Bridges 1995;645–52.
- [3] Billington DP. Building bridges: perspectives on recent engineering. Ann NY Acad Sci 1984;424:309–24.
- [4] Lafranchi M. Robert Maillart's curved concrete arch bridges. J Struct Eng 1997;123(10):1280–6.
- [5] Zastavni D. Typological decision-making tree for the design of arch bridges from historical studies. In: 7th international conference on arch bridges, 2013. p. 325–32.
- [6] Heim E. Eisenbetonbogenbrücken im Landschaftsbild. Internationales Organ Für Betonbau 1914;(Heft 6):121–4.
- [7] Protective measures make possible winter construction of concrete arch bridge. Constr Methods 1929; 11(11): 38–9.
- [8] Hutchinson D. Application and design of segmental precast arches. Geotech Spec Publ 2004;126(1):452–9.
- [9] Boughton B. Precast reinforced concrete arch and portal units. Concrete (London) 2005;39(3).
- [10] Homepage of Macrete Flexiarch. Ireland. <www.macrete.com> [Last accessed March 2015].
- [11] Proctor P, Seow K. Bridge replacement using low profile three hinged pre-cast arch in Newfoundland. In: 2000 annual conference abstracts – canadian society for civil engineering, 2000. p. 254–60.
- [12] Tan GE, Ong TB, Choong KK, Ong CY. A new form of precast closed spandrel arch bridge system. In: 7th international conference on arch bridges, 2013. p. 195–202.
- [13] FlexiArch. Bendy bridge. New civil engineering international, November 2008. p. 20–1.
- [14] Mekitnick D. Contractor design and design build finance and operate, the increasing use of manufactured arches. Arch Bridges 1995:683–91.
- [15] Mondorf PE. Concrete bridges. Polyteknisk forlag; 2006.
- [16] Han M, Lee S, Sim J, Jeon S. The effects of design parameters on structural behavior of arch rib. In: 7th international conference on arch bridges, 2013. p. 125–32.
- [17] Long DBE, McPhee D, Kirkpatrick J, Gupta A, Courtenay D. FlexiArch : from concept to practical application. Struct Eng 2014;92(7):10–5.
- [18] Halding PS, Hertz KD, Viebæk NE, Kennedy B. Assembly and lifting of pearl-chain arches. In: Proceedings of FIB symposium 2015, 2015. p. 185–6.
- [19] Hertz K, Castberg A, Christensen J. Super-light concrete decks for building floor slabs. Struct Concr 2014;15(4):522–9. <http://dx.doi.org/10.1002/suco.201300062>.
- [20] Hertz KD, Halding PS. Super-light pearl-chain arch vaults. In: Proceedings of the IASS-SLTE 2014 symposium, 2014.
- [21] Hertz KD. Super-light concrete with pearl-chains. Mag Concr Res 2009;61(8):655–63. <http://dx.doi.org/10.1680/jmcr.2008.61.8.655>.
- [22] Lund MSM, Arvidson M, Hansen KK. Homogeneity and strength of mortar joints in pearl-chain bridges. In: Proceedings of fib symposium, 2015. p. 187–8.
- [23] Halding PS, Hertz KD. Concrete hinges. In: Proceedings of the IASS-SLTE 2014 symposium, 2014.
- [24] Elmont VJ. Test-loading until breaking point of a 100-foot arch bridge. Can Eng 1913;24:739–44.
- [25] Binley AH. Deck participation in concrete arch bridges. Civ Eng 1932;2(11):685–9 [New York].
- [26] Wilson WS. Reinforced concrete arch bridges. Surveyor 1935;88(2272):143–6.
- [27] Wilson WM. Tests of reinforced concrete arch bridges. Association Internationale Des Ponts Et Charpentiers – Memoires 1938;5:375–422.
- [28] Ruzicka J, Vrablik L. Shape optimization of arch and shells centerline. In: 7th international conference on arch bridges, 2013. p. 211–6.
- [29] Lai LLY. Thermal effects on load rating of reinforced concrete arch bridges. In: Structures congress 2013: bridging your passion with your profession – proceedings of the 2013 structures congress, 2013. p. 479–90.
- [30] Hackstedt OHF. Three-hinged concrete arch bridge, Brookside Park, Cleveland. Eng News 1906;55(18):507.
- [31] Steinberg HE. Eliminating initial stresses in concrete arch bridges. Concr Constr Eng 1932;2(6):326–7.
- [32] EN 1991-2. Traffic loads on bridges, 2003; 1: 35–8.
- [33] Autodesk Robot Structural Analysis Professional 2013, SP3. Structural software. <www.autodesk.com>.



# *B* CONCRETE HINGES FOR PEARL-CHAIN BRIDGES

# Concrete Hinges for Pearl-Chain Bridges

**Philip S. Halding<sup>a</sup>, Kristian D. Hertz<sup>a</sup>, Jacob W. Schmidt<sup>a</sup>.**

<sup>a</sup>Technical University of Denmark, Department of Civil Engineering, building 118, DK-2800 Kgs. Lyngby, Denmark.

## **Abstract:**

Pearl-Chain Bridges is a pre-fabricated concrete arch bridge concept, where pre-tensioned elements are post-tensioned together in a low rise to span arch shape. Pearl-Chain Bridges therefore have a relatively high level of normal force which possible concrete hinges must accommodate. Two specially designed hinges are tested: A Mesnager inspired hinge, and an orthogonal saddle bearing hinge. Both types are full-scale tested. The Mesnager inspired hinge is lab-tested, while the orthogonal saddle bearing is implemented in a load test of two 13 m span Pearl-Chain Arches.

Numerical models are created for both, and results show only little deviation between tested and modeled behavior in the elastic region. The Mesnager inspired hinge fits well with a universal hinge response rotation-moment-curve from the literature despite of the high level of normal stress. The model of the orthogonal saddle bearing hinge is used in finding the influence of the mortar stiffness and mortar layer thickness on the rotation behavior.

Finally, the influence of local hinge response in a global arch structure is illustrated with the Mesnager inspired hinge being implemented in a model of the tested 13 m span Pearl-Chain Arches in Robot Structural Analysis.

## **1. INTRODUCTION**

The resistance of hinges used in arch structures has a significant influence on the overall static system. A resistance during rotation of the hinge means that the static system does not behave as desired - with the assumption of ideal, zero bending moment hinges. An ideal hinge response, with no resistance, is difficult to obtain in real life structures which often results in magnitudes of section forces and bending moments somewhere in between the ideal hinge, and a fixed connection, Figure 1.

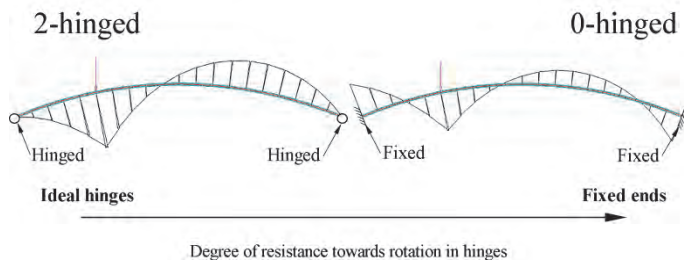


Figure 1: Influence of hinge rotational resistance on bending moment distribution in a loaded two-hinged arch.

The first type of concrete hinge was a so called saddle bearing (originally developed by German Claus Köpcke in 1880) where basically two concrete surfaces with similar radii were connected in compression – one with concave and one with convex shape [3]. The rotation would then happen with a resistance from the friction between the surfaces. Sometimes a thin sheet of lead was put in between the concrete surfaces to reduce friction.

The saddle bearing evolved into two surfaces with different radii, which means that the rotation in the hinge had more of a rolling character compared to the sliding in the first saddle bearing type [4-6].

In the start of the 20<sup>th</sup> century Mesnager and Freyssinet each developed a new type of concrete hinge by reducing the cross section height,  $b_2$ , of the concrete at the hinge position to  $b_1$ , see Figure 2. The reduced cross section is called the hinge throat. First, Augustin Mesnager created such hinge with crossing reinforcement through the hinge throat. His design was focused on the mild steel reinforcement and disregarded the concrete in the throat area. The steel bars were designed to transfer both shear and normal forces and the job of the concrete was to protect against corrosion.

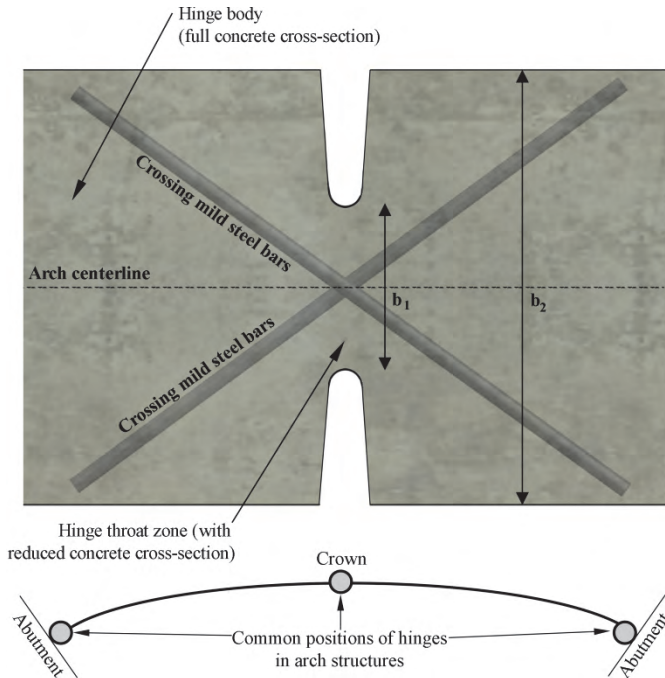


Figure 2: Mesnager and Freyssinet type concrete hinge with reduced height at the hinge throat.

Freyssinet had a similar design but without the crossing mild steel bars in the throat so that section forces had to entirely be transferred through the concrete. In the throat the concrete is subjected to multi-axial stress as described by Base [5]. The normal stress from the arch structure changes direction in a bottleneck shape near the throat and creates a lateral confinement of the concrete in the throat. The confined concrete has a capacity up to several times higher than the unconfined cylinder strength. For “one-way hinges” Griezic et al. [7] introduced an empirical confinement factor based on test results. The factor is very conservatively limited to the value 1.7 regardless of the  $b_1$  to  $b_2$  ratio:

$$c = \frac{1}{1 - 0.5k_1 \left[ 1 - \frac{b_1}{b_2} \right]} \quad (1.1.)$$

The parameter  $k_1$  is 1.1 for “one-way hinges”. Moreell [6] describes how Mesnager tested full-scale hinges and found that the concrete in the hinge throat, that he would ignore in regard to load carrying capacity, would actually increase the fracture load in the order of 33 % compared to a throat with exposed mild steel bars only.

For use of the Mesnager type of concrete hinges in constructions the rotation limits are important and were investigated several times [4-6, 8-11]. The limits vary in the literature and there seem to be no consensus in the definition of the limits for use in SLS state. Values between 0.004 rad and 0.01 rad were proposed based on hinge testing for different

geometries and normal forces. Leonhardt [9, 11] developed design guidelines including a suggested size of the maximum rotation,  $\alpha_{Rd}$ , in ‰:

$$\alpha_{Rd} = \frac{12800N_d}{b_1 \cdot d \cdot E_{c0m}} \quad (1.2.)$$

The area of the hinge throat in  $m^2$  is  $b_1 \cdot d$ , and  $N_d$  and  $E_{c0m}$  are the normal force in MN, and the Young's modulus in  $MN/m^2$ , respectively.

Leonhardt's guidelines included also suggested sizes of the hinge throat, the geometry of the recesses at the throat, transverse tensile forces in the hinge body, and rotation-moment characteristics. In the literature tested hinge characteristics are most often presented as rotation-moment plots. Leonhardt though proposed a universal rotation-moment relationship applicable for different geometries, normal forces, and concrete stiffnesses:

$$m = \frac{M}{N \cdot b_1} \quad (1.3.)$$

$$K = \frac{8N}{9 \cdot b_1 \cdot d \cdot E} \quad (1.4.)$$

$$\frac{\alpha}{K} = \frac{1}{(1 - 2m)^2} \quad (1.5.)$$

$m$  is a dimensionless parameter taking into account the normal force,  $N$ , and is the ordinate of the universal hinge response curve. It is valid for  $m > 1/6$ . In the interval of  $0 < m < 1/6$  the hinge response is assumed linear with a straight line from origo to the response curve. The angle of rotation in the hinge,  $\alpha$ , is divided by a constant,  $K$ . This ensures that the calculated abscissa take into account the concrete stiffness,  $E$ , the geometry of the hinge, and the normal force. The universal hinge response curve is verified by several tests with different sizes of normal force. The curve is seen in Figure 3. The hinge rotation limit in Eq. 1.2. is based on the point in the figure, where the crack reaches the middle of the throat ( $m = 1/3$ ).

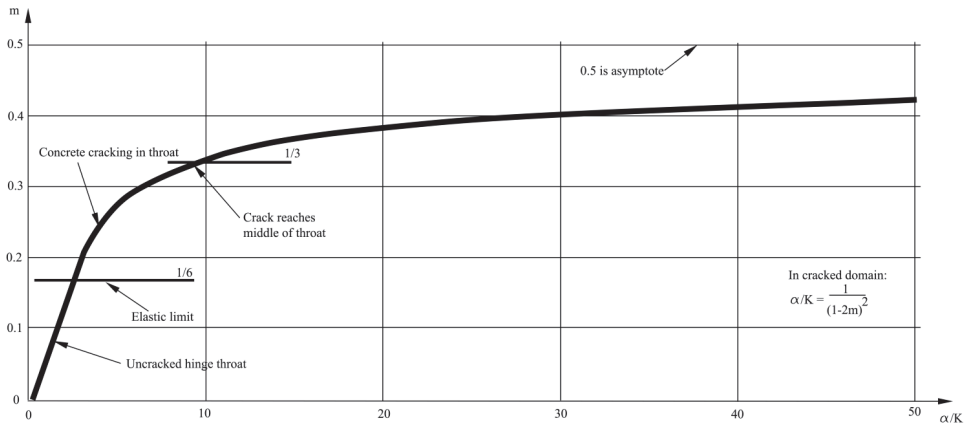


Figure 3: Universal hinge response proposed by Leonhardt and Reimann [9].

The Two types of concrete hinges which were investigated for use in Pearl-Chain Bridges (concrete arch bridge concept) [1]: i) a Mesnager and Freyssinet inspired hinge, and ii) an orthogonal saddle bearing type hinge, both shown in Figure 4. The Mesnager inspired type hinge has been used many times in arch bridges in the beginning of the last century [2], while the orthogonal saddle-bearing hinge is specially invented for use in Pearl-Chain Bridges.



Figure 4: The two types of investigated hinges for PC-Arches. The Mesnager hinge can be used as abutment hinge as well as crown hinge.

The objective of this paper is to:

- Investigate the response of the two hinge systems using component-scale testing and numerical modelling.
- Implement the hinge responses into a global structural model of the Pearl-Chain Bridge to investigate the changes in structural response compared to the ideal hinge, and a fixed connection.

## 2. LOCATIONS- AND REQUIREMENTS RELATED TO THE HINGES IN PEARL-CHAIN ARCHES

Pearl-Chain Bridges consist of a number of adjacent concrete arches (Pearl-Chain Arches), and a filling material on top [1, 12]. Above the filling is a road or path for pedestrians. The number of adjacent arches depends on the required total width of the bridge, and the width of each Pearl-Chain Arch (typically 1.75 m). The Pearl-Chain Arches are fixed together transversely by in-situ cast joints, but each arch consist of several pre-fabricated concrete elements (called SL-Decks). The individual low-weight SL-Decks are straight, and pre-tensioned with a number of strands in top and bottom. A curved duct is cast into the concrete longitudinally in every element, and the elements are assembled by post-tensioning cables through the ducts – similar to pearls on a string. To ensure an arch shape of the post-tensioned Pearl-Chain Arch, each SL-Deck element has inclined ends, so that when elements join, they form a pre-determined curved shape (piecewise), which has a curvature equal to the ducts. See Figure 5 for a photograph of a Pearl-Chain Arch, and illustrations of the cross-section (I – I) and longitudinal-section (II – II) of the SL-Decks used. In the photograph the arch is built with orthogonal concrete end surfaces that will work as an orthogonal saddle bearing hinge when positioned on a foundation. One challenge for hinges in a Pearl-Chain Arch is the practical solution when implementing a hinge in combination with having post-tensioning.

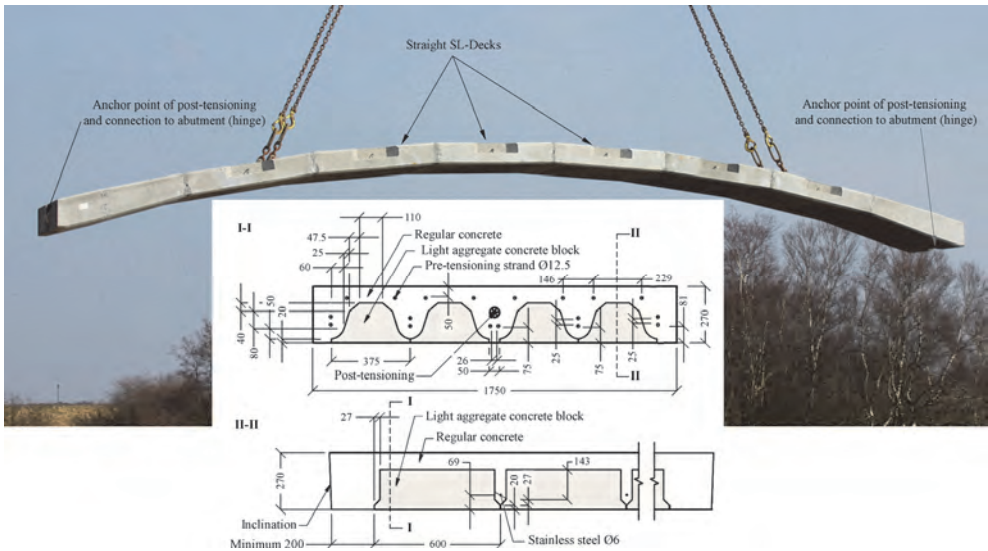


Figure 5: A single lifted Pearl-Chain Arch and section views of typical SL-Deck.

The Pearl-Chain Bridges differs from many other closed-spandrel arch bridge types by having a high level of normal force applied to the cross section. The self-weight contributes to the normal force in all arches, but having post-tensioning at the same time in-

creases the normal force significantly compared to “plain” concrete arches with only mild steel reinforcement. Furthermore, the concept so far has been intended for low rise to span constructions ( $R/S = 1/13$ ), where the normal force from the self-weight and payload is high. The relatively high level of normal force may affect the functionality of the hinges in these arches. It is a requirement for the Pearl-Chain Arch hinges to be functional at this high level of normal force.

It has been shown via full-scale tests that transfer of forces between Pearl-Chain arches occurs via the transverse joints [13]. This means that the hinges in each individual Pearl-Chain Arch have to resist only a distributed average value of the normal force produced by a live load on the road-surface of one of the Pearl-Chain Arches.

Pearl-Chain Arches behave like an ordinary concrete arch when loaded, and the point in having hinges is therefore the same as for any other concrete arch. Implementing abutment hinges can decrease the bending moments in the abutment areas. A three-hinged arch will reduce problems with increased moments from creep, shrinkage, temperature changes, and abutment settlement, and create a potentially statically determinate system. By correct dimensioning of concrete hinges the arch could be expected to crack in the hinge region first. This can be used to quickly evaluate the condition of a bridge with visible hinges. According to the approach in Figure 4 another requirement for the hinges is to stay below  $m = 1/3$  (crack half way through throat) in the Ultimate Limit State (ULS), and  $m = 1/6$  (first crack initiation) in the Serviceability Limit State (SLS). It may be necessary to use stainless steel where cracks are expected to occur.

Hinge-less arches are more rigid and can often have a higher load carrying capacity. Having less flexibility basically means that temperature changes, horizontal abutment settlements etc. are withstood as an increased bending moment in the arch, and this can be an advantage for low rise to span arches. Furthermore, it is practical not having to produce the hinges, which are expensive and time consuming because of complex reinforcement solutions and molds.

### 2.1. Materials and geometry of test-specimens

The regular concrete in Pearl-Chain Arches has characteristic compressive cylinder strength of 55 MPa, and Characteristic Young’s modulus of 41 GPa. The same type of concrete was used in both types of hinges. In the Mesnager inspired hinge type the concrete properties were tested to be  $f_{ck\_mes} = 55$  MPa, and  $E_{c0k\_mes} = 33$  GPa. For the orthogonal saddle bearing hinge the same test values were  $f_{ck\_ort} = 59$  MPa, and  $E_{c0k\_ort} = 39$  GPa. The mild steel was the same in both types of specimens as well. The strength of the steel was 550 MPa.

Figure 6 shows the test specimens for the Mesnager inspired hinge test. Three geometries of the throat was tested which is the reason for the three different length values given in the close-up on the right in the figure. To more easily handle the elements in the lab, the

test specimens had reduced width compared to a Pearl-Chain Arch. The tested specimens had crossing reinforcement through the throat with a total of four crosses of two Y10 mild steel bars at each cross. The hinge body was sufficiently reinforced to avoid splitting from transverse forces next to the throat.

In Figure 7 the specimen for testing the orthogonal saddle bearing hinge is shown. The orthogonal concrete surfaces at the end of the specimen are connected to a rigid foundation with similar surfaces. Mortar is poured between the opposite surfaces, and this connection has the studied hinge-behavior. The test-specimens have full width of 1.75 m.

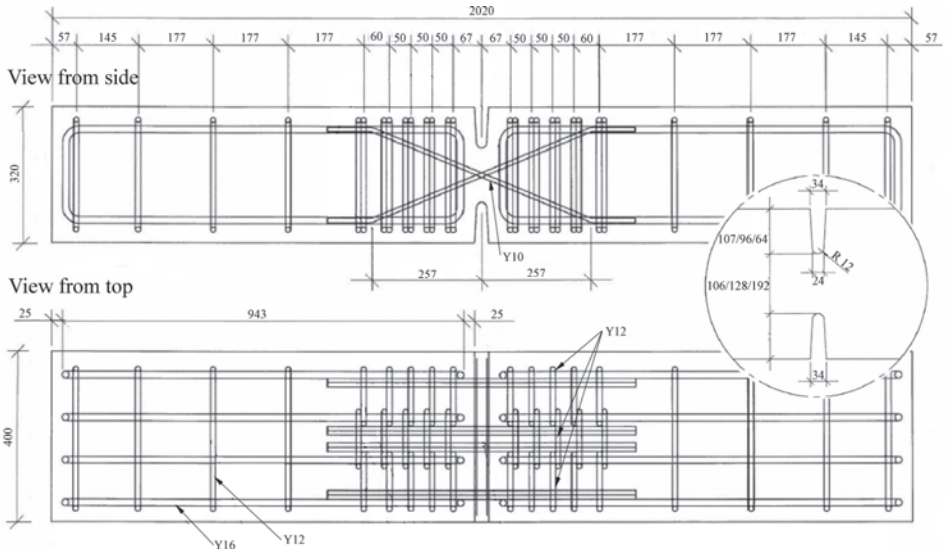


Figure 6: Geometry of test-specimen for the Mesnager inspired hinge test. Unit is mm.

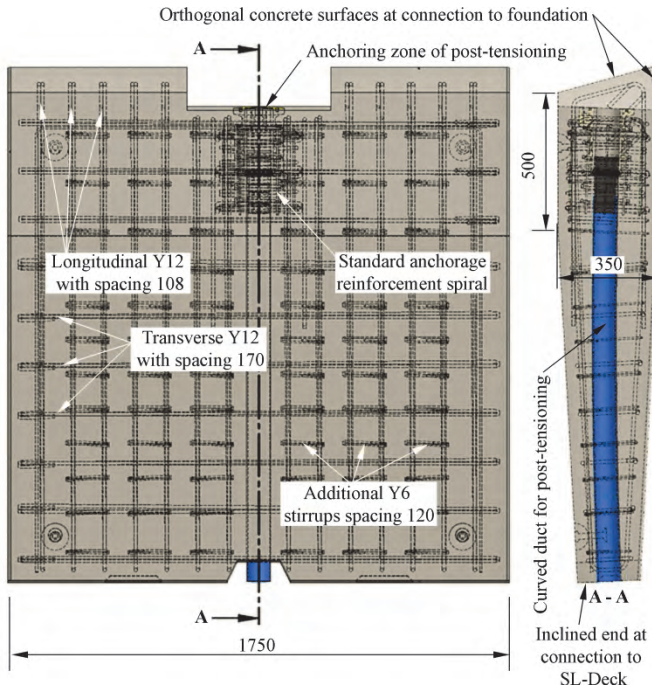


Figure 7: Concrete element specimen used for orthogonal saddle bearing hinges. Unit is mm. By courtesy of Perstrup Betonindustri.

### 3. TESTING OF THE HINGES

The two developed hinge candidates for possible application in Pearl-Chain Bridges were tested and analyzed. Full-scale tests were performed on both types: The Mesnager inspired hinge type was tested at the Technical University of Denmark, and the orthogonal saddle bearing was implemented in two loaded Pearl-Chain Arches tested in Jutland in Denmark.

#### 3.1. Testing of the Mesnager inspired hinges

Previously, a brief presentation was made in [2]. It was found that the best hinge ratio,  $b_1/b_2$ , was  $1/3$  based on tests of three different ratios. Larger hinge ratios of  $4/10$  and  $6/10$  were unfit for use in Pearl-Chain structures due to cracking from the throat into the hinge body. Hence, the more detailed investigations in this paper includes the ratio  $b_1/b_2 = 1/3$  alone. Eight specimens were tested with the  $1/3$  ratio, five with the  $4/10$  ratio, and three with the  $6/10$  ratio.

### 3.1.1. Test method

Extensive efforts were made to create a test-setup that would simulate the conditions of the hinge in a Pearl-Chain Arch. Instead of having a post-tensioning duct inside the test specimens and two complex anchorage zones, it was chosen to compress the specimens on the end surfaces to create the large normal force similar to the one from pre-stressing, and arch loads. This was the best possible practical solution when having specimens of only 2 m in length.

First, specially designed steel profiles were pre-stressed to the ends of the test-specimen to achieve the required normal force. The steel profiles were two HEB 300 welded together, and the pre-stressing was applied via two threaded rods of M42 – one next to the specimen in each side. Six Belleville springs were used in each connection between steel profile, and threaded rod to ensure free rotation. The normal force was initially 1000 kN (changed with up to 8 % during testing). The deviation in normal force was measured by four strain gauges on the M42 threaded rods.

The test-setup was a four-point-bending creating a constant bending moment between the presses. A rigid steel test-frame was built with two hydraulic presses pushing down onto the top surface of the test specimen positioned on two supports on the floor. The setup is seen in Figure 8.

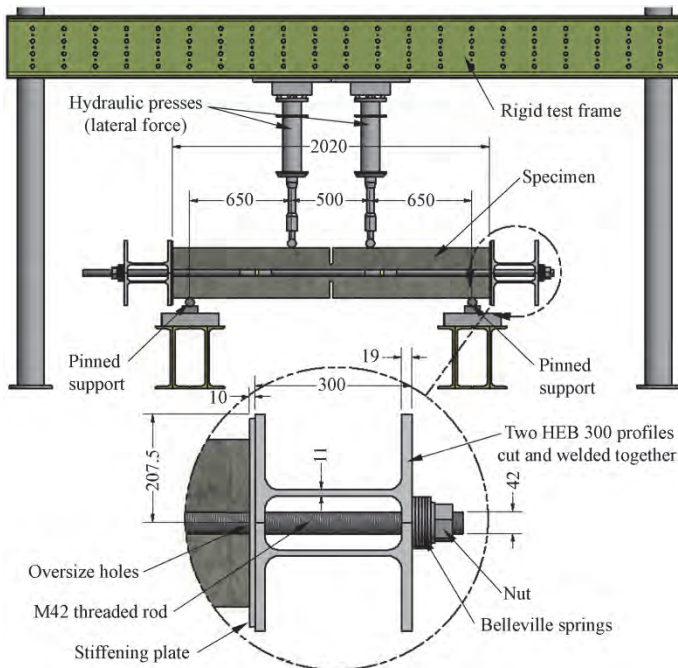


Figure 8: Test-setup for Mesnager inspired hinge type tested at DTU [2].

Measurements of rotation were performed on the top surface of the hinge body, and across the recesses in the throat. The top surface measurements were of the vertical deflections in six locations – three in each side of the throat with spacing 300 mm. These measurements were intended to show if any significant bending occurred in the hinge body during testing. Any interfering vertical settlements of the arch supports were recorded at both supports. Figure 9 shows the measuring equipment and the position of it.

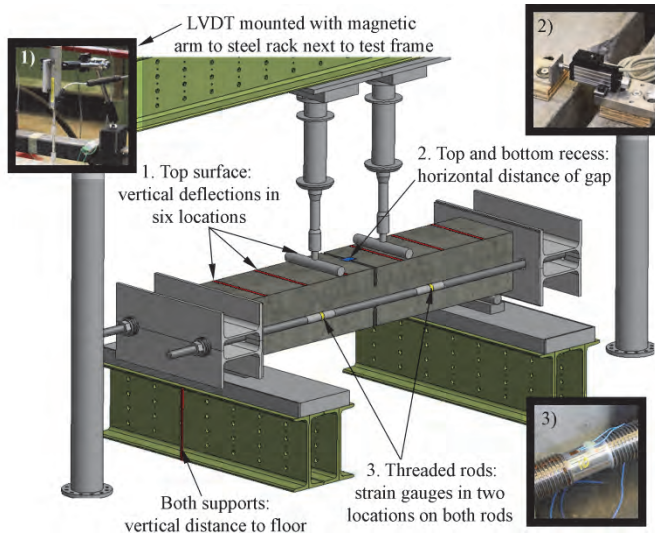


Figure 9: Measuring equipment positions and types.

The measurements across the recesses in the top and bottom of the throat were more directly recording the deformations, though it was expected that the bottom recess measurement would be affected by cracking in the throat when exceeding the elastic limit ( $m = 1/6$ ).

The tests were video recorded and the rotations were verified by visual interpretation from the recordings.

### 3.1.2. Test results

Results for the hinge ratio  $1/3$  showed that the elastic limit for the hinge type at the given normal force was at a rotation of  $0.0018$  rad, and moment of  $20$  kNm. The rotational stiffness was hence  $10,600$  kNm/rad, and there was a  $3\%$  deviation in this value depending on the measuring method: top surface of body or in recess of throat. Failure (max bending moment) occurred at  $0.019$  rad and  $40$  kNm. The specimens showed no cracks except for in the hinge throat, which was anticipated. The hinge responses are seen in

Figures 10, 11, and 12 (measured on top of test specimen), where the average curves, and fracture points for the different specimens are shown as well.

The hinge ratios  $b_1/b_2 = 4/10$  had a rotational stiffness of 14,200 kNm/rad, and  $b_1/b_2 = 6/10$  had 37,600 kNm/rad. In the figure, points of largest moment for ratio  $b_1/b_2 = 6/10$  are not given due to large deviations depending on the measuring method used.

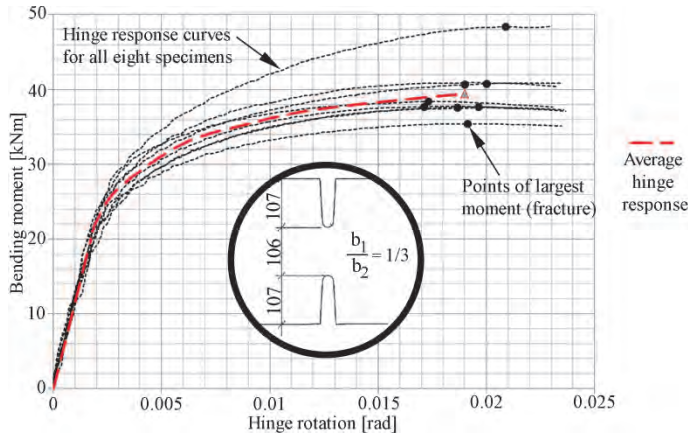


Figure 10: Hinge responses from the tested specimens,  $b_1/b_2 = 1/3$ . Unit is mm.

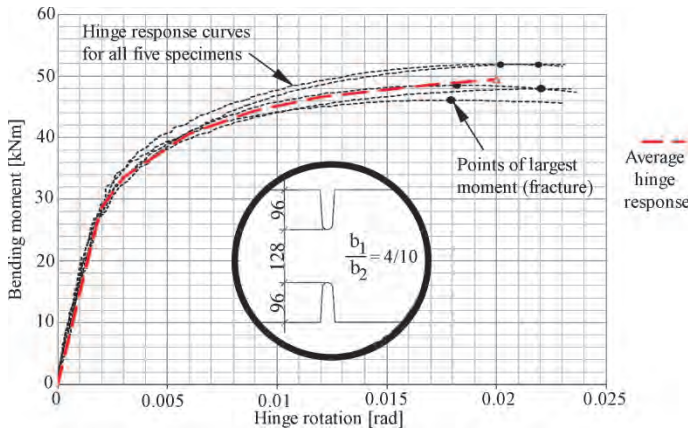


Figure 11: Hinge responses from the tested specimens,  $b_1/b_2 = 4/10$ . Unit is mm.

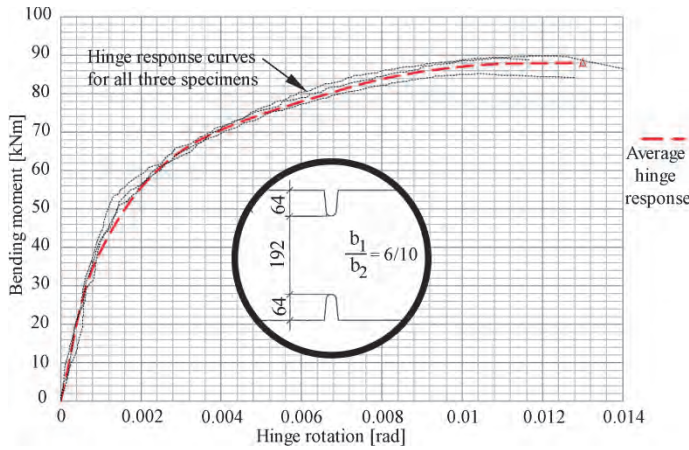


Figure 12: Hinge responses from the tested specimens,  $b_1/b_2 = 6/10$ . Unit is mm.

### 3.1.3. Comparison between test, model and theory.

To compare the universal hinge response curve by Leonhardt and Reimann to the hinge response from the tests we use Eq. 1.3., 1.4., and 1.5. The altered plot of the average hinge response from the tested hinge specimens are matched with the one proposed in Figure 4. When testing the hinges measurements showed that the normal force deviated with up to 8 % during testing. Therefore, two alternate curves are given as well with a plot of the hinge response assuming 8 % higher or 8 % lower normal force, see Figure 13.

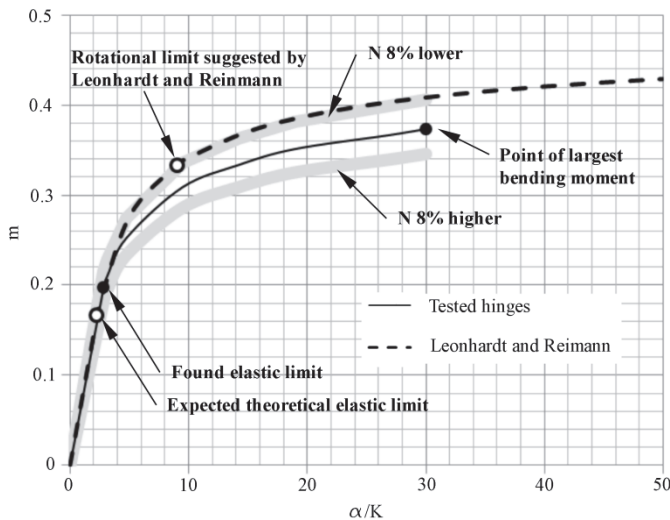


Figure 13: Tested hinge response ( $b_1/b_2 = 1/3$ ) compared to universal response model by Leonhardt and Reimann.

The comparison shows that the tested hinge response is comparable to the universal hinge response curve. It is therefore found that the relatively high level of normal force is not a hindrance for applying the model by Leonhardt and Reimann. Still, the reason why the rotational limit should be  $m = 1/3$  (crack half way through throat) is unclear. Base [5] tested Mesnager hinges in working condition with cracks up to  $2/3$  through the throat. This can be explained by two observations: i) the crossing reinforcement go into tension to help resist the moment, when the crack becomes larger than  $b_1/2$ , and ii) the concrete confinement increases as the crack length develops cf. Eq. 1.1.

There is a high margin of safety using the  $m = 1/3$  limit but even then there might be a challenge with ingress of water to the crossing reinforcement. An even more conservative approach is to stay below the  $m = 1/6$  limit to avoid corrosion in the mild steel in the throat. Use of this type of hinge in the domain between  $m = 1/6$ , and  $m = 1/3$  would require stainless steel in the hinge throat region.

A numerical model is created in Abaqus [14] (without the reinforcement) to compare with the tested response in the elastic un-cracked domain. The results are seen in Figure 14. The geometry, material properties, and applied loads are similar to the tested hinges. The numerical model gives a 9 % higher rotation compared to the tested hinge. Creating a denser mesh than the shown does not change the output significantly. As shown in the figure the effect of the normal force does not account for the difference either. The reason for the 9 % dissimilarity is a degree of fixation of the test-setup that does not exist in the numerical model or in a real concrete hinge in an arch structure. If we fix the supports of the hinge specimen in the model the rotation decreases to approximately half. When there is a degree of fixation at the supports the static system changes, and the bending moment becomes less than expected for a given load.

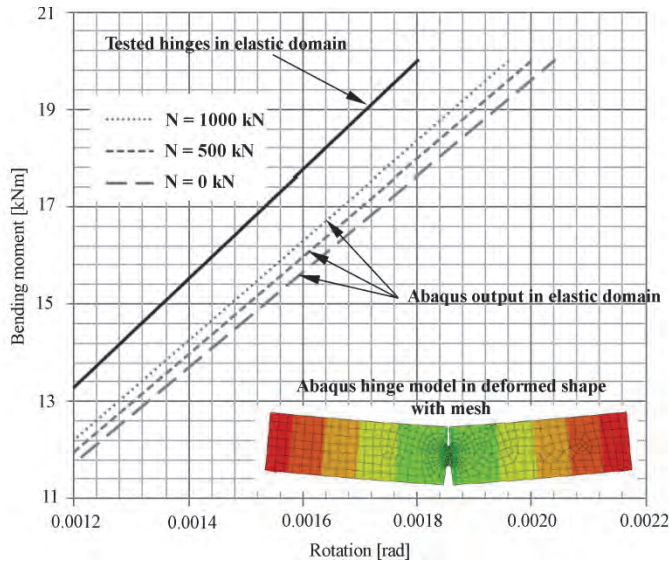


Figure 14: Abaqus model output vs. tested hinge in elastic domain.

### 3.2. Testing of the Orthogonal bearing hinge

This type of hinge was developed to be implemented in a load test of two full-scale Pearl-Chain Arches of 13 m span. The test was performed in two tempi: 1) A test to 2/3 of the load carrying capacity and 2) a test to fracture. The relevant results of the behavior of the orthogonal saddle bearing hinges were primarily gathered from the non-destructive first test.

#### 3.2.1. Test method

Two Pearl-Chain Arches of 1.75 m width were positioned next to each other on a stiff concrete foundation,  $E_{cf} = 36$  GPa, with no possibility of horizontal settlement [15], see Figure 15. The span was 13 m, and rise 1 m. A plateau was cast in concrete on top of the arches at the  $\frac{1}{4}$  point of the span, and heavy steel weights were positioned on the plateau during the test. The abutment elements (elements in each end of each arch) were designed with orthogonal concrete surfaces to fit to two similar surfaces in the foundation. When positioning the arches, wedges were placed between arch and foundation, and the gap was poured with a mortar of stiffness,  $E_m = 23$  GPa. The mortar gap was approximately 6 cm in the loaded side and 8 cm in the non-loaded side.

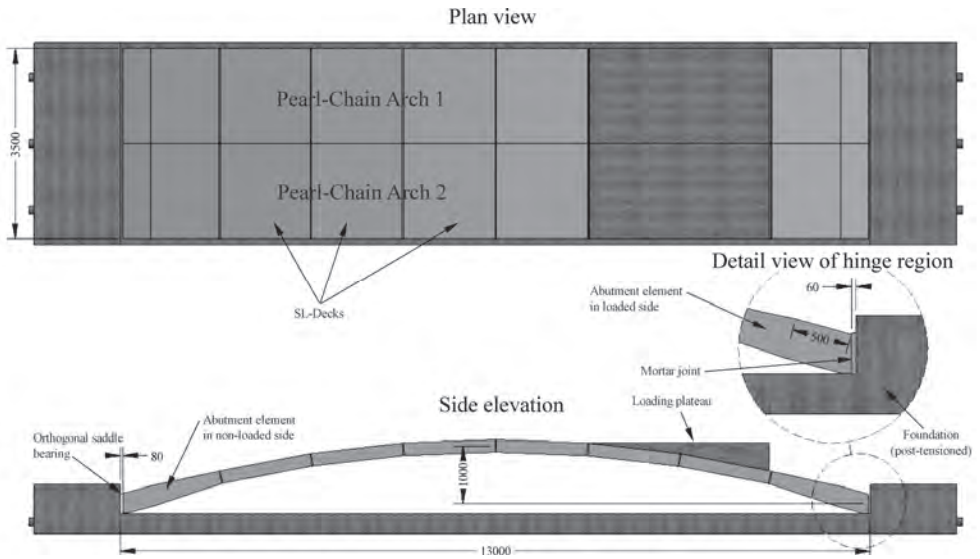


Figure 15: Test setup for full-scale Pearl-Chain Arch test with orthogonal saddle bearing hinges. Unit is mm.

Measurements of the hinge behavior were performed using ARAMIS DIC software (Digital Image Correlation) [16]. After taking photographs of the relevant surface, the software compares the photo taken during loading to a reference photo. The output from ARAMIS was utilized in finding the rotation of the hinges, and to spot the first appearing cracks, see Figure 16. The figure shows a fully formed crack in top of the hinge in the loaded side of the arch.

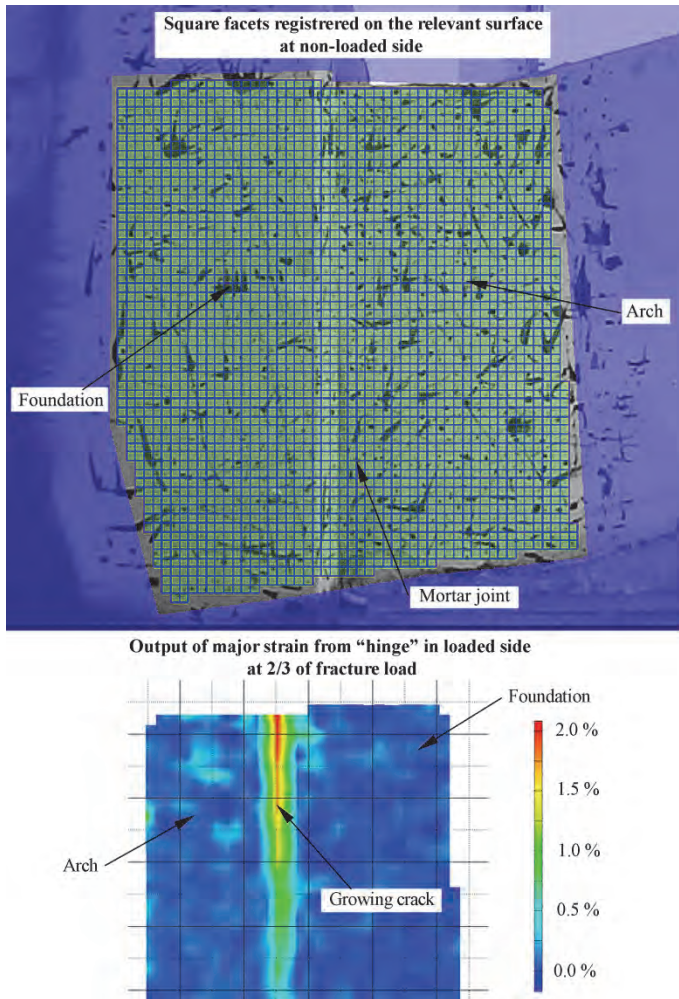


Figure 16: ARAMIS. Top: The used facets (non-loaded side). Bottom: Cracking in surface between foundation and mortar (loaded side).

The normal force was calculated based on the arch geometry and the applied load and self-weight. Post-tensioning was anchored in the abutment elements and do in this case not contribute to the normal force in the hinges.

At the point of first cracking in the hinge regions at the elastic limit, the load was approximately,  $P_{\text{elastic}} = 300 \text{ kN}$  (including load from plateau), giving a normal force in the hinges of approximately,  $N_{\text{elastic}} = 891 \text{ kN}$ . This value is applied in a numerical model of the orthogonal saddle bearing created in Abaqus.

The deflections of the tested arches were monitored by LVDT's during loading. At  $d_{\text{hinge}} = 500 \text{ mm}$  from the hinge point in the loaded side the deflection was  $\delta_{\text{down}} = 0.30 \text{ mm}$

downwards, and at the same distance from the hinge point in the non-loaded side the deflection upwards was  $\delta_{up} = 0.29$  mm. Both measurements of the deflections were at the load  $P_{elastic}$ .

### 3.2.2. Test results

Figure 17 and 18 show comparisons between ARAMIS results from the test, and the numerical model in Abaqus. In the figures the influence of the thickness of the mortar joint,  $t$ , and the Young's modulus,  $E_m$ , have been investigated. The response of the joints is evaluated by two different methods: 1) The rotation is shown coming from the deformation of the mortar joint alone, and 2) the total rotation is shown at the surface between the arch, and the mortar joint (not including the deformations in the 500 mm of arch). An ideal hinge would in the tested setup give a total rotation of:

$$rot_{ideal} = \tan^{-1} \left( \frac{\delta_{down}}{d_{hinge}} \right) = 0.0006 \text{ rad}$$

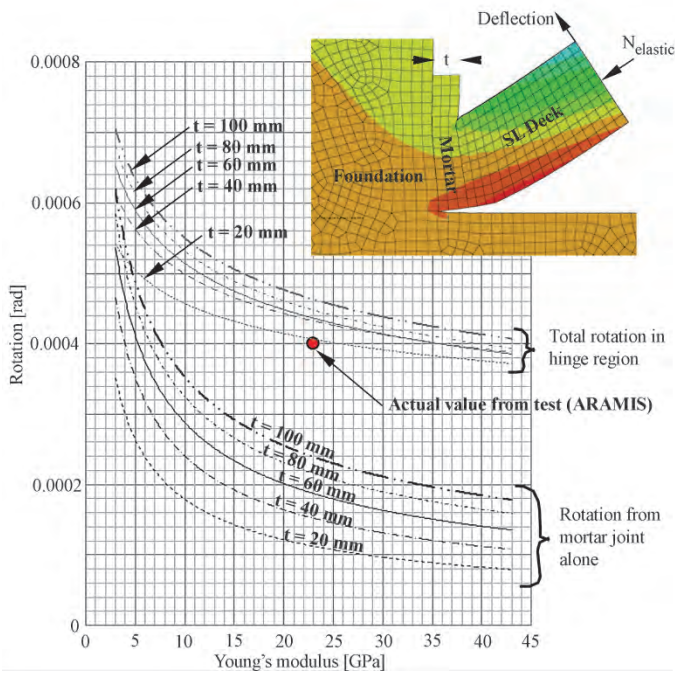


Figure 17: Rotation in non-loaded side for different thicknesses,  $t$ , and values of Young's modulus of the mortar.

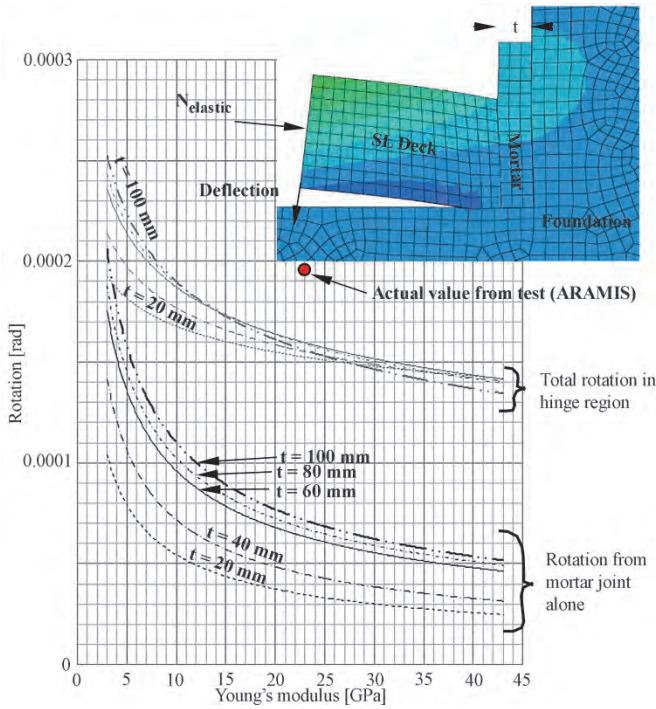


Figure 18: Rotation in loaded side for different thicknesses,  $t$ , and values of Young's modulus of the mortar.

### 3.2.3. Comparison between test and model

The measured values from ARAMIS are within 22 % of the total values from the Abaqus model, when applying the same properties of stiffness and mortar thickness. When comparing to the rotation of an ideal hinge though, the rotation measured in ARAMIS is only around  $1/3$  of  $rot_{ideal} = 0.0006$  rad. This indicates that the joints perform as practically fixed in the un-cracked region.

The results show that it is possible to some extent to affect the level of rotation in the elastic region from altering the mortar thickness, and Young's modulus. The effect of such alteration on the other hand is not abundant. For instance it is seen in Figure 18 that the trend line curves of the total rotations from the model are close to each other and even overlapping for stiffness above 15 GPa.

Beyond the elastic limit of the material cracking occurs. The elastic to plastic behavior was recorded with ARAMIS as well, see Figure 19.

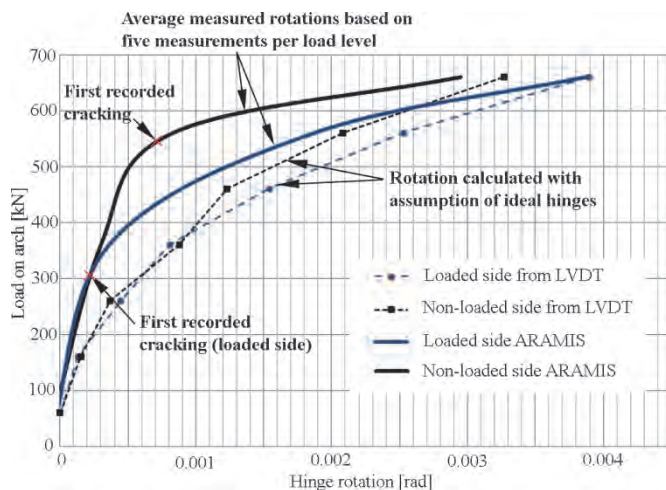


Figure 19: Comparison between measured and ideal hinge behavior.

It is seen from the figure that the hinges behave fixed primarily in the elastic region of the response curves (prior to cracking). After cracking initiates the gap between the measured rotations with ARAMIS and the calculated ideal rotations (from LVDTs) decreases. Actually, the transition from un-cracked to cracked state happens prior to the recorded first visible signs of cracks. This may be due to unrecorded micro-cracking in front of the crack tip.

#### 4. IMPLEMENTATION OF HINGE RESPONSE INTO THE PEARL-CHAIN ARCHES

The normal force in the tested Mesnager inspired hinges were 1000 kN which corresponds to 7.8 MPa of normal stress in the hinge body. The level of normal stress is based on what is found in a fully traffic loaded Pearl-Chain Bridge with rise to span of 1/13 and span of 30 m. In the orthogonal saddle bearing hinges from the 13 m span test the normal stress was 1.3 MPa. This 83 % difference could have an influence when comparing the hinges. In Figure 14 we found that the effect of the normal force on the hinge response in the elastic region was relatively small.

The proportionality limit for the Mesnager inspired hinge was 0.0018 rad, which is close to four times the value of the orthogonal saddle bearing hinge (Figure 19). Despite of the smaller rotation capacity in the elastic domain, the orthogonal saddle bearing hinge has several practical advantages compared to the Mesnager type:

- For application in pre-fabricated arches, the developed abutment element is easy to implement as a pre-fabricated “pearl” in the Pearl-Chain, and the mortar connection to the foundation is simple to create.

- The hinge (mortar joint) has fewer problems with corrosion of reinforcement. Nevertheless, observations from loading at 2/3 of collapse load of the two tested 13 m span arches showed cracks propagating into the abutment element.
- The abutment element works as an anchorage block for the post-tensioning, which means no pre-stressing in the hinge. In the Mesnager hinge the post-tensioning would conceivably have to propagate through the hinge throat, and be anchored outside that region.
- Even beyond the 2/3 of collapse load the hinges still acted as intended (despite of large cracks), and the final collapse of the two arches occurred in the span of the arch – not in the springing hinges.

Advantages of the Mesnager inspired hinge type:

- The larger rotation in the elastic region is important in certain types of arches.
- A well-defined rotation-moment curve from lab-testing exists for simple implementation in programs for global structural analysis such as Robot Structural Analysis [17]. A true rotation-moment curve for the orthogonal saddle bearing hinge can only be found in the future by complicated lab testing.
- The hinge type is well tested and documented for use in other arch structures over a range of years.
- Can be used as crown hinge.

To exemplify the influence of the local hinge response, the curve from Figure 10 is implemented in a global model in Robot Structural Analysis. The model is similar to the tested 13 m span Pearl-Chain Arches. Figure 20 shows the difference in bending moment going from ideal hinges to the true hinge response to fixed ends. The load in the figure is equal to 2/3 of the fracture load in the full-scale test.

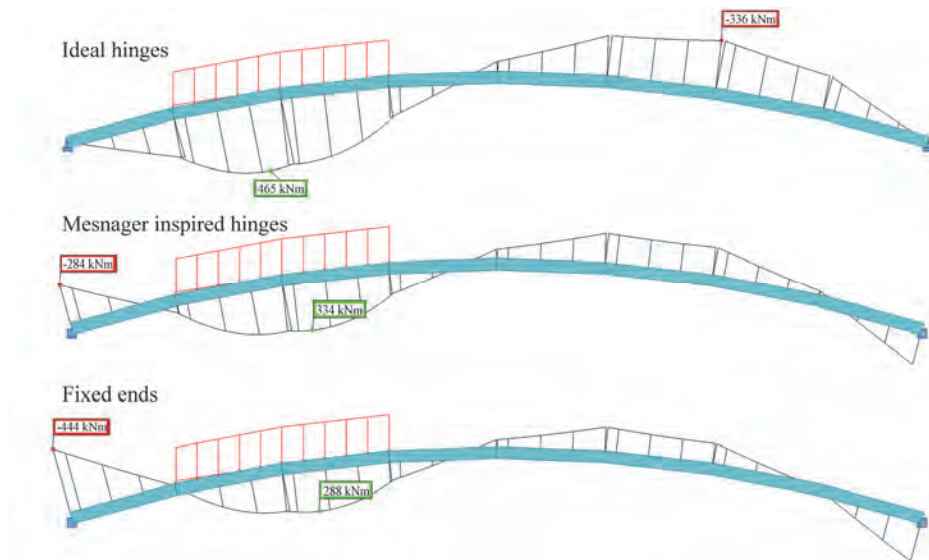


Figure 20: Behavior of global structure depending on support properties.

In the example in the figure the hinge is in the plastic domain of the hinge response curve, which is beyond the limit for serviceability state (at first cracking  $m = 1/6$ ). Actually, the hinge in the loaded side is exactly at the  $m = 1/3$  limit suggested in the ULS by Leonhardt and Reimann, where the crack has reached the middle of the throat.

In the real test of the two Pearl-Chain Arches, the orthogonal saddle bearing hinge in the loaded side had a crack of  $3/4$  of the height of the mortar joint. At that stage the crack followed the surface between mortar and foundation in one side of the bridge, while the crack at the opposite side grew into the abutment element.

Due to the simplicity, the practical advantages, and the behavior seen at the test, the orthogonal saddle bearing hinge has been chosen for use in the first ever build Pearl-Chain Bridge in the summer of 2015 in Denmark.

## 5. CONCLUSION

The Mesnager inspired hinge was full-scale tested with hinge ratios,  $b_1/b_2$ , of  $1/3$ ,  $4/10$ , and  $6/10$ . The results of the ratio  $1/3$  specimens showed that the hinge response (relationship between rotation and bending moment) was comparable to a universal hinge response curve by Leonhardt and Reimann. An Abaqus model of the tested Mesnager inspired hinges gave results within 9 % of the tested. Changing the normal force did not seem to have a significant effect on the hinge response in the elastic region of the hinge in the model.

Orthogonal saddle bearing type hinges were tested as part of a full-scale Pearl-Chain Arch load test. The arch span was 13 m and loaded in the  $1/4$  point of the span. The hinge

type was monitored with digital image correlation software, ARAMIS, in both the loaded and non-loaded side. An Abaqus model was created for comparison to the test results. At the elastic limit, the rotation difference was up to 22 % between test and model. The numerical model was applied to illustrate the hinge behavior when the two parameters: mortar stiffness, and mortar joint thickness was varied.

Advantages were listed for both hinge types in regard to being implemented in a Pearl-Chain Bridge. The orthogonal saddle bearing was evaluated as being practical, and easy to implement, but with only the hinge response data available found in this paper. The Mesnager inspired hinge type is tested and documented over many years, but the combination of a hinge throat and post-tensioning is an obstacle for practical use.

To show the significance of the local hinge response, the rotation-moment-data from the test of the Mesnager inspired hinge was built into a global model of the 13 m span Pearl-Chain Arches in Robot Structural Analysis. The results from this exercise revealed that the Mesnager inspired hinge would be beyond the elastic limit ( $m = 1/6$ ) when the arches were loaded to  $2/3$  of the fracture load. The load level corresponded with the rotation limit suggested by Leonhardt and Reimann ( $m = 1/3$ ). At the same load level in the actual test, the orthogonal saddle bearing hinge had cracking of approximately  $3/4$  of the height of the mortar joint in the loaded side.

Based on the available data the orthogonal saddle bearing hinge was implemented in the first ever built Pearl-Chain Bridge in 2015.

## Acknowledgements

The authors wish to thank Innovationsfonden for funding the project.

## References

- [1] Halding, P. S., Hertz, K. D., & Schmidt, J. W. (2015). Precast Pearl-Chain concrete arch bridges. *Engineering Structures*, *103*, 214–227. doi:10.1016/j.engstruct.2015.09.012
- [2] Halding, P. S., & Hertz, K. D. (2014). Concrete Hinges. In *Proceedings of the Iass-slte 2014 Symposium*.
- [3] Marx, S., & Schacht, G. (2010b). Gelenke im massivbau. *Beton- Und Stahlbetonbau*, *105*, 27–35. doi:10.1002/best.200900061
- [4] Dix, J. (1962). Betongelenke unter oftmals wiederholter Druck- und Biegebeanspruchung. *Deutscher Ausschuss Für Stahlbeton*, *150*, 1–41.
- [5] Base, G. D. (1965). Tests on four prototype reinforced concrete hinges. *Cement and Concrete Association -- Research Report*.

- [6] Moreell, B. (1935). Articulations for concrete structures -- Mesnager hinge. *American Concrete Institute -- Journal*, 7(1), 123 – 124.
- [7] Griezic, A., Cook, W. D., & Mitchell, D. (1998). Stress-strain characteristics of confined concrete in column “hinges.” *Aci Materials Journal*, 95(4), 419 – 428.
- [8] Kluge, R. W. (1940). Tests of reinforced concrete hinges. *Concrete and Constructional Engineering*, 35(12), 605 – 615.
- [9] Leonhardt, F., & Reimann, H. (1965). Betongelenke -- Versuchsbericht, Vorschlaege zur Bemessung und konstruktiven Ausbildung. *Deutscher Ausschuss Für Stahlbeton*, 1 – 34.
- [10] Nilsson, I. H. E. (1977). Belastningsförsök på ofullständiga betongleder. *Nord Betong*, (6), 17 – 22.
- [11] Marx, S., & Schacht, G. (2010). Concrete Hinges – Historical Development and Contemporary Use. In *Proceedings of the 3rd fib International Congress – 2010* (pp. 1–22).
- [12] Hertz, K. D. (2010). Light-weight load-bearing structures reinforced by core elements made of segments and a method of casting such structures. Denmark.
- [13] Halding, P. S., Hertz, K. D., Schmidt, J. W., & Kennedy, B. (2016). Full-Scale Load Tests of Pearl-Chain Arches. To be in *Engineering Structures*.
- [14] Abaqus/CAE. (2012). Dassault Systèmes.
- [15] Halding, P. S., Hertz, K. D., Schmidt, J. W., & Viebæk, N. E. (2015). Assembly and lifting of Pearl-Chain arches. *Proceedings of Fib Symposium 2015*.
- [16] Aramis. (2013). GOM mbH.
- [17] Robot Structural Analysis Professional. (2013). Autodesk.



# C CONCRETE HINGES

## Concrete Hinges

Philip Skov HALDING\*, Kristian Dahl HERTZ<sup>a</sup>, Jacob Wittrup SCHMIDT<sup>b</sup>

\* Department of Civil Engineering, Technical University of Denmark  
Building 118, DTU, 2800 Kgs. Lyngby, Denmark  
phsh@byg.dtu.dk

<sup>a</sup> Department of Civil Engineering, Technical University of Denmark

<sup>b</sup> Department of Civil Engineering, Technical University of Denmark

### Abstract

In the first part of the 20<sup>th</sup> century concrete hinges developed by Freyssinet and Mesnager were widely tested and implemented in concrete structures. The concrete hinges were used a great deal in closed-spandrel arch bridges. Since such a bridge type has not been competitive for the past 40 years, the research in concrete hinges has not evolved significantly in that period. But introducing a new state-of-the-art concrete arch bridge solution (Pearl-Chain arches invented at the Technical University of Denmark) creates a necessity of a concrete hinge research based on modern standards.

Back when research in concrete hinges was more common different designs were proposed for the geometry and reinforcement. Previous research focused on fatigue, multi-axial stresses around the hinge throat, and the relation between rotation- and moment. But many different test-setups were proposed by different researchers. The present paper uses the prior research results to optimize a test-setup for concrete hinge testing by means of a universal method taking into account the application of the hinge in an arch structure. 3D CAD is utilized in all steps of the planning to reduce errors during assembly of the parts in the test-setup, to create detailed drawings for the workman crew, and to produce visualizations. The test-setup is created for testing of full scale concrete hinges, and actual tests are successfully made on 18 specimens with three different hinge geometries.

**Keywords:** Concrete Hinges, Closed-Spandrel Arch Bridges, Test-Setup, Pearl-Chain Arches, Hinge Response Curves, Test Specimen Geometry, Rotational Stiffness, Elastic Limit, 3D CAD, Full-Scale Testing.

### 1. Introduction

Earlier closed spandrel arch bridges were used widely and plenty of literature is available on the topic (e.g. Billington [2] and Mondorf [13]). By use on new inventions and contemporary technology by Hertz ([6] and [7]) at the Technical University of Denmark it is possible to "reinvent" the closed spandrel concrete arch bridge in a modern version (the Pearl-Chain Arch), but with inspiration from the knowledge gained during the period, where concrete arch bridges were most popular. An example is concrete hinges, which were widely used in concrete arch bridges in the first part of the 20<sup>th</sup> century.

Much literature exists on concrete hinges, but there does not seem to be a consensus in the test-setups used by different scientist for concrete hinge testing. This paper focuses on the local behavior – the hinge responses – and does not consider the effects on the structural system in which the concrete hinge is placed. The method used when creating the specimens and the functional test-setup can be applied in any type of test situation. The goal of the hinge-tests is to find rotation- and moment relationships for three types of hinges having different hinge throat sizes.

#### 1.1. The concrete hinge

In the beginning of the 20<sup>th</sup> century two Frenchmen developed a new generation of concrete hinges (Marx and Schacht [12], Dix [3] and Base [1]). They both created hinges where the stiffness was reduced in the zone of the hinge by reducing the cross section height, see Figure 1. The area of reduced cross section is called the throat of

*Copyright © 2014 by the authors.*

*Published by the International Association for Shell and Spatial Structures (IASS) with permission.*

1

the hinge. Firstly, Augustin Mesnager shaped such hinge having a large amount of crossing reinforcement through the rotation point in the middle of the throat. Mesnager's design was based on the properties of the reinforcement and therefore did not take into account the stiffness of the concrete in the throat. The reinforcement was hence designed to resist both shear and normal forces and the role of the concrete in the throat was purely as corrosion protection.

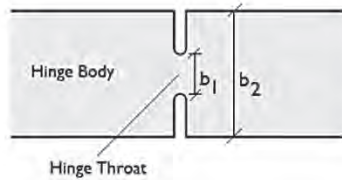


Figure 1: Mesnager and Freyssinet type concrete hinge with reduced height at the hinge throat.  $b_1$  is the throat height and  $b_2$  is the body height.

Another leading French researcher was Freyssinet who basically had the same concrete hinge design as Mesnager but without the reinforcement in the throat so that section forces had to entirely be transferred through the concrete.

Mondorf [13] explains the stress distribution in a Freyssinet type hinge and presents design rules which originally came from Leonhardt and Reimann [10]. Leonhardt has had the most significant influence on the design of concrete hinges from the 1960's and onwards.

Many of the difficulties of having a throat area – sometimes as small as a quarter of the area of the body – can be overcome because the concrete in the throat is subjected to multi-axial stresses as described by Base [1]. The normal stresses from the arch must “bend” in towards the bottleneck in the throat and this change of direction of the normal force produces a lateral confinement of the concrete in the throat. Laterally confined concrete has a capacity up to several times higher than the unconfined cylinder strength. Griezic et al. [4] introduces a confinement factor based on test results for “one-way hinges”. The factor is conservatively limited to the value 1.7 regardless of the geometry. The equation for the stress confinement factor is:

$$\alpha_1 = \frac{1}{1 - 0.5k_1 \left[ 1 - \frac{b_1}{b_2} \right]} \quad (1)$$

The parameter  $k_1$  is 1.1 for “one-way hinges” and the  $b_1$  to  $b_2$  ratio is the relation between the height of the throat and the height of the body of the hinge.

The  $b_1$  to  $b_2$  ratio is investigated in several papers (e.g. [1], [10], Guyon [5] and Sastry [16]) and generally it is agreed that a ratio of 0.3 to 0.33 always is an acceptable interval. However, there have been performed tests on hinges with ratios down to 0.11 and up to 0.4. Except for increasing the stiffness in the throat a larger ratio will also decrease the effect of the confinement as seen from the above equation. Dix [3] found that not only does multi axial stresses in the throat increase the proportionality limit but also the deformation capacity before reaching fracture: Two substantial parameters for concrete hinges.

There also exist recommendations for e.g. the length of the throat (Nilsson [15]), the amount of crossing reinforcement bars in the throat [9] and stirrup distances in the body [6] due to transverse tensile forces in the body (Jensen [8] and Leonhardt [11]). Fatigue is tested as well on several occasions ([3], [10] and [16]) but there has not been found problems for concrete hinges having been through up to two million cycles.

## 1.2. Previous concrete hinge test-setups

In order to assess how a concrete hinge design will behave when being subjected to load and rotation a rotation- and moment curve is useful. Different methods have been used in the past to be able to evaluate the dependency of the moment on the hinge rotation. As mentioned the common use of concrete hinges are in arch structures, and arch structures do always intend to utilize the good compressive properties of the construction material, inducing a relatively large normal force and a relatively small bending moment. A concrete hinge test will need an applied normal force and some sort of lateral force to be able to generate the rotation.

Copyright © 2014 by the author(s).

Published by the International Association for Shell and Spatial Structures (IASS) with permission.

Moreell [14] and Nilsson [15] have used the method of only investigate one rotation at a time. This is done by using a test machine where the test specimen is compressed to represent the normal force in an arch. Between the machine and the specimen is then put in a wedge given the desired angle so that the specimen will be forced to rotate to the desired angle when compression is applied.

Others have tried to divide the normal force and bending force contribution into two different independent machines, meaning that it then is possible to change one of the forces without it having an effect on the other ([3], [1], [6] and Kluge [9]). This way at a given normal force a curve for the rotation- and moment relationship can easily be determined. A difficult detail though, when applying a longitudinal force and a lateral force independently, is how to secure a free rotation of the ends of a test specimen and still keep the normal force constant at the same time. Base [1] tested some specimens inside a rigid frame and secured free rotation by a series of steel rollers at the ends of the test-specimen. Dix [3] created a vertical three point bending test setup inside a compressive testing machine. He had a hydraulic press pushing in on the test specimen at the hinge region in a horizontal direction. The free rotation of the top and bottom of the specimen was assured by curved pieces of steel between the concrete specimen and the test-machine. Kluge [9] describes a test-setup with pre-stressing of specimens, and use of large springs to ensure the free rotation at the ends of the specimen.

## 2. Method

The idea of the setup was to maintain a constant normal force while increasing the moment in the hinge throat until failure. To be sure to monitor the correct moment a four-point bending setup was chosen giving a constant moment in the specimen between the two points of applied load. The supports were designed to rotate freely. The distance between supports and applied load from the presses was 650 mm, see Figure 2.

When recording the rotation against the moment it is then possible to find the rotational stiffness and other parameters from the curve.

Parameters that may influence the shape of the rotation- and moment curve include: The concrete strength and stiffness, the reinforcement strength and stiffness, the  $b_1$  to  $b_2$  ratio of the hinge, the normal force, the rate of moment increase, the ability for the supports to rotate and the measurement method.

The main interest is regarding the  $b_1$  to  $b_2$  ratio and hence the other parameters are kept constant while observing the change in rotation and moment for different  $b_1$  to  $b_2$  ratios of: 1/3 (8 specimens), 4/10 (5 specimens) and 6/10 (3 specimens). By testing cylinders the 5<sup>th</sup> percentile values of strength and stiffness of the concrete was found to be 54.9 MPa and 33.1 GPa, respectively.

The normal force used in the tests are equal to the normal force in a 30 m span Pearl-Chain Bridge when fully loaded by uniformly distributed traffic load. The normal force is 1000 kN for the specimen size given in Figure 3 having a width of 400 mm, and the shown longitudinal reinforcement solution is repeated four times over the width. The normal force is applied to the specimen by post-tensioning specially designed steel profiles (two HEB 300 welded together) to the ends of the specimen by use of threaded rods (M42). To ensure the free rotation of the specimen 4x6 Belleville springs were put in the connections between the threaded rods and the steel profiles, and the holes through the steel profiles were large enough to permit rotation as well.

When the final geometry of the test-setup was in place the whole assembly procedure of the many components was performed in the program Autodesk Inventor. This gave the possibility of checking the fit of the whole setup before it was built in the test lab. Also, the creation of a three dimensional model gives the option of quickly producing technical drawings of the test-setup or test-specimens if necessary. In the present case technical drawings were sent to the workers making the steel profiles and setting up the test-frame. Figure 2 is an example of such drawing.

### 2.1. Measurements

The moment is found from the geometry, distance between supports and presses, and the force in the presses. The max force needed in the presses was beforehand estimated using the concrete confinement factor. The rotation is found both by measuring the vertical deflection of the top surface of the specimen at several locations and by measuring the horizontal distance between the sides in the top or bottom recess. It is more precise to measure the horizontal distances in the recesses because that directly relates to what happens in the throat. But a measurement of the vertical deflection on the top surface gives an opportunity of also monitoring if any bending occurs in the body of the hinge. Therefore, it was chosen to measure six points at the top surface of the concrete specimen placed symmetrically around the recesses with an equal distance between the deflectometers (LVDTs).

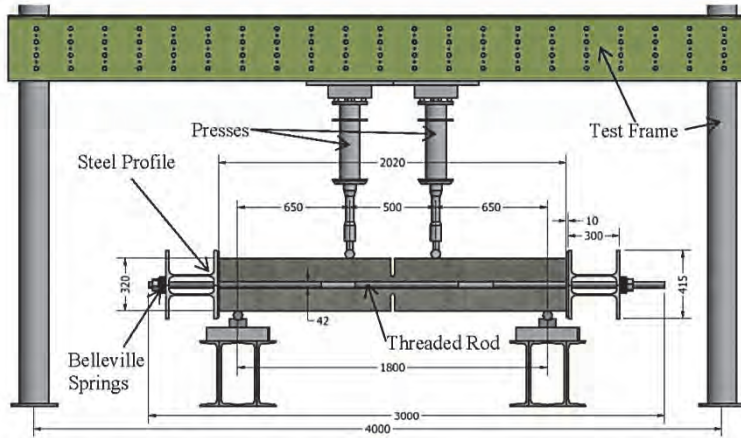


Figure 2: Example of a side-elevation view of the test-setup created from a 3D drawing in Autodesk Inventor. A constant normal force is applied and lateral forces increasing during testing creating an increasing bending moment. The test continues to failure of the specimen.

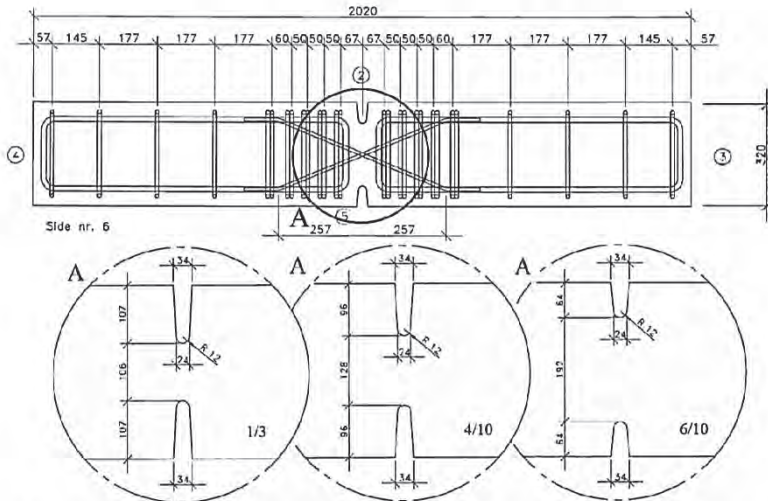


Figure 3: The reinforcement solution is similar for all three  $b_1$  to  $b_2$  ratios. The specific dimensions of each one of the ratios – 1/3, 4/10 and 6/10 – is shown in the bottom. Y12 stirrups are used together with Y16 longitudinal steel bars. The crossing throat reinforcement is Y10.

In order to evaluate if the forces in the threaded rods remained constant, when moment was applied to the specimen, two strain gauges were put on each one of the threaded rods. Lastly, there was placed LVDTs between the supports and the floor to make sure that any settlement of the supports would be registered and in addition all tests were being video-recorded.

Copyright © 2014 by the author(s).  
 Published by the International Association for Shell and Spatial Structures (IASS) with permission.

### 3. Results

The rotation of a hinge was – as mentioned previously – found in four different ways: The first two methods were by calculations based on the change in deflection measured on the top surface either close to ("Close") or far from the top recess ("Far"). The last two methods were from the horizontal movements of the top ("Top") and bottom recess ("Bottom"), respectively. If the main rotation occurs in the hinge throat of the test-specimens, the expectation is to find that the top and bottom recess measurements give the same rotation as the measurements from the top surface. If significant rotation was to happen as well in the hinge body of the test-specimen a difference in the output would be expected as a result of that. Also, the expectation prior to testing is that a large  $b_1$  to  $b_2$  ratio will result in a higher rotational stiffness and a larger fracture moment.

Figure 4 shows average curves of the three types of specimens tested with different  $b_1$  to  $b_2$  ratios. The rotational stiffness is found as the inclination of the linear part of the hinge response curves. 8 specimens were tested having the small ratio (1/3) and the largest difference between rotational stiffness's in that group was 3 %. The average rotational stiffness was 10,600  $kNm/rad$ . For the 5 tested specimens of the medium ratio (4/10) the difference was 8%, and the average rotational stiffness was 14,200  $kNm/rad$ . For the 3 specimens having the large ratio (6/10) the largest difference was 40%, the rotational stiffness was 37,100  $kNm/rad$ .

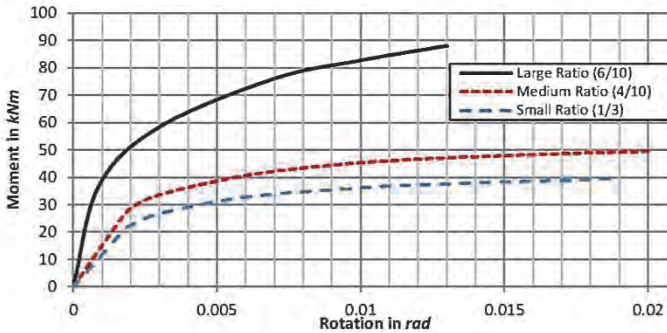


Figure 4: Average hinge responses from the three different ratios of  $b_1$  to  $b_2$ .

A summary of the average points of the elastic limit and failure limit is given in figure 5 for each hinge size ratio. The largest moment for both the linear limit and at failure is found for the specimens having the largest hinge size ratio. The small ratio specimens on the other hand have the largest rotation at the linear limit.

$b_1/b_2$	Max Linear Moment	Max Linear Rotation	Failure Moment	Failure Rotation
Large ratio (6/10)	37	0.0009	88	0.013
Medium ratio (4/10)	23	0.0015	49	0.020
Small ratio (1/3)	20	0.0018	40	0.019

Figure 5: Average rotation ( $rad$ ) and corresponding moment ( $kNm$ ) for the elastic limit and for the point of failure of the tested specimens.

### 4. Discussion

The curves in Figure 4 are limited to include only increase in moment. All curves would return towards the starting point when the specimen was unloaded after the failure moment had occurred, though having a level of permanent plastic deformation. Figure 6 shows a typical full hinge response. It must be recommended not to exceed the elastic limit during normal service of such hinges in order not to develop permanent deformations. The results showed a larger difference between values of the rotational stiffness for the large hinge size ratio of 6/10. The tested large ratio specimens (and few of the medium specimens) showed problems in regard to crack formation between the applied load and the bottom of the recess.

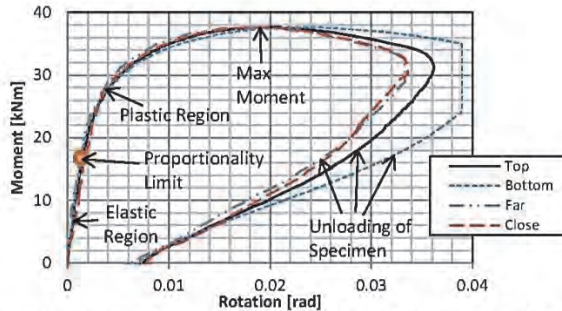


Figure 6: Hinge response curves of one typical test specimen (in this case a hinge  $b_1$  to  $b_2$  of 1/3). Each curve represents one of the four types of rotation measurement, and all curves have a similar inclination in the elastic region. The elastic area continues until the orange dot which illustrates the limit to the plastic domain.

The recess depth was only 64 mm for the large ratio specimens and this meant that a crack could occur from the top recess, where none or almost none of the reinforcement could reach. This together with the knowledge of the stiffness in the throat being six times larger for the large ratio (6/10) than for the small ratio (1/3), makes the large  $b_1$  to  $b_2$  ratio specimens useful only in cases where they can act as a point of crack initiation or if there are requirements of large concrete covers to the crossing reinforcement in the throat.

All specimens showed very similar results in the elastic region for measurements at the recesses as well as at the top surface of the concrete. The measurement from the bottom recess, though, often showed a larger rotation at the point of failure compared to the other methods.

The rotation at the elastic limit of the hinge is 7 to 10 % of the rotation at failure, and this indicates that the hinges are not suited for arch constructions with large deformations. Instead, the design is applicable in situations where e.g. it is important to control where cracks are forming in the structure.

#### 4.1. Test-setup evaluation

The Test-Setup functionality was first of all based on a constant normal force during testing. If the normal force was to deviate too much, the output of the tests would not replicate the actual situation of a concrete hinge in a loaded hinged arch. To be able to assess the normal force, strain gauges were put on the threaded rods.

For each of the  $b_1$  to  $b_2$  ratios a mean percentage increase in the force in the threaded rods was found: 8% for the small ratio (1/3), 10% for the medium ratio (4/10), and 12% for the large ratio (6/10). There was a tendency that the change in force in the rods got smaller with a decreasing  $b_1$  to  $b_2$  ratio. This means that the influence on the results was less significant for the small ratios. Generally, a value up to the 12% recorded as the largest change was expected.

### 5. Conclusion

The method used to create the test setup worked as intended, and the monitoring of the threaded rods in the test setup showed that there was only an average deviation of approximately 10% in the normal stress during testing, when bending was applied at the same time as the normal force.

The test of rotational stiffness gave results with up to 10% difference no matter which of the four measuring methods was used. This was true for both medium (4/10) and small (1/3) ratios of  $b_1$  to  $b_2$ , but for the tests performed on the specimens having the large ratio (6/10) the difference was 40%. The large ratio results gave more different results possibly because of crack development between the top recess and the load application areas. The hinge responses showed similar curves for all measuring methods in the elastic part but few differences in the plastic part of the curves.

The rotation in the elastic part of the hinge represents 7 to 10% of the rotation at the full capacity, and therefore, application of the tested hinges is not practicable for structures with large deformations in service state. The hinges can be used controlling cracks in an arch structure, with minor deformations in service state.

## References

- [1] Base G.D., Tests on four prototype reinforced concrete hinges. *Research Report of the Cement and Concrete Association*, 1965; 1-48.
- [2] Billington D., The Revolutionary Bridges. *Scientific American*, 2000; **283**; 84-91.
- [3] Dix J., Betongelenke unter oftmals wiederholter Druck- und Biegeanspruchung. *Deutscher Ausschuss für Stahlbeton*, 1962; **150**; 1-41.
- [4] Griezic A., Cook W.D. and Mitchell D., Stress-strain characteristics of confined concrete in column 'hinges'. *Journal of ACI materials*, 1998; **95**; 419-428.
- [5] Guyon Y., Long span prestressed concrete bridges constructed by the Freyssinet system. *Proceedings of the Institution of Civil Engineers*, 1957; **7**; 110-168.
- [6] Hertz K.D. and Anne B., Super-Light Structures with Pearl-Chain Reinforcement, in *IASS 2010. Spatial Structures – Temporary and Permanent*, 2010, 2697-2708.
- [7] Hertz K.D., Super-Light concrete with pearl-chains. *Magazine of Concrete Research*, 2009; **61**; 655-663.
- [8] Jensen B.C., *Betonkonstruktioner efter DS/EN 1992-1-1*. (1st ed.), Nyt teknisk forlag, 2008.
- [9] Kluge R.W., Tests of Reinforced Concrete Hinges. *Concrete and Constructional Engineering*, 1940, **12**; 605-615.
- [10] Leonhardt F. and Reimann H., Betongelenke – Versuchsbereich, Vorschläge zur Bemessung und konstruktiven Ausbildung. *Deutscher Ausschuss für Stahlbeton*, 1965; **175**; 1-34.
- [11] Leonhardt F., *Spannbeton für die Praxis*. (2<sup>nd</sup> ed.), Verlag von Wilhelm Ernst & Sohn, 1962.
- [12] Marx S. and Schacht G., Gelenke im Massivbau. *Beton und Stahlbetonbau*, 2010; **1**; 27-35.
- [13] Mondorf P.E., *Concrete Bridges*. (1<sup>st</sup> ed.), Polyteknisk Forlag, 2006.
- [14] Moreell B., Articulations for concrete structures – Mesnager hinge. *American Concrete Institute*, 1935; **6**; 368-381.
- [15] Nilsson I.H.E., *Belastningsförsök på ofullständiga betongleder*. (1st ed.), Nordisk betong, 1977.
- [16] Sastry M.V., Detailing of reinforcement in concrete hinges and reinforced concrete pendulum bearings. *Indian Concrete Journal*, 1981; **55**; 157-159.

# *D* ASSEMBLY AND LIFTING OF PEARL-CHAIN ARCHES



## ASSEMBLY AND LIFTING OF PEARL-CHAIN ARCHES

Philip S. Halding<sup>1</sup>, Kristian D. Hertz<sup>1</sup>, Nicky E. Viebæk<sup>2</sup>, and Bryan Kennedy<sup>3</sup>.

<sup>1</sup>Technical University of Denmark, Department of Civil Engineering, 2800 Kgs. Lyngby, Denmark.

<sup>2</sup>Abeo A/S, 2000 Fr. Berg, Denmark.

<sup>3</sup>University of Washington, Seattle, Washington, 98195, USA.

### Abstract

Pearl-Chain arches were invented at the Technical University of Denmark in cooperation with the company Abeo A/S. The system uses specially designed, pre-fabricated concrete elements that are post-tensioned together into an arch shape, which is then lifted into place. The arches can be used both in buildings and bridges.

The assembly and lifting of two Pearl-Chain arches, with a span of 13 m and rise of 1 m, is considered in this paper. Precast “Super-Light Deck” elements were used for the arches, which had a thickness of 22 cm. Both arches were successfully lifted, rotated in mid-air, and placed adjacent to one another on prepared footings. The arches’ span and shape were continuously monitored during the entire construction sequence, and deformations stayed within an anticipated level.

**Keywords:** Pearl-Chain Bridge, Post-tensioning, Super-Light concrete decks, full-scale testing, pre-fab elements, arch erection method, Hammerhead joints.

### 1 Introduction

Pearl-Chain (PC) arches consist of a number of straight pre-fabricated concrete elements called Super-Light (SL) decks which are post-tensioned together into a desired shape (Halding & Hertz 2015; Hertz & Halding 2014).

The SL-deck technology uses normal concrete (cylinder compressive strength of 55 MPa, and density of 2300 kg/m<sup>3</sup>) in combination with a lightweight aggregate concrete (cylinder compressive strength of 3 MPa, and density of 700 kg/m<sup>3</sup>). SL-decks are produced by pouring the normal concrete over lightweight aggregate concrete blocks. Using lightweight concrete reduces the weight of the elements without compromising their rigidity or stability (in contrast to using thinner slabs). Therefore, a lower capacity crane can be used to safely erect the arches. However, normal, strong concrete is used for the full slab thickness at the ends of the SL-decks where compressive stresses need to be transferred from one SL-deck element to the next. The use of the lightweight aggregate concrete also makes the construction more environmentally friendly (Hertz & Bagger 2011).

A whole PC bridge would consist of several PC arches next to each other, giving the desired bridge width. The following challenges are posed for the assembly and erection of each arch:

First of all, the assembly of SL-deck elements on the ground is essential. To reach the correct shape, each SL element must be positioned accurately before being post-tensioned, and not to significantly change shape due to the post-tensioning. Each PC arch in a bridge must be identical concerning the span and shape, since even small errors in the geometry will be visible after erection.

Secondly, the arches need to have sufficient moment capacity to withstand the static and dynamic loading while lifted by crane. Special attention has to be given to the position of lifting

points and the lifting method. The weight of the arches should also be minimized in order to reduce the bending stresses during lifting, and to be able to lift with a larger lever arm of the crane.

Thirdly, the distance between the abutments has to be sufficiently large for the arches to be placed correctly – even when being slightly deformed hanging from a crane. Placing an arch requires the abutment not to settle horizontally more than intended, since even relatively small unended horizontal movements can significantly increase the bending moment in an arch. Therefore, the abutments must be placed far enough from each other to accommodate any deformations due to lifting. In a perfect lifting process the arch span should be slightly shorter when being put into position. This means that the lifting points are moved a bit toward the middle of the arch, and a negative moment is introduced in the structure. This can be good from a static point of view, but of course both the sub-structure and super-structure must be prepared. The test arches are two-hinged, with a hinge at each of the springings.



**Fig. 1** Four-point transportation of a 13 m Pearl-Chain arch by truck.

### *1.1 Previous assembly and lifting methods*

Prior to the middle of the 20<sup>th</sup> century, all concrete arch bridges were cast in situ, which requires significant time and energy for formwork and scaffolding construction. Increasing labor costs have created a market for pre-fabricated bridges, and the following pre-fabricated concrete arch bridges are examples of this:

TechSpan produces pre-cast concrete arch bridges with higher rise (relative to PC arches), and with spans of up to approximately 20 m. They assemble their arches from two smaller pieces put together. This requires one crane per arch half, and hence, two small cranes are required for the erection of at least the first two full arches. The arch segments are lifted at four points. Finally, the crown (the top of the arch where the pieces meet) is grouted (Hutchinson 2004; Proctor & Seow 2000). Similar to a Pearl-Chain bridge, the width of a TechSpan arch bridge can be increased by simply adding more arches adjacent to each other.

BEBO is another manufacturer of pre-cast concrete arch bridges. Their system is similar to Techspan's, but permits spans up to 30 m. For spans over 14.6 m they use a twin leaf method that requires two cranes for erection. The crown is cast in situ (Bernini et al. 2000; Bebo 2014).

The Nucon arch system differs from the above in regard to its assembly and lifting. Straight pre-cast concrete segments are placed flat on the ground, which are chained to a specially designed

lifting beam. An arch consists of several smaller pieces (similar to PC arches), and the arch does not take the intended shape until the lifting beam is elevated by a crane (Wakeman 1995).

Macrete Flexiarch uses even more smaller concrete segments than the Nucon arch system. All the segments are connected by a flexible membrane bonded to the top of all the elements. The arch, like the Nucon arch, is flat when on the ground, and obtains its design shape when being lifted. The longest available Flexiarch has a span length of 17 m, and requires six lifting points, including two at the crown (Macrete 2014; Mokhtar et al. 2011).

### 1.2 Scope

The assembly, lifting, and final placement of the first 8-element Pearl-Chain arches of 13 m is assessed in this paper. Lifting points were found by FE modeling in order to minimize bending moments (not presented in this paper). Different ways of placing the arches are also evaluated: both by use of wedges and by hydraulic flat jacks.

## 2 Positioning and post-tensioning the elements

The 13 m Pearl-Chain arches for testing of the assembly procedure consisted of six Super-Light deck elements, and two specially designed abutment-elements. All the elements had an interior cable duct for a 7C15 post-tensioning cable. Fig. 2 shows an overview of the components in one arch. The elements were cast at least seven days before the assembly.

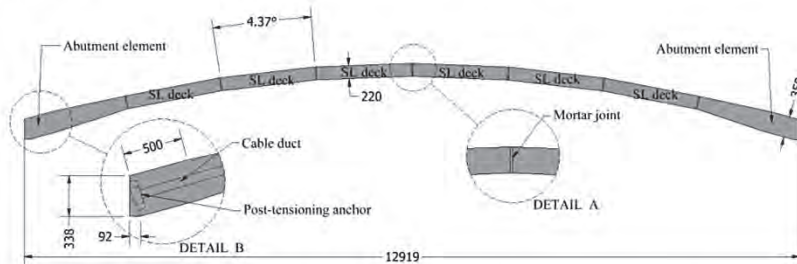


**Fig. 2** One PC arch consisting of six SL-elements and two abutment elements. It is held together by a post-tensioning cable running through all the elements. Detail A shows a mortar joint at the crown, and similar joints exist in all element connections. The rise is 1 m, and all units are mm.

The width of each test arch was 1.75 m, and the SL-deck elements were 220 mm thick. Other SL-deck widths and thicknesses are possible. The thickness of the abutment elements was tapered from 350 mm at the anchorage end for the post-tensioning (500 mm from the anchorblock location) to 220 mm at the connection to the SL-decks.

All elements were pre-cast, transported to the site, and then placed on their edge on shims on the ground for post-tensioning. Ends of cable ducts from each element were connected and formwork was put up for in situ casting of the mortar joints between the elements. The compressive cylinder strength of the mortar was: >20 MPa after 24 hours, >60 MPa after 7 days, and >80 MPa after 28 days. The mortar was designed and tested to remain homogeneous when being poured over a height of up to 2.4 m (Lund et al. 2014).

Two days later, the mortar was hardened enough for the post-tensioning to take place. The cable was post-tensioned to 90 % of the 0.1 percent proof strength of the steel, giving a force of 221 kN per wire. This force will decrease over time with up to 20 % due to anchorage seating loss, shrinkage, creep, and relaxation. See Fig. 3 for pictures of the assembly steps.

The last part of the pre-lifting assembly was grouting the cable duct.



**Fig. 3** Assembly steps for PC arch. 1) Top left: Vertical positioning of the elements in the desired arch shape. The dark surfaces are light aggregate concrete blocks. 2) Top right: Formwork put up and joints are cast between elements. 3) Bottom left: Two days later the formwork is removed and post-tensioning is performed. 4) Bottom right: Grouting of cable duct and the arch is ready for lifting.

This method was selected in order to minimize crane time, which is often a costly component of bridge construction. If the PC arches were assembled on temporary scaffolding or on a ground excavation (that followed the arch profile), a large, mobile crane would be required to lift and erect the arch before the next arch assembly could begin. By assembling each arch on its side, a smaller, less expensive crane mounted on a truck can be used to handle the individual SL-elements. After assembling several PC arches, a larger crane can then be brought to the site to erect all the arches at the same time.

### 3 Lifting process of one arch

The optimal lifting method was determined on beforehand with analyses in the FE program: Autodesk Robot Structural Analysis, and by simple hand calculations (not presented in this paper). Mid-air rotation of the arch was necessary, and the number and position of lifting points were studied to minimize bending moments during the lift. The lifting sequence can be summarized as:

- 1) Using two lifting points to vertically lift the arch from its "on-side" orientation.
- 2) Connecting two additional lifting points, and then rotating the assembly in mid-air.
- 3) Transporting the arch in its horizontal orientation.

At first the arch was lifted in two points. This first vertical lift should be performed without the arch slanting to the side when leaving its supports. The balance points were found to be slightly into the first SL-decks next to the abutment elements.

When hanging in the air, the arch was then rotated and transported to the site of erection. Rotating and lifting the arch in its horizontal orientation with the same lifting points used for the

initial vertical lift resulted in bending moments less than the arch's capacity. Therefore, the same lifting points were chosen for both vertical and horizontal lifting (although two additional points were added for the horizontal lift). The optimal position for the four-point, horizontal lifting of the arch is two points approximately in the middle of the first SL-decks adjacent to the abutment elements on each end. However, positioning the lifting points here was not chosen due to the light-aggregate concrete in the SL-decks in this area. Fig. 4 shows the position of the final lifting points.

A factor of 1.65 was applied to the static analysis results in order to account for dynamic loading.



**Fig. 4** Top: Lifting points for PC arch (circled in red). The two top points were used for the initial vertical lift. Bottom: Subsequently, the two bottom lifting points were connected, and the arch was rotated, positioned on temporary supports, and transported by truck to the erection site.

During this assembly and lifting test, the mid-air rotation was performed by a small crane as well as a large truck working together. They lowered the arch onto a temporary support, supporting the arch at the  $\frac{3}{4}$  points. Thereafter, the truck could lift and transport the arch to the erection site, see Fig. 1. In future Pearl-Chain bridge erections, such maneuvering can be performed with one mobile crane alone, by means of a crane hoist. In future Pearl-Chain bridges, the arch elements should be assembled next to the erection site so that the total number of arches for the PC bridge can be lifted and put on prepared foundations one by one with a mobile crane.

#### 4 Positioning and post-lifting assembly

Positioning of the arches on a prepared foundation was a significant part of the assembly process. As seen in Fig. 2, the theoretical span for an arch alone is less than the 13 m, and this is because of the need for space between the foundation and the arch when positioning it on the foundation. Arches transfer horizontal forces as well as vertical forces to the abutments, so the positioning has to be precise, since even small horizontal settlements of the arch springings will incorporate undesired bending moments in the arch.

Two methods were tried when positioning the arches: The first PC test arch was positioned on the foundation, and plastic and wood wedges were put in the space to regulate the span length. The span of the second PC test arch was adjusted by two hydraulic flat jacks at each springing. The latter method was less time consuming.

The remaining space between the arches and the foundation was later cast out with a mortar. Because the springings were designed to behave as hinges, no reinforcement was used between arches and footings. Fig. 5 shows the two methods for positioning the arches at the foundation.



**Fig. 5** Connection detail between foundation and arch. Left: First PC test arch was connected by plastic pieces and wood wedges. Right: Second PC test arch was connected by pumping up hydraulic flat jacks (requiring 6 bars of pressure).

After the placement, the two arches were tied together with shear connections called “Hammerhead joints”, which were prepared on the side of every SL-deck element. The Hammerhead joints consisted of a transverse, 550 MPa Y12 reinforcement steel bar embedded in a recess formed in the strong concrete. The steel bar goes from the concrete into the Hammerhead recess where it bends 180 degrees (with a bending radius of 96 mm) and continues back into the concrete again, see Fig. 6. The recess length was 500 mm, the depth was 113 mm, and the width was 110 mm. After placing the second arch, the Hammerhead joint recesses of each arch became aligned with each other and pieces of rebar were put on the inside of the bended Y12 in the longitudinal direction. Then, the longitudinal rebar pieces were connected by a rebar hoop that went around both bars. The longitudinal bars and the hoops were both 550 MPa Y16. Finally, the whole thing is cast out with a >55 MPa mortar. The arches are positioned 10 mm apart, and therefore it is necessary to use a construction foam as a formwork between the two arches to contain the mortar during the Hammerhead joint pour.

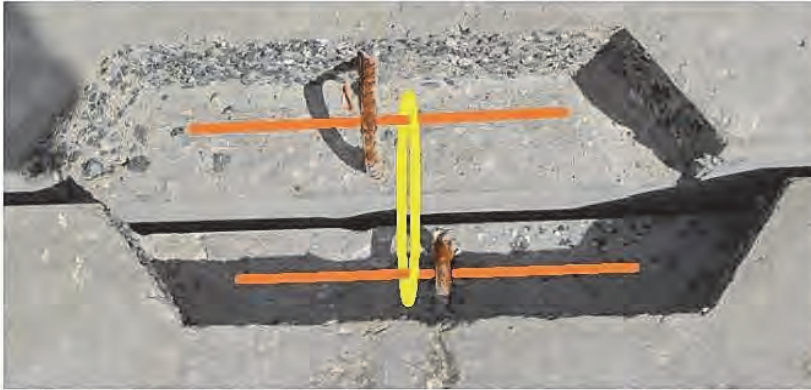


**Fig. 6** Hammerhead joint recesses on sides of two adjacent SL decks before assembly. Y12 rebars are seen on both sides. Later longitudinal bars (drawn in orange), a steel hoop (drawn in yellow), and construction foam will be applied before pouring the mortar. The aggregates are exposed for better shear transfer.

Each Hammerhead joint can transfer a shear force of more than 2.5 tons. Due to the hoop around the longitudinal bars, the joint remains functional even if the arches are not perfectly aligned.

## 5 Lessons learned

Shortly after the post-tensioning of both arches, visible cracks were formed in the longitudinal direction through the mortar joints between the elements. The cracks were only found between SL-decks and not at the joints to the abutment elements. They also only occurred in the bottom face of the elements, see Fig. 7.

When the arches were post-tensioned with a cable through the curved ducts in the elements, the curvature of the cable resulted in a downwards force along the duct. Increasing the deck thickness and the cross reinforcement will increase the crack resistance. Also, the curing time of the concrete and mortar before post-tensioning has an influence (in this case the curing time was less than two days). In a previous test where the concrete had been cured for a longer time these cracks did not appear although the thickness of the deck and the prestressing force were identical. In future PC arches additional reinforcement will be applied transversely below the ducts in the SL decks and sufficient curing time will be applied to avoid any cracking which potentially could lead to corrosion of the tendon.



**Fig. 7** Crack forming in the longitudinal direction in the bottom of the SL-deck in the joints between SL-elements. Joints between abutment elements and SL-decks did not crack due to larger number of transverse reinforcement. The dark areas are the bottom of the light aggregate concrete blocks.

Before and after the assembly and lifting of both PC arches, the arch span lengths were measured, see Table 1. Before post-tensioning, the span length was within 10 mm of the design shown in Fig. 2. After positioning the arch on the foundation, the span lengths ended up being 15 mm longer than after the post-tensioning had been completed. In addition to the above measurements, arch 2 were measured right after post-tensioning as well as in mid-air during the transportation.

**Table 1**  
**Span of the two PC arches in the assembly and lifting test.**

Time	Span of arch 1 (m)	Span of arch 2 (m)
Before post-tensioning	12.910	12.910
After post-tensioning, before lifting	-	12.885
During lifting; hanging at four points	-	12.880
Final position with wedges/flat jacks	12.900	12.900

A deformation of 15 mm was within the expected range for the span after post-tensioning compared with the span at the final position. The first arch was lifted the day after the post-tensioning, and the second arch was lifted three weeks after the post-tensioning. Possibly, creep could be a small part of the reason why the first arch, ended up with a 25 mm lower rise than the second arch when they were placed next to each other. Though this difference was easily observed, it did not affect the structural behavior except for the “built-in” bending moments, since the Hammerhead joints were designed to provide some tolerance for misalignment. Two other significant reasons for the difference in the rise was measuring accuracy of more than  $\pm 5$  mm when measuring the span, and inaccurate assembly by the workman crew. Fig. 8 shows the misaligned arches and Hammerhead joints.



**Fig. 8** Top: Close up of difference in height between the two arches at the crown showing the requirement of high accuracy during the assembly process. The first arch (closest) was placed on the foundation three weeks prior to the second arch (furthest away). Bottom: The first 13 m span PC arches in their final position.

## 6 Conclusion

Two 13 m span Pearl-Chain arches were successfully assembled, post-tensioned, lifted, and positioned on a prepared foundation. Each arch was composed of eight pre-fabricated, Super-Light deck elements. The arches were placed adjacent to one another, and formed a single span bridge.

The arches were assembled by first placing the elements vertically (on edge) in the desired arch shape before casting the joints between the elements with a fluid mortar. Two days later, post-tensioning took place, and one arch was measured to reduce its span by 25 mm due to the post-tensioning. Minutes after the post-tensioning, longitudinal cracks developed in the mortar joints under the cable ducts; the cracks were investigated and assessed to only have aesthetic concern in regard to the rest of the test.

Lifting, including mid-air rotation, went smoothly for both arches, and two different methods were tried when placing the arches on the foundation. The method using flat jacks was less time consuming.

In the final position, the arch span length was within 15 mm of the span lengths measured after post-tensioning (for arch 2). This produced “built-in” bending moments in the arches, but the deformations were within the expected limit of deviation for the span. The final rise of the arches differed by 25 mm at the crown. The main reason for the difference was span measuring inaccuracy

and assembly errors by the workman crew. The two arches were tied together with Hammerhead joints, which were designed to permit some misalignment between the arches. The joints were completed without incident.

### Acknowledgements

The authors wish to thank the workman crew at Perstrup Betonindustri for their great efforts during the test (Lasse Hejdenhejm Hoyer should receive a special appreciation), and for the project main funding by the Innovationsfonden and a Valle Scholarship from the University of Washington.

### References

- Bebo (2014). [www.beboarch.com](http://www.beboarch.com).
- Bernini, J., Fitzsimons, N. & Heierli, W. (2000). Overfilled Precast Concrete Arch Bridge Structures. In IABSE Congress Report. pp. 380–387.
- Halding, P.S. & Hertz, K.D. (2015). Precast Pearl-Chain Concrete Arch Bridges. To be in Journal of Structural Engineering.
- Hertz, K.D. & Bagger, A. (2011). CO2 emissions from Super-light Structures. In Proceedings of the International Association for Shell and Spatial Structures (iabse-iass) Symposium 2011 “taller, Longer, Lighter”. London, UK.
- Hertz, K.D. & Halding, P.S. (2014). Super-Light Pearl-Chain Arch Vaults. R. M. L. R. F. Brasil & R. M. O. Pauletti (Eds.). In Proceedings of the IASS-SLTE 2014 Symposium “Shells, Membranes and Spatial Structures: Footprints”. Brasilia, Brazil.
- Hutchinson, D. (2004). Application and design of segmental precast arches. Geotechnical Special Publication, (126 I), pp.452 – 459.
- Lund, M.S.M., Arvidson, M. & Hansen, K.K. (2014). Homogeneity and Strength of Mortar Joints in Pearl-Chain Bridges.
- Macrete (2014). [www.macrete.com/flexiarch](http://www.macrete.com/flexiarch).
- Mokhtar, M.R. et al. (2011). Arch-bridge lift Process Monitoring by Using Packaged Optical Fibre Strain Sensors with Temperature Compensation. Journal of Physics: Conference Series, 307.
- Proctor, P. & Seow, K. (2000). Bridge replacement using low profile three hinged pre-cast arch in Newfoundland. In 2000 Annual Conference Abstracts - Canadian Society for Civil Engineering. p. 254.
- Wakeman, A. (1995). The nucon arch - Plain precast concrete arch systems. In ARCH BRIDGES. pp. 645 – 652.



***E*** FULL-SCALE LOAD TESTS OF PEARL-CHAIN ARCHES

# Full-Scale Load Tests of Pearl-Chain Arches

Philip S. Halding<sup>a</sup>, Kristian D. Hertz<sup>b</sup>, Jacob W. Schmidt<sup>c</sup>, Bryan J. Kennedy<sup>d</sup>

<sup>a</sup>Technical University of Denmark, Department of Civil Engineering, building 118, DK-2800 Kgs. Lyngby, Denmark, +45 4525 1811, [psh@byg.dtu.dk](mailto:psh@byg.dtu.dk).

<sup>b</sup>Technical University of Denmark, Department of Civil Engineering, building 118, DK-2800 Kgs. Lyngby, Denmark, +45 4525 1950, [khz@byg.dtu.dk](mailto:khz@byg.dtu.dk).

<sup>c</sup>Technical University of Denmark, Department of Civil Engineering, building 118, DK-2800 Kgs. Lyngby, Denmark, +45 4525 1773, [jws@byg.dtu.dk](mailto:jws@byg.dtu.dk).

<sup>d</sup>University of Washington, Seattle, Washington, 98195, USA, [bryanken@uw.edu](mailto:bryanken@uw.edu).

**Abstract:** Specially designed, pre-fabricated, lightweight, concrete deck elements (SL-Decks) can be post tensioned together into an arch shape (Pearl-Chain arch). Individual arches can then be erected adjacent to one another in order to form a bridge span. Two Pearl-Chain arches, each with a span of 13 m and a rise of 1 m, were erected onto a prepared test foundation. The arches were tested with load control by applying a gravity load to the  $\frac{1}{4}$  point of the bridge span. Two tests were completed on the same specimen in order to determine the behavior of an arch bridge formed with SL-Decks. The first test investigated the system's elastic response (maximum load of 648 kN), and the second test demonstrated its collapse mechanism and ultimate capacity (maximum load of 970 kN). Analytical calculations showed that the loaded  $\frac{3}{8}$  point of the span and the non-loaded  $\frac{1}{4}$  points of the span were critical locations for the structure. Failure initiated at the  $\frac{3}{8}$  and  $\frac{5}{8}$  points. Plastic hinges were observed at a load near the fracture load, and different warning signs were seen at 84% to 94% of the fracture load. The ultimate, experimental load capacity was 14 % higher than the calculated result (load of 849 kN), and the difference was mainly due to the assumed static system used in the calculations. Measurements performed in Test 1 showed that the SL-Decks, which contained lightweight aggregate concrete blocks (LAC blocks) in the bottom of their cross sections, may have benefited from multiaxial compression effects. Furthermore, the pair of test arches were connected with so called Hammerhead joints in order to transfer forces from one arch to the other. The displacement data suggested that when a load was applied to a single arch, some proportion of that load was transferred to the adjacent arch.

**Keywords:** *Full-Scale; Pearl-Chain Arches; Ultimate capacity; Arch bridge; Concrete; Post-tensioning; Structural behavior; Plastic hinges; Super-Light Deck elements; Testing to fracture.*

## 1. INTRODUCTION

This article presents and summarizes the results from two experimental tests of full-scale, Pearl-Chain, concrete arches. The test method was developed by considering previous analytical and experimental research of full-scale, traditionally constructed, reinforced concrete arches.

The difference between elastic and plastic ultimate strength calculations for statically indeterminate, concrete arches was addressed by Jain [1]. He studied circular, two-hinged arches subjected to a concentrated load at the  $\frac{1}{4}$  point of the span. Beyond the elastic limit, when the concrete starts cracking, and the moment of inertia and material stiffnesses decrease, his proposed plastic calculation method gave a load carrying capacity 50% to 100% larger than obtained elastically. The plastic response of a two-hinged arch begins when approaching the ultimate load. First, a plastic hinge forms below the load, due to the maximum, positive bending moment there. After further loading, another plastic hinge forms on the non-loaded side at the location of the largest negative bending moment. The second plastic hinge leads to collapse of the structure.

Jain dealt with a static system with a steel tension tie of a given stiffness,  $E_s$ , and area,  $A_2$ , to resist the horizontal force from the concrete arch of span,  $L$ . The arch had stiffness,  $E_c$ , cross sectional area,  $A_1$ , and moment of inertia,  $I$ . Without taking areas of plastic deformations into account, the horizontal reaction force,  $H$ , was:

$$H_{elastic} = \frac{\int \mu \cdot y \cdot ds}{\int y^2 ds + L \left( \frac{I}{A_1} + \frac{E_c}{E_s} \cdot \frac{I}{A_2} \right)} \quad (1)$$

The parameter,  $y$ , is the equation of the arch shape, and  $\mu$  is the bending moment distribution of a similar beam (with no horizontal force). The small length,  $ds$ , is along the arch centerline axis. From having the arch reactions he calculated the thrust line, and found the normal force in the arch at any point on the span. The positive bending moment was much larger below the load compared to the negative moment in the non-loaded  $\frac{1}{4}$  point. To achieve the optimal load carrying capacity, moment redistribution had to occur. That happened when the first plastic hinge was formed below the load where the moment was largest. At a certain length of the span below the point load, the concrete was in the plastic domain of the working curve. This additional angular deformation generated an increase in the horizontal reaction force and the line of thrust therefore became less inclined, compared to the purely elastic case. This change is illustrated in Figure 1.

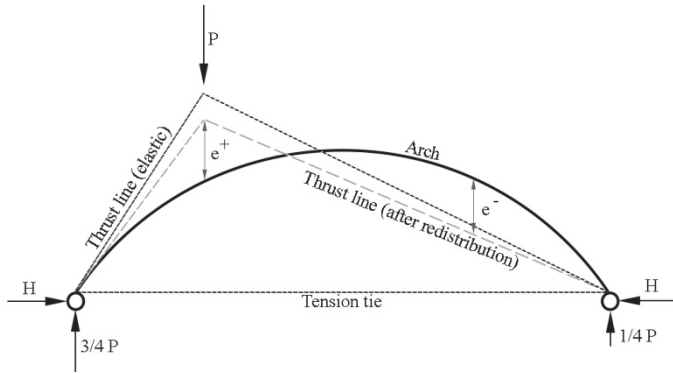


Figure 1: Thrust lines of arch loaded in 1/4 point of span.

In the figure the thrust line is shown for the elastic case and for the case with moment redistribution from plastic hinges. The optimal condition was a situation where the concrete could undergo enough angular deformation in the plastic hinge for the bending moment to reach the same level in the non-loaded 1/4 point of the span as in the loaded 1/4 point of the span. The eccentricity of the thrust line to the arch shape is shown in Figure 1 in the loaded-,  $e^+$ , and the non-loaded side,  $e^-$ . The horizontal reaction including plastic hinges was:

$$H_{pl\_hinge} = \frac{\int \mu \cdot y \cdot ds + E_c I \sum \Delta \phi \cdot y \cdot ds}{\int y^2 ds + L \left( \frac{I}{A_1} + \frac{E_c}{E_s} \cdot \frac{I}{A_2} \right)} \quad (2)$$

$E_c I \sum \Delta \phi \cdot y \cdot ds$  was extra outward movement of the arch ends due to the part of the arch span that had developed plastic strains. The potential extra outward movement was withstood as an increased H.  $\Delta \phi$ , is the extra angular deformation compared to the elastic case.

Jains proposed theory only included arches with the same cross section properties along the span. With that limitation the method was verified after several tests.

Marshall et al. [2] provided practical engineering guidelines based on experimental tests of three closed-spandrel, reinforced concrete arches. Those arches had span lengths 12.8 m, 6.1 m, and 11 m. Their arches were cast into abutment walls, and soil-structure interaction was considered. Their 12.8 m span arch was tested during erection, during the compaction of the filling material, and later for a live load of 253 kN. The 6.1 m and the 11 m span arches were tested in a lab to fracture with symmetric point loads at the crown and close to the crown. Strain gauges were implemented in both tests, and were applied on the top and bottom of the arches at various positions along their spans. With this instrumentation, bending curvature (and therefore moment) could be calculated and correlated to the applied load for various points in the span. The 6.1 m span arch failed in a

brittle, shear fracture mechanism, close to the fixed connection at the abutment support. Conversely, the 11 m span displayed a more ductile failure, with larger bending deformations before the ultimate load was applied.

Zhang et al. [3] used a similar method to determine the ultimate capacity of two existing, 20 m long, arch ribs. They measured strains at different span locations by instrumenting the top, bottom, and ribs of the arches. The vertical displacements were monitored at several span locations, and the abutments' horizontal settlement was also measured. The arches were loaded with point loads of same magnitude in both  $\frac{1}{4}$  points and in the crown. A plastic hinge was observed in the  $\frac{1}{8}$  point of the span as the load increased and large cracks became visible before the ultimate load was applied. Their tested arches failed with a sudden shear fracture at the springings.

Another full-scale test was described by McGrath and Mastroianni [4]. An 8.5 m long, closed-spandrel arch bridge was loaded with a real, tandem-load truck. The bridge was further tested with a loading beam. That beam was connected to adjacent ground anchors, which were used to pull the beam downward onto the bridge. This loading simulated one axle of a heavy vehicle. Cracking was observed, but the bridge was not loaded to fracture.

### **1.1. Pearl-Chain Bridges**

Pearl-Chain (PC) Bridges are a relatively new arch bridge technology [5]. A PC-Bridge consists of several adjacent Pearl-Chain arches, with each arch assembled from a number of Super-Light (SL), pre-fabricated, concrete deck elements [6]. The SL-Decks are individually pre-stressed, mainly to resist forces from transport. The deck elements have a rectangular cross section, and are cast with a combination of normal concrete and a lightweight aggregate concrete (LAC). The normal concrete is used to form a top flange and ribs, while the LAC blocks stabilize the ribs and reduce the element's self-weight. In this paper, normal concrete is defined as regular concrete with compressive cylinder strength of 55 MPa. The SL-Decks are then assembled into a desired arch profile by means of Pearl-Chain reinforcement. Additional details on this reinforcing design were published by its inventor, Kristian Hertz [7]. Basically, a Pearl-Chain design uses a post-tensioning cable to fasten several SL-Deck elements together. Post-tensioning ducts are draped within those elements so that the eventual, continuous duct follows the elevation profile of the complete structure. Furthermore, the ducts are situated so that the post-tensioning cable will perpendicularly cross each joint along the arch. This prevents shear forces from developing across the joint interfaces between the deck elements when they are post-tensioned together and the arch is subjected to its self-weight.

A 6 m span, PC-Arch was previously tested [8]. The 6 m span arch was mainly produced to verify the assembly method of the three SL-Decks it consisted of. A pair of 13 m span arches were recently assembled (of 8 elements each), lifted, and positioned on a prepared foundation [9].

This paper presents experimental results on the behavior of the SL-Decks when used in an arch (Test 1), and the ultimate load capacity of the 13 m span, PC-Arches (Test 2). It is noted that a PC-Bridge would also include a filling material between the arches and road surface. A filler was not included with these arches, which is considered as a conservative design. Furthermore, it has to be emphasized that the test was performed on the two 13 m span arches only, and that the results therefore solely gives indications of a behavior. Figure 2 shows the two arches in their test position, after being assembled and erected.



Figure 2: Two adjacent PC-Arches after assembly and lifting.

The scope of the tests addressed in this paper was:

- Monitor deflections and strains during loading, and determine if forces are transferred between arches during loading.
- Investigate the behavior of the straight SL-Decks during loading, when used in an arch structure.
- Compare the ultimate load from testing with an analytical model.
- Find indication of clear warnings before the ultimate capacity is reached.

## 2. PREPARING THE TEST

The bridge assembly was tested two times. In Test 1, the arches were loaded with a total of 66 tonnes (648 kN) at the  $\frac{1}{4}$  point of the span. Ten months later, they were re-tested in Test 2 to determine the load capacity, which was 98.8 tonnes (970 kN). Both tests were scheduled for the same day, but due to problems with the loading crane, Test 2 was delayed.

## 2.1. Geometry and materials

Each arch consisted of eight elements (six SL-Decks and two abutment elements), which were post-tensioned together by 7C15 cables. All elements were made of the same concrete mix. The cables were first tensioned to 90% of the 0.1% proof stress of the steel ( $f_{p0,1k} = 1634$  MPa), and then grouted. The SL-Decks were approximately 1.60 m long, 1.75 m wide, and 220 mm in section height. This gave space for four LAC blocks across and two lengthwise in each deck element. The resulting area of the normal concrete in an arch cross section with LAC blocks was  $0.196$  m<sup>2</sup>. The SL-Decks had 10 pre-stressed mono strands in the bottom of the cross section with a concrete cover of 60 mm, and 10Y20 bars (550 MPa mild steel) in the top of the cross section with concrete cover of 30 mm. The material properties of the strands were the same as the previously mentioned post-tensioning cables. See Figure 3 for section cuts of the SL-Decks.

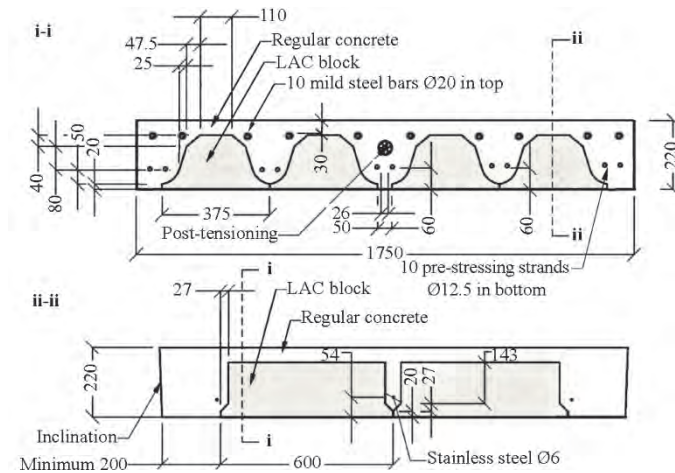


Figure 3: Detailed section cuts of SL-Deck type in the test arches.

The normal concrete had a characteristic compressive cylinder strength of  $f_{ck} = 59$  MPa and a Young's modulus of  $E_{cm} = 39$  GPa. The concrete's theoretical strain at maximum stress was  $\epsilon_{c1} = 0.26\%$ . Figure 4 is based on 28 day tests of the uniaxial compressive strength ( $f_{cm}$ ) combined with values of the Young's modulus ( $E_{cm}$ ) and strains ( $\epsilon_{c1}$  and  $\epsilon_{cu1}$ ) calculated with the Eurocode 2 [10]. Cored specimens were tested after the collapse in Test 2 and gave approximately the same Young's modulus and strength. The true curve would have been dependent on a variety of factors (e.g., mix design, aggregate size and type, and admixtures).

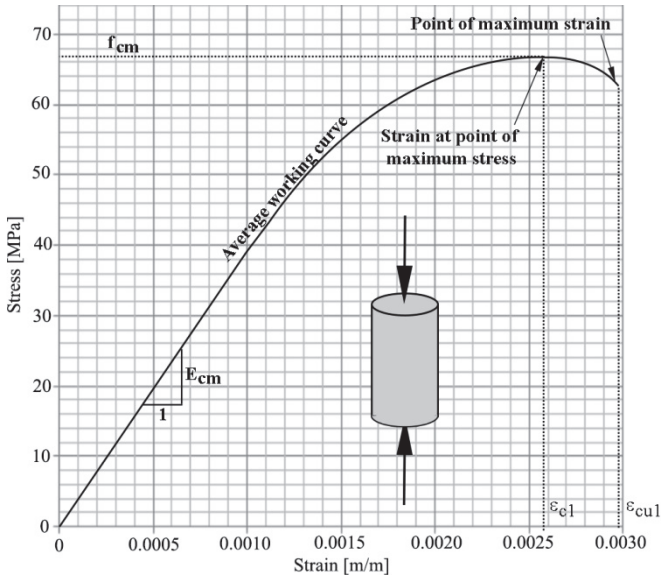


Figure 4: Theoretical working curve for the normal concrete in the SL-Decks.

Reinforced concrete plateaus were cast on top of the arches between the 1/8 and 3/8 points of the span. These plateaus provided a level, horizontal surface for load application at the span's 1/4 point. Both arches had their own, isolated plateau, each weighing an estimated 30 kN. Individual plateaus were chosen because one goal was to determine if an asymmetrical load would be shared between the arches. Therefore, a gap between the plateaus prevented the premature transfer of force at the load point. A layer of polyethylene was placed between each arch and plateau to reduce friction between the surfaces, and to hereby ensure that the load would act vertically.

The two arches were tied together with Hammerhead joints. These connections were designed to transfer forces from one arch to the other, and are shown in Figure 5. The connections are completed by first forming recesses in the sides of the SL-Deck elements. Once the arches are erected and aligned, a series of rebars are used to tie adjacent deck elements together. Finally, each recess is filled with mortar. The Hammerhead joint mortar had compressive cylinder strength of 12MPa, and a Young's modulus of 23 GPa. The rebar of a Hammerhead joint consists of Y12 (550 MPa mild steel) stirrups that protrude from the side of each SL-Deck, which are connected to a Y16 hoop with a Y16 steel bar. The connection detail is often used between deck elements in buildings, and is explained further in [9].

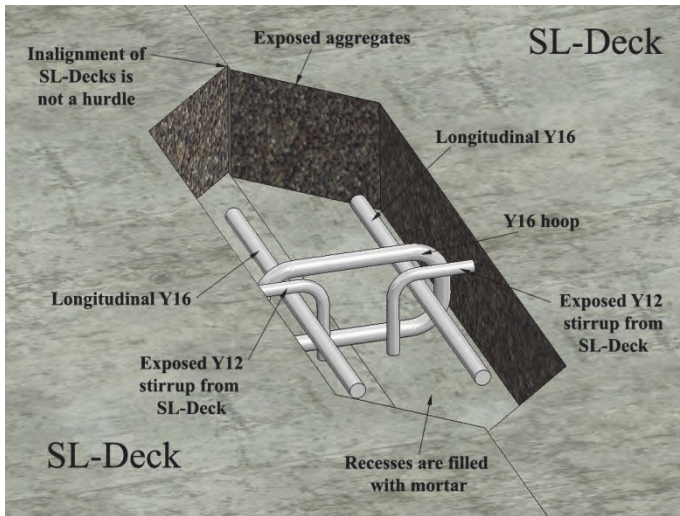


Figure 5: Explanation of transverse Hammerhead joint.

The mortar used in the joints between SL-Decks had a compressive strength greater than 80 MPa at the time of the first test.

To avoid test result interference from horizontal settlement of the abutments, a post-tensioned abutment plate was cast as a foundation for the test arches. It consisted of concrete with characteristic compressive cylinder strength of 43 MPa, and a corresponding Young's modulus of 36 GPa. Three 7C15 post-tensioning cables were used to post-tension the abutment plate (similar to those in the arches). The distance between the ducts was 1.2 m. The ends of the abutment plate were also heavily reinforced with mild steel.

Figures 6 shows the test setup.

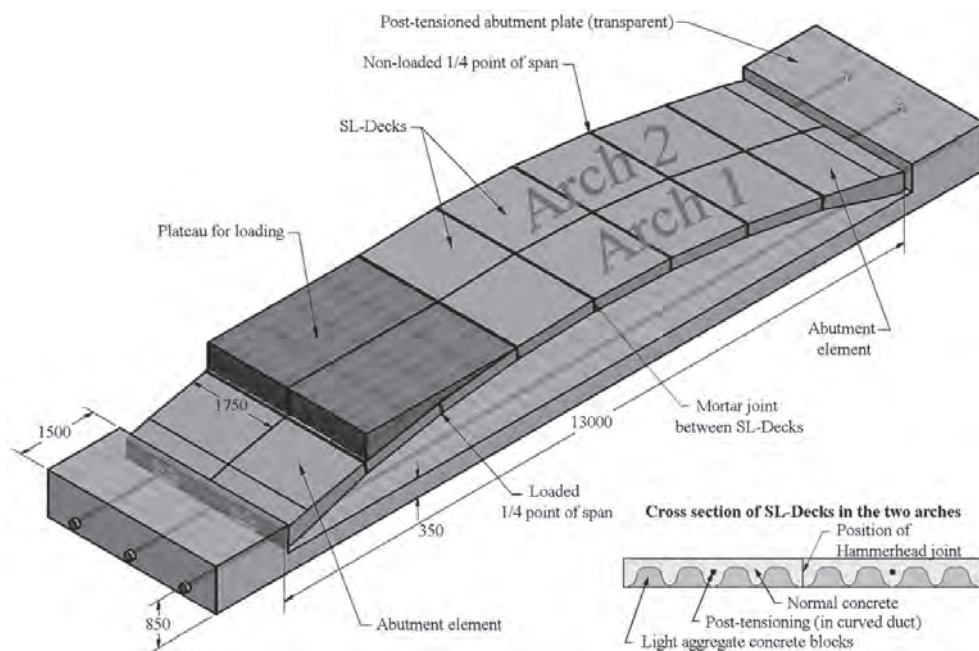


Figure 6: Test setup of two 13 m span PC-Arches placed on a post-tensioned abutment plate. All given dimensions are in mm.

Mortar was poured between the PC-Arches and the abutment plate. This mortar had similar properties as the one used in the Hammerhead joints. This was done to provide a smooth, continuous bearing surface for the lateral and vertical support reactions. Statical-ly, it was expected that these joints – which lacked any sort of crossing reinforcement – would behave as hinges, so that the whole system would behave as a two-hinged arch.

## 2.2. Measurement Methods

### 2.2.1. Arch Deflections

Deflections were measured with three different methods: LVDT's, a leveling instrument, and a digital image correlation system.

Twelve linear variable differential transformers (LVDT's) were attached to different locations of the arches. Two of the LVDT's measured the horizontal settlement of the abutments, while the other 10 measured vertical deflections along the span length. Vertical deflections were also measured by using a leveling instrument. The instrument was placed approximately 7 m from the side of "arch 1". Rulers were attached to the sides of both arches, and the deflection was measured through the leveling instrument when the load was applied. A total of 12 rulers were attached: 7 on "arch 1" and 5 on

“arch 2”. The leveling instrument was used both to verify the readings from the LVDT’s, which were more accurate and precise, and to measure the deflections at locations where the LVDT’s could not be applied. This was at the loading plateau, and at the  $\frac{3}{4}$  joint, where detailed photographs were taken.

Figure 7 shows the position and notation of all LVDT’s and rulers. The measuring devices were positioned as close to the joints between SL-Decks as possible, and the joints were each given a location name: A, B, C, etc. The LVDT’s named 1 and 2 measured the horizontal movement of the abutments at the end of “arch 1”.

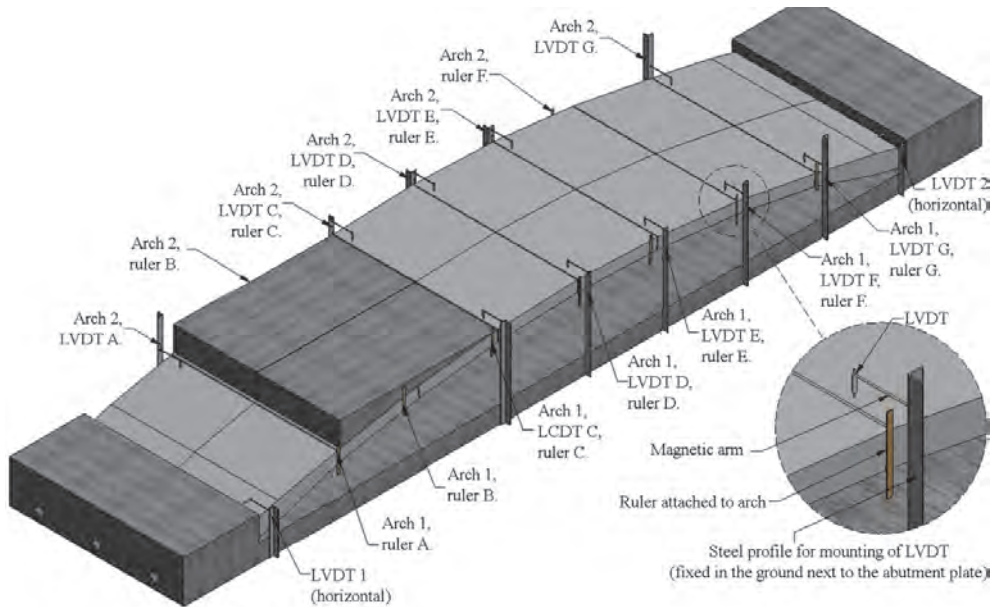


Figure 7: Position of all LVDT’s and rulers for measurement of deflections on “arch 1” and “arch 2”.

The third method relied on a digital image correlation system (DIC) system - ARAMIS.

### 2.2.2. Strain Measurements

Two methods were used to acquire strain measurements on the arches: ARAMIS and concrete strain gauges.

ARAMIS is a software package with digital image correlation technology [11]. After taking several pictures of a surface, the software can recognize and track facets of a defined size, and then compare the movement and deformation of these areas with a reference picture. The program can then generate several outputs, such as two-dimensional strains and deformations of the photographed surface.

Photographs were taken on the side of the arches for processing in ARAMIS. The first two cameras were in location B (the loaded  $\frac{1}{4}$  point of the span), two other cameras were in location F (the non-loaded  $\frac{1}{4}$  point of the span), and the last two cameras were placed at the joints to the abutment plate in both ends of “arch 2”. All cameras were perpendicularly aligned to the arch surface, and several spot lights gave indirect light for best possible pictures. The 2d ARAMIS version was used.

Strains were also obtained with concrete strain gauges, which were applied underneath “arch 2”. Eight, 50 mm long, concrete strain gauges were attached, which measured the strain in the longitudinal direction of the arch. They were positioned at location F, in two rows of four strain gauges, as shown in Figure 8. The first row was aligned with the middle of the SL-Deck and continued along its rib. The second row was placed along the side of the SL-Deck. A longitudinal spacing of 200 mm between gauges was used for each row, and all gauges were placed on the deck’s normal concrete. In Figure 8, the dark rectangles are the bottoms of the LAC blocks. Line A is the position of a cross section in the SL-Deck through only normal concrete, and line B is the position of a cross section with both normal concrete and LAC blocks. The bottom of the non-loaded side was expected to be in compression during testing. Furthermore, it was expected to be one of two critical locations when approaching the ultimate load carrying capacity. The other important location was in the  $\frac{1}{4}$  point of the span in the loaded side.

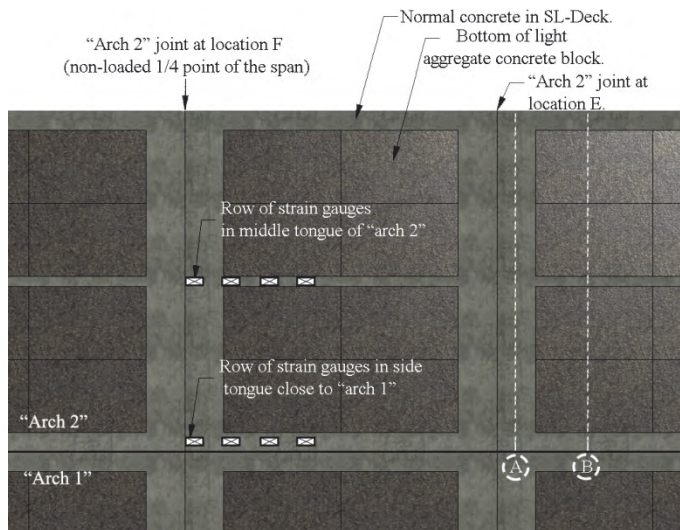


Figure 8: View from underneath “arch 2” at the joint at location F (for locations see Figure 7).

### 2.3. Analytical calculations

Before testing the arches, analytical calculations were performed in order to determine the initial strains at the most critical positions, and the expected load at fracture.

### 2.3.1. Initial strains

The self-weight (including the plateaus), pre-tensioning force within the individual SL-Decks, and the post-tensioning force were included in this calculation. Figure 9 shows the sequence of initial loadings. State I is the strain distribution after pre-tensioning the SL-Deck. State II represents the post-tensioning of the arch and the application of its self-weight. States IIIA and IIIB represent the strain distributions at the loaded and non-loaded  $\frac{1}{4}$  points, respectively, after applying the weight of the loading plateau. Those  $\frac{1}{4}$  points were the theoretically most critical locations in the span assuming the load as being concentrated at the  $\frac{1}{4}$  point. In reality the load on the plateaus was expected to be uniformly distributed from the  $\frac{1}{8}$  to  $\frac{3}{8}$  of the span in the first load steps. Later as the arch deflects, the load would be expected to concentrate in the regions of the  $\frac{1}{8}$  of the span, and the  $\frac{3}{8}$  of the span. This is due to the plateaus having a bending stiffness as well.

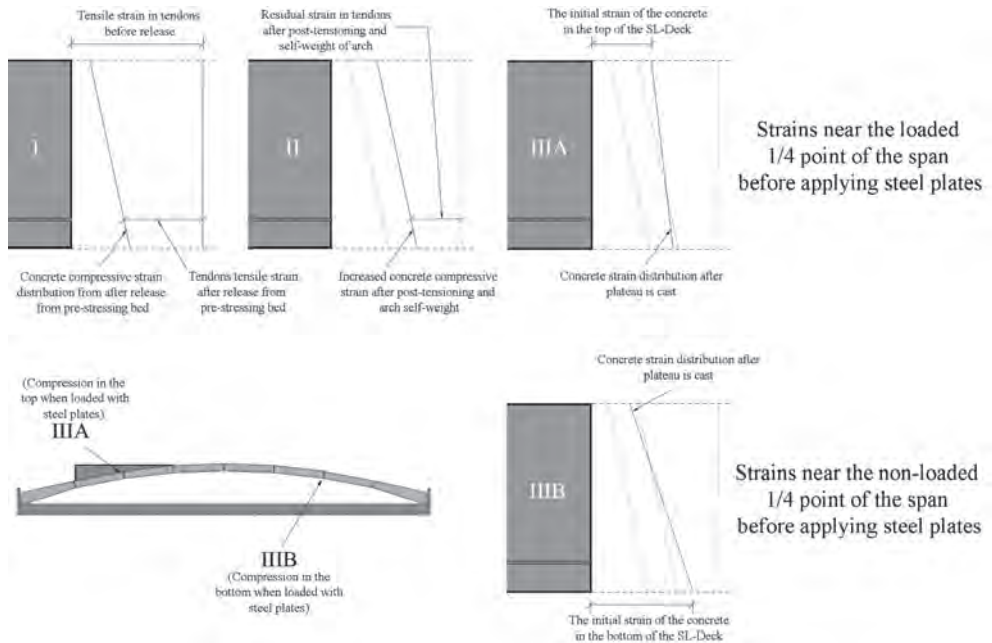


Figure 9: Initial elastic strain distributions in a SL-Deck in two positions before loading with steel blocks. The size of the strain distributions are not to scale.

The normal force in each arch from the initial contributions, less the expected initial losses, was 3251 kN. The calculated contributions to the normal force were: 166 kN for the arch dead load, 1520 kN for the eccentric pre-stressing strands, 1544 kN for the central post-tensioning cable, and 107 kN for the plateau dead load. The bending moment

from the eccentric pre-tensioning was negative. In a cross section with LAC blocks it was -111 kNm, and in a cross section of only normal concrete it was -76 kNm. In the joints between SL-Decks there were no contributions from pre-tensioning.

The moment contribution from the dead load of the plateau was 43 kNm close to the loaded ¼ point of the span, and -28 kNm close to the non-loaded ¼ point of the span. By Navier's formula we achieve the following elastic, compressive strains:

- In the bottom of the non-loaded side around location F:
  - With a full cross section of normal concrete the strain was 0.038%.
  - With a cross section including LAC blocks the strain was 0.10%.
  - In the joints between SL-Decks the strain was 0.0136%.
- In the top of the loaded side around location B:
  - With a full cross section of normal concrete the strain was 0.0142%.
  - With a cross section including LAC blocks the strain was 0.0073%.
  - In the joints between SL-Decks the strain was 0.0049%.

The SL-Decks were chosen to have pre-tensioning in the bottom of the cross section only (cf. Figure 3), and this, along with the position and mass of the plateau, is the reason for the largest initial strain in the bottom of the non-loaded side.

### 2.3.2. Expected load at fracture

The load at fracture was at first calculated to be 56 tonnes (550 kN) with the assumption of the full load being concentrated in the ¼ point of the span. As mentioned, the true static system is closer to two point loads in the 1/8 point, and 3/8 points of the span. This is the basis of the following simplified calculation:

By using Eq. 1 the horizontal reaction is determined. The steel tension tie properties are changed to fit the properties of the abutment plate in the test:

$$H_{elastic} = \frac{\int \mu(x) \cdot y(x) \cdot ds}{\int y(x)^2 ds + L \left( \frac{I_{arch}}{A_{arch}} + \frac{E_{arch}}{E_{plate}} \cdot \frac{I_{arch}}{A_{plate}} \right)}$$

Then the bending moment,  $M(x)$ , and normal force,  $N(x)$ , is found. An example of the shape of the moment distributions is seen in Figure 10.

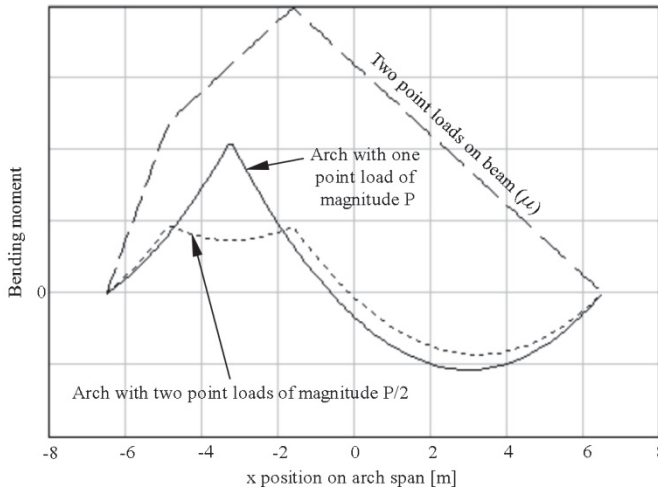


Figure 10: Bending moment in the arch from applied load.

The  $M(x)$ , and  $N(x)$  depend on the total load,  $P$ . The bending moment capacity of the arch depends on the normal force. Using an iterative approach the direct load carrying capacity is found in terms of  $P$ :

5. Choose a  $P$ , calculate  $H$ , and find  $M(x)$ , and  $N(x)$ .
6. In the assumed most critical positions ( $1/8$ ,  $1/4$ , and  $3/8$  of the span in the loaded side, and the  $1/4$  point of the span in the non-loaded side) calculate  $N$  and  $M$ .
7. For the different magnitudes of  $N$  find the moment carrying capacity,  $M_d$ , of the three possible cross sections in the arch: A section with LAC blocks in the SL-Deck (Figure 3), a section with no LAC blocks in the SL-Deck, and a section through a joint between SL-Decks. In this step the value of  $N$  from the load,  $P$ , is increased by the normal force from pre-stressing and dead load.
8. Compare the numerical value of  $M$  and  $M_d$  for all the positions on the arch span, and all types of cross sections in these positions. In this step the relevant initial bending moments are added to  $M$  found from the load,  $P$ . If  $|M| < |M_d|$  in all possible combinations, then increase  $P$  and repeat the iteration.

By means of this purely elastic approach the load carrying capacity was found to be  $P = 86.5$  tonnes. The capacity is found to be reached in the non-loaded side in the  $1/4$  point of the span in a cross section with LAC blocks. At that point only little capacity is left in the loaded side in the  $3/8$  point of the span in the joint between SL-Decks. Therefore, the effect of possible plastic hinges is presumably insignificant.

### 3. TEST RESULTS

The bridge assembly was tested with two separate phases, with different investigative objectives for each test. In Test 1, deflections and strains were measured during loading to 66 tonnes (648 kN), when the test was stopped for safety reasons. This first test gave evidence for the transfer of forces through the Hammerhead joints, and permitted the study of the distribution of strains within an SL-Deck. Test 2, on the other hand, was conducted in order to determine the specimen's ultimate load capacity, and to observe its collapse mechanism. Figure 11 shows a photograph taken during Test 1.



Figure 11: Test 1. Six steel blocks, each weighing 10 tonnes, were set on the plateaus on “arch 1” (near side in photograph) and “arch 2”.

Test 1 was performed with the following procedure. The two arches were loaded with steel blocks, each weighing 10 tonnes (98 kN). First “arch 1” was loaded with one block, and then “arch 2” was loaded with one block. This sequence repeated until three blocks were positioned on each arch, and then the arches were unloaded in reverse order. In Test 1, the maximum applied load at the  $\frac{1}{4}$  point of the span was 66 tonnes (648 kN), which included the mass of the plateaus. Test 2 was executed similarly, but with blocks weighing 6.4 and 10 tonnes. The specimen was loaded to failure of the arches, which occurred at a total load of 98.8 tonnes (970 kN). Figure 12 shows the loading as function of time for Test 2.

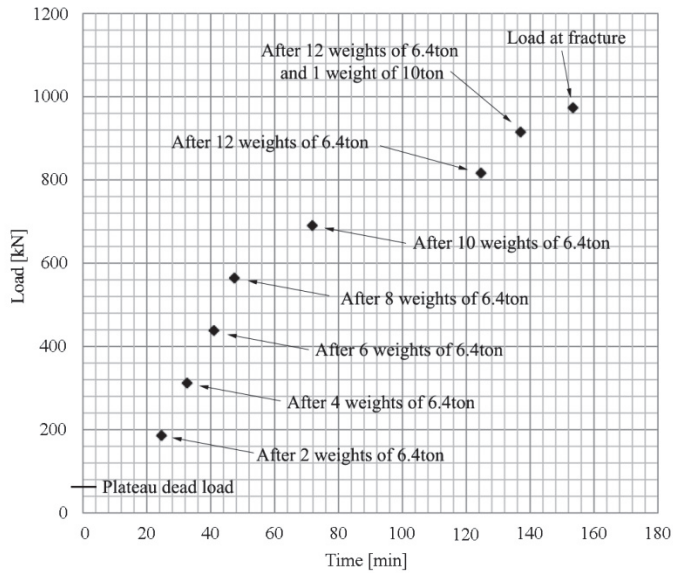


Figure 12: Loading sequence for Test 2.

### 3.1. Test 1 – testing in the linear elastic range

#### 3.1.1. Deflections and deformations

The deflections measurements from the LVDT's were similar to those measured by the leveling instrument. Because of the LVDT's gave readings every five seconds, whereas the rulers were only read after every change in loading, only the LVDT data is presented here. In Figure 13, the deflection of "arch 1" is given, and in locations of no LVDT instruments, the deflections given by adjacent LVDT's have been supplemented with readings from the leveling instrument. For very small deflections, however, the leveling instrument lacked the resolution needed for useful results. During Test 1, the largest deflection on the loaded side was 15 mm. In Test 2, this value was 32 mm at the load level before fracture.

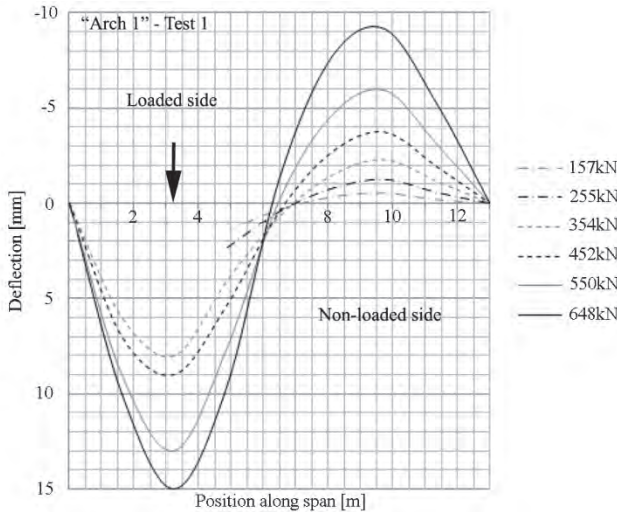


Figure 13: Deflection of “arch 1” for various total loads (accumulated from both arches) at the  $\frac{1}{4}$  point of the span, not including self-weight.

Figure 14 shows the measured deflections of each arch as the loading progressed. The plot indicates that the Hammerhead joints transferred forces between the arches. However, there was some deviation between the deflections because of the unsymmetrical loading. The deflection in “arch 1” increased both when load was applied to “arch 1”, but also when applied to “arch 2”. The results from LVDT 1 and LVDT 2, measuring horizontal settlement of the abutments, showed insignificant deflections of less than  $\frac{1}{3}$  of a mm. Therefore, all deflections in “arch 1” when applying load on “arch 2” must come from forces being transferred through the Hammerhead joints.

By comparing the arches’ deflections at locations C, D, E, and G, it appears that the position closest to the loading plateau, had the largest difference in the deflection between the two arches. In Figure 14, it is seen that at position C, “arch 1” deflected more than “arch 2” when the load was applied to “arch 1”, and vice versa. This did not happen in the same way for positions D, E, and G. This trend was expected because the forces being transferred through the Hammerhead joints were likely largest at the location of applied load, but were smaller when moving away from that position. The Hammerhead joints for the test bridge were designed to transfer more than 100 kN each.

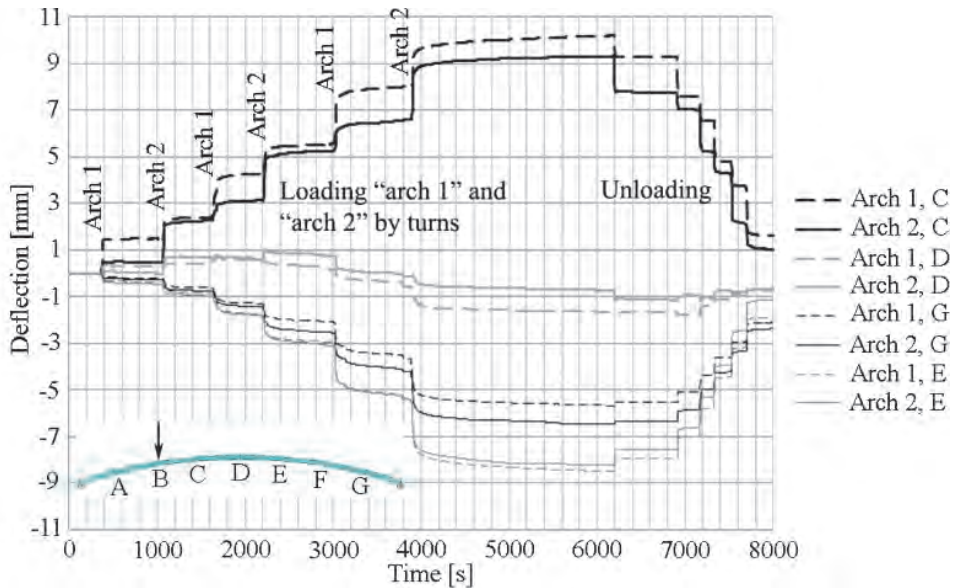


Figure 14: Test 1. Comparison of deflections of “arch 1” and “arch 2” at location C, D, E, and G (downwards is considered positive).

An ARAMIS system was used to monitor the arch deformation at the loaded and non-loaded  $\frac{1}{4}$  points of the span (locations B and F, respectively). Vertical deformations found by ARAMIS corresponded well with the measurements from the LVDT’s and the leveling instrument. Digital image correlation enables crack growth analysis by limiting the display output to strains above a certain value. Such analyses were complete for both the loaded and non-loaded  $\frac{1}{4}$  points of the span. The non-loaded  $\frac{1}{4}$  point (location F) did not show any cracking after applying the total of 66 tonnes, while some cracks appeared in the loaded  $\frac{1}{4}$  point of the span (location B). Figure 15 shows the location of the DIC measurements (a), the vertical deflection contour plot at 648 kN load (b), and the identified cracks at 648 kN load (c). One crack developed between the plateau and arch, and another one from the arch into the plateau. Neither of those cracks affected the behavior of the arch itself. The plateau was not designed to transfer any significant shear to the arch – only direct vertical load. Therefore, some sliding between the two surfaces was expected. The separation was expected and verified the assumption of the static system being with two concentrated forces: one force at the  $\frac{1}{8}$  of the span, and one at the  $\frac{3}{8}$  of the span. The plateaus likely had a large bending stiffness, and as the arch settled below the plateau, the load went from being uniformly distributed on the arch to being two point loads on the arch – one close to the  $\frac{1}{8}$  point of the span, and one close to the  $\frac{3}{8}$  point of the span. This was due to the arch deflecting more than the plateau, so that the contact surface was limited to the two areas close to the  $\frac{1}{8}$  and  $\frac{3}{8}$  points.

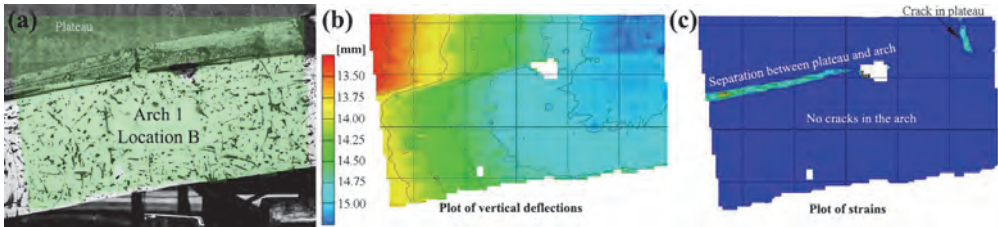


Figure 15: At 648 kN load: ARAMIS output for the loaded quarter point at location B on the side of arch 1.

### 3.1.2. Strains in SL-Decks

At location F on “arch 2”, concrete strain gauges were attached to the underside of the arch, see Figure 8. The measured strains (in the longitudinal direction of the span) are shown in Figure 16. The vertical tick marks on the time axis indicate the time when each new 98 kN load was applied.

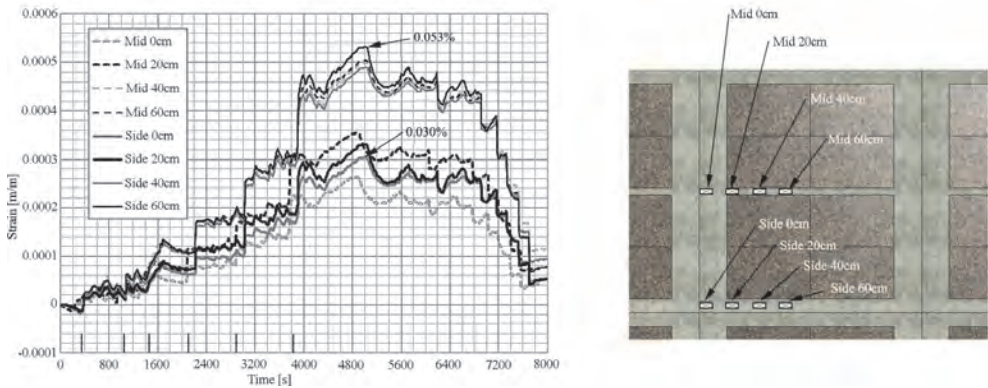


Figure 16: Strains from the eight strain gauges during Test 1 (not including initial strains).

The results show that the largest measured strains developed in the concrete ribs in a cross section of the SL-Deck where the LAC blocks were located. This was expected, since the cross sectional area of the normal concrete was smaller in this zone compared to the zone with no LAC blocks at the ends of an SL-Deck. The thinnest rib was in the middle of the element, and the strains there were approximately 100% larger (at location “Mid 60 cm”) compared to the cross section without LAC blocks (at location “Mid 0 cm”). The strain gauge at “Mid 20 cm” was positioned at the transition between the cross sections with and without LAC blocks. Here, the magnitude of the strain was between the two extremes, since the normal force in the SL-Deck was being transferred from the large rectangular concrete section to the rib, which had a smaller cross sectional area.

The same trend occurred for the strain gauges at the side of the SL-Deck, although the concentration of the strains occurs a little further into the side rib. Where the “Mid 40 cm” and the “Mid 60 cm” measurements are almost similar, the difference between the “Side 40 cm”, and “Side 60 cm” measurements are up to 9%. Also, the increase in strain from “Mid 0 cm” to “Mid 20 cm” was close to 40%, while the increase from “Side 0 cm” to “Side 20 cm” was less than 9%. The reason for the difference in how fast the strains concentrated was due to the ribs’ relative sizes - the side rib was wider than the middle rib. Furthermore, a Hammerhead joint was located in proximity of the strain gauges “Side 40 cm” and “Side 60 cm”. This could have had an effect on the results.

### **3.2. Test 2 – Testing to failure**

The fracture load was 98.8 tonnes (970 kN) which was 14% higher than the analytically calculated result of 86.5 tonnes (849 kN). Plastic hinges formed in both the loaded and non-loaded side of the arches during the last loading interval: from 94% to 100% of the fracture load. So they did not contribute to a 50% to 100% larger load capacity as explained by Jain [1], who stated that this occurs for arches with rectangular concrete cross sections and mild steel reinforcement.

Several different damage warnings were observed in the structure before the ultimate capacity was applied. Figure 17 shows three photographs at the moment of collapse: 1. Plastic hinges forming on the loaded side, and then on the non-loaded side. 2. Loss of structural stability (a four hinged arch which is free to move) at the moment of fracture. 3. Final collapse.

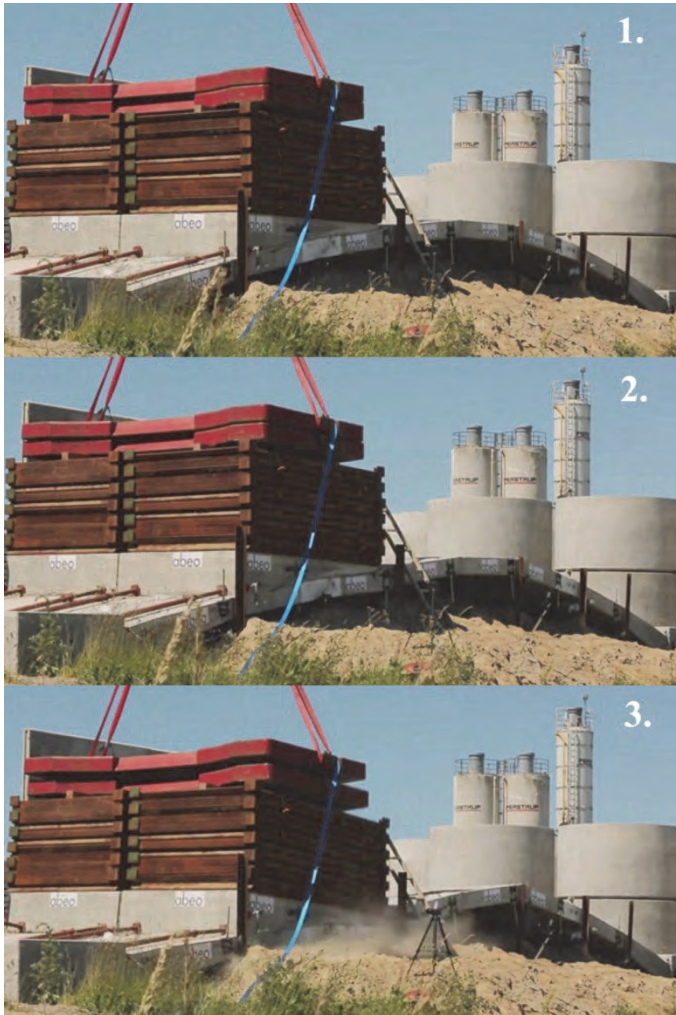


Figure 17: Sequence of observed failures preceding collapse.

### 3.2.1. Test of theory

The collapse occurred after two plastic hinges developed in the arch. The plastic hinges formed at the  $3/8$  and  $5/8$  points of the span. Theoretically, the most critical positions were found to be in the  $3/8$  of the span in the loaded side, and at the  $1/4$  point of the span in the non-loaded side, but only if the specimen behaved as a two-hinged arch. The cross sections where the hinges formed though were the same as predicted: In the joint in the loaded side, and in the SL-Deck with LAC blocks in the non-loaded side.

Hinge behavior was assumed at the interfaces between the foundation plate and the arch ends because reinforcement was not used to tie those elements together. At a low level of

load ( $< 300$  kN), however, the ARAMIS analysis showed limited rotation at the abutments, which suggested that the support connections were close to being fixed instead of hinged. At larger loads ( $> 300$  kN), clear hinge effect was observed, although it remained far from an ideal hinge with zero bending moment. A plot based on numerical calculations in the program Robot Structural Analysis [12] shows the difference in bending moment distributions, see Figure 18.

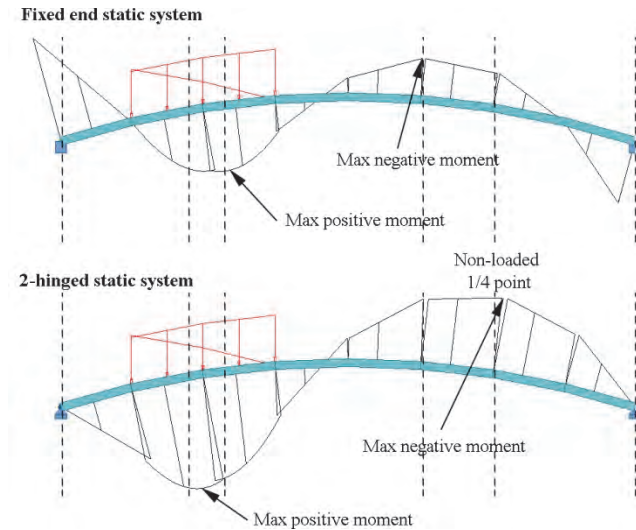


Figure 18: Bending moment distribution in fixed vs. 2-hinged arch of same geometry as the tested arches.

The true static system would have been somewhere between the two extremes. This may be the reason why the fracture occurred closer to the crown of the arch in the non-loaded side. Also, a small degree of fixation in the hinges may have reduced the bending moments and hereby give an increase in the load carrying capacity compared to the calculated value. In fact, when checking the load carrying capacity based on an arch with fixed ends, and a load corresponding to the fracture load from the test, there would still be a remaining moment capacity of  $+102$  kNm and  $-105$  kNm in the loaded and non-loaded side, respectively.

The expected failure mechanism was compressive crushing of the concrete in the bottom of the non-loaded side, or in the top of the cross section in the loaded side of the span. The actual failure was more complex due to the rotation in the points of the plastic hinges and the SL-Deck geometry in combination with the local stresses from the plateau used for loading. The following observations were made just before the ultimate capacity was reached:

6. A plastic hinge formed at the  $3/8$  point of the span on the loaded side of the arch. The plastic hinge concentrated the stresses in that location, since the concrete crushed at the top and a transverse crack opened at the bottom. A longitudinal crack developed in the middle of the adjacent deck element, which was likely caused by a splitting mechanism that resulted from the concentrated normal load being transferred between the deck elements.
7. A plastic hinge formed in the  $5/8$  point of the span, at which point the arch became an unstable structure (having four hinges). The  $3/8$  point was pushed downwards, and the  $5/8$  point was lifted upwards. This movement would have created a shear force, which would exacerbate the cracking at the  $3/8$  point of the span.
8. The deflections and crack propagation occurred very quickly. As the plastic hinges moved upwards and downwards, the longitudinal crack lengthened in the mid-depth of the SL-Deck. The crack stayed in the middle of the cross section, probably because of the mild steel reinforcement and the pre-stressing strands in the top and bottom of the cross section.

Figure 19 depicts the observations leading to collapse.

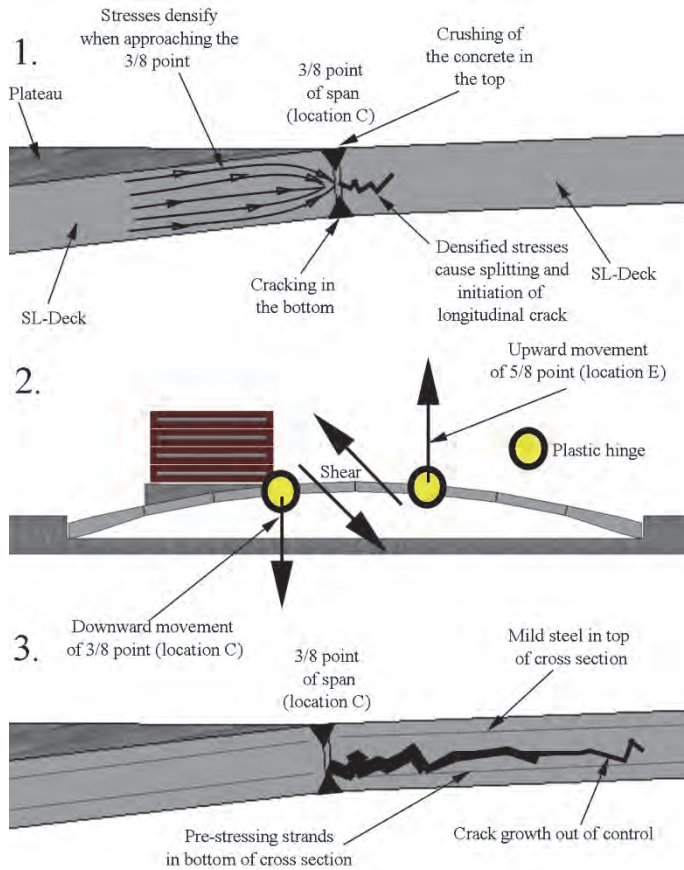


Figure 19: Sequence of events leading to final collapse.

Figure 20 shows photographs of the large longitudinal crack in the loaded side (3/8 point of span – location C), and crushing of concrete on the underside of the arch in the non-loaded side (5/8 point of span – location E).



Figure 20: Photographs taken after collapse: longitudinal crack at 3/8 point (top) and crushed concrete at 5/8 point (bottom).

The PC-Arches seemed to form both plastic hinges nearly simultaneously. If this was true, then the same load resulted in concrete crushing strains at the 3/8 and 5/8 locations. With this damage observation, the results from the elastic analyses can be used to predict the load at failure.

Other reasons for the 14% difference between the calculated load capacity and the actual capacity are:

- Multiaxial stresses in the SL-Decks. We have shown how the stresses concentrate inside the SL-Deck and the confinement of the concrete may give a different working curve with a higher compressive strength compared to the one presented earlier.

- The strength of the LAC blocks has not been accounted for in the analytical calculations. The load bearing capacity is based on the normal concrete only.

### 3.2.2. Warnings before fracture

Highly pre-stressed construction members (arches in particular) are often assumed to have a brittle, unwarned fracture. However, the tested PC-Arches showed several warning signs before the collapse occurred. Figure 21 shows the change in system stiffness. On the main vertical axis the load is plotted as function of the deflections for all load levels in the loaded  $\frac{1}{4}$  point – locations B – and the non-loaded  $\frac{1}{4}$  point – location F. On the secondary vertical axis the corresponding stiffnesses are seen. There is clear system ductility since the stiffness decreases as the load and deflections increase. The figure is based on data from Test 2.

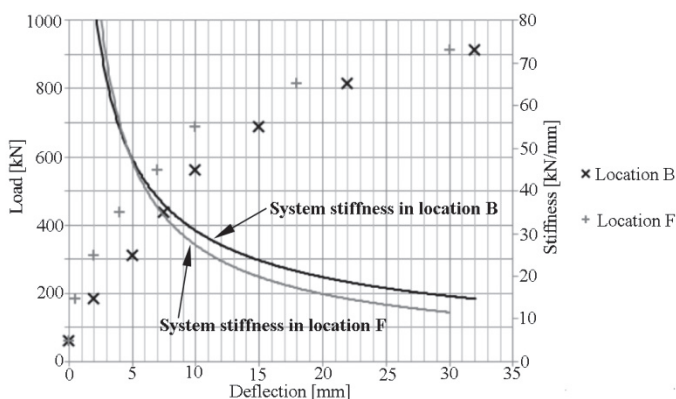


Figure 21: Deflections in location B and F at different loads, and corresponding system stiffness.

The first visible cracks were seen at the connection to the abutments where the hinge rotation took place. Figure 18 compared analyses of the two-hinged and fixed end static systems, and showed that the largest bending moment resulted at the abutments if fixed. The cracks at the support “hinges” were initially observed at a load of approximately 300 kN, and grew as a result of additional loading. This means that visible cracks at the abutments were seen at a load level of 31% of the fracture load. At several locations, cracks were observed in the bottom of the loaded side of the arch at 84% to 94% of the fracture load. The non-loaded  $\frac{1}{4}$  point of the span was closely monitored, but cracks were not observed there. However, cracking was observed in the top of the cross section at the  $\frac{5}{8}$  point of the span, where the plastic hinge developed before the collapse. Extensive concrete spalling was observed in the bottom of the arch close to that same location, also at 84% to 94% of the fracture load.

An interesting observation was that all cracking initiated at the connections between the SL-Decks and mortar joints, which seemed to be the weakest link.

#### 4. CONCLUSION

The straight SL-Decks in PC-Arches worked as intended. The LAC blocks formed ribs in the SL-Decks which lead to a concentration of the stresses and multiaxial compression. The Hammerhead joints transferred forces between arches, and the two arches deflected similarly when loaded on one arch only.

Analytical calculations predicted the critical locations to be the  $3/8$  point of the span in the loaded side, and the  $1/4$  point of the span in the non-loaded side. Two plastic hinges formed – one on the loaded side, and one on the non-loaded side of the span. However, those hinges formed at the  $3/8$  and  $5/8$  points, as opposed to the predicted,  $1/4$  point on the non-loaded side. This discrepancy could have resulted from the difference between the actual test setup and the ideal setup that would represent the theoretical static system. Most importantly, loading plateaus were used to transfer the gravity load to the arches. These plateaus had a significant bending stiffness and the bending deformation of the plateaus applied the load concentrated to the  $1/8$  and  $3/8$  points. This loading change affected the location of the plastic hinge on the unloaded side of the span.

The load at collapse was 970 kN which was 14% higher than the calculated ultimate load of 849 kN based on ideal abutment hinges. Possible reasons for the difference were: i) the abutment hinges had a rotational resistance, and must have decreased the bending moment and increased the capacity, ii) the strength in the SL-Decks close to the ribs may have been higher due to multiaxial stresses, iii) the stabilizing effect of the LAC blocks was not considered.

Several damage warnings were observed before final collapse. First, the connections to the abutments started cracking at around 31% (300 kN) of the fracture load. Later, the arches cracked on the bottom of the loaded side, and concrete began spalling off from the bottom of the non-loaded side. This damage occurred at 84% to 94% of the fracture load. At this level of load, the largest measured deflection was 32 mm in the loaded  $1/4$  point of the span. All cracks initiated at the interfacial, mortared joints between SL-Deck elements. Finally, large deformations occurred in the arches when the last 6% of the fracture load was applied.

The capacity calculations were correct. The tested fracture load was between the calculated capacity loads for a two-hinged (below), and a fixed end static system (above). Consequently, the tests demonstrated that the arches can be used to construct Pearl-Chain Bridges. A field implemented PC-Bridge would be a closed spandrel type of arch bridge. Such a bridge would include a filling material on top of the arches, in order to produce a level road surface. Additionally, this filling material would more evenly distribute traffic loads to the arches. After Test 1 was completed, the first PC-Bridge was successfully

constructed in Denmark. That bridge had the same type of span and design as the test specimen, but used thicker SL-Deck elements.

The concept of PC-Bridges already includes the option of larger spans [5]. Furthermore, experimental tests of small scale models at the Technical University of Denmark showed that the design could be developed into a “sandwich arch” structure. If the backfilling material transfers shear between the arch and a concrete road-surface-plate, the load bearing capacity could increase by a factor of up to 86. This interesting observation may be the basis of further research.

### **Acknowledgements**

Many thanks for the help from the construction crew of Perstrup Betonindustri, the cooperation with the project manager Nicky Eide Viebæk, and the funding provided by Innovationsfonden.

### **References**

- [1] Jain, O. P. (1960). Ultimate strength of reinforced concrete arches. *American Concrete Institute -- Journal*, 32(6), 697 – 713.
- [2] Marshall, J. D., Anderson, J. B., Meadows, R. L., & Jensen, T. J. (2014). Full-Scale Testing of Three-Sided Precast Concrete Arch Sections. *Journal of Bridge Engineering*, 19(12), 04014051. doi:10.1061/(ASCE)BE.1943-5592.0000630
- [3] Zhang, J., Li, C., Xu, F., & Yu, X. (2007). Test and Analysis for Ultimate Load-Carrying Capacity of Existing Reinforced Concrete Arch Ribs. *Journal of Bridge Engineering*, 12(1), 4–12. doi:10.1061/(ASCE)1084-0702(2007)12:1(4)
- [4] McGrath, T. J. (2002). Finite-element modeling of reinforced concrete arch under live load. *Transportation Research Record*, (1814), 203 – 210.
- [5] Halding, P. S., Hertz, K. D., & Schmidt, J. W. (2015). Precast Pearl-Chain concrete arch bridges. *Engineering Structures*, 103, 214–227. doi:10.1016/j.engstruct.2015.09.012
- [6] Hertz, K., Castberg, A., & Christensen, J. (2014). Super-light concrete decks for building floor slabs. *Structural Concrete*, 15(4), 522 – 529.
- [7] Hertz, K. D. (2009). Super-light concrete with pearl-chains. *Magazine of Concrete Research*, 61(8), 655–663. doi:10.1680/macr.2008.61.8.655
- [8] Hertz, K. D., & Halding, P. S. (2014). Super-light pearl-chain arch vaults. *Proceedings of the Iass-Slste 2014 Symposium*.

[9] Halding, P. S., Hertz, K. D., Viebæk, N. E., & Kennedy, B. (2015). Assembly and lifting of Pearl-Chain arches. *Proceedings of Fib Symposium 2015*.

[10] EN 1992-1-1 (2008), Design of concrete structures, 3<sup>rd</sup> Ed.

[11] [www.gom.com](http://www.gom.com). Webpage of ARAMIS software. Last visited March 10, 2015.

[12] Autodesk Robot Structural Analysis Professional (2012), version 26.0.3.4375 (x64).

Arches once were a popular construction type for bridges, but in the past 50 years the number of constructions has been limited because in-situ cast arch bridges require complicated formwork which is expensive and slow to build. Pearl-Chain Bridges use straight pre-fabricated light-weight concrete elements, post-tensioned together in an arch shape. The elements are patented SL-Decks with a number of pre-tensioning strands. The thesis presents a calculation method for Pearl-Chain Bridges, two types of tested concrete hinges, a fast erection procedure, full-scale tests, and two applied cases.

**DTU Civil Engineering**  
Technical University of Denmark

Brovej, Bygning 118  
2800 Kongens Lyngby

[www.byg.dtu.dk](http://www.byg.dtu.dk)

ISBN 9788778774439  
ISSN 1601-2917